

Critical Tests in the Theory and Application of  
Nonstatistical Dynamics

Lawrence Michael Goldman

A thesis submitted for the Degree of Doctor of Philosophy  
School of Chemistry  
Cardiff University

June 2010

UMI Number: U516851

All rights reserved

INFORMATION TO ALL USERS

The quality of this reproduction is dependent upon the quality of the copy submitted.

In the unlikely event that the author did not send a complete manuscript and there are missing pages, these will be noted. Also, if material had to be removed, a note will indicate the deletion.



UMI U516851

Published by ProQuest LLC 2013. Copyright in the Dissertation held by the Author.  
Microform Edition © ProQuest LLC.

All rights reserved. This work is protected against  
unauthorized copying under Title 17, United States Code.



ProQuest LLC  
789 East Eisenhower Parkway  
P.O. Box 1346  
Ann Arbor, MI 48106-1346

**DECLARATION**

This work has not previously been accepted in substance for any degree and is not concurrently submitted in candidature for any degree.

Signed *Laurence Goldin* (candidate) Date *24/6/10*

**STATEMENT 1**

This thesis is being submitted in partial fulfillment of the requirements for the degree of PhD

Signed *Laurence Goldin* (candidate) Date *24/6/10*

**STATEMENT 2**

This thesis is the result of my own independent work/investigation, except where otherwise stated.  
Other sources are acknowledged by explicit references.

Signed *Laurence Goldin* (candidate) Date *24/6/10*

**STATEMENT 3**

I hereby give consent for my thesis, if accepted, to be available for photocopying and for inter-library loan, and for the title and summary to be made available to outside organisations.

Signed *Laurence Goldin* (candidate) Date *24/6/10*

## ABSTRACT

Nonstatistical dynamics were searched for in two organic systems. Both of these systems presented properties that were not commonly conducive to nonstatistical effects. Chapter one provides an overview of nonstatistical dynamics and the methodology presented in this work to search for such effects.

Chapters two and three discuss a singlet biradical which was specifically designed to search for nonstatistical effects in the ring opening of a cyclopropylmethyl radical. These effects could be seen experimentally by observing the reactivity of the biradical as a function of the pressure of the supercritical fluid solvent. While several syntheses were designed to synthesise the biradical precursor, they were ultimately unsuccessful. Computational study of the biradical system highlights the convenience and accuracy of density functional theory in studying singlet biradicals. Molecular dynamics carried out on the biradical system is then discussed. The molecular dynamics confirms that this biradical should be a useful system to search for nonstatistical dynamics.

Chapter four discusses cyclopentadiene. When cyclopentadiene is formed from bicyclo[2.1.0]pent-2-ene, it can undergo a [1,5] hydrogen shift. We proposed that this hydrogen shift shows evidence for nonstatistical dynamics. Molecular dynamics calculations at the density functional theory level showed that hydrogen shift breaks the expected symmetry of the system. This symmetry breaking is caused by normal mode coupling which is a hallmark of nonstatistical dynamics. We have proposed a mechanism for the transformation of bicyclo[2.1.0]pent-2-ene into cyclopentadiene that explains the oscillatory behaviour of the hydrogen shift which is able to break the symmetry. We have also proposed isotope-labelling experiments that can be used to confirm the existence of nonstatistical behaviour for the cyclopentadiene system.

“Nothing is impossible. Not if you can imagine it. That’s what being a scientist is all about.” – Professor Hubert Farnsworth, *Futurama*

## ACKNOWLEDGMENTS

First and most importantly I would like to thank my supervisor, Barry Carpenter for taking me on as a student and for all guidance, advice, and patience he has offered me. He is one of the most astute chemists I have ever met and I am glad I had the chance to work with him. I'm also very thankful for Thomas Wirth and Ian Williams for serving as my examiners.

I would not have been able to do this research on my own. I'm very appreciative of the members of the POC for chemistry discussions and general socialising. Steve, Aviva, and Vishu were very welcoming back at Cornell. And Alex, who was the other Carpenter group member to come to Cardiff. Having a fellow Yankee made it that much easier for me to adapt to being in a new country for the first time. And while not officially in the group, thanks to Scott and Sean for the occasional game of pool in the Baker basement.

At Cardiff, the POC flourished, thanks to the addition of Drs Niek Buurma and Eric Tippmann as lecturers. And an extra thanks to Niek for the many chemistry discussions we had, and for being the default person to drive the group to conferences. And I'm appreciative of the members of the POC, Rob, Julia, Jamie, Ed, Andy, Mihaela, Stefania, Mazin, Ismail, Azzedine, Mandeep, Ian, Alicja, Zuzka, Carol, Sundaram, Becky, and Amy. Rob in particular was very good at mentoring me and other people as they joined the group. And a special mention for Mandeep introducing mandatory coffee breaks, especially for people like me who don't actually drink coffee.

I began my PhD at Cornell, and so there are many other people to thank on both sides of the Atlantic. At Cornell, I'd like to thank Ivan Keresztes and Anthony Condo for their helps with NMR and other instrumentation. And Pat, June, Sharon, and Sharon in the office for help with all things clerical and for aiding in the process of transferring universities to Cardiff.

At Cardiff, I want to thank all the people who make the department work behind the scenes. Terrie, Trish, Jo, Alison, and Stephanie in the office for helping with clerical things on this side of the pond. And well as Dr Benson Kariuki for X-ray crystallography and technicians Rob, Robin, and Dave for help with the NMR and MS. Any lab needs to be kept well stocked which is thanks to Gaz and Jamie in stores. And Alun, JC, and Mal for keeping the mechanical bits and bobs working, particularly Mal maintaining our nitrogen supply even though we had a tendency to guzzle cylinders.

And finally, I'd like to thank my family for their love and support throughout my life. I would not be where I am not if it was not for their constant support and encouragement, and the occasional trans-Atlantic gift basket. And of course to Damian, for making my life better.

So to all of these people, and anyone I might have accidentally left out, thank you so very much.

# TABLE OF CONTENTS

## Introductory Sections

Declaration	ii
Abstract	iii
Acknowledgments	v
Table of Contents	vii
List of Abbreviations	x
Journal Abbreviations	xiv
List of Figures	xv
List of Tables	xviii
List of Graphs	xix

## Chapter 1 Introduction to Nonstatistical Dynamics and Computational Chemistry

Section 1.1	Introduction to Chapter 1	1
Section 1.2	Conventional Kinetic Theories	1
Section 1.3	Nonstatistical Behaviour	3
Section 1.4	Examples of Nonstatistical Dynamics	6
Section 1.4.1	Acetone Radical Cation	6
Section 1.4.2	2,3-Diazabicyclo[2.2.1]hept-2-ene	9
Section 1.4.3	Vinylcyclopropane	11
Section 1.4.4	Ethyl Radical	12
Section 1.5	Computational Methodology	13
Section 1.5.1	Hartree-Fock	14
Section 1.5.2	Post Hartree-Fock Methods for Dynamical Electron Correlation	16
Section 1.5.3	Post Hartree-Fock Methods – Multireference Methods	17
Section 1.5.4	Density Functional Methods	19
Section 1.5.5	Molecular Dynamics	20
Section 1.6	Summary and Project Goals	21
Section 1.7	References for Chapter 1	22

## Chapter 2 Nonstatistical Effects in Singlet Biradicals

Section 2.1	Introduction to Chapter 2	26
Section 2.2	Pressure, Nonstatistical Dynamics, and Supercritical Fluids	26
Section 2.3	Clock Reactions	27
Section 2.4	Cytochrome P450 – An Example of the Use of Ultrafast Clock Reactions	28
Section 2.5	A Singlet Biradical to Test for Nonstatistical Effects	31
Section 2.6	Revised Biradical System	33
Section 2.7	DFT Benchmarks and Calculations	34
Section 2.7.1	Computational Studies on Biradical <b>31</b>	34
Section 2.7.2	Computational Studies on Biradical <b>37</b>	40
Section 2.7.3	Molecular Dynamics	45
Section 2.8	Synthetic Work Toward Biradicals <b>31</b> and <b>37</b>	54
Section 2.8.1	Attempted Synthesis of Ketones <b>30</b> and <b>36</b> Using Late Cyclopropanations	55
Section 2.8.2	Attempted Synthesis of Ketones <b>30</b> and <b>36</b> Using Early Cyclopropanations	63
Section 2.9	Summary and Conclusions	75
Section 2.10	References for Chapter 2	75

## Chapter 3 Experimental Section for Chapter 2

Section 3.1	General Experimental	80
Section 3.2	Instrumentation	80
Section 3.3	Experimental Procedures	82
Section 3.4	References for Chapter 3	102

## Chapter 4 Nonstatistical Effects in Cyclopentadiene

Section 4.1	Introduction to Chapter 4	105
Section 4.2	Cyclopentadiene and Bicyclopentene	105
Section 4.3	Nonstatistical Effects in the CP/BCP System	108
Section 4.4	Proposed Experimental Tests for Nonstatistical Dynamics	111
Section 4.5	Computational Work	113

Section 4.5.1	DFT Benchmarks	113
Section 4.5.2	Molecular Dynamics	117
Section 4.5.2.1	Experimental Design to Study the CP/BCP System	118
Section 4.5.2.2	High Temperature MD Studies of The CP/BCP System	125
Section 4.5.3	Reaction Mechanism	129
Section 4.5.4	Statistical Analysis of the CP Work	130
Section 4.6	Summary and Conclusions	139
Section 4.7	References for Chapter 4	139
<b>Appendix</b>		
Section A.1	X-ray Structure for Compound <b>74</b>	142
Section A.2	Computational Details for Chapter 2	146
Section A.2.1	Molecular Dynamics Details	146
Section A.2.2	Computed Energies and Geometries	146
Section A.3	Computational Details for Chapter 2	195
Section A.3.1	Molecular Dynamics Details	195
Section A.3.2	Computed Energies and Geometries	196

## LIST OF ABBREVIATIONS

Å	Ångström
Ac	Acetyl
B	Becke functional
BCP	Bicyclo[2.1.0]pent-2-ene
BOMD	Born-Oppenheimer Molecular Dynamics
br	Broad (IR data)
Bu	Butyl
BuLi	n-Butyllithium
CASPT2	Complete active space 2 <sup>nd</sup> order perturbation theory
CASSCF	Complete active space self consistent field
Cat.	Catalyst
CC	Coupled-Cluster theory
CI	Configuration-Interaction theory
COSY	Correlation spectroscopy
CP	1,3-Cyclopentadiene
Cycl.	Cyclisation
d	Day (in experimentals)
d	Doublet (NMR data)
DBH	2,3-Diazabicyclo[2.2.1]hept-2-ene
DBU	1,8-Diazabicyclo[5.4.0]undec-7-ene
DCM	Dichloromethane
DDQ	2,3-Dichloro-5,6-dicyano-1,4-benzoquinone
DEPT	Distortionless enhancement by polarisation transfer
DFT	Density functional theory
DMAP	4-(Dimethylamino)pyridine
DMF	N,N-Dimethylformamide
DMPU	N,N'-Dimethylpropyleneurea
DMSO	Dimethylsulphoxide
<i>E</i>	Energy
EI	Electron ionisation
Eq.	Equivalentents
ES	Electrospray

Et	Ethyl
Ether	Diethylether
Frag.	Fragmentation
FT	Fourier transform
<i>G</i>	Gibbs (Free) Energy
GC	Gas Chromatography
<i>h</i>	Planck's constant
h	Hour (in experimentals)
<i>H</i>	Enthalpy
hν	UV irradiation
HF	Hartree-Fock
HMBC	Heteronuclear multiple bond coherence
HMDS	Hexamethyldisilazane (K or Li salt as given)
HRMS	High resolution mass spectrometry
HSQC	Heteronuclear single quantum coherence
IBX	2-Iodoxybenzoic acid
IR	Infrared (spectroscopy)
IVR	Intramolecular Vibrational Relaxation (or redistribution)
<i>k</i>	Rate constant
<i>k<sub>b</sub></i>	Boltzmann's constant
<i>KE</i>	Kinetic energy
LDA	Local density approximation
LTMP	Lithium tetramethylpiperidide
LYP	Lee-Yang-Parr functional
MD	Molecular dynamics
m	Medium (IR data)
m	Minute (in experimentals)
m	Multiplet (NMR data)
<i>m/z</i>	Mass per charge
Me	Methyl
MO	Molecular Orbital
MP	Moller-Plesset theory
MRMP2	Multireference 2 <sup>nd</sup> order MP theory
MS	Mass Spectrometry

MVK	Methyl vinyl ketone
n	normal (hydrocarbons)
N/A	Not applicable
n-BuLi	n-Butyllithium
NBS	N-Bromosuccinimide
NCS	N-Chlorosuccinimide
NMO	N-Methylmorpholineoxide
NMR	Nuclear Magnetic Resonance
NOESY	Nuclear Overhauser effect spectroscopy
Ox.	Oxidation
PBE	Perdew-Burke-Ellison functional
PES	Potential Energy Surface
Ph	Phenyl
$pK_a$	$-\log$ (acid dissociation constant)
Ppm	parts per million
Prod.	Product
PW	Perdew-Wang functional
q	Quartet (NMR data)
quin	Quintet (NMR data)
$R$	Gas constant
$R_f$	Retention factor
RMS	Root-mean-square
ROHF	Restricted open-shell Hartree-Fock
Rot.	Rotation
RRKM	Rice-Ramsperger-Kassel-Marcus
RT	Room temperature
s	Singlet (NMR data)
s	Strong (IR data)
SOMO	Semi-occupied molecular orbital
t	tertiary (hydrocarbons)
t	Triplet (NMR data)
$T$	Temperature
<i>t</i> -BuLi	<i>t</i> -Butyllithium
THF	Tetrahydrofuran

TLC	Thin layer chromatography
TMS	Tetramethylsilane
Tol	Toluyl
Ts	Tosyl
TS	Transition State
TST	Transition State Theory
UV	Ultraviolet
UHF	Unrestricted Hartree-Fock
w	Weak (IR data)
ZPE	Zero point energy

## JOURNAL ABBREVIATIONS

Acc. Chem. Res.	Accounts of Chemical Research
Angew. Chem. Int. Ed.	Angewandte Chemie-International Edition
Annu. Rev. Phys. Chem.	Annual Reviews of Physical Chemistry
Biochem. Biophys. Res. Commun.	Biochemical and Biophysical Research Communications
Chem. Ber.	Chemische Berichte
Chem. Phys. Lett.	Chemical Physics Letters
Helv. Chim. Acta	Helvetica Chimica Acta
Int. J. Quantum Chem.	International Journal of Quantum Chemistry
J. Am. Chem. Soc.	Journal of the American Chemical Society
J. Chem. Phys.	Journal of Chemical Physics
J. Chem. Soc.	Journal of the Chemical Society
J. Chem. Soc., Chem. Commun.	Journal of the Chemical Society Chemical Communications
J. Chem. Soc., Perkin Trans.	Journal of the Chemical Society Perkin Transactions
J. Comp. Chem.	Journal of Computational Chemistry
J. Org. Chem.	Journal of Organic Chemistry
J. Phys. Chem.	Journal of Physical Chemistry
J. Phys. Org. Chem.	Journal of Physical Organic Chemistry
Mol. Phys.	Molecular Physics
Mol. Spect.	Molecular Spectroscopy
Organomet. Chem.	Organometallic Chemistry
Org. Biomol. Chem.	Organic and Biomolecular Chemistry
Org. Lett.	Organic Letters
Org. Syn.	Organic Synthesis
Phys. Rev.	Physical Reviews
Pract. Synth. Proc.	Practical Synthetic Procedures
Tetrahedron Lett.	Tetrahedron Letters

## LIST OF FIGURES

Figure 1.1	A One Step Reaction	2
Figure 1.2	A Two Step Reaction	3
Figure 1.3	PES Showing Symmetrical Pathways	5
Figure 1.4	Reactions Involving the acetone radical cation	6
Figure 1.5	Isotope labelling for the acetone radical cation	7
Figure 1.6	Oscillatory behaviour of the acetone radical cation	9
Figure 1.7	Reaction of DBH	9
Figure 1.8	Deuterium labelled reactions of DBH	10
Figure 1.9	Mechanism of DBH Reactivity	10
Figure 1.10	Vinylcyclopropane rearrangement	11
Figure 1.11	Stepwise mechanism for vinylcyclopropane	11
Figure 1.12	Chemistry of the ethyl radical	13
Figure 1.13	Two electronic configurations for a singlet biradical	18
Figure 1.14	Electronic configurations for bond cleavage	19
Figure 2.1	Radical clock ring-opening reaction	28
Figure 2.2	Mechanism for Cytochrome P450	29
Figure 2.3	Kinetics of the cyclopropane ring-opening	29
Figure 2.4	Norrish Type II reaction	32
Figure 2.5	Potential reactivity for singlet biradical <b>21</b>	32
Figure 2.6	Actual reactivity of singlet biradical <b>21</b>	33
Figure 2.7	Revised biradicals and their reactivity	34
Figure 2.8	Orbital overlap in biradical <b>31</b>	34
Figure 2.9	Biradical conformations	36
Figure 2.10	Reactions of biradical <b>31</b>	37
Figure 2.11	Multireference enthalpies for the clock reaction of <b>42</b>	40
Figure 2.12	Conformations of Biradical <b>37</b>	42
Figure 2.13	Reactions of Biradical <b>37</b>	43
Figure 2.14	Conformations of biradical <b>42</b>	46
Figure 2.15	Retrosynthetic analysis of biradicals <b>31</b> and <b>37</b>	54
Figure 2.16	First proposed synthesis of ketone <b>30</b>	55
Figure 2.17	First attempted synthesis of ketone <b>30</b>	56
Figure 2.18	Reactions of diazofluorene	56
Figure 2.19	Alternative proposed route to halide <b>45</b>	57

Figure 2.20	Alternative attempted route to halide <b>45</b>	57
Figure 2.21	Proposed route to ketone <b>47</b>	57
Figure 2.22	Attempted route to ketone <b>47</b>	58
Figure 2.23	Proposed route to ketone <b>30</b> bypassing ketone <b>47</b>	59
Figure 2.24	Attempted route to ketone <b>30</b> bypassing ketone <b>47</b>	59
Figure 2.25	Proposed alternative route to diene <b>48</b>	60
Figure 2.26	Attempted alternative route to diene <b>48</b>	61
Figure 2.27	Mechanism of the Chugaev elimination	61
Figure 2.28	Attempted route to ketone <b>36</b>	62
Figure 2.29	Initial proposed route to ketone <b>74</b> and then ketone <b>30</b>	63
Figure 2.30	First alternative proposed route to ketone <b>74</b>	64
Figure 2.31	Attempted alternative route to ketone <b>74</b>	64
Figure 2.32	Next proposed route to ketone <b>74</b> <i>via</i> ketone <b>78</b>	65
Figure 2.33	Next attempted route to ketone <b>74</b> <i>via</i> ketone <b>78</b>	66
Figure 2.34	Alternative proposed route to ketone <b>74</b>	67
Figure 2.35	Alternative attempted route to ketone <b>74</b>	68
Figure 2.36	Proposed rearrangement route to ketone <b>74</b> <i>via</i> ketone <b>88</b>	68
Figure 2.37	Proposed rearrangement route to ketone <b>88</b>	69
Figure 2.38	Optimised synthesis of ketones <b>74</b> and <b>94</b>	70
Figure 2.39	Proposed endgame from ketones <b>74</b> and <b>94</b> to final ketones <b>30</b> and <b>36</b>	71
Figure 2.40	Tebbe reagent	71
Figure 2.41	Attempted reactions of ketones <b>74</b> and <b>94</b>	72
Figure 2.42	X-ray structure of ketone <b>74</b>	73
Figure 2.43	Proposed alternative route to ketones <b>30</b> and <b>36</b>	73
Figure 2.44	Attempted alternative route to ketones <b>30</b> and <b>36</b>	74
Figure 4.1	Formation of cyclopentadiene	105
Figure 4.2	Reactions involving bicyclopentene and their energetics	106
Figure 4.3	Possible mechanisms of the thermal opening	107
Figure 4.4	Revised mechanism of ring-opening	108
Figure 4.5	Important vibrational modes	109
Figure 4.6	Isotopic labelling to study CP/BCP	111
Figure 4.7	Isotopically labelled syntheses	112
Figure 4.8	Atom numbering used by Gaussian	116

Figure 4.9	Isotope effects for cyclopentadiene chemistry	117
Figure 4.10	Proposed mechanism for the hydrogen shift	129
Figure 4.11	Geometric coordinates important to the Fourier analysis	130

## LIST OF TABLES

Table 2.1	Relative energies of the compounds in Figure 2.10	38
Table 2.2	Relative energies of the compounds in Figure 2.11	44
Table 2.3	Summary of molecular dynamics on biradical <b>42b</b>	47
Table 2.4	Results of the biradical MD trajectories	49
Table 2.5	Comparing the subsets of the MD trajectories	50
Table 4.1	DFT Energy benchmarks	114
Table 4.2	DFT Frequency benchmarks	115
Table 4.3	DFT method comparisons	115
Table 4.4	Summary of important geometric parameters	116
Table 4.5	Summary of hypothetical variables	119
Table 4.6	Design of experiments and results for the experiments	120
Table 4.7	Results of the hypothetical experimental design	121
Table 4.8	A small subset of data from the experimental trajectories	124
Table 4.9	Optimum quanta of energy according to the statistical analysis	124
Table 4.10	Summary of the statistically designed trajectories	125
Table 4.11	Summary of trajectories at various temperatures	126

## LIST OF GRAPHS

Graph 2.1	Number of reactions as a function of time	51
Graph 2.2	Cumulative selectivity of the reactions as a function of time	51
Graph 2.3	Portion of the reactions complete after a given amount of time	52
Graph 2.4	Number of D-labelled reactions as a function of time	52
Graph 2.5	Cumulative selectivity of the D-labelled reactions as a function of time	53
Graph 2.6	Portion of the D-labelled reactions complete after a given amount of time	53
Graph 4.1	Shift vs. time	127
Graph 4.2	Branching ratio vs. time	128
Graph 4.3	Reaction “completion” vs. time	129
Graph 4.4	Fourier Transform of the geometrical data	131
Graph 4.5	Fourier Transform for trajectories undergoing the “17” H-shift	133
Graph 4.6	Fourier Transform for trajectories undergoing the “18” H-shift	133
Graph 4.7	Fourier Transform for trajectories undergoing the “57” H-shift	134
Graph 4.8	Fourier Transform for trajectories undergoing the “59” H-shift	134
Graph 4.9	Kinetic energies for all trajectories	135
Graph 4.10	Kinetic energies for trajectories undergoing the “17” ( <i>endo</i> ) H-shift	135
Graph 4.11	Kinetic energies for trajectories undergoing the “18” ( <i>endo</i> ) H-shift	136
Graph 4.12	Kinetic energies for trajectories undergoing the “57” ( <i>endo</i> ) H-shift	136
Graph 4.13	Kinetic energies for trajectories undergoing the “58” ( <i>endo</i> ) H-shift	137
Graph 4.14	Relative number of shifts seen from exciting methylene or non-methylene bending modes.	138

# CHAPTER 1

## INTRODUCTION TO NONSTATISTICAL DYNAMICS AND COMPUTATIONAL CHEMISTRY

### 1.1 Introduction to Chapter 1

This chapter serves as a general introduction to the conventional theories of kinetics and dynamics. Core assumptions that are made in the development of these theories are discussed. Special focus is on the statistical approximation, because the failure of this approximation forms the basis of the research on both singlet biradicals (Chapters 2 – 3) and cyclopentadiene (Chapters 4 – 5). The potential consequences of this nonstatistical dynamics will be introduced, and a short survey will be provided of reactions already known to exhibit this behaviour. The chapter closes with a discussion of various common computational methods that can be used to study these systems.

### 1.2 Conventional Kinetic Theories

While a full discussion of theories of chemical kinetics is beyond the scope of this work<sup>1</sup>, it will cover the basic concepts behind the two theories most commonly used today, RRKM theory<sup>2</sup> and Transition State Theory (TST).<sup>3</sup>

RRKM theory was first formulated by Rice and Ramsperger, and then augmented by Kassel and Marcus. RRKM theory can predict reaction rates by comparing the rotational and vibrational energy states of the reactant and activated complex. Given the starting energy of the molecule, the vibrational-rotational spectrum of the reactants (available from either spectroscopy or computational study), and the vibrational-rotational spectrum of the activated complex, the rate constant can be predicted. RRKM is a microcanonical theory, that is, it predicts rate constants as a function of energy –  $k(E)$ . In contrast to that, TST is a canonical theory, that is, it predicts rate constants as a function of temperature –  $k(T)$ . Aside from that, the two theories are equivalent. If a Boltzmann distribution of reactant energies is assumed, and the corresponding  $k(E)$  from RRKM theory is weighted by those Boltzmann populations, the resulting  $k(T)$  will be identical to the  $k(T)$  from TST.

Consider a simple reaction coordinate diagram as in Figure 1.1. TST assumes equilibrium between the reactant and the activated complex (which from now on will be referred to as the transition state). That equilibrium constant can be calculated from the

difference in Gibbs energy between the transition state (TS) and the reactant(s). The Eyring equation<sup>3</sup> (equation 1.1) converts this equilibrium constant into a rate constant  $k$  by multiplying it by a prefactor, where  $k_b$  is Boltzmann's constant,  $T$  is the temperature,  $h$  is Planck's constant,  $R$  is the gas constant, and  $\Delta G^\ddagger$  is the difference in Gibbs energy between the TS and reactant(s). The prefactor represents an estimate from statistical mechanics for the reaction of a system already energised to the same energy as the TS. It serves as an upper limit on the rate constant, roughly  $2 \times 10^{10} T \text{ s}^{-1}$  for unimolecular chemical reactions. At room temperature, this is approximately  $6 \times 10^{12} \text{ s}^{-1}$ .

$$k = \frac{k_b T}{h} e^{\frac{-\Delta G^\ddagger}{RT}} \quad \text{Equation 1.1}$$

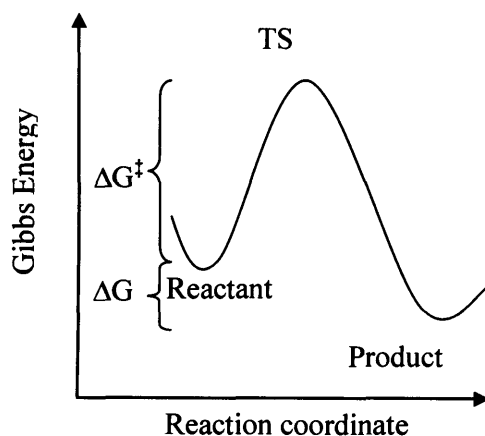


**Figure 1.1:** A one step reaction

The derivation of RRKM theory explicitly invokes the statistical approximation, which assumes that vibrational energy in a set of molecules is always statistically distributed amongst the available vibrational modes. For this to be true, intramolecular vibrational energy relaxation (IVR) must be much faster than product formation. The equivalent assumption in the derivation of TST is the equilibrium between the reactant(s) and the TS.<sup>4</sup>

TST and RRKM theory were originally developed for single-step reactions. However they are often assumed to apply to multi-step reactions with additional assumptions. Consider the more generalised reaction coordinate in Figure 1.2. Here a reactant must pass over two barriers in order to reach the final product. There is an

intermediate between the barriers characterised by a local minimum in energy. In order to cross the first barrier and enter the intermediate region, the system must not only have sufficient total energy, but must also have that energy localised in the correct vibrational modes that correspond to the reaction coordinate. To put this another way, the first TS acts as a filter for only those molecules which have the correct vibrational energy distribution. Consequently, those molecules in the intermediate region will initially not have a statistical distribution of energies in their vibrational modes. However, this has no consequence for the second step because rapid IVR would re-establish a statistical distribution of vibrational energy of the intermediate before it underwent the second reaction.

Intermediates would therefore be expected to lose all “memory” of where they have come from. Any differences in where they started would be reflected in different distributions of vibrational energy, and all of those would be wiped out by fast IVR. This makes an important (and intuitive) prediction that an intermediate should always behave the same way, regardless of how it was generated, and that reactions passing through achiral intermediates should only give achiral/racemic products

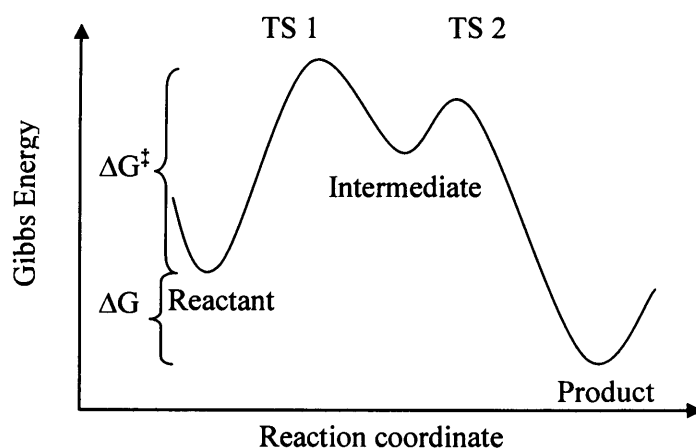


**Figure 1.2:** A two step reaction

### 1.3 Nonstatistical Behaviour

To a first approximation, the decay of a set of nonstatistically distributed molecules to being statistically distributed can be treated with first-order kinetics.<sup>5</sup> A number of experiments suggest that the “rate constant” for IVR ( $k_{IVR}$ ) is in the order of

$10^{12} \text{ s}^{-1}$ .<sup>6</sup> In the first few decades following the development of RRKM and TST theories, experiments looking for failures of the statistical approximation would focus on systems where  $k_{IVR}$  might be considerably slowed by phase-space bottlenecks.<sup>16a</sup> The overall rate of these reaction should be significantly smaller than that calculated by either TST or RRKM theories. Some examples of this were found for small systems such as  $\text{H}_3^+$  or  $\text{HeI}_2$ ,<sup>7</sup> though the phase-space bottleneck criterion is sufficiently strict that this is not expected to be a common phenomenon. An example that is more applicable to organic chemistry is described in Section 1.4.4.

More recently, it has been recognised that nonstatistical behaviour might still be observable even if  $k_{IVR}$  has a normal value. Any molecular motion can be decomposed into a linear combination of normal modes of a nearby stationary point.<sup>8</sup> If the modes excited by the intermediate after it has passed through TS1 are sufficiently similar to the modes that need to be excited in order to pass through TS2, the second step may occur significantly faster than predicted by RRKM/TST theories. Whereas the phase-space-bottleneck only occurs infrequently, it appears that rate enhancement through mode coupling is a relatively common phenomenon. See the discussion of the cyclopropylmethyl radical (Chapter 2) for more details.

This coupling has potential consequences for product ratios in cases where a single intermediate has several seemingly degenerate exits. Normally product ratios are determined from the rate constants for each of the potential reactions, which the Eyring equation says come from the relative barrier heights of each reaction. Consider the case (Figure 1.3) where an intermediate can form several equivalent products. The TSs leading towards the products must have the same energy, therefore the barrier heights are the same. According to TST, the products will be formed with the same rate and in the same amount. Intuitively, this explains how the  $\text{S}_{\text{N}}1$  reaction can transform chiral alkyl halides into racemic products by passing through an achiral carbocation. But memory effects can cause symmetry-breaking to occur. There may be significant mode coupling between the achiral intermediate as it is being formed (from a previous TS where the asymmetry was still present) and **only one** of the TSs leading towards the chiral product. That will increase the rate of formation for **only one** of the seemingly-equivalent products and lead to an unexpected product distribution. This symmetry-breaking is one of the hallmarks of nonstatistical dynamics. See sections 1.4.1 and 1.4.2 for examples.

As a corollary to the symmetry-breaking behaviour, there can also be unexpected changes in product distributions as a function of time. Initially, a nonstatistical distribution of vibrational energies leads to favouring one product over another. Once IVR has been completed, both products will be favoured equally. Therefore, the product distribution must change as a function of time. It is even possible that a different product will be favoured midway through IVR. Contrast this with the statistical approximation which suggests that since rapid energy redistribution occurs completely before any subsequent reactions, product formation will be time-invariant. See sections 1.4.1 and 1.4.3 for examples of time-dependence of product formation.

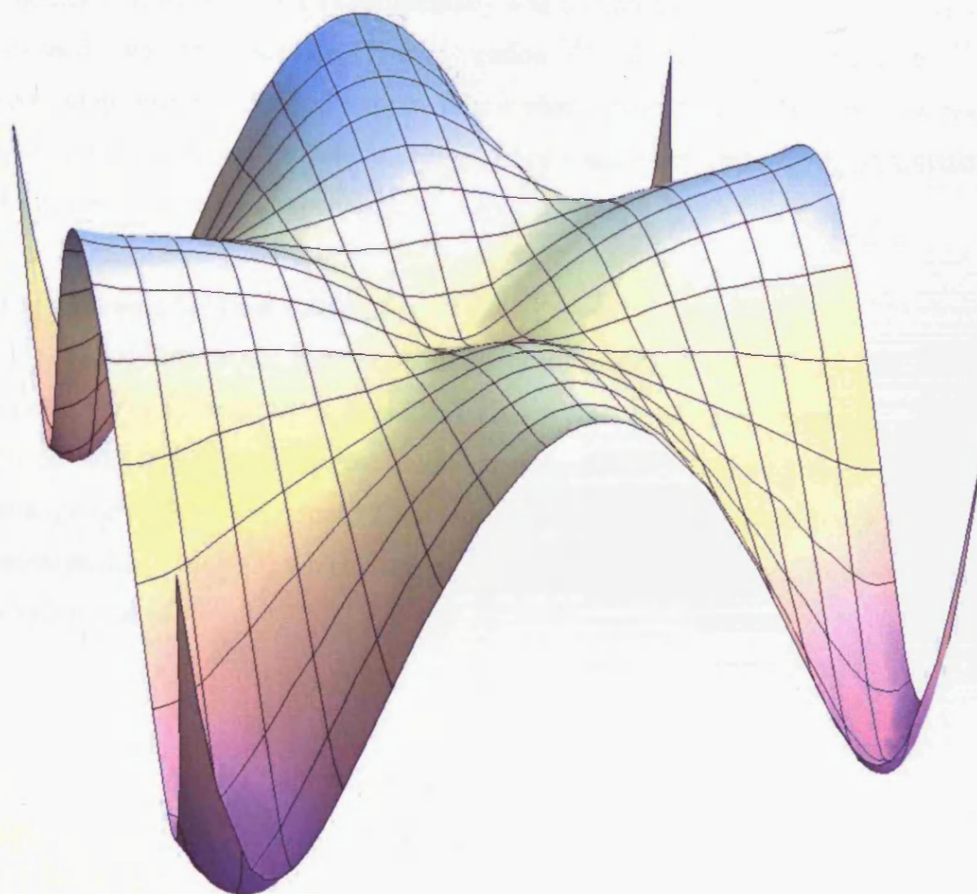


**Figure 1.3, Potential energy surface showing symmetrical pathways**

## 1.4 Examples of Nonstatistical Dynamics

As stated in the previous section, the initial investigations into nonstatistical dynamics involved looking for systems where the rate constant of IVR was substantially slower than expected. Some reactions that showed this included the decomposition of  $\text{H}_3^+$ ,  $\text{HeI}_2$ , carbonyl sulfide, and the isomerisation of hydrogen isocyanide to hydrogen cyanide.<sup>7</sup> These are small systems that are not directly applicable to the organic chemist. Instead, a more recent approach has been to look for larger systems where vibrational mode coupling in high-energy intermediates leads either to kinetics or product distributions not predicted by RRKM/TST. This evidence has been seen with such energetic intermediates such as radicals<sup>9</sup>, biradicals (also called diradicals)<sup>10</sup>, cations<sup>11</sup>, and radical cations<sup>12</sup>. While a comprehensive survey of this evidence is beyond the scope of this work, a selection of examples will be presented in which nonstatistical dynamics is observed both experimentally and computationally. The cases that will be discussed are the acetone radical cation<sup>12,13</sup>, 2,3-diazabicycloheptene<sup>10,14</sup>, and vinylcyclopropane<sup>15</sup>. As an example of how phase space bottlenecks can slow reactions down, the ethyl radical<sup>9</sup> will be discussed. For a more detailed survey of nonstatistical effects, see reviews by Carpenter<sup>16</sup>.

### 1.4.1 Acetone Radical Cation

The nonstatistical behaviour of the acetone radical cation was first studied by McLafferty<sup>13</sup> and later by Schwarz<sup>17</sup>. The overall scheme is shown in Figure 1.4. 2-Hexanone (**1**) is placed into the mass spectrometer (MS) and undergoes a McLafferty rearrangement to acetone enol (**2**) with loss of propene. The enol tautomerises to the acetone radical cation (**3**) which eventually fragments to form an acylium ion (**4a**) and a methyl radical (**4b**).

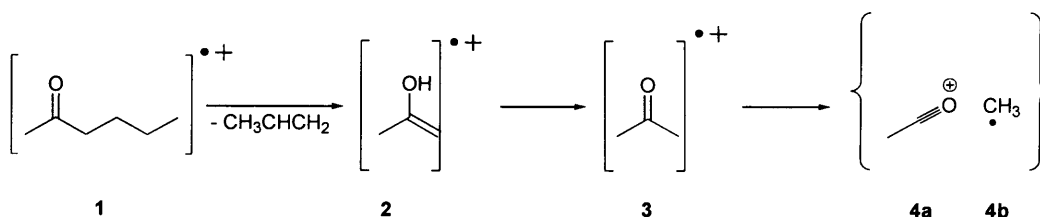
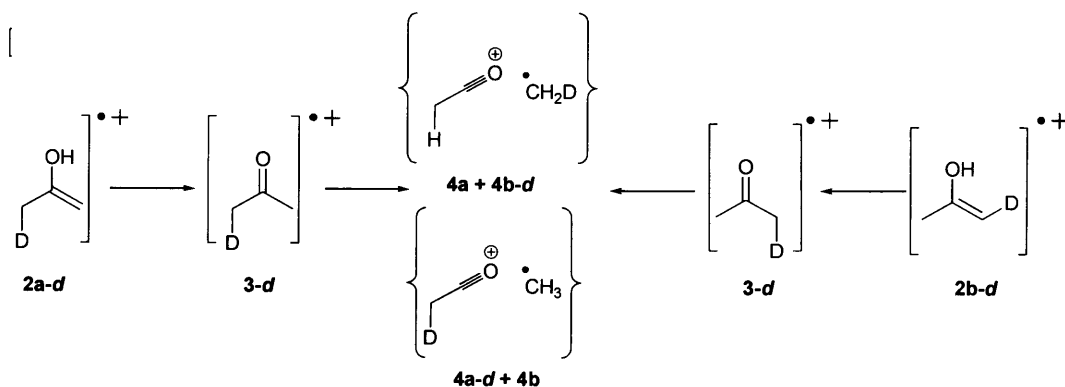


Figure 1.4: Reactions involving the acetone radical cation

When McLafferty deuterium labelled the different alpha protons of **1**, there was an asymmetry in where the label wound up. The methyl groups in **3** are related by symmetry so the C-C bonds should cleave with equal probability. Ignoring any isotope effects, a single  $^2\text{H}$  or  $^{13}\text{C}$  atom on either of the methyl groups would have an equal chance of ending up in the acylium ion or the methyl radical as shown in Figure 1.5. If the deuterium atom was introduced on the existing methyl group (**2a-d**), there was a 1.3 : 1 preference for the deuterium ending up on the acylium ion (**4a-d**). And if the deuterium atom was introduced on the vinyl group (**2b-d**), there was again a 1.3 : 1 preference, except that this time the deuterium preferentially ended up on the methyl radical (**4b-d**). It appeared that when the acetone radical cation was generated in this manner, the existing methyl group in enol **2** preferentially ended up in the acylium ion **4a**. Some of this asymmetry could be explained with isotope effects. This could be seen in either the tautomerisation step or the fragmentation step. The tautomerisation could show a secondary isotope effect, but is irrelevant because reaction of compounds **2a-d** and **2b-d** make the same intermediate **3-d**. The fragmentation step could also show a secondary isotope effect, but since **3-d** is a common intermediate, the isotope effect should favour the same fragmentation pathway in both cases (*ie.* **4a-d** or **4b-d**), rather than the **2a-d** and **2b-d** favouring different isotope distributions. The nail in the coffin for isotope effects was work by Schwarz<sup>14</sup> where instead of  $^2\text{H}$  labels,  $^{13}\text{C}$  labels were used. He found the same product asymmetry, with the initial methyl group ending up in the acylium ion with a similar ratio. As  $^{13}\text{C}$  isotope effects are generally much smaller than  $^2\text{H}$  primary and secondary isotope effects, and are too small to cause the observed product ratios, this precludes isotope effects being the cause of the symmetry breaking.<sup>18</sup>



**Figure 1.5:** Isotope labeling for the acetone radical cation

McLafferty postulated that the energy of intermediate **3** had not fully relaxed, leading to a memory effect when the acetone radical cation was formed. Computational evidence for this was found by Carpenter.<sup>12</sup> Molecular dynamics calculations on the acetone radical cation reproduced the asymmetric fragmentations for the methyl groups. Trajectories starting from **3** lost both methyl groups with equal frequency, whilst trajectories starting from the TS between **2** and **3** showed a 1.1 : 1 preference for losing the newly-formed methyl group. The molecular dynamics also allowed a confirmation of the explanation of the origin for the nonstatistical behaviour. The original mechanism was proposed by Brauman<sup>18</sup>, and as McLafferty hypothesised, ketone **3** was indeed formed with a selective localisation of vibrational energy in the CCO bending mode of the newly formed methyl group, whilst the bending mode for the other carbon did not have localised energy. Fortuitously, this mode is also important for the methyl fragmentation, but according to conventional theories, this would have been irrelevant as **3** would simply have redistributed its vibrational energy. However, the molecular dynamics suggested that a large portion of the molecules dissociate very soon after forming **3**, before any relaxation could occur. As only one of the CCO bending modes had the large amount of vibrational energy, only one of the two “equivalent” fragmentations is accelerated. Accordingly, the MD shows an excess of the new methyl group being lost as the methyl radical during the initial time period. As vibrational energy oscillates between the two bending modes (which for symmetry reasons are strongly coupled to each other), the original methyl group’s bending mode becomes coupled with the dissociation. Hence, the original methyl group is preferentially lost during the next time-period. This oscillation continues until the system has undergone full IVR, and by then in the MD, the remaining molecules of **3** show statistical behaviour in which methyl group is lost. But as with a damped oscillation, the initial asymmetry was large enough to explain the overall product distribution. This is shown graphically in Figure 1.6.<sup>19</sup> The blue curve is the ratio of newly-formed methyl loss to initial methyl loss as a function of time. The red curve is the cumulative ratio of methyl loss. Note that it is above one, even in the long time limit. The theme of oscillating product formation will be seen in several of the other examples, including diazabicycloheptene (Section 1.4.2) and cyclopentadiene (Chapter 5).

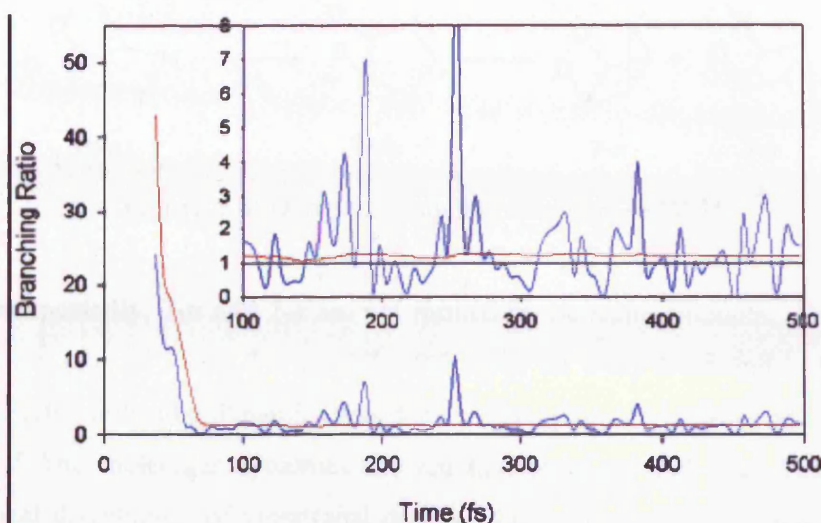


Figure 1.6: Oscillatory behaviour of the acetone radical cation<sup>20</sup>

#### 1.4.2 2,3-Diazabicyclo[2.2.1]hept-2-ene (DBH)

DBH is another system that has been seen to show symmetry-breaking behaviour. The overall reaction scheme is shown in Figure 1.7. DBH (**5**) thermally extrudes a molecule of nitrogen to form biradical **6** which can then ring close to bicyclo[2.1.0]pentane **7**. That the reaction proceeds through biradical **6** rather than a fully concerted mechanism or stepwise breakage of the C-N bonds was a matter of considerable debate. The debate was settled through computational work<sup>10</sup> at the CASSCF and CASPT2 levels<sup>20</sup>.

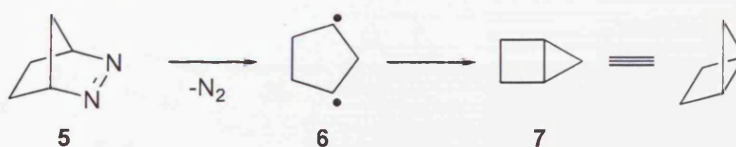
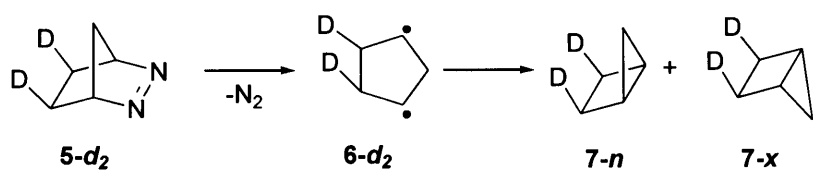


Figure 1.7: Reaction of DBH

In the process of probing the mechanism experimentally, deuterated DBH **5-exo-d<sub>2</sub>** was synthesised which could lead to one of two products, **7-x** and **7-n** (excluding the possibility that the D-containing carbons scramble their stereochemistry), as shown in Figure 1.8. As with the acetone radical cation, because intermediate **6-d<sub>2</sub>** is symmetrical (ignoring isotope effects), the *endo* and *exo* products should be formed in equal amounts. Baldwin showed that the secondary isotope effect will be negligible enough to ignore in order to compare product ratios.<sup>14b</sup>



**Figure 1.8:** Deuterium labelled reactions of DBH

Unexpectedly, *7-n* and *7-x* are not formed in the same amounts. Experimental values for the ratio of *7-x* to *7-n* are  $4.7 \pm 0.9$ , quite far away from unity. As with the acetone system, molecular dynamics was done on the system to understand why it broke symmetry. The molecular dynamics showed that biradical *6-d<sub>2</sub>* was formed with a nonstatistical distribution of vibrational energy. In order to conserve momentum, the loss of nitrogen forced the two radical centres to move away from the N<sub>2</sub> molecule (Figure 1.9). Even though the biradical is formed closer in appearance to conformation *6-d<sub>2-n</sub>*, that momentum causes the ring to bend into conformation *6-d<sub>2-x</sub>* before any ring-closing chemistry can occur. Once the system reaches conformation *6-d<sub>2-x</sub>*, the coupling between the system and the ring-closing reaction is so great that virtually all molecules with a nonstatistical distribution of energy ring close to form product *7-x*. Only those molecules which have undergone IVR would remain and they would form a statistical distribution of products *7-n* and *7-x*. It is the behaviour of the intermediates with nonstatistical vibrational energy distributions at short timescales that explain the overall nonstatistical behaviour.

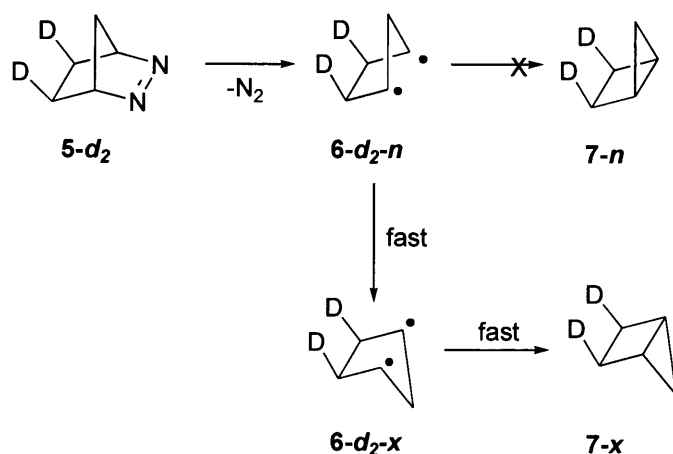


**Figure 1.9:** Mechanism of DBH reactivity.

### 1.4.3 Vinylcyclopropane

Vinylcyclopropane thermally isomerises to the more stable cyclopentene as shown in Figure 1.10. As with the previous examples, isotope labeling proved to be a useful tool in elucidating the mechanism of this rearrangement.<sup>15a</sup>

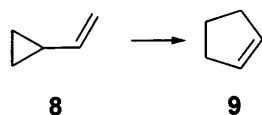


Figure 1.10: Vinylcyclopropane rearrangement

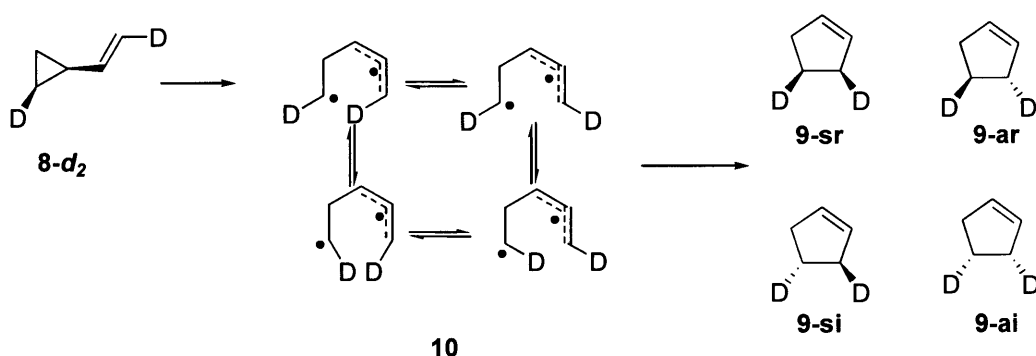


Figure 1.11: Stepwise mechanism for vinylcyclopropane

Consider labelled vinylcyclopropane **8-d<sub>2</sub>** in Figure 1.11. If it goes through a stepwise pathway, it would form biradical **10** which could equilibrate into four conformations *via* internal rotations. These biradicals can all ring-close onto the other end of the allylic radical to give four cyclopentenenes, **9-sr**, **9-ar**, **9-si**, and **9-ai** (the letters correspond to the stereochemistry of the reaction if it occurred in a concerted manner, with *s/a* representing suprafacial or antarafacial ring closure and *i/r* representing inversion or retention of the stereochemistry of the D-labelled cyclopropyl methylene). Statistical behaviour would suggest that by symmetry arguments the pairs of enantiomeric biradicals should have the same energy, barring a small isotope effect. They should therefore be formed in equal amounts. Therefore, the four diastereomers of **9** should be formed in equal pairs (*i.e.* **9-si** = **9-ar** and **9-sr** = **9-ai**). If the reaction is concerted and does not involve biradical **10**, this argument does not apply. Instead, the Woodward-Hoffmann rules<sup>21</sup> would dictate the product distribution. In this reaction, products **9-si** and **9-ar** are nominally allowed, while **9-sr** and **9-ai** are nominally forbidden. This does not mean that they would not be formed at all, just that there should be considerably more [**9-si** + **9-ar**] than [**9-sr** + **9-ai**]. When performed

experimentally<sup>15a</sup>, the observed ratio is 23 : 13 : 40 : 24 (**9-sr** : **9-ar** : **9-si** : **9-ai**). This is in disagreement with the biradical mechanism because diastereomers **9-si** and **9-ar** should be formed in equal amounts, but are clearly not. In addition, this ratio is not consistent with the concerted pathway. The ratio of Woodward-Hoffmann allowed vs. forbidden products is 53% allowed, 47% forbidden. Two potential explanations are that either the biradical and concerted mechanisms are competing with each other, or that there are nonstatistical effects at play. The former explanation is possible though it requires the  $k_{birad}$  and  $k_{concert}$  rate constants to be similar (meaning that their barrier heights must be nearly identical), which is often not the case. To check for nonstatistical effects, Doubleday performed molecular dynamics on this system<sup>15b</sup>. The molecular dynamics predicted that the mechanism did indeed pass through biradicals **10-i** and **10-r** and the overall product ratio from the dynamics matched the experimental values. An explanation into the mechanism was gleaned from the time dependence of the shifts. The quickest reactions, namely those that took less than 200 fs, gave 96% suprafacial products **9-sr** and **9-si**. Reactions that took longer than 600 fs gave a roughly 1:1:1:1 mixture of all four products, consistent with the statistical biradical mechanism. An explanation is that after crossing the TS barrier between vinylcyclopropane and the biradical, some molecules have the correct excited vibrational modes to immediately perform the suprafacial ring-closing to the cyclopentene. The remaining molecules survive long enough to undergo full IVR and form a statistical distribution of both biradicals, which react to form all four cyclopentenes equally. The combination of short-time nonstatistical products and long-time statistical products gives rise to the overall complicated ratio of the four cyclopentenes.

#### 1.4.4 Ethyl Radical

The previous three sections discussed reactions that give unsymmetrical product distributions from seemingly symmetrical intermediates. This comes from those intermediates maintaining nonstatistical distributions of vibrational energies. In contrast to those, the example of the ethyl radical shows a different kind of nonstatistical behaviour, more akin to the original work on phase-space bottlenecks.<sup>7</sup> Figure 1.12 shows the chemistry Chen used to make and use the ethyl radical<sup>9a</sup>. Ethyl iodide was pyrolysed to form the ethyl radical. A molecular beam of the ethyl radical was then struck by a UV laser to give a hydrogen atom and ethene. The rate of the reaction was found by detecting the hydrogen atoms *via* their Lyman emission at 121 nm.

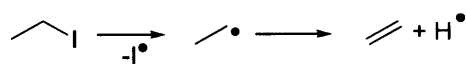


**Figure 1.12:** Chemistry of the ethyl radical.

Chen found a rate constant for the formation of ethene to be between  $10^6 \text{ s}^{-1}$  and  $10^7 \text{ s}^{-1}$  given laser excitation energies of 108 – 117 kcal/mol<sup>9a</sup>. While this number on its own may not seem interesting, the rate constant calculated by RRKM theory was approximately  $10^{12} \text{ s}^{-1}$ . The reaction was 5 – 6 orders of magnitude slower than predicted. The full details of the RRKM calculation goes beyond this work, but can be found in reference 9b. Chen deemed the accuracy of the RRKM calculation to be sufficiently good to require an explanation for the difference between the predicted and experimental lifetimes for the ethyl radical.

Chen's approach was to perform molecular dynamics on the ethyl radical<sup>9b</sup>. Many trajectories were run and the results agreed with the experimental results. Several of the ethyl radicals survived orders of magnitude longer than predicted, despite the system having at least three times as much energy as needed to cross the reaction barrier. The explanation for the slow reactivity of the ethyl radical is that a large portion of this excess energy is tied up in an unreactive mode, that is, a mode that is not coupled to the second reaction coordinate. In terms of vibrational mode coupling, this is the opposite of previously discussed systems in Sections 1.4.1 and 1.4.2. Having excess energy in a mode coupled to the second reaction coordinate greatly increased the observed reactivity of those systems relative to the theoretical reactivity. Specifically, the major observed motion in the dynamics simulations was the rotation of the methyl group. Slow IVR prevents that energy from being redistributed to the necessary CH stretching mode. Until that energy is redistributed amongst the other modes, the molecule is unable to react further and the overall system has a lifetime that is much longer than expected.

## 1.5 Computational Methodology

Computational chemistry is an increasingly used tool to help understand chemical systems<sup>22</sup>. It is particularly useful for highly reactive systems that can not be easily observed. In the cases described in Section 1.4 and Chapter 2, computational chemistry was used to find additional evidence for nonstatistical dynamics. This section begins by giving an overview of some areas of computational chemistry. Again as a detailed discussion of computational chemistry is beyond the scope of this work, only the basic

details will be presented and will focus on areas of computational chemistry related to the current projects.

### 1.5.1 Hartree-Fock (HF)

The Hartree-Fock<sup>23</sup> method is one of the simplest for approximately solving the Schrödinger equation. HF starts with the time-independent Schrödinger equation<sup>24</sup> (Equations 1.2 and 1.3 ).

$$\hat{H}\Psi = E\Psi \quad \text{Equation 1.2}$$

$$\hat{H} = \hat{K}_N + \hat{K}_e + \hat{V}_{NN} + \hat{V}_{Ne} + \hat{V}_{ee} \quad \text{Equation 1.3}$$

Here  $\hat{H}$  is the Hamiltonian,  $E$  is the energy of the system, and  $\Psi$  is the wavefunction. The Hamiltonian is an operator that represents each of the contributions to the overall energy. This can be broken down into the kinetic energy of each nucleus ( $\hat{K}_N$ ) kinetic energy of each electron ( $\hat{K}_e$ ), potential energy interactions between each pair of nuclei ( $\hat{V}_{NN}$ ), potential energy interactions between each nucleus-electron pair ( $\hat{V}_{Ne}$ ), and the potential energy interactions between each pair of electrons ( $\hat{V}_{ee}$ ). For systems containing more than one electron, the Schrödinger equation is impossible to solve exactly<sup>25</sup>. Instead, several approximations are made and the simplified equation is solved numerically. The first approximation is the Born-Oppenheimer approximation<sup>26</sup> which assumes that because the nuclei are much heavier than the electrons, the nuclei will be essentially motionless on the time-scale of electron motions. With this assumption in place, the term in Equation 2.2 for the kinetic energy of the nuclei drops out and the potential energy between nuclei becomes a constant. The form of the wavefunction is also assumed to be a linear combination of molecular orbitals, which in turn are formed from combinations of atomic orbitals. In order to simplify the calculations, electron correlation is ignored. While greatly simplifying the calculation, it also introduces a great deal of inaccuracy. Post-HF methods reintroduce the electron correlation in various ways.

Another of the assumptions in HF theory is that the wavefunction is described by a single Slater determinant<sup>27,28</sup>. The Slater determinant represents the molecular wavefunction in terms of the electrons. As an example, Equation 1.4 shows a possible wavefunction for two electrons.

$$\Psi = N[\chi_1(x_1)\chi_2(x_2) - \chi_1(x_2)\chi_2(x_1)] \quad \text{Equation 1.4}$$

Here,  $N$  is simply a normalisation constant. The  $\chi_1, \chi_2, \dots, \chi_M$  represent the  $M$  spin orbitals (which include both spin and spatial components). The  $x_1, x_2, \dots, x_J$  represent the  $J$  electrons ( $J=2M$ ). What this means is that  $J$  electrons are placed into  $J/2$  molecular orbitals, so that if two electrons are in the same orbitals than they must have opposite spin. Hartree-Fock theory assumes that each electron belongs in a specific orbital. It can be computationally expensive to use hydrogenic atomic orbitals, so instead the molecular orbitals are linear combinations of Gaussian functions. The term basis set refers to the specific set of Gaussian functions used to approximate the orbitals. A problem can arise when the electronic structure is best described by more than one Slater determinant because there is more than one configuration of electrons what would suit the structure. Limitations of only using a single Slater determinant will be discussed in Section 1.5.3.

Another assumption of standard (restricted) HF theory is that the molecules are all closed-shell, *ie.* all orbitals are doubly occupied. While this is fine in many cases, it breaks down in open shell species or when there are an odd number of electrons, for instance in ions, radicals, and biradicals. There are two variants of HF that can be used in these cases. In restricted open-shell HF (ROHF), all orbitals are considered to be doubly occupied except for the orbitals of interest (*ie.* the singly occupied orbitals in biradicals). In unrestricted HF (UHF), all electrons are considered to occupy their own orbitals.<sup>30</sup> This allows for the consideration of open shell systems, but can cause spin contamination by higher multiplicity states (eg. triplets and quartets contaminating singlets and doublets respectively).

The exact form of the wavefunction is not known, but is approximated at the beginning of the calculation. At each step in the calculation, that approximation is refined so that the energy of the system decreases. This is in accordance with the variational principle which says that the result of the HF calculation will be an overestimate of the true energy of the system, so that the lowest calculated energy will be the most accurate.<sup>29</sup> The iterative process is carried out until the numerical wavefunction converges to the desired tolerance. This is the best wavefunction for the system and can be used to calculate properties such as energy, enthalpy, vibrational frequencies, etc.

As stated above, a major problem with HF methods is the omission of electron correlation. Electron correlation comes in dynamical and nondynamical varieties<sup>31</sup>. Dynamical correlation relates to the fact that all of the electrons are moving rather than

static. An approximation of HF is when calculating the energy of one electron, to treat the remaining (N-1) electrons as an average field rather than discrete moving particles. This can be improved by using perturbative methods as described in Section 1.5.2. Nondynamical electron correlation occurs when there are multiple electronic configurations needed to fully describe the system. Methods like HF or perturbative methods are not able to accurately describe this. Instead, multireference methods must be used and these will be described in Section 1.5.3.

### 1.5.2 Post-HF Methods for Dynamical Electron Correlation

As stated above, ignoring electron correlation reduces the accuracy of HF methods. Dynamical electron correlation can be included in the calculation through the use of perturbative methods such as Moeller-Plesset theory (MP)<sup>32</sup> configuration interaction (CI) methods<sup>33</sup>, or coupled cluster (CC) theory<sup>34</sup>.

MP perturbation theory begins with the HF wavefunction and Hamiltonian, which is termed the zeroth order Hamiltonian. It then applies an nth order perturbation to the standard Hamiltonian. (Equation 1.5) where  $H_0$  is the HF Hamiltonian,  $V$  is the perturbation, and  $\lambda$  is a number that can be optimised. The MP wavefunction and energy can be expressed as a power series of any arbitrary order (Equations 1.6 – 1.7). Brillouin's theorem<sup>35</sup> says that a first order perturbation will not actually change the energy, but the levels of theory containing up to second, third, and fourth order perturbations are commonly used in quantum chemistry (called MP2, MP3, and MP4).

$$\hat{H} = \hat{H}_0 + \lambda V \quad \text{Equation 1.5}$$

$$\Psi = \Psi_0 + \lambda \Psi_1 + \lambda^2 \Psi_2 + \dots \quad \text{Equation 1.6}$$

$$E = E_0 + \lambda E_1 + \lambda^2 E_2 + \dots \quad \text{Equation 1.7}$$

CI theory begins with the Slater determinant from HF theory. Recall that the Slater determinant assigns each electron to a specific orbital. The orbitals are chosen according to the Aufbau principle, meaning that low energy orbitals are fully filled before moving onto higher energy orbitals. CI theory allows for electronic excitations in the calculation of the energy. For instance, the ground state of lithium is  $1s^2 2s^1$ . A single excitation might be  $1s^1 2s^2$  or  $1s^2 2p^1$ . A double excitation might be  $1s^1 2s^1 2p^1$ . Full CI includes all possible excitations, but is prohibitively expensive. CI is often truncated to second order, CISD or CID.

CC theory shares characteristics with both CI and MP theories. Once again, the starting point is the HF wavefunction. A cluster operator,  $T$  is formulated that applies up to  $n$ th order excitations (Equations 1.8 – 1.10) where  $\Phi_0$  is the Slater determinant and  $T_n$  is applies the  $n$ th order excitation. The power series for the new Hamiltonian is truncated at the desired level. This truncation affects both A) the number of terms that comprise the cluster operator that are used, and B) the power to which those terms are raised. That means that second order CC theory would include all combinations of  $T_1$  and  $T_2$  where each of those terms can be raised to the second power. The optimal coefficients for each of those terms are then found which will yield the optimised Hamiltonian and wavefunction. Whilst this seems similar to CI, a major difference is that CC is size-extensive, *ie.* the energy of 2 particles infinitely separated is equal to the sum of the energies calculated individually. Common CC methods use second, third, or fourth order excitations (CCSD, CCSDT, CCSDTQ). A more cost effective approach use second order excitations, and then simulates the third order excitations perturbatively (CCSD(T)). CCSD(T) is one of the highest levels of theory used for small-medium sized molecules.

$$\Psi = e^T \Phi_0 \quad \text{Equation 1.8}$$

$$e^T = \sum \sum T_1^n T_2^m \dots \quad \text{Equation 1.9}$$

$$T = T_1 + T_2 + \dots + T_n \quad \text{Equation 1.10}$$

MP, CI, and CC theories are all based on a single Slater determinant which is then perturbed in some manner. This approach is good for dealing with dynamical electron correlation. However, the approaches do not account for nondynamical electron correlation.

### 1.5.3 Post-HF Methods – Multireference Methods

While the methods of Section 1.5.2 are useful for dealing with dynamical electron correlation, they do not help with nondynamical electron correlation. This is especially important for singlet biradicals and TSs that contain partially broken bonds. Consider the molecular orbitals of an arbitrary singlet biradical (Figure 1.13).<sup>36</sup> In most cases, the semi-occupied molecular orbitals (SOMOs) will be the highest energy occupied orbitals and will have similar energies (the right orbital is meant to have a slightly higher energy than the left orbital in the diagram). By the definition of a singlet biradical, the unpaired electrons will have different spins. There will be four potential

configurations. At face value, it might appear that the first and last configurations correspond to a zwitterionic structure and are unimportant. However, these are molecular orbitals, not atomic orbitals. Even though both electrons in the first configuration are in the same MO, that MO is still a combination of AOs from both radical centres. The first configuration corresponds to both electrons spending equal amounts of time on both radical centres. The electrons act independently of each other, but will tend to spend time near opposite nuclei. This configuration will be primarily “biradical” in nature, but with some “zwitterionic” character. Of the two middle cases, one correspond to the *triplet* state (the triplet state where  $S=0$  as opposed to  $S = +1$  or  $-1$ ) and the other corresponds to a singlet state that is primarily “zwitterionic” in character. The last configuration is the reverse of the first configuration. It corresponds primarily to “zwitterionic” character, albeit with some “biradical” character. The specific chemical environment will determine how much “zwitterionic” and “biradical” character the biradical has. For symmetry reasons, RHF includes the first and fourth configurations equally, even if the zwitterionic configuration should not contribute substantially. For molecules of low symmetry, the second and third configurations can also contribute. The resulting combination of configurations is unlikely to simply be a small perturbation of the first state (*i.e.* an equal mixture of biradical and zwitterionic configurations). For this reason, the perturbative methods of the previous section (MP, CC, CI) will not describe singlet biradicals correctly.

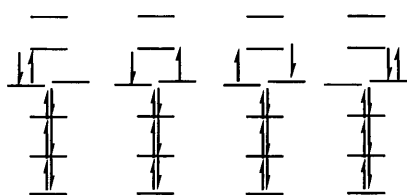


**Figure 1.13:** Two electronic configurations for a singlet biradical

A similar effect happens in bond breaking (and is thus important for nearly all TS calculations). This is shown in Figure 1.14. Consider the breakage of the bond between X-X. This can occur either homolytically to yield two X radicals, or heterolytically to yield  $X^+ + X^-$ . For most organic systems in the gas phase, the former is preferred. But as before, there are actually four configurations to consider. They will correspond to a similar mix of “ionic” and “covalent” states. All states would need to be considered in order to accurately describe the dissociation.

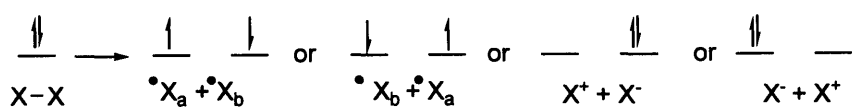


**Figure 1.14:** Electronic configurations for bond cleavage

This can be solved by using multireference methods, such as CASSCF<sup>37</sup>. Again starting with the HF wavefunction, some or all of the M electrons and N orbitals are put into an active space. Inside the active space, every possible configuration of the electrons being distributed into the orbitals is considered.<sup>38</sup> The molecular orbitals for these configurations are optimised and their energies are calculated. Contrast this to methods in section 1.5.2 where the same molecular orbitals are used for all of the excited states. It can be seen that this approach will take into account all of the important configurations in Figures 1.13 or 1.14. This approach is very expensive though, so the active space is chosen to be as small as possible, whilst still including all sources of the nondynamical electron correlation. CASSCF is one of the few methods that deals well with nondynamical electron correlation. However, it is also one of the most expensive.

There exist perturbative multi-reference methods such as CASPT2 that combine the multireference nature of this section with the perturbative approach of the previous section.<sup>39</sup> While even more expensive, this allows both dynamical and nondynamical electron correlation to be included in the calculation.

#### 1.5.4 Density Functional Methods (DFT)

DFT is currently the most commonly used method for doing electronic structure calculations on organic molecules. A detailed review of DFT is beyond the scope of this thesis. DFT presents an alternative method for doing electronic structure calculations. All of the previous methods involve numerically solving for the wavefunction ( $\Psi$ ). This has no physical meaning, however, the square of the wavefunction<sup>40</sup> represents the probability density function for the electrons. A function is a process that converts a number into a number. An example might be  $f(x)=x^2$ . A functional is a process that converts a function into a number. An example of this might be  $f[g\{x\}] = \int_0^1 g(x)dx$  where the function  $g(x)$  is converted into a number. In DFT, the density functional converts the wavefunction (the function) into electron density (the number). An exact form of this density would give an exact solution to the Schrödinger

equation, equivalent to knowing the exact wavefunction in HF theory. Unfortunately according to the Kohn-Hohenberg theorems, the exact form of this density is not known and can not be determined exactly<sup>41</sup>. Instead approximations to the density are used. The most common of these is called the local density approximation (LDA).<sup>42</sup> Within the LDA approximation are two functionals that describe electronic interactions, the exchange functional and the correlational functional.<sup>22</sup> There are many combinations of exchange and correlation functionals which are popular in modern computational chemistry. One common one is BLYP<sup>43</sup> which includes the exchange functional of Becke and the correlation functional of Lee, Yang, and Parr. Another popular approach is the use of hybrid methods. These combine standard DFT exchange and correlation functionals with HF energies and can often give better results, usually due to fortuitous error cancellation. The general syntax is “AXB”, where A represents the exchange functional, B represents the correlation functional, and X represents how much HF energy is mixed in. Some common hybrid functionals include B3LYP<sup>44</sup>, O3LYP<sup>45</sup>, PBE1PBE<sup>46</sup>, and MPW1PW91<sup>47</sup> amongst many others.

At this point, DFT might seem too good to be true. It is not much more computationally expensive than HF, but it claims to give results as nearly good as more expensive methods such as CASSCF and MP2. Even though DFT includes electron correlation, DFT is not necessarily valid for multireference systems. However, DFT does tend to give good experimental results for many systems. The debate over multireference systems such as singlet biradicals tends to be between “It works” and “But it shouldn’t”. Cremer has recently shown that DFT should be able to accurately describe most singlet biradicals<sup>48</sup>.

### 1.5.5 Molecular Dynamics (MD)

All of the previously mentioned methods calculate molecular properties that are time-independent. These include properties such as enthalpies, vibrational frequencies, and geometries. Chemists are interested not just in properties of systems, but in how those systems behave over time. In particular, for the examples mentioned in sections 1.4.1 – 1.4.4, it was crucial for the computational simulations to show evidence that nonstatistical effects were occurring. Molecular dynamics represents a way to watch systems evolve over time<sup>49</sup>. Essentially, the system is started with an initial potential energy (which is calculated quantum mechanically from the initial geometry) and kinetic energy (either given for each atom, or for each vibrational mode). Newton’s

Laws of Motion are then solved based on the quantum mechanical potential energy surface and a new set of potential and kinetic energies are found. The particular approach of mixing quantum mechanics and classical physics is called Born-Oppenheimer Molecular Dynamics (BOMD).<sup>49</sup>

There are some caveats to BOMD. Firstly, the system is closed. That means that things such as solvent collisions and intermolecular interactions are ignored. Secondly, and more importantly, at the beginning of the calculation some quanta of vibrational energy are assigned to each vibrational mode in addition to zero-point energy (ZPE). But as the system evolves and energy passes between modes, there is the potential for certain modes to wind up with less than their ZPE. This is not compatible with quantum mechanics and trajectories that have reached this stage are no longer valid. The approximate timescale for this vibrational leakage is 1 ps. In contrast, the step size for a small molecule is roughly 0.5 fs, so this allows the dynamics to be run for a long time, just as long as the dynamical simulation is not excessively long and the system is checked to make sure vibrational leakage has not occurred.

## 1.6 Summary and Project Goals

While conventional kinetics theories such as RRKM and TST have worked well for most chemistry so far, they are based on assumptions such as rapid IVR that are not always obeyed. In the cases described above, the breakdown of assumptions leads to unexpected and unintuitive results. The results can include reactions breaking symmetry, ultrafast reactions, and ultraslow reactions. As the field of nonstatistical dynamics is still growing, it is important to understand the phenomenon better. What types of reactions lend themselves to nonstatistical effects? How will they change our understanding of these commonly used kinetics theories? This project will seek to answer these questions by investigating two main systems.

The first system is a singlet biradical that will be discussed in Chapter 2 – 3. Work investigated whether the biradical reacted faster than RRKM/TST theories predicted, a sign of nonstatistical dynamics described in Sections 1.4.1 – 1.4.3. Computational work was done to study the time and isotope dependence of the biradical to determine what vibrational modes remained coupled to each other in the chemistry, in contrast with the rapid IVR assumption in conventional theories.

The second system involves the formation and reaction of cyclopentadiene that will be discussed in Chapter 4 – 5. It was hypothesised that cyclopentadiene can be

formed in a “hot” state where the vibrational energy is not statistically distributed. If there was again mode coupling between the cyclopentadiene formation and consumption reactions, this would lead to symmetry breaking (Section 1.4.1). Isotopic labelling was used to see if the symmetrical intermediates involved were able to retain a “memory” of what precursors they were made from, so as to have formed an asymmetrical product distribution that violated the predictions of conventional kinetics theories.

### 1.7 References for Chapter 1

1. For a discussion of kinetic theories, see (for example) Houston, P. L. *Chemical Kinetics and Reaction Dynamics.*, McGraw Hill: London., 2001.
2. (a) Rice, O. K.; Ramsperger, H. C. *J. Am. Chem. Soc.* **1927**, *49*, 1617 – 1629. (b) Rice, O. K.; Ramsperger, H. C. *J. Am. Chem. Soc.* **1928**, *50*, 617 – 620. (c) Kassel, L. S. *Chem. Rev.* **1932**, *10*, 11 – 25. (d) Marcus, R. A.; Rice, O. K. *J. Phys. Colloid Chem.* **1951**, *55*, 894 – 908..
3. Eyring, H. *J. Chem. Phys.* **1935**, *3*, 107 – 115.
4. Stannard, P. R.; Gelbart, W. M. *J. Phys. Chem.*, **1981**, *85(24)*, 3592 – 3599.
5. This first order decay of nonstatistical vibrational energy can be compared with other kinetics that do not deal with chemical reactivity, such as nuclear spin relaxation in NMR.
6. Rynbrandt, J. D.; Rabinovitch, B. S. *J. Phys. Chem.* **1971**, *75*, 2164 – 2175.
7. (a) Decomposition of  $\text{H}_3^+$ : Berblinger, M.; Schlier, C. *J. Chem. Phys.* **1994**, *101*, 4750 – 4758. (b) Decomposition of  $\text{HeI}_2$ : Davis, M. J.; Gray, S. K. *J. Chem. Phys.* **1986**, *84*, 5389 – 5411. (c) Behaviour of carbonyl sulfide ( $\text{O}=\text{C}=\text{S}$ ): Gibson, L. L.; Schatz, G. C.; Ratner, M. A.; Davis, M. J. *J. Chem. Phys.* **1987**, *86*, 3263 – 3272. (d) Isomerisation of hydrogen cyanide to isocyanide: Waalkens, H.; Burbanks, A.; Wiggins, S. *J. Chem. Phys.* **2004**, *121*, 6207 – 6225.
8. In this way, the set of normal modes acts as a basis set for the vector space of molecular motions. In linear algebra, any combination of basis sets spans the associated vector space. For instance, the unit coordinate vectors (0,1) and (1,0) span two dimensional Cartesian space.

9. (a) For experimental work, see: Gilbert, T.; Grebner, T. L.; Fischer, I.; Chen, P. *J. Chem. Phys.* **1999**, *110*, 5485 – 5488. (b) For computational work, see: Bach, A.; Hostettler, J. M.; Chen, P. *J. Chem. Phys.* **2005**, *123*, 021101 – 021104.
10. Reyes, M. B.; Carpenter, B. K. *J. Am. Chem. Soc.* **2000**, *122*, 10163 – 10176.
11. Ussing, B. R.; Singleton, D. A. *J. Am. Chem. Soc.* **2005**, *127*, 2888 – 2899..
12. Nummela, J. A.; Carpenter, B. K. *J. Am. Chem. Soc.* **2002**, *124*, 8512 – 8513.
13. (a) For experimental work, see: McLafferty, F. W.; McAdoo, D. J.; Smith, J. S.; Kornfeld, R. J. *J. Am. Chem. Soc.* **1971**, *93*, 3720-3730. (b) For computational work, see reference 12.
14. (a) For experimental work, see: Roth, M. W.; Martin, M. *Justus Liebigs Ann. Chem.* **1967**, *702*, 1 – 7. (b) Baldwin, J. E.; Ollerenshaw, J. *J. Org. Chem.* **1981**, *46*, 2116 – 2119 and references therein. (c) For computational work, see reference 10.
15. (a) For experimental work, see: Baldwin, J. E.; Villarica, K. A.; Freedberg, D. I.; Anet, F. A. L. *J. Am. Chem. Soc.* **1994**, *116*, 10845 – 10846. (b) For computational work, see: Doubleday, C.; Li, G.; Hase, W. L. *Phys. Chem. Chem. Phys.* **2002**, *4*, 304 – 312.
16. (a) Carpenter, B. K. *Annu. Rev. Phys. Chem.* **2004**, *56*, 57 – 89. (b) Carpenter, B. K. *J. Phys. Org. Chem.* **2003**, *16*, 858 – 868.
17. Depke, G.; Lifshitz, C.; Schwarz, H.; Tzidony, E. *Angew. Chem. Int. Ed. Eng.* **1981**, *20*, 792 – 793.
18. In general,  $^{12}\text{C}/^{13}\text{C}$  isotope effects are significantly smaller than even secondary H/D isotope effects. For an exception to this, see: de Petris, G.; Troiani, A. *J. Phys. Chem. A* **2008**, *112*, 2507 – 2510. However, an isotope effect this large is not expected for the acetone system.
19. Osterheld, H. T.; Brauman, J. L. *J. Am. Chem. Soc.* **1993**, *115*, 10311 – 10315.
20. Graph taken with permission from reference 12.
21. Woodward, R. B.; Hoffmann, R. *Conservation of Orbital Symmetry*; Academic Press, Inc., **1970**.
22. For a more complete discussion of computational chemistry, see Cramer, C. J. *Essentials of Computational Chemistry*. John Wiley and Sons, Ltd: West Sussex, England., 2003.
23. (a) Hartree, D. R.; Hartree, W. *Proc. Roy. Soc.* **1935**. (b) Fock, V. *Z. Physik* **1930**, *61*, 126 – 148. (c) Slater, J.C. *Phys. Rev.* **1930**, *35*, 210 – 211 and also reference 22 for more information.

24. Schrödinger, E. *Phys. Rev.* **1926**, *28*, 1049 – 1070 and reference 22 for more information.
25. There are specific conditions for when it is possible to solve equations involving three bodies. For larger systems, there is no theorem about when a solution exists. In general, systems with more than three bodies must be solved numerically.
26. (a) Born, M.; Oppenheimer, R., *Annalen der Physik* **1927**, *84*, 457 - 484 (b) Eckart, C. *Phys. Rev.*, **1935**, *46*, 383 – 387.
27. Slater, J. C. *Phys. Rev.* **1929**, *34*, 1293 – 1322 and reference 22 for more information.
28. The use of the word determinant comes from linear algebra, where it is an operation performed on square matrices. While it is not important exactly how the determinant of a matrix is found (there are many algorithms), it gives a very useful mnemonic for construction a wavefunction. Slater determinants are used to guarantee that the wavefunction obtained is antisymmetric with respect to interchanging two electrons, in accordance with the Pauli principle.
29. The variational principle can be proved as being equivalent to the Schrödinger equation. For the original proof, see: Eckert, C. E. *Phys. Rev.* **1930**, *36*, 878 – 892. For a more easily understood explanation of the proof, see: Pilar, F. P. *Elementary Quantum Chemistry*. McGraw Hill Publishing Company: New York, 1990.
30. (a) Roothaan, C. C. J. *Rev. Mod. Phys.* **1951**, *23*, 69 – 89. (b) Pople, J. A.; Nesbet, R. K. *J. Chem. Phys.* **1954**, *22*, 571 – 572.
31. Lowdin, P-O. *Phys. Rev.* **1955**, *97*, 1509 – 1520 and reference 22 for more information.
32. (a) Moller, C.; Plesset, M. S. *Phys. Rev.* **1934**, *46*, 618 – 622. Second order perturbations are often used (MP2): (b) Head-Gordon, M.; Pople, J. A.; Frisch, M. J. *Chem. Phys. Lett.* **1988**, *153*, 503 – 506.
33. Nesbet, R. K. *Proc. Royal. Soc. London Ser. A* **1955**, *230*, 312 – 321 and reference 22 for more information.
34. (a) Bartlett, R. J.; Purvis, J. D., III. *Int. J. Quantum Chem.* **1978**, *14*, 561 – 581. Oftentimes, single and double excitations are performed explicitly and triple excitations iteratively (CCSD(T)): (b) Pople, J. A.; Head-Gordon, M.; Raghavachari, K. *J. Chem. Phys.*, **1987**, *87*, 5968 – 5975.
35. Hegarty, D.; Robb, M. A. *Mol. Phys.* **1979**, *38*, 1795 – 1812. and reference 22 for more information.

36. Salem, L; Rowland, C. *Angew. Chem. Int. Ed.* **1972**, *11*, 92 – 111.
37. For M electrons and N orbitals and distinguishing between  $\alpha$  and  $\beta$  spin, there are:
- $$C(2N, M) = \frac{2N!}{M!(2N - M)!}$$
- configurations. This will clearly grow intractable very quickly. In practice, the best supercomputers can handle roughly (12,12) active spaces.
38. Parr, R. G.; Yang, W. *Ann. Rev. Phys. Chem.* **1995**, *46*, 701 -728.
39. Andersson, K.; Malmqvist, P.-A.; Roos, B. O.; Sadlej, A. J.; Wolinski, K. *J. Chem. Phys.* **1990**, *94*, 5483 – 5488.22
40. Technically, it is not the square of the wavefunction. Since the wavefunction can be complex, that is of the form  $ai + b$  where  $i$  is the square root of -1, the density is the wavefunction times its complex conjugate, which is guaranteed to be real.
41. (a) Hohenberg, P.; Kohn, W. *Phys. Rev.* **1964**, *136*, 864 – 871. (b) Kohn, W.; Sham, L. J. *Phys. Rev.* **1965**, *140*, 1133 – 1138.
42. For a description of LDA and other DFT information, see Parr, R. G.; Yang, W. *Density-Functional Theory of Atoms and Molecules*. Oxford University Press: Oxford, 1994.
43. Becke exchange: (a) Becke, A. D. *Phys. Rev. A* **1988**, *38*, 3098 – 3100. Lee, Yang, and Parr correlation: (b) Lee, C.; Yang, W.; Parr, R. G. *Phys. Rev. B* **1988**, *37*, 785 – 789.
44. Becke exchange, Lee, Yang, and Parr correlation (reference 40). Hybridisation: Becke, A. D. *J. Chem. Phys.* **1993**, *98*, 5648 – 5652.
45. Cohen, A. J.; Handy, N. C. *Mol. Phys.* **2001**, *99*, 607 – 615.
46. Perdew, Burke, and Ernzerhof exchange and correlation: (a) Perdew, J. P.; Burke, K.; Ernzerhof, M. *Phys. Rev. Lett.* **1996**, *77*, 3865 – 3868. Hybridisation: (b) Adamo, C.; Barone, V. *J. Chem. Phys.* **1999**, *110*, 6158 – 6169.
47. Perdew, Wang exchange and correlation: (a) Perdew, J. P.; Chevary, J. A.; Vosko, S. H.; Jackson, K. A.; Pederson, M. D.; Singh, D. J.; Fiolhais, C. *Phys. Rev. B* **1992**, *46*, 6671 – 6687. (b) Perdew, J. P.; Wang, Y. *Phys. Rev. B* **1992**, *45*, 13244 – 13249. Hybridisation: (c) Adamo, C.; Barone, V. *J. Chem. Phys.* **1998**, *108*, 664 – 675.
48. Cremer, D. *Mol. Phys.* **2001**, *99*, 1899-1940.
49. Bolton, K.; Hase, W. L.; Peslherbe, G. H. *Modern Methods for Multidimensional Dynamics Computation in Chemistry*, Ed. Thompson, D. L., World Scientific, Singapore, **1998**, 143.

## CHAPTER 2

# NONSTATISTICAL EFFECTS IN SINGLET BIRADICALS

### 2.1 Introduction to Chapter 2

This chapter gives an overview of the singlet biradical project. It starts by explaining the underlying concepts of clock reactions, singlet biradicals, and the reactivity of singlet biradicals. Two examples of ultrafast radical reactions that are related to the proposed work are described. An earlier unsuccessful attempt to connect this biradical chemistry to nonstatistical dynamics is presented. Finally, the design of a revised biradical system is given and the computational and experimental results and discussion follow. Experimental details are in Chapter 3; computational details are in the appendix.

### 2.2 Pressure, Nonstatistical Dynamics, and Supercritical Fluids

One of the ways in which nonstatistical dynamics can be detected is by looking for a product variance as a function of pressure. According to the statistical approximation, IVR is fast relative to any subsequent chemistry. That implies that small changes to the exact rate of IVR would not change the fact that IVR is still happening rapidly relative to the other chemistry. Hence, this would not be experimentally observable. However, if IVR is happening competitively with two or more pathways, small changes to IVR could have an impact on the exact favourability of each pathway, which would change the exact product distribution that would form. This would in principle be experimentally observable.

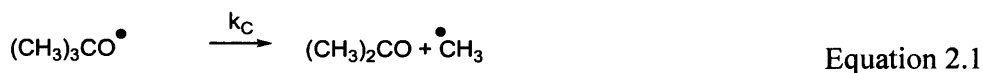
One of the factors that can cause the rate of IVR to change is the number of intermolecular collisions. Even though it is intramolecular, IVR can be mediated through molecular collisions, *e.g.* with solvent molecules. The more collisions that occur, the faster IVR occurs.<sup>1</sup> In solution phase, the rate of molecular collisions cannot be changed much, but in the gas phase the number of molecular collisions is a direct function of pressure, which can be easily changed. When the pressure is raised, there are more collisions. In fact, pressure can be defined by the number of collisions of the gas particles with the walls of the container per unit time. Additionally, the collision rate must be sufficiently high to trap short-lived intermediates such as biradicals. If the rate constant for the reaction of interest is  $\sim 10^{12} \text{ s}^{-1}$ , (as with the clock and oxidation reactions described in Sections 2.3 and 2.4) then it is necessary to have a solvent

collision frequency of more than that, at least  $10^{13} \text{ s}^{-1}$ . Supercritical fluids offer a compromise between gas phase and solution phase. Supercritical fluids offer similar solubilising properties to liquid solvents, have collisional frequencies on par with liquid solvents, but can have their pressure varied as with gases to tune the absolute collisional frequency. Section 2.5 will describe how supercritical fluids could be used to test for nonstatistical dynamics in a particular singlet biradical.

### 2.3 Clock Reactions

One of the most important pieces of information about a chemical reaction is its rate. Unfortunately, the rate constants of some elementary reactions cannot be directly measured, especially if they occur after the rate-determining step in a complex sequence. One solution is to measure the relative rate constants of such steps against other reactions with known absolute rate constants. From there, the absolute rate constants of the desired reactions can be found. The reference reactions with known rate constants are often called clock reactions<sup>2</sup> and those involving a radical rearrangement are termed radical clock reactions. It is important to use a clock reaction that occurs on roughly the same timescale as the reaction being studied so that the products of both reactions can be detected in comparable amounts.

An example of a radical clock involves *tert*-butoxy radical; it can be used to determine the relative rate constants of hydrogen-atom abstraction reactions.<sup>2</sup> The relevant chemical reactions and kinetics are shown by equations 2.1 – 2.3. The only measurements required are the initial concentration of the organic substrate RH ( $[RH]_i$ ), and the final ratio of acetone to *tert*-butanol products ( $[(CH_3)_2CO]_f$  and  $[(CH_3)_3COH]_f$  respectively). Because the rate constant for methyl loss from the *tert*-butoxy radical is known, these measurements give the absolute value for  $k_R$ .



$$\frac{k_R}{k_C} = \frac{[(CH_3)_3COH]_f}{[RH]_i [(CH_3)_2CO]_f} \quad \text{Equation 2.3}$$

Amongst the most widely used radical clocks are derivatives of cyclopropylcarbinyl radicals, shown in Figure 2.1. These radicals (11) can open the cyclopropane ring, forming alkenes (12). Newcomb determined the absolute ring-opening rates as follows.<sup>3</sup> Relative rate constants were determined by trapping both

radicals **11** and **12** with freshly prepared benzenselenol at various temperatures. The relative rate constants at each temperature were then combined with the known absolute rate constant for H abstraction from benzenselenol at the same temperature, yielding an absolute rate constant for the ring-opening. Fitting the combined data to an Arrhenius plot ( $\log k$  vs.  $1/T$ ) gave the Arrhenius A factor and activation energy for each radical, which could be used to determine the absolute rate constant for the ring-opening at any desired temperature. These rate constants at 25 °C are given below the structures.

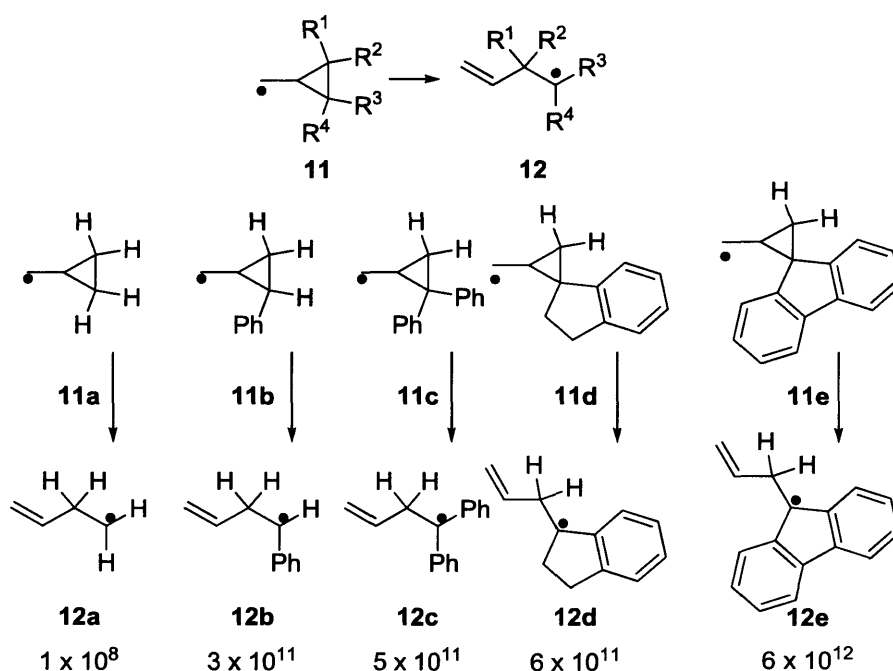


**Figure 2.1.** Radical clock ring-opening reaction (rate constants in  $s^{-1}$  at 25 °C)

#### 2.4 Cytochrome P450 – An Example of the Use of Ultrafast Clock Reactions

Cytochrome P450 is a family of enzymes found in all living organisms.<sup>4</sup> An important function of Cytochrome P450 is to detoxify the cell by monooxygenating compounds. The enzyme is able to oxygenate many types of C-H bond, even those which are not very reactive. The enzyme contains an iron atom in the middle of a porphyrin cofactor which is critical to this chemistry. The mechanism of Cytochrome P450 has been well studied.<sup>5</sup> The complete mechanism is beyond the scope of this work<sup>6b</sup>, but the two primary steps (Figure 2.2) are believed to be H-abstraction from the substrate to form an iron-hydroxy complex, followed by oxygen donation from the iron to the substrate radical to form the product alcohol. The latter step is often called the “rebound” because the radical recombines with the iron complex to give the alcohol product.

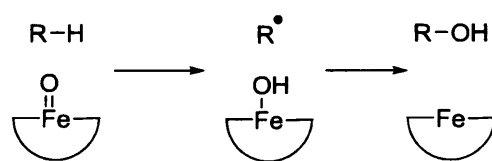


**Figure 2.2.** Mechanism for Cytochrome P450. The semicircle represents the porphyrin.

Because the rate of the rebound step of the reaction could not be measured directly, it was probed using radical clocks. Figure 2.3 shows the reaction scheme for the radical clocks. A C-H bond in cyclopropane **13** is broken to form cyclopropylmethyl radical **11**, which can ring-open to form radical **12**. Either of radicals **11** and **12** can be oxidised to yield alcohols **14** and **15** respectively. Given the known rate of ring-opening from radical **11** to radical **12**, the rates of the oxidation step can be determined. The rate constants<sup>6</sup>,  $k_{ox}$  are given below the appropriate structures in  $s^{-1}$ . The ring-opening rate constants,  $k_{clock}$  were determined in earlier work<sup>3</sup> and are given below  $k_{ox}$ , which was determined through the use of Equation 2.4.

$$\frac{k_{ox}}{k_{clock}} = \frac{[14]}{[15]} \quad \text{Equation 2.4}$$

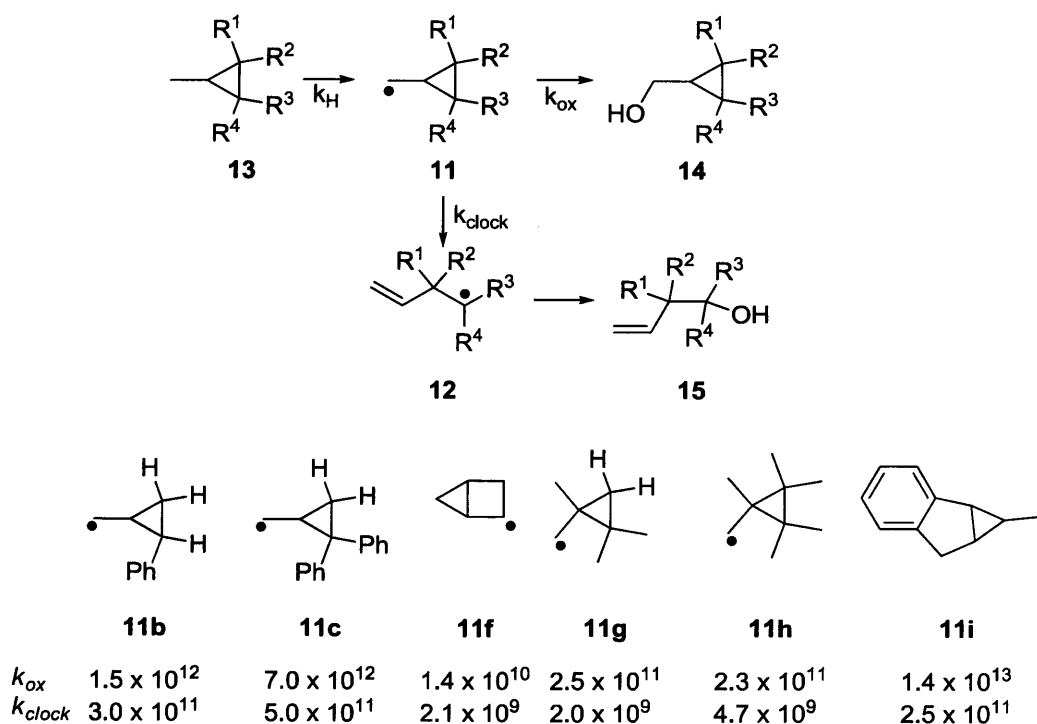


**Figure 2.3.** Kinetics of the cyclopropane ring-opening

There are two striking results from this kinetic data. Firstly, there is a very wide range in  $k_{ox}$ . And secondly, radical **11i** oxidises faster than the Eyring equation allows (see section 1.2), which would require a negative activation Gibbs energy. While some range in  $k_{ox}$  would be expected, it does not seem obvious what would cause **11b** – **11i** to have such different oxidation rates as the radical is not in conjugation with the aromatic system in **11b** – **11i**. A possible explanation is that the enzyme active site serves to force radical **11** into a specific conformation. There may be unfavourable steric interactions for some of the radicals which could change  $k_{ox}$  considerably relative to a small molecule like **11f**. This explanation would not resolve the matter of how radical **11i** could ring-open faster than the Eyring equation allows. This is only a factor of two larger than the Eyring limit and could possibly be an experimental error. It is also possible that the mechanism for Cytochrome P450 oxidation is incorrect and the extremely fast rate was a consequence of utilising the wrong clock. For instance, if the enzymatic reaction involves ions rather than radicals, a radical clock would not be correct to use. Further work by Newcomb<sup>7</sup> suggested that there are both radical and cation intermediates in the oxidation with separate mechanisms, but the rate of the radical oxidation was indeed  $10^{13} \text{ s}^{-1}$ . Further work by Shaik<sup>8</sup> casts doubt on this. His computational work at the valence bond level of theory suggested that in addition to the ground state radical and cation intermediates, there were higher-multiplicity radical intermediates. For instance, while the ground state of a radical is a doublet state, the Cytochrome P450 system also involved quartet radicals that were lower in energy than the corresponding doublets.

There is another possible explanation. If the ring-opening clock reaction itself shows nonstatistical effects, the actual ring-opening rate may differ from the literature value. Depending on the cause of the nonstatistical effects, observed rate constants can either be larger or smaller than predicted with conventional theories.<sup>9a</sup> If the nonstatistical behaviour is due to a phase-space bottleneck, the rate constant will be smaller than predicted. This is what happens with the ethyl radical (Section 1.4.4). If, however, the effect arises from strong normal mode coupling, the result can be an increase in the apparent rate constant for reaction of a reactive intermediate. Such mode coupling was seen for the reactions described in Chapter 1, and this work proposes that it may be occurring for the clock system as well. If  $k_{clock}$  is higher than predicted, the calculated value for  $k_{ox}$  will be too large as well; in the case of **11i** this was above the Eyring limit. IVR has been observed to occur on a timescale of picoseconds. This

suggests that in general, reactions that have rate constants above approximately  $10^{12} \text{ s}^{-1}$  are candidates for nonstatistical behaviour. This would include the oxidation reaction, and perhaps the clock reaction as well.<sup>9b</sup> Additionally, Carpenter<sup>10</sup> has proposed that certain enzymes might have evolved to take advantage of this nonstatistical behaviour. This is not to say that enzymes have any knowledge of what reactions might show nonstatistical behaviour; just that nonstatistical dynamics allows an opportunity for natural selection to choose enzymes best suited to exploit these ultrafast reactions. If nonstatistical effects are occurring in the radical clock reaction, there would be no reason to expect the radical clocks to give meaningful results for the oxidation reaction, nor in fact even to expect the reactions to obey the rate limit imposed by the Eyring equation.

## 2.5 A Singlet Biradical to Test for Nonstatistical Effects

In most of the examples in Chapter 1, nonstatistical effects were detected using isotopically labelled compounds to probe for symmetry-breaking. This symmetry is not present for compounds such as **11i**. Rather, the dynamics must be probed more directly. In order to test for nonstatistical effects in radicals such as **11**, there must be other reactions that can compete with the ring-opening. As the ring-opening is near the Eyring limit, the competing reaction must also be extremely fast.

Radicals are compounds with a single unpaired electron. As the name suggests, biradicals have two unpaired electrons. The unpaired electrons in biradicals normally occupy orbitals that have very similar energies and can either have parallel or antiparallel spins.<sup>11</sup> In the former case, the compound is a triplet biradical, in the latter a singlet biradical. While there is a wide variety of chemistry available to triplet biradicals<sup>12</sup>, this work will focus on singlet biradicals.

One of the reactions available to biradicals is the Norrish Type II reaction<sup>13</sup>, shown in Figure 2.3. Biradical **17** is formed photochemically by  $\gamma$ -H abstraction of an excited ketone **16**. This biradical can then either ring-close to form cyclobutanol **18** or fragment to form alkene **19** and the acetone enol **2**. Because of the high energy of the singlet biradical and the low barrier to bond formation, the Norrish II reaction is often very rapid. As will be seen later, a 1,4-singlet biradical where one of the radicals is cyclopropylmethyl might show both ring-opening and Norrish Type II reactivity.

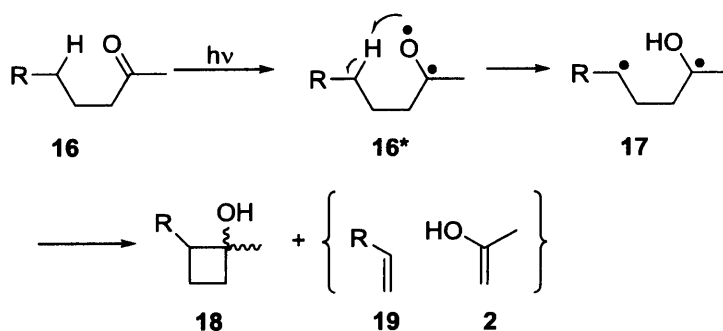


**Figure 2.4.** Norrish Type II Reaction

To test for nonstatistical behaviour, work by previous Carpenter group member Dave Broyles synthesised biradical precursor **20**.<sup>14</sup> Ketone **20** reacts to form biradical **21** upon irradiation which is capable of Norrish type II reactions to form cyclised product **22** and fragmented product **23**. Biradical **21** is also capable of undergoing the clock-type cyclopropyl ring-opening to give biradical **24** which can itself react to give stable products **25** and **26**. The scheme is shown in Figure 2.5.

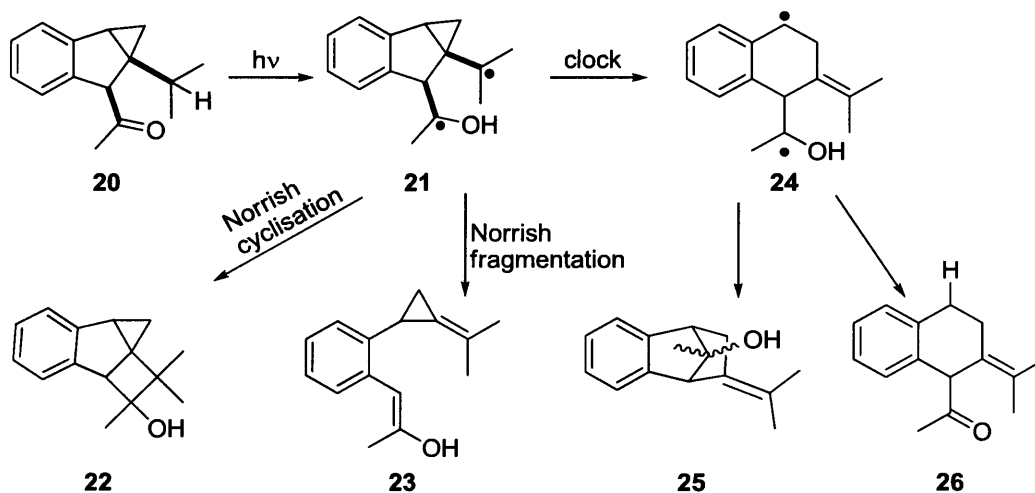


**Figure 2.5.** Potential reactivity of singlet biradical **21**

Nonstatistical effects were searched for in the previous biradical system as follows. At least one of the Norrish products (**22** or **23**) and one of the clock products (**25** or **26**) would need to be formed. If the behaviour were statistical, then no amount of molecular collisions could affect the subsequent rates of reaction and the ratio of Norrish : clock =  $[\mathbf{22}] + [\mathbf{23}] : [\mathbf{25}] + [\mathbf{26}]$  would be constant. But if IVR were occurring competitively with the clock reaction<sup>15</sup> the product distribution could be changed by changing the supercritical fluid pressure. The exact product ratio would depend on the exact amount of IVR that had occurred, which itself would depend on factors including

the pressure.<sup>16</sup> There may also be factors due to the volumes of activation, but these are likely to be small relative to the changes in the rate of IVR. Unfortunately for biradical **21**, as shown in Figure 2.6, the photolysis provided only Norrish Type II products **22** and **23** (the latter of which rapidly decomposed), and Norrish Type I products **27**, **28**, and **29**. Neither of the clock products **25** and **26** was formed. It was postulated that one of the methyl groups of **21** faced a steric repulsion with one of the phenyl hydrogen atoms. This favoured a geometry where the cyclisation to **22** was still essentially barrierless, but the clock reaction to **24** was no longer feasible. Unfortunately, all attempts to get biradical **21** to undergo the ring-opening were unsuccessful. Without either clock product **24** or **25** being formed, the supercritical fluid work would not have yielded any information about nonstatistical behaviour.

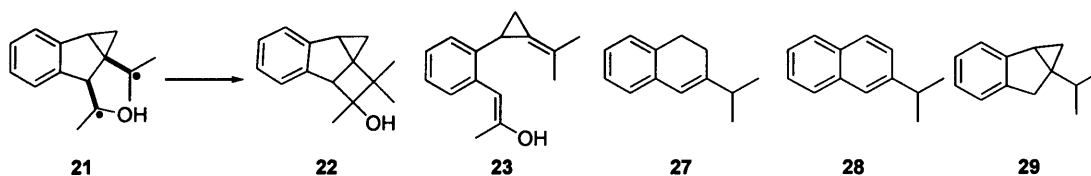


**Figure 2.6.** Actual products formed by biradical **21**

## 2.6 Revised Biradical System

To overcome the slow clock reaction seen in biradical **21**, new biradicals **31** and **37** were devised, as shown in Figure 2.7. Similarly to biradical **21**, **31** and **37** are made from ketone precursors (**30** and **36**) and can undergo Norrish cyclisation and fragmentation as well as clock ring-opening, followed by H-abstraction. Additionally, the geometry of the biradical allows for good orbital overlap between the cyclopropylmethyl radical and the neighbouring cyclopropyl bond (Figure 2.8). It was hoped that this would allow the clock reaction to take place competitively with the standard Norrish reactions. Because of the large rate enhancement for radicals when an additional phenyl group is introduced (Figure 2.1), the clock rate could be tuned if it was too fast or too slow. The goal would be to see clock product **35/41** and at least one of the Norrish products **33/39** or **34/40**. In addition to the synthetic work towards biradicals **31** and **37**, there was also a computational study of how nonstatistical effects could be seen in the biradical system.

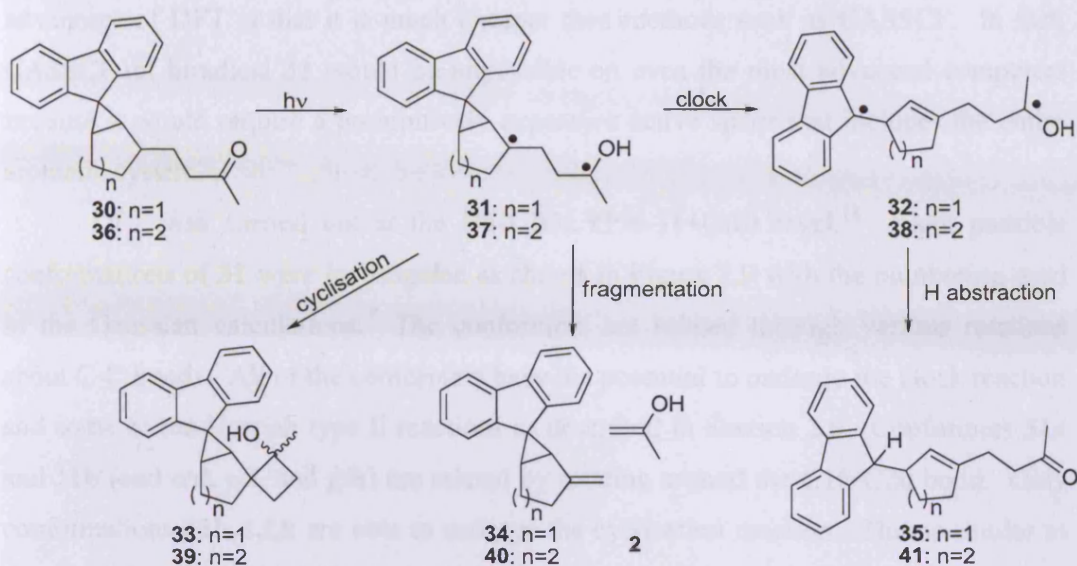


Figure 2.7. Revised biradicals and their reactivity

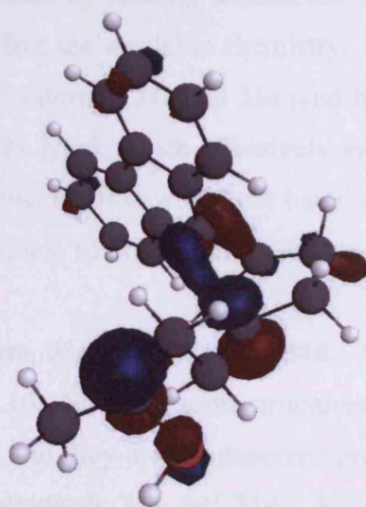


Figure 2.8. Orbital overlap in biradical 31. Both the cyclopropane bonding orbital and biradical orbitals are shown.

## 2.7 DFT Benchmarks and Calculations

### 2.7.1 Computational Studies on Biradical 31

As stated in Section 1.5.3, singlet biradicals **31** and **37** are likely to have significant multireference character. As such, methods such as HF, MP2, and CCSD are unlikely to accurately describe them. According to Cremer, broken-symmetry unrestricted density functional theory, BS-UDFT, is able to describe these systems even though it does not explicitly take into account multireference effects.<sup>17</sup> A large

advantage of DFT is that it is much cheaper than methods such as CASSCF. In fact, CASSCF on biradical **31** would be impossible on even the most advanced computers because it would require a prohibitively expensive active space that includes the entire aromatic system.

DFT was carried out at the BS-UB3LYP/6-31+G(d) level.<sup>18</sup> Eight possible conformations of **31** were investigated as shown in Figure 2.9 with the numbering used in the Gaussian calculations. The conformers are related through various rotations about C-C bonds. All of the conformers have the potential to undergo the clock reaction and some of the Norrish type II reactions as described in Section 2.6. Conformers **31a** and **31b** (and **c/d**, **e/f**, and **g/h**) are related by rotating around the C19-C20 bond. Only conformations **31b,d,f,h** are able to undergo the cyclisation reaction. This is similar to the reactivity of tetramethylene which exists in cisoid and transoid conformations. Only the cisoid conformer is able to ring-close to cyclobutane.<sup>19</sup> Conformers **31a** and **31c** (and **b/d**, **e/g**, and **f/h**) are related by rotating around the C18-C19 bond. While this rotation would not seem to affect the available chemistry, steric clashes could change their relative favourabilities. Conformer **31a** and **31e** (and **b/f**, **c/g**, and **d/h**) are related by rotating around the C20-C21 bond, which effectively switches the OH and methyl groups. It was assumed that this rotation would not have a large effect on the relative energetics of the various reactions, so conformers generated by this rotation were not considered.

That left four conformers, **31a**, **31b**, **31c**, and **31d**. The overall scheme of their reactivity is shown in Figure 2.10. Note that some structures relating to conformers **31c** and **31d** are omitted for space, but they are the expected products and transition states that would be formed from biradicals **31c** and **31d**. Relative enthalpies and Gibbs energies for the biradicals, products, and transition states are given in Table 2.1. Activation enthalpies are shown in bold.

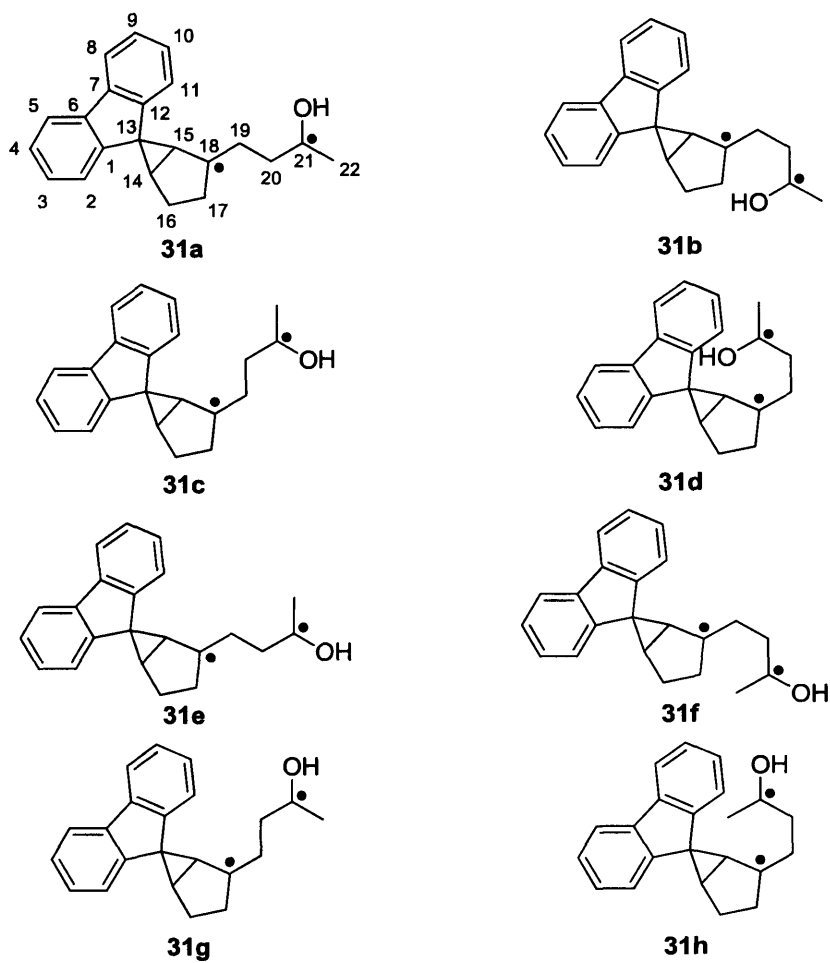


**Figure 2.9.** Biradical conformations (numbering as used in the calculations)

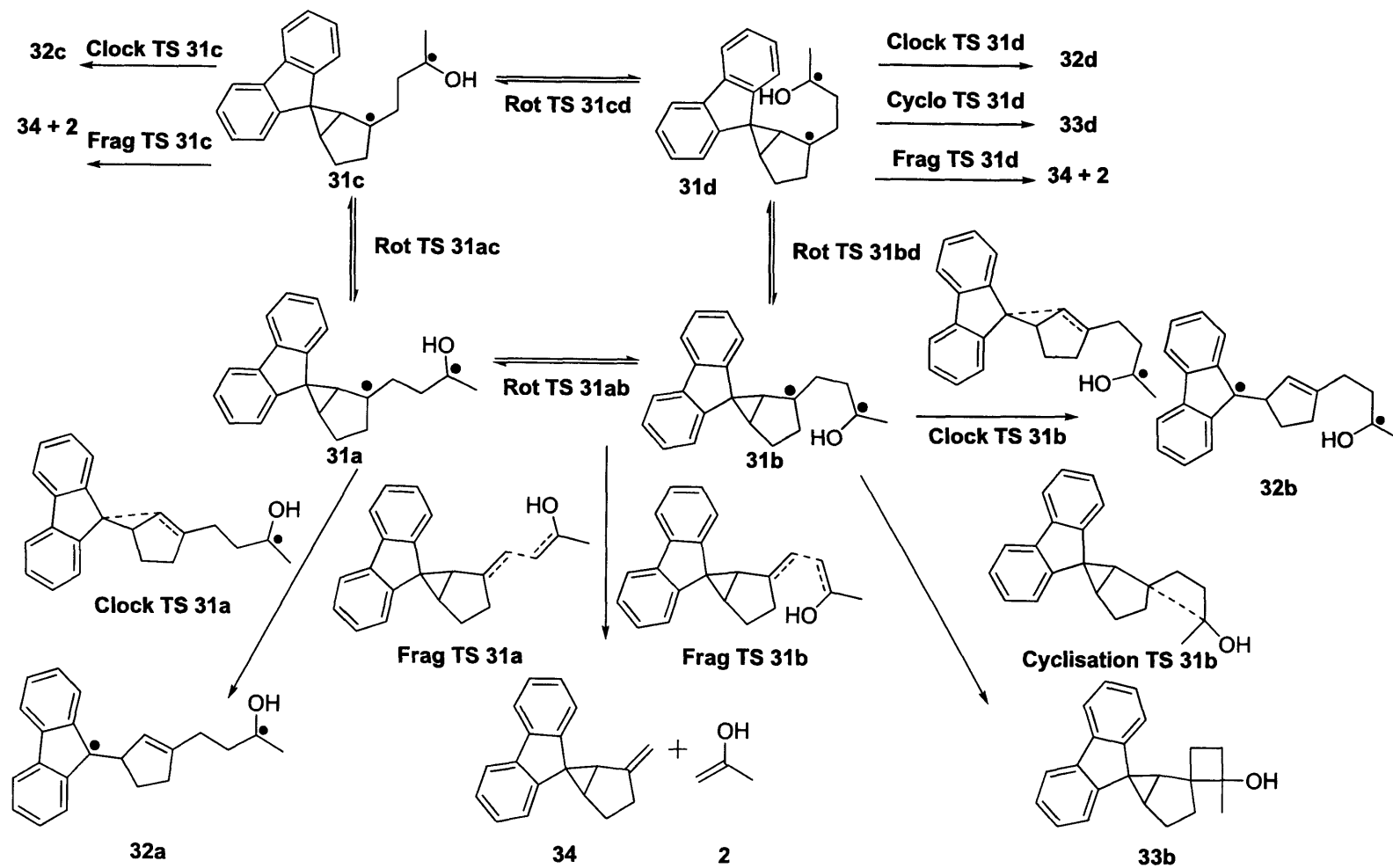


Figure 2.10. Reactions of biradical 31

<i>Compound</i>	<i>Relative enthalpy (kJ mol<sup>-1</sup>)</i>	<i>Relative Gibbs energy (kJ mol<sup>-1</sup>)</i>	<i>Relative enthalpy (kJ mol<sup>-1</sup>)<sup>a,b</sup></i>
<b>Biradical 31a</b>	[0]	[0]	-
<b>Clock TS 31a</b>	12	10	<b>12</b>
<b>Clock Prod 32a</b>	-89	-94	-89
<b>Frag TS 31a</b>	4	6	<b>4</b>
<b>Frag Prod 34 + 2</b>	-141	-188	-141
<b>Rot TS 31ab</b>	19	12	<b>19/8<sup>c</sup></b>
<b>Rot TS 31ac</b>	Not Found	Not Found	N/A
<b>Biradical 31b</b>	11	12	-
<b>Clock TS 31b</b>	11	13	<b>0</b>
<b>Clock Prod 32b</b>	-85	-89	-96
<b>Cycl. TS 31b</b>	Not Found	Not Found	N/A
<b>Cycl Prod 33b</b>	-164	-147	-180
<b>Frag TS 31b</b>	16	17	<b>5</b>
<b>Frag Prod 34 + 2</b>	-141	-188	-152
<b>Rot TS 31bd</b>	Not Found	Not Found	N/A
<b>Biradical 31c</b>	13	9	-
<b>Clock TS 31c</b>	11	11	<b>-2<sup>21</sup></b>
<b>Clock Prod 32c</b>	-90	-94	-103
<b>Frag TS 31c</b>	Not Found	Not Found	N/A
<b>Frag Prod 34 + 2</b>	-141	-188	-154
<b>Rot TS 31cd</b>	20	25	<b>7/8<sup>c</sup></b>
<b>Biradical 31d</b>	12	11	-
<b>Clock TS 31d</b>	11	12	<b>-1<sup>21</sup></b>
<b>Clock Prod 32d</b>	-88	-92	-100
<b>Cycl. TS 31d</b>	Not Found	Not Found	N/A
<b>Cycl Prod 33d</b>	-160	-144	-172
<b>Frag TS 31d</b>	Not Found	Not Found	N/A
<b>Frag Prod 34 + 2</b>	-141	-188	-153

<sup>a</sup>: Enthalpies are relative to their parent biradical

<sup>b</sup>: Activation enthalpies are bolded

<sup>c</sup>: For rotational TSs, activation enthalpies from both biradicals are given

**Table 2.1.** Relative energies of the compounds in Figure 2.10.

In general, errors in DFT energies are likely to be  $\sim 5\text{--}10\text{ kJ mol}^{-1}$ , though this number cannot be given with any precision. No transition states could be found for the cyclisation reaction, and that reaction is predicted to be essentially barrierless. This is similar to the experimental result found for the previous biradical<sup>14</sup> where the main reaction product was from the Norrish type II cyclisation reaction and none of the clock ring-opening was detected. Transition states for some of the rotations could also not be found, but presumably, the barriers to all of the rotations are similar, and in fact they are quite comparable to known rotations around hydrocarbon C-C bonds which tend to be around  $15\text{ kJ mol}^{-1}$ . While conformation **31a** is the lowest in energy, because the biradical is being formed kinetically, there is no guarantee that biradical **31a** will be the conformation formed.<sup>22</sup> It is also possible that all four conformations will equilibrate on the same timescale that the clock and Norrish reactions are occurring. However, the clock reaction appears competitive with the Norrish reactions for all of the biradical conformations. If the DFT results are valid, this suggests that biradical **31** is a valid target to test for nonstatistical effects. In the biradical conformers, the cyclopropane C-C bond that would open in the clock reaction had an average bond length of  $1.60\text{ \AA}$ , and the C-C bond that breaks in the fragmentation had an average length of  $1.55\text{ \AA}$ . In the clock TSs, the average length for the cyclopropane C-C bond was  $1.70\text{ \AA}$ . In the fragmentation TSs, the average length for the fragmenting C-C bond was  $1.80\text{ \AA}$ .

While the DFT results implied that both the Norrish and clock reactions would occur, the question of the validity of using DFT on a singlet biradical remained. To test how well the DFT method captured nondynamical electron correlation, CASSCF was tried next. Because of the computational cost of CASSCF, the system was simplified to **42**. Unfortunately, the ring-opening TS could not be found for **42** at DFT level, so instead an approximate structure for the TS was estimated for the CASSCF single-point calculations. Also, only one conformation was calculated, corresponding to **31a** for computational ease, with the assumption that all conformations would behave similarly. A (10,9) active space was chosen to include the major orbitals involved with the clock reaction. This included the two cyclopentadiene  $\pi$ -bonds and antibonds, the radical singly occupied orbitals, the oxygen p-type lone pair, and either the cyclopropane  $\sigma$  bond that breaks or the

cyclopentene  $\pi$  bond that forms and the corresponding antibond. The orbitals involved in the active space are highlighted in red in Figure 2.11. This was done at both CASSCF and RS2<sup>23</sup> levels (RS2 is the version of MRMP2 implemented in Molpro, see section 1.5.3) as the latter would take into account both dynamical and non-dynamical electron correlation. The relative energies are given in Figure 2.11. Enthalpies for CASSCF and MRMP2 were estimated using the same approach as for MP2.

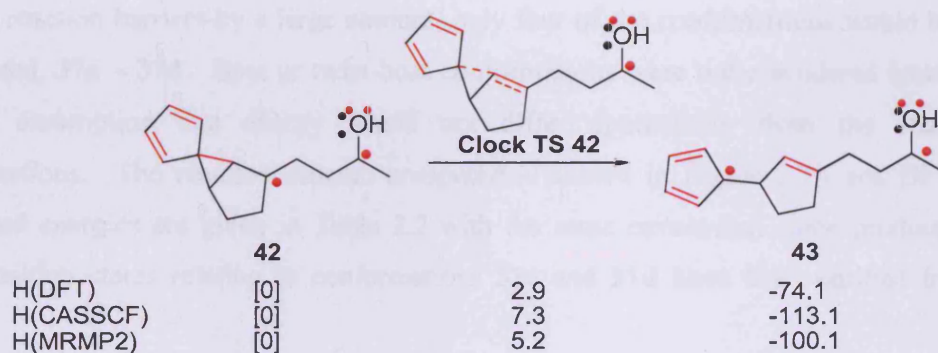


**Figure 2.11.** Multireference enthalpies for the clock reaction of **42** (in  $\text{kJ mol}^{-1}$ )

The CASSCF and MRMP2 results were in quite good agreement with each other and with DFT. If it was assumed that MRMP2 is more accurate than CASSCF and was essentially the “gold standard” for the system, then DFT errors were roughly  $2\text{--}3 \text{ kJ mol}^{-1}$  for the activation energy and about  $25 \text{ kJ mol}^{-1}$  for the (less important) reaction exothermicity. This suggested that DFT was able to describe the clock ring-opening for biradical **42** well. Additionally, since DFT could describe biradical **42** well, it should be able to describe biradicals **31** and **37** well. This was one of the core questions to be answered. Now that the DFT results were confirmed to be valid, the above conclusion was confirmed that the clock reaction should be competitive with the Norrish reactions.

### 2.7.2 Computational Studies on Biradical **37**

The computational results for biradical **31** were encouraging, suggesting that the clock reaction would be competitive. As biradical **37** was also a target, it was important to know if the clock reaction would also be competitive for it. As DFT had previously been shown to be an acceptable method for biradical **31**, the very intensive

MP2, CASSCF, or MRMP2 calculations would not have to be performed. In addition to the eight conformations that were seen for biradical **31**, there is now a question of the conformation of the cyclohexane ring in biradical **37**. It could either be in one of two ring-flip conformations. Figure 2.12 shows the conformers considered. The rotations are the same as in Figure 2.9 with the addition that conformers **37a** and **37i** (and the other seven pairs) are related by performing a ring-flip. It was decided that based on the results for **31** and the assumption that the ring-flip would not change the relative reaction barriers by a large amount, only four of the conformations would be considered, **37a** – **37d**. Boat or twist-boat conformations were not considered based on the assumption that energy would not differ appreciably from the chair conformations. The reaction scheme computed is shown in Figure 2.13 and DFT calculated energies are given in Table 2.2 with the same caveat that some products and transition states relating to conformations **31c** and **31d** have been omitted for space.

As with biradical **31**, biradical **37** shows the same general trends. All of the conformers are of similar energy and have similar reaction profiles. Most importantly, the clock reaction is predicted to have a very similar barrier as the Norrish reactions and the rotations. Overall, computational work predicted both biradicals **31** and **37** would be feasible targets to test for nonstatistical effects. As DFT on biradical **31** had already been benchmarked against multireference methods, there was no need to benchmark the results from biradical **37**.

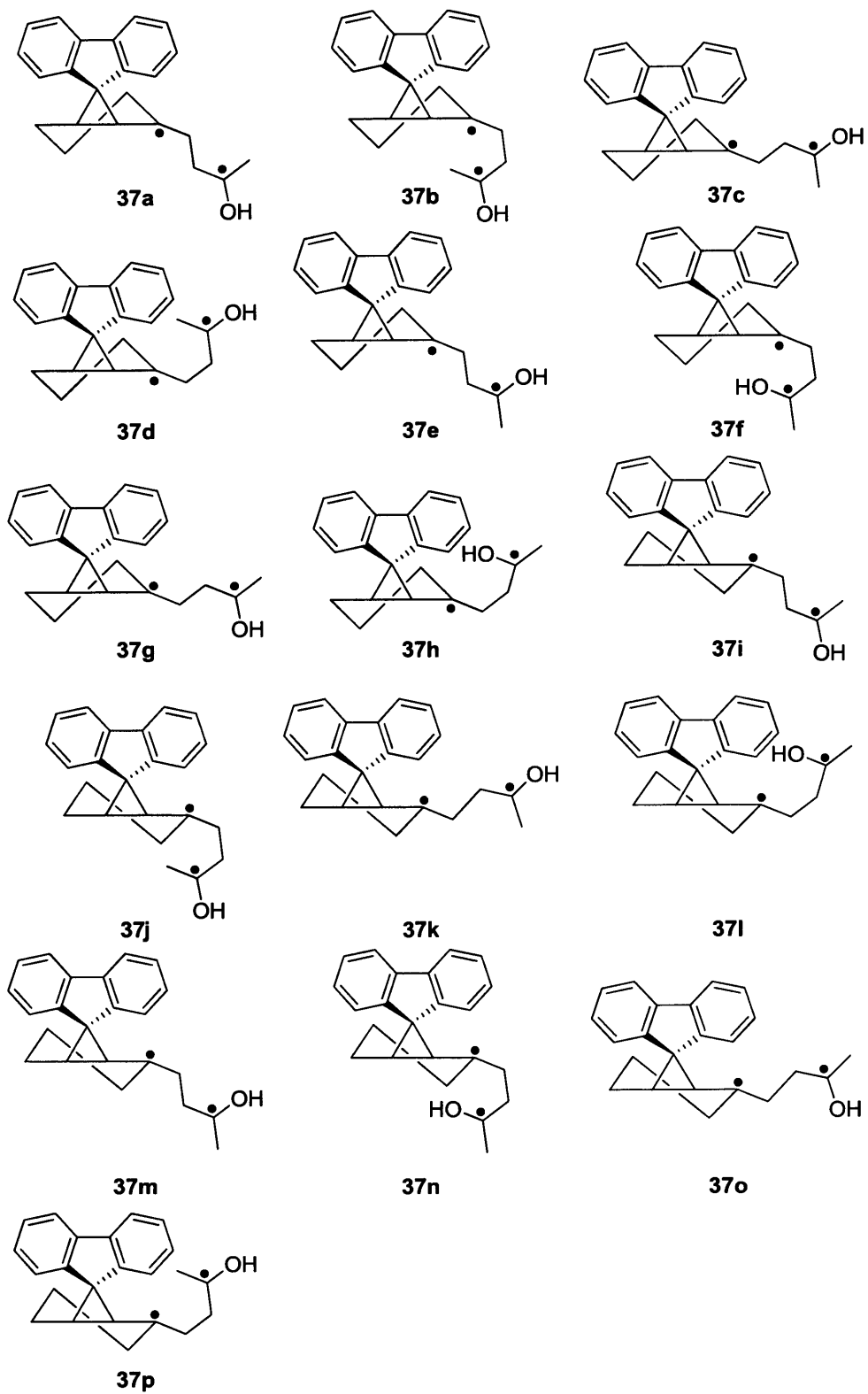


**Figure 2.12.** Conformations of Biradical 37

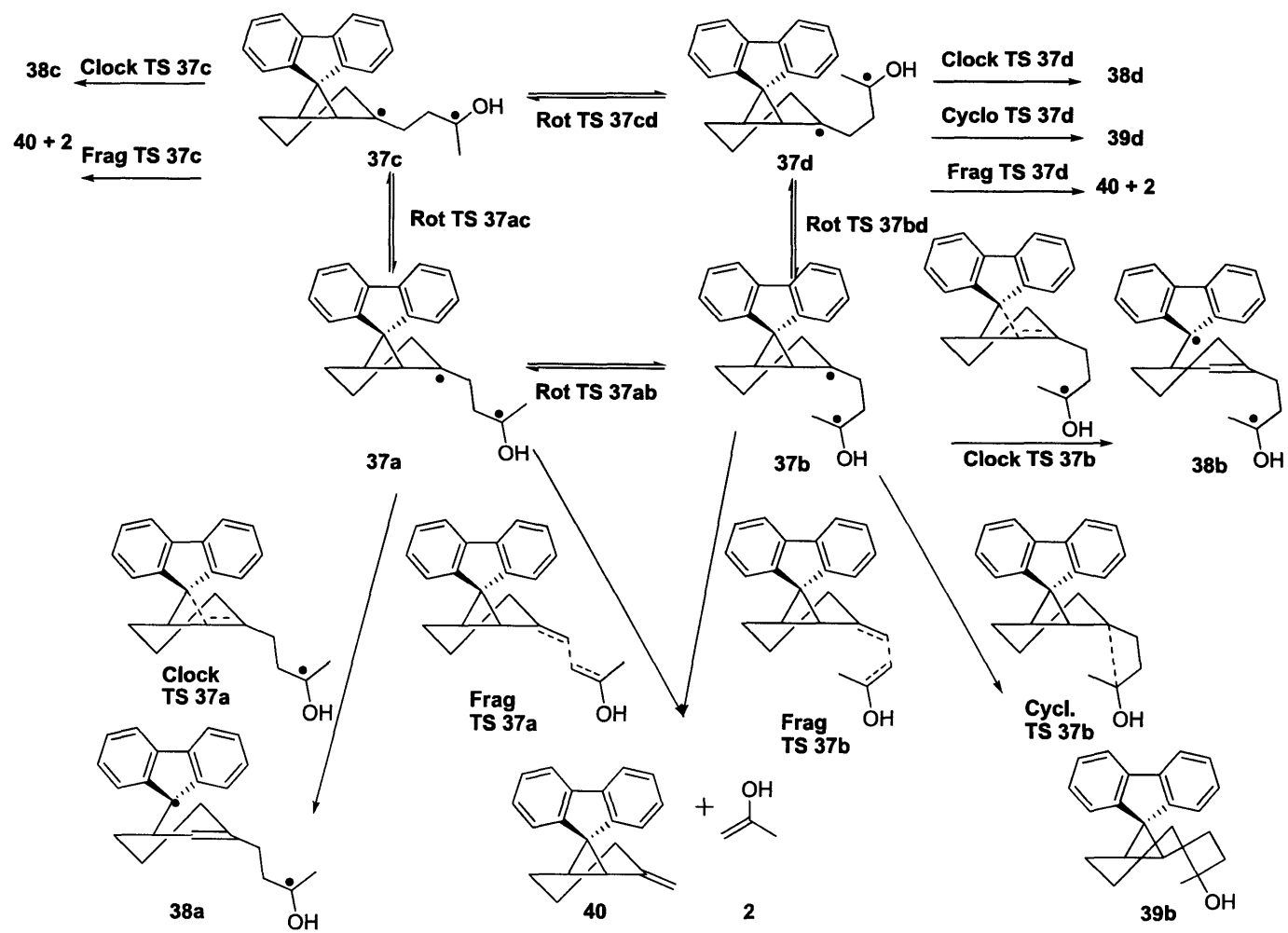


Figure 2.13. Reactions of Biradical 37

<i>Compound</i>	<i>Relative Enthalpy (kJ mol<sup>-1</sup>)</i>	<i>Relative Gibbs Energy (kJ mol<sup>-1</sup>)</i>	<i>Relative enthalpy (kJ mol<sup>-1</sup>)<sup>a</sup></i>
<b>Biradical 37a</b>	[0]	[0]	-
<b>Clock TS 37a</b>	0	1	<b>0</b> <sup>21</sup>
<b>Clock Prod 38a</b>	-101	-104	-101
<b>Frag TS 37a</b>	Not Found	Not Found	N/A
<b>Frag Prod 40 + 2</b>	-146	-194	-146
<b>Rot TS 37ab</b>	13	19	<b>13</b>
<b>Rot TS 37ac</b>	Not Found	Not Found	N/A
<b>Biradical 37b</b>	8	11	-
<b>Clock TS 37b</b>	11	13	<b>3</b>
<b>Clock Prod 38b</b>	-95	-94	-103
<b>Cycl. TS 37b</b>	Not Found	Not Found	N/A
<b>Cycl Prod 39b</b>	-159	-141	-167
<b>Frag TS 37b</b>	14	18	<b>6</b>
<b>Frag Prod 40 + 2</b>	-146	-194	-154
<b>Rot TS 37bd</b>	Not Found	Not Found	N/A
<b>Biradical 37c</b>	0	0	-
<b>Clock TS 37c</b>	0	0	<b>0</b> <sup>21</sup>
<b>Clock Prod 38c</b>	-101	-104	-101
<b>Frag TS 37c</b>	Not Found	Not Found	N/A
<b>Frag Prod 40 + 2</b>	-146	-194	-146
<b>Rot TS 37cd</b>	Not Found	Not Found	N/A
<b>Biradical 37d</b>	8	11	-
<b>Clock TS 37d</b>	11	13	<b>3</b>
<b>Clock Prod 38d</b>	-91	-91	-99
<b>Cycl. TS 37d</b>	Not Found	Not Found	N/A
<b>Cycl Prod 39d</b>	-137	-120	-145
<b>Frag TS 37d</b>	14	18	<b>6</b>
<b>Frag Prod 40 + 2</b>	-146	-194	-154

<sup>a</sup>: See footnotes for Table 2.1

**Table 2.2.** Relative energies of the compounds in Figure 2.13.

### 2.7.3 Molecular Dynamics

Molecular dynamics simulations were also used to probe the biradical system and yield more information about whether or not the dynamical product distribution was similar to that based on computed energies, *i.e.*, would both the clock and Norrish products be seen in the MD simulations? Nonstatistical effects would be harder to detect for the singlet biradical than for the various examples in Chapter 1 or the cyclopentadiene work described in Chapter 4, as there was no symmetry element present in the biradical that could be used to search for unexpected product ratios. Instead, evidence could be inferred if there appeared to be vibrational mode coupling between the reactions that form and consume biradicals **31** and **37**. Additionally, the rate of the clock and Norrish reactions seen in the MD simulations could be compared to an RRKM calculation to see if the MD reactions were happening faster or slower than expected by conventional kinetic theories.

Unfortunately, molecular dynamics calculations are very time intensive. For a system of this size, it could only be done on either a semiempirical method<sup>24</sup> or a small DFT method. Semiempirical methods probably do not account well for the nondynamical correlation present in a singlet biradical, and in general are not as well-regarded as DFT. Initially, DFT MD was performed on the smaller biradical **42**. The reactions would be analogous to those shown in Figures 2.7 and 2.10. Ideally, the molecular dynamics would start at the highest energy point on the reaction coordinate. This would correspond to the excited-state TS between biradical **42** and its excited ketone precursor. Because it would be difficult to find an excited-state TS, the next-best alternative was to find the conical intersection linking the ground-state and excited-state PESs containing biradical **42** and its ketone precursor. Depending on how the system behaved, it might explore all of the biradical conformations before it underwent the Norrish or clock reactions. Regardless of whether or not it did this, the MD would still provide valuable information about the behaviour of the system. Unfortunately, finding the conical intersection would have required a multireference method such as CASSCF, which would be too expensive to perform MD on. Instead, trajectories would be started from the four major biradical conformations shown in Figure 2.14. While this approach would not search for nonstatistical dynamics, it

would give some insight into the biradical system, such as checking that all of the expected products are indeed formed.

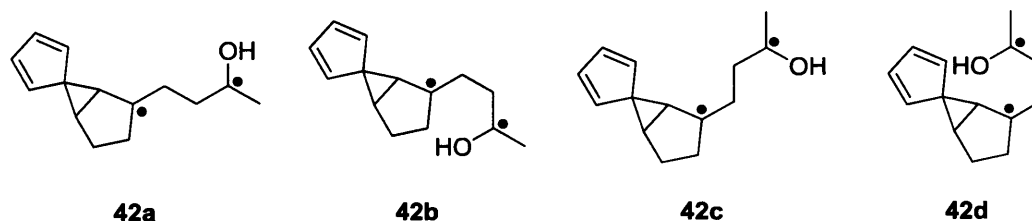


**Figure 2.14.** Conformations of biradical **42**

Attempts were made to optimise biradicals **42a-d** at several levels of theory, including UB3LYP/3-21G<sup>18</sup>, UO3LYP/3-21G<sup>25</sup>, UPBEPBE/3-21G<sup>26</sup>, UBLYP/3-21G<sup>18b,c</sup>, and UMPW1PW91/3-21G.<sup>27</sup> Of these, the only biradical conformer that could be located was **42b** and only for the UMPW1PW91 method. Additional problems arose because only the fragmentation and clock transition states could be located with this method, while the cyclisation and rotational transition states could not. This limited the reactivity that could be searched for. Luckily, at least one Norrish reaction, and the clock reaction transition state were found, so the MD could at least show if the clock and Norrish fragmentation reactions were competitive with each other. Dynamics trajectories were started from the fragmentation transition state, clock transition state, and biradical **42b**. Trajectories were run with initial kinetic energy selected by quasiclassical normal-mode sampling from a canonical ensemble at 300 K. The results of the trajectories are shown in Table 2.3.

The cyclisation and rotation reactions were not observed at all. It appeared that the biradical was not in a favourable conformation for cyclisation. It was unclear why rotation was not seen, but a plausible explanation was that the Norrish and clock reactivity were outcompeting the conformation interconversions. Rather than a dihedral of 0° (conformer **42b**) or 180° (conformer **42a**), the dihedral was closer to 40° for most of the trajectories. The relative amounts of fragmentation and clock product are interesting. Starting from either the biradical or clock TS, both products are formed in approximately equal amounts, but when the trajectories started from the fragmentation TS, the fragmentation is seen almost exclusively. This may be due to the division of potential energy. Some of the total energy is given in

potential energy, which is done by perturbing the starting structure. For a reaction with a very small or flat barrier, this geometrical perturbation may be sufficient to cross the barrier to the fragmentation reaction and form that product both rapidly and exclusively. In this case, the perturbation of the fragmentation transition state may have sufficiently lengthened the C–C bond to the point that the fragments could not recombine. The most important results are from the biradical. All of the trajectories showed a reaction, and the Norrish (fragmentation) and clock reactions were indeed competitive with each other.

<i>Starting Point</i>	<i>Direction<sup>a</sup></i>	<i>% Frag</i>	<i>%Clock</i>	<i>%Cyclo</i>	<i>%Rotation<sup>b</sup></i>
Biradical	Forward	47	53	0	0
Biradical	Reverse	46	54	0	0
Biradical	Overall	47	53	0	0
Frag. TS	Forward	100	0	0	0
Frag. TS	Reverse	85	15	0	0
Frag. TS	Overall	92	8	0	0
Clock TS	Forward	47	53	0	0
Clock TS	Reverse	40	60	0	0
Clock TS	Overall	43	57	0	0

<sup>a</sup>: When kinetic and potential energy are divided amongst the modes, this is done with an arbitrary sign convention corresponding to one of the two directions along the reaction coordinate. Forward from the fragmentation TS is toward the fragmentation products, forward from the clock TS is back toward the biradical, and forward from the biradical itself is not well defined. See the discussion in Section 4.5.2.1 for further information.

<sup>b</sup>: For purposes of this table, trajectories that rotated to a different biradical conformer are not counted as having undergone any other reactions.

**Table 2.3.** Summary of molecular dynamics on biradical **42b**

Further MD simulations were desired for biradicals **31** and **37**, rather than the simplified model **42**. Only biradical **31** was considered to save resources. While it was not feasible to find the excited-state TS between excited ketone **30** and biradical

**31**, the conical intersection could be found with a reduced (6,5) active space. The active space (starting from biradical **31**) contained the O p-type lone pair, the two radical SOMOs, and the O–H bonding and antibonding orbitals. This reduced active space omits the aromatic portion of the molecule, and the result is therefore invalid for considering the clock reaction. However, it is optimised for the hydrogen-abstraction from ketone **30** to biradical **31**. The located conical intersection appeared to be very similar to biradical **31** in structure and roughly 40 kJ mol<sup>-1</sup> higher in energy. One CASSCF MD trajectory was carried out from the conical intersection with no vibrational energy at all, not even ZPE. This would allow the intrinsic PES to be observed. This trajectory led directly to the biradical and eventually to the cyclisation product. Caution is advised with interpreting this result because only one trajectory was carried out and because of the choice in active space, the cyclisation reaction might be biased over the fragmentation or clock reactions (*vide infra*).

This single CASSCF trajectory took several weeks using a supercomputer cluster, so it would be impractical to carry out multiple CASSCF trajectories. Rather, a method of performing MD at the DFT level was desired. However, at any level other than this specific CASSCF, the conical intersection geometry would be a meaningless point on the PES. Rather, the single CASSCF trajectory passed through a biradical conformation *en route* to the cyclised product. While this particular biradical differed from conformations **31a-h** given in Figure 2.9 and could not be optimised as a singlet, it was instead optimised as a triplet. The assumption was made that the triplet and singlet states would have very similar geometries. This triplet geometry was then used as the starting point for the DFT MD trajectories on the singlet PES.

According to the CASSCF calculation, the conical intersection was approximately 40 kJ mol<sup>-1</sup> above the biradical. This corresponded to roughly one quantum of energy in the OH stretching mode, where nearly all of the energy produced by coming down from the conical intersection to the biradical was initially deposited. This energy appeared to redistribute very slowly to the remainder of the molecule, which suggested additional evidence for nonstatistical effects. At the triplet geometry, one quantum of energy was added in either the forward or reverse direction (one direction would push the system toward the starting material, while the other

direction would push the system toward products), and many trajectories were run on the singlet biradical. It should be noted that these trajectories were run with ZPE energy, in contrast to the CASSCF trajectory. It was not known which corresponded to moving toward the biradical, rather than the ketone, so both directions were chosen. After the trajectories were run, it became clear that “forward” meant toward the Norrish and clock products and “reverse” meant back toward the ketone. The trajectories were analysed based on what product was formed, either the fragmentation product, cyclisation product, clock ring-opening product, or a retro-Norrish reaction to form ketone **30**. Trajectories were run on both biradical **31** and **31-d** where the OH was replaced with OD. This would probe whether poor vibrational coupling between the OH (or OD) stretching modes and other vibrational modes explained the relatively slow IVR observed. This is similar to what Chen found with the ethyl radical (Section 1.4.4). These results are summarised in Table 2.4.

<i>Isotopomer</i>	<i>Direction</i>	<i>% Frag</i>	<i>%Clock</i>	<i>%Cyclo</i>	<i>%Retro Norrish</i>
H	Forward	6	43	0	51
H	Reverse	1	33	0	66
D	Forward	5	44	0	52
D	Reverse	1	29	0	70

**Table 2.4.** Results of the biradical MD trajectories

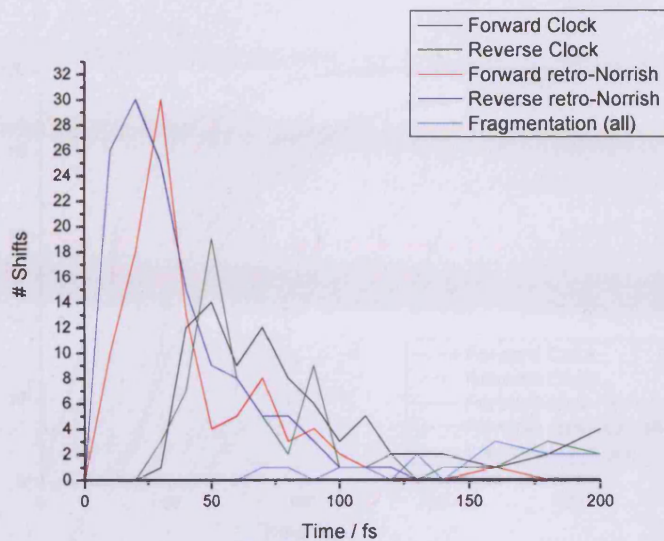
A statistical analysis to 95% confidence (Table 2.5) compared the various reactions and directions and suggested the following conclusions: First, there is essentially no difference between trajectories that assign energy in the forward and reverse directions. Second, there is not a significant difference between the H and D isotopomers or between the forward and reverse directions. It is not obvious why there was no difference seen for the H and D isotopomers.

From Graphs 2.1 – 2.6, there is a large difference between the timings of the clock, fragmentation, and retro-Norrish reactions. Graphs 2.1 – 2.3, respectively show the number of reactions as a function of time, the running selectivity as a function of time, and what portion of a specific reaction will have occurred by a given

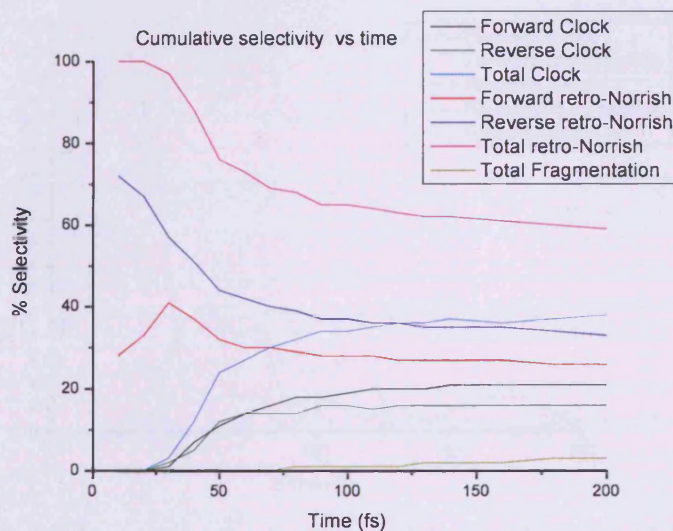
time. Graphs 2.4 – 2.6 show the same information for the D isotopomer. It is not surprising that the retro-Norrish, clock, and fragmentation reactions would behave differently.

<i>Variable 1</i>	<i>Variable 2</i>	<i>Statistical Test</i>	<i>Significance (%)</i>
<i>H</i> forward clock	<i>H</i> reverse clock	Student's t-test	87
<i>H</i> forward retro-Norrish	<i>H</i> reverse retro-Norrish	Student's t-test	94
<i>H</i> forward clock	<i>H</i> forward retro-Norrish	Student's t-test	<b>99.99</b>
<i>H</i> reverse clock	<i>H</i> reverse retro-Norrish	Student's t-test	<b>99.99</b>
<i>D</i> forward clock	<i>D</i> reverse clock	Student's t-test	83
<i>D</i> forward retro-Norrish	<i>D</i> reverse retro-Norrish	Student's t-test	<b>98</b>
<i>D</i> forward clock	<i>D</i> forward retro-Norrish	Student's t-test	<b>99.99</b>
<i>D</i> reverse clock	<i>D</i> reverse retro-Norrish	Student's t-test	<b>99.99</b>
<i>H</i> forward	<i>D</i> forward	Chi-squared	4
<i>H</i> reverse	<i>D</i> reverse	Chi-squared	77
<i>H</i> overall	<i>D</i> overall	Chi-squared	61

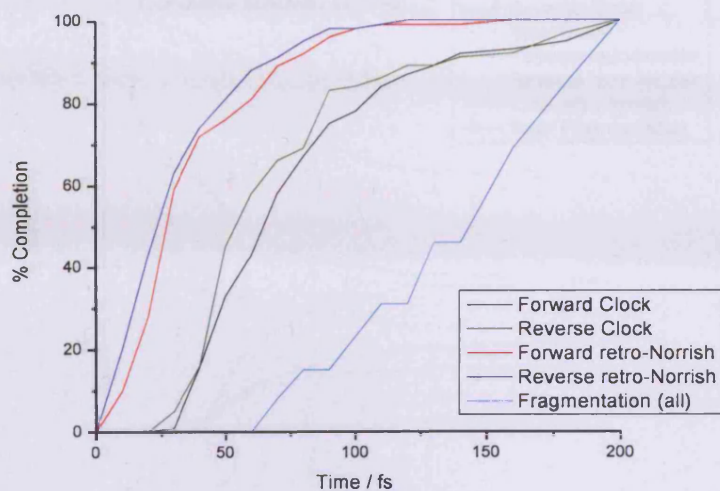
**Table 2.5.** Comparing the subsets of the MD trajectories. The differences between two populations are meaningful above 95% significance.



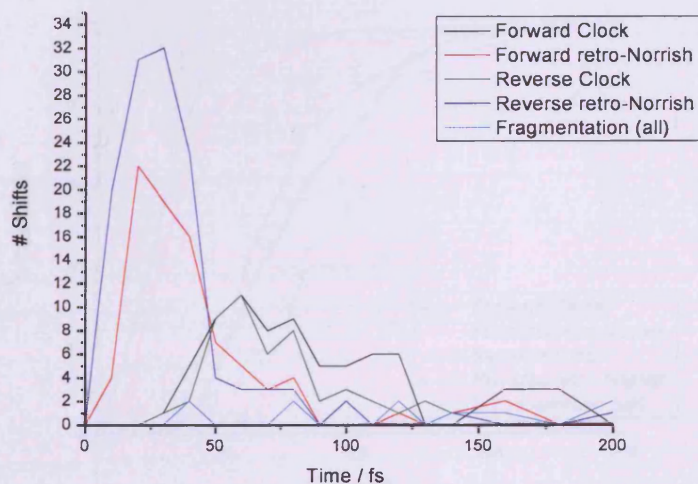
**Graph 2.1.** Number of reactions as a function of time



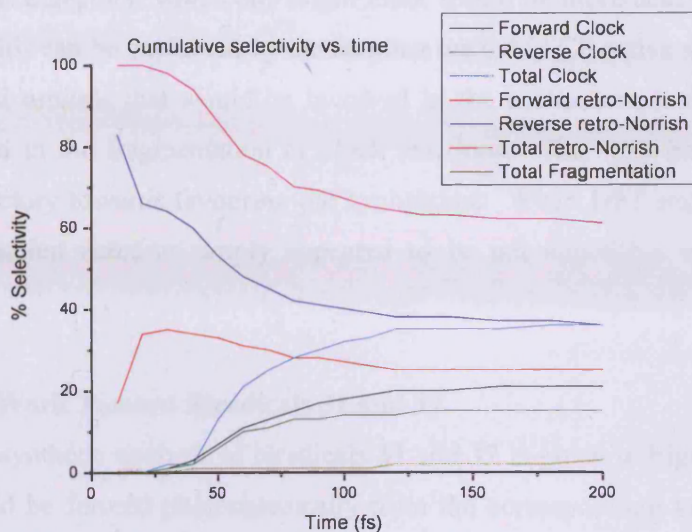
**Graph 2.2.** Cumulative selectivity of the reactions as a function of time



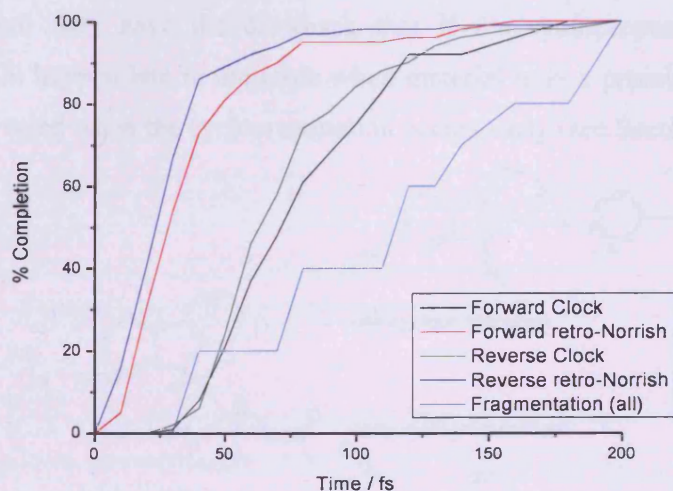
**Graph 2.3.** Portion of the reactions complete after a given amount of time



**Graph 2.4.** Number of D-labelled reactions as a function of time



**Graph 2.5.** Cumulative selectivity of the D-labelled reactions as a function of time



**Graph 2.6.** Portion of the D-labelled reactions complete after a given amount of time

The graphs highlight the conclusion that the forward and reverse directions are essentially the same. Further, the retro-Norrish reaction occurs first (10 – 40 fs), followed by the clock reaction (40 – 100 fs) and then the fragmentation reaction (120+ fs). The retro-Norrish reaction being earliest is consistent with the biradical geometry being closer to ketone **30** than any of the other conformations previously studied. Additionally, no cyclisations were observed, while that was the product seen

in the CASSCF trajectory, which one might think would be more accurate than DFT trajectories. This can be explained by the fact that the CASSCF active space included the two radical orbitals that would be involved in the cyclisation, but not the C–C bonds involved in the fragmentation or clock reactions. This may have biased the CASSCF trajectory towards favouring the cyclisation. When DFT trajectories were run, the cyclisation reaction simply appeared to be uncompetitive with the other reactions.

## 2.8 Synthetic Work Toward Biradicals 31 and 37

A retrosynthetic analysis of biradicals **31** and **37** is given in Figure 2.15. The biradicals could be formed photochemically from the corresponding ketones **30** and **36**. The major step in the syntheses is the cyclopropanation, which can either occur early or late in the synthesis. Routes that cyclopropanate late (see Section 2.8.1) have the advantage that the relatively sensitive cyclopropane will not be around for long in the synthesis, but they have the drawback that if the cyclopropanation is poor yielding, that will happen late in the route when material is at a premium. The pros and cons are reversed when the cyclopropanation occurs early (see Section 2.8.2).

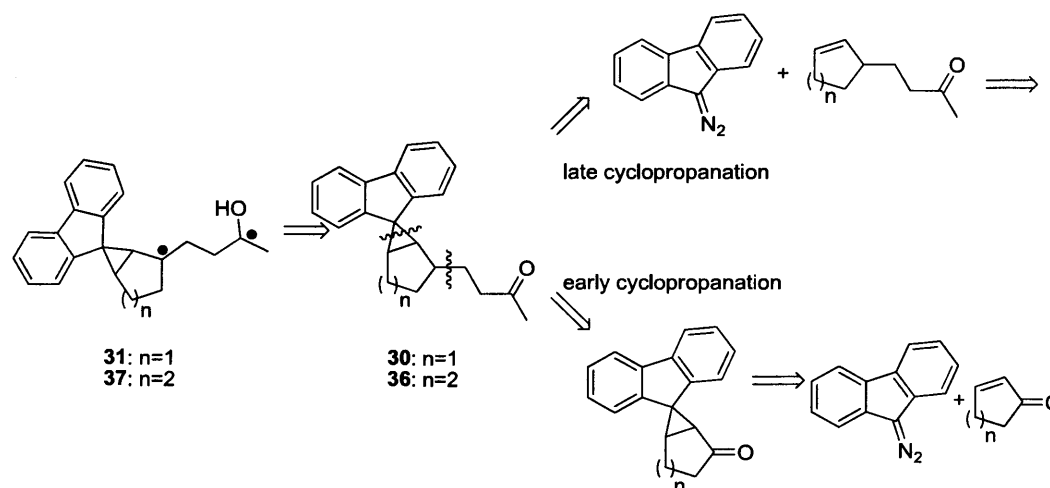


**Figure 2.15.** Retrosynthetic analysis of biradicals **31** and **37**

### 2.8.1 Attempted Synthesis of Ketones 30 and 36 Using Late Cyclopropanations

The first proposed synthesis of ketone **30** is shown in Figure 2.16. Commercially available cyclopentene (**44**) could either be allylicly brominated or chlorinated to form halide **45**. The halide could then either be reacted with Grignard reagent **46** or turned into a cuprate before undergoing Michael addition to methyl vinyl ketone (MVK).<sup>29</sup> The latter could produce enone **47**. The former could produce diene **48**, which could be Wacker oxidised<sup>30</sup> to **47**. Enone **47** could be cyclopropanated with 9-diazafluorene (**49**) (itself prepared from 9-fluorenone hydrazone (**50**)<sup>31</sup>) to give ketone **30**.

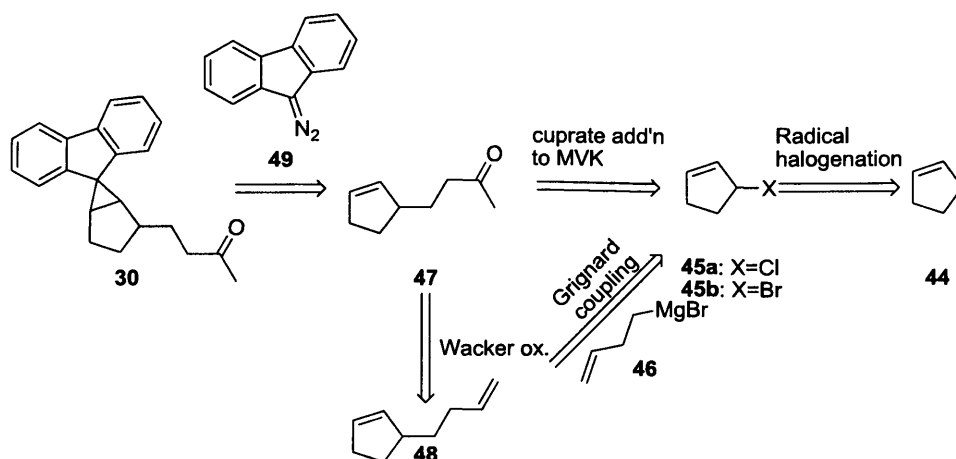


**Figure 2.16.** First proposed synthesis of ketone **30**

Unfortunately, this scheme did not work as expected (Figure 2.17). Halides **45** were unstable even at subzero temperatures and decomposed nearly as rapidly as they were formed. The small amounts of halide that did not decompose were coupled with Grignard reagent **46** in poor overall yield to give diene **48**. Michael addition to MVK was unsuccessful. Wacker oxidation was successful to give ketone **47**, however the cyclopropanation did not give ketone **30** as expected. The major products (Figure 2.18) formed by the fluorenyl carbene were fluorene **51** (hydrogen abstraction), fluorenone **52** (oxidation), and bifluorenylidene **53** (dimerisation). It was the last of these that was the most problematic, because as long as diazofluorene was sluggish in reacting with a target alkene, it would begin to react with itself.

These products were seen regardless of how the cyclopropanation was attempted, either thermally, photochemically, or with rhodium acetate as a catalyst.

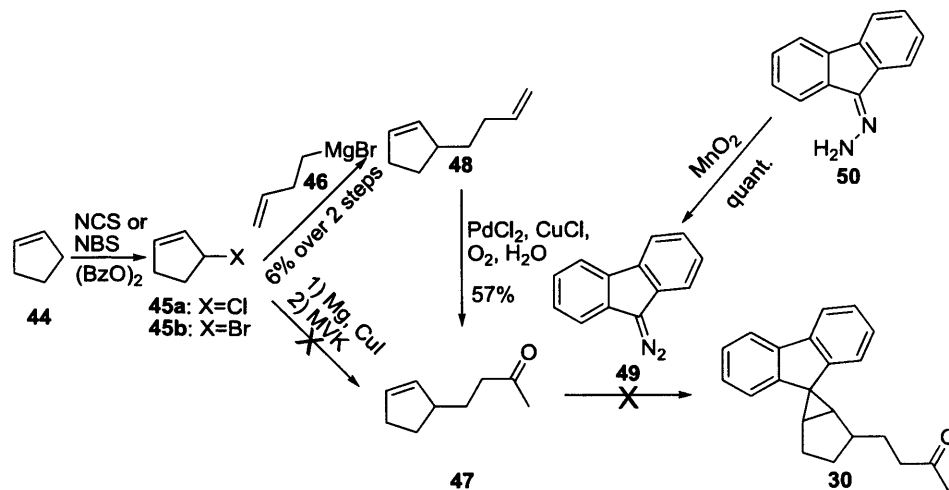


**Figure 2.17.** First attempted synthesis of ketone 30

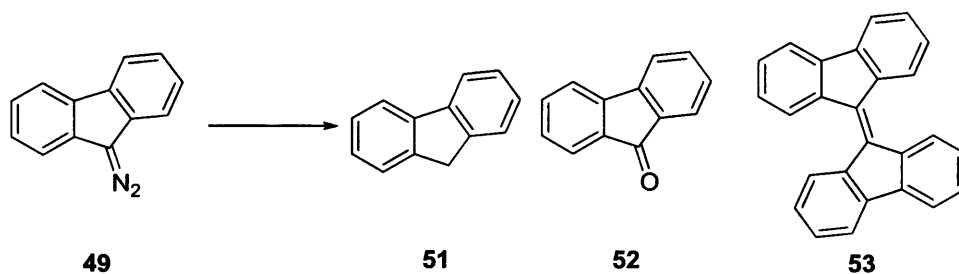


**Figure 2.18.** Reactions of diazofluorene

It was hoped that if halides **45** could be generated in a different manner, the coupling reaction to produce ketone **47** or diene **48** could be more successful. To that end, the alternative route of Nefedov to form halide **45** from bicyclopentadiene (**54**) was considered.<sup>32</sup> (Figure 2.19). Cyclopropanation with either chloroform or bromoform could lead to dihalocyclopropane **55**. Vacuum pyrolysis of **55** could lead to halide **45** and halobenzene **56**<sup>32</sup>.

In practice (Figure 2.20), the cyclopropanation was successful, but the pyrolysis to form halide **45** appeared to crack dihalocyclopropane **55**, but only gave brown tar.<sup>33</sup>

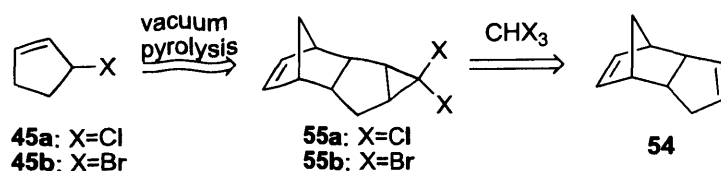


**Figure 2.19.** Alternative proposed route to halide 45

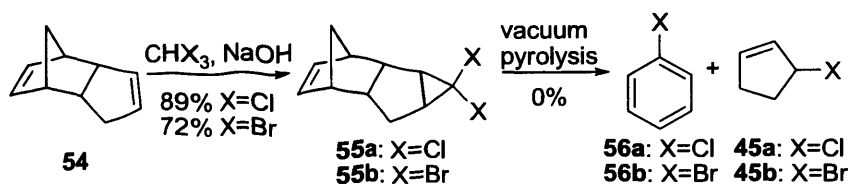


**Figure 2.20.** Alternative attempted route to halide 45

Rather than try to work with unstable halide 45, a new synthesis was designed that would also lead to ketone 47. It was hoped that access to a large amount of ketone 47 would allow the cyclopropanation to form final ketone 30 to be optimised. The new proposed synthesis is shown in Figure 2.21. This route differs from the previous ones by adding the last two carbons of the alkyl chain, rather than adding the whole chain at once. In the route, commercially available acid 57 could be reduced to alcohol 58. The alcohol could be brominated to form 59. Bromide 59 could be turned into the Grignard reagent and added to acetaldehyde to form alcohol 60, which could then be oxidised under standard conditions to yield ketone 47.

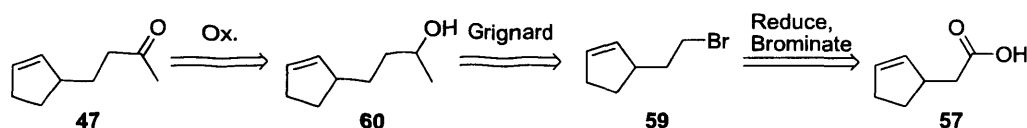


**Figure 2.21.** Proposed route to ketone 47

In practice (Figure 2.22), the reduction worked well, but the bromination was problematic. Under Appel conditions with freshly bought triphenylphosphine and carbon tetrabromide<sup>35</sup>, the reaction formed very little product and would stall after 2 – 3 days at approximately 20% conversion. Using an old bottle of carbon tetrabromide inherited from the previous research group occupying the lab yielded considerably better results, but the reaction still stalled at approximately 50%

completion. Additional reagents were able to restart the reaction. Attempts to determine why old carbon tetrabromide worked better than new carbon tetrabromide were unsuccessful. The presence of hydrogen bromide and molecular bromine were ruled out. Attempts to artificially “age” the new carbon tetrabromide, for instance by irradiating it, were similarly unsuccessful. Our current theory is that that new carbon tetrabromide contains a reaction inhibitor that eventually decomposes, although the identity of such an inhibitor remains unknown. Attempts to brominate alcohol **58** with phosphorous tribromide were similarly unsuccessful. A successful approach used triphenylphosphine and NBS, which formed bromide **59** in very good conversion (by NMR). Unfortunately, the boiling point of bromide **59** was too close to the reaction and column solvents and **59** could not be satisfactorily purified. Ultimately, this route was deemed to be unsuccessful.

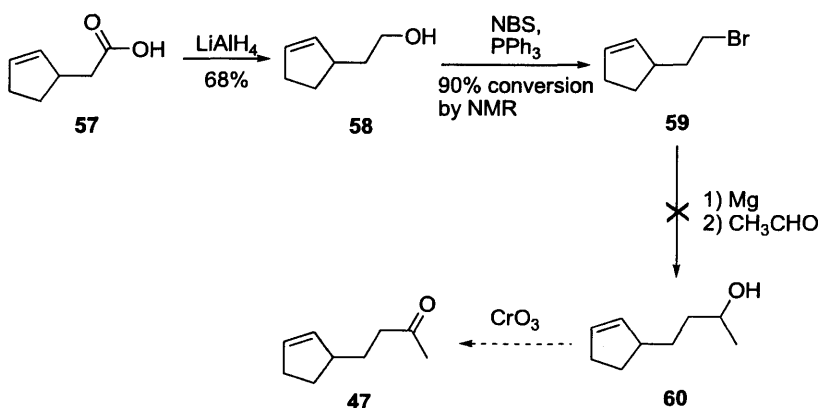


**Figure 2.22.** Attempted route to ketone **47**

A new proposed route to ketone **47** is shown in Figure 2.23. Here, commercially available carboxylic acid **57** could be esterified to **61**. After cyclopropanation with diazofluorene<sup>36</sup>, ester **62** could be reduced to alcohol **63**. From here, a route analogous to Figure 2.22 could be followed where the alcohol could be brominated to form bromide **64**, turned into a Grignard reagent, added to acetaldehyde, and finally oxidised to lead to ketone **30**.

However the cyclopropanation was unsuccessful (Figure 2.24) on ester **61**, leading once again to primarily bifluorenylidene dimer **53**.

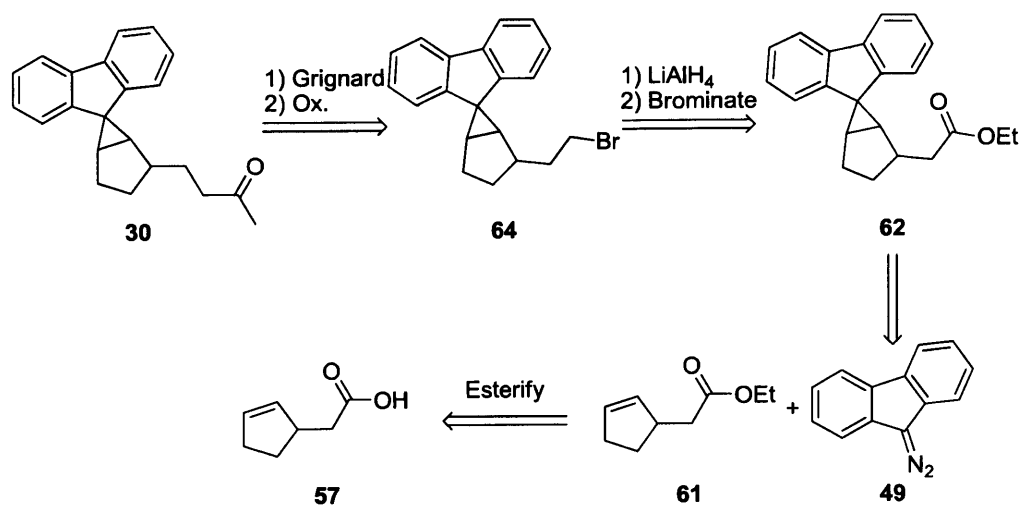


**Figure 2.23.** Proposed route to ketone **30** bypassing ketone **47**

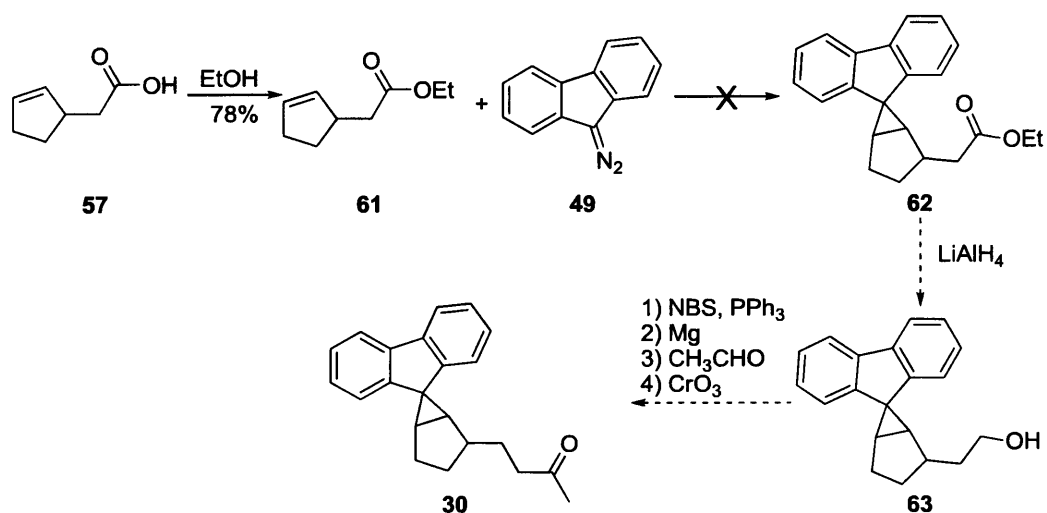


**Figure 2.24.** Attempted route to ketone **30** bypassing ketone **47**

Instead, a different route to ketone **47** was devised (Figure 2.25).<sup>37</sup> Commercially available ketoester **65** could be alkylated with 4-bromo-1-butene to give ketoester **66**. This could be hydrolysed and decarboxylated to give ketone **67**, which is related to ketone **47** by interchange of the ketone and alkene groups. Stereoselective reduction could give alcohol **68-syn** where the alcohol is *syn* to the alkyl chain. This stereochemistry is required because *syn*-xanthate **69-syn** is poised to undergo a Chugaev elimination<sup>38</sup> to yield diene **48**. *Anti*-xanthate **69-anti** could undergo the Chugaev elimination in either direction to give dienes **48** and **70** (*vide*

*infra* and Figure 2.27). The oxidation of diene **48** to ketone intermediate **47** had already been shown to work (Figure 2.17), and would hopefully give enough material to optimise the cyclopropanation to give final ketone **30**.

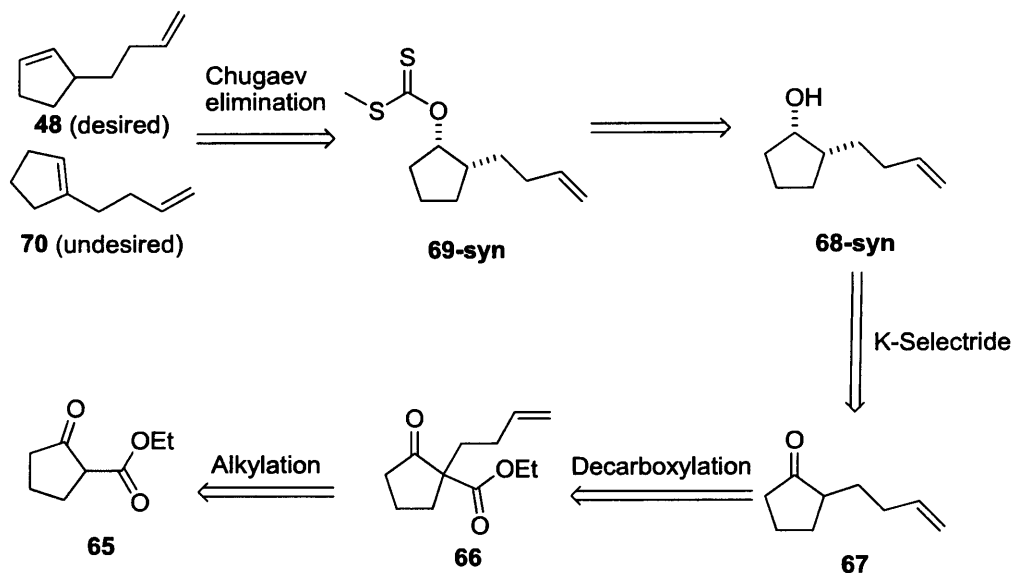


**Figure 2.25.** Proposed alternative route to diene **48**

Unfortunately, this route also had difficulties (Figure 2.26). The alkylation to form **66** worked well, however the decarboxylation could only be accomplished sluggishly and with poor yield. Various conditions were tried such as hydrolysing the ester with acid, hydrolysing with base followed by acidification, or using lithium chloride to aid in the decarboxylation.<sup>39</sup> None of those conditions improved the reaction yield. The reduction was also problematic. The use of K-selectride<sup>40</sup> gave only one diastereomer. Chugaev elimination on the xanthate derived from this alcohol gave primarily diene **70**, rather than the desired diene **48**. This is most likely due to the wrong diastereomer of alcohol **68-anti** being formed. Figure 2.22 gives the mechanisms of the Chugaev elimination for each diastereomer of **69**. The reaction proceeds through a six-membered transition state. For compound **69-syn**, only the methylene has a hydrogen atom in the correct position, so only alkene **48** is formed. For compound **69-anti**, both of the neighbouring carbons has a hydrogen atom in the correct position, and this can lead to either alkene **48** or **70**. In retrospect, since only

compound **70** was seen, that implies that alcohol **68-anti** must have been formed by the K-selectride reduction instead of the desired **68-syn**.

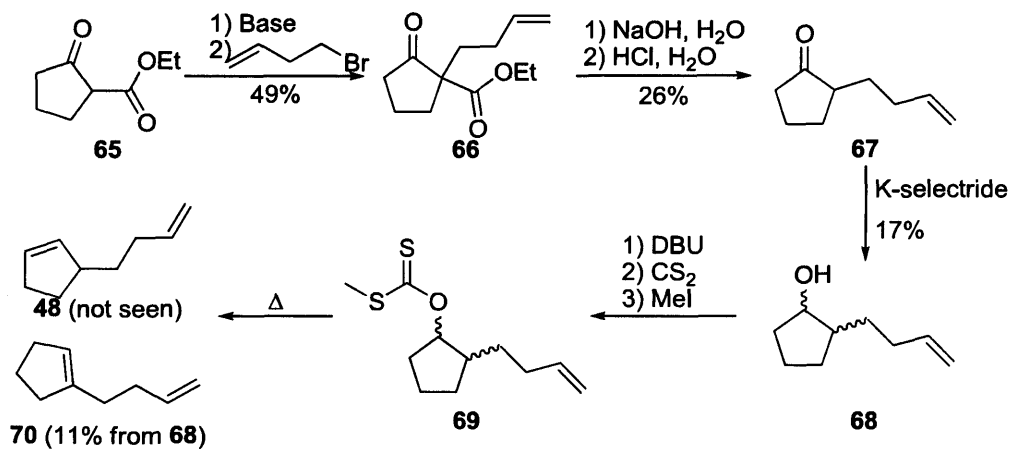


Figure 2.26. Attempted alternative route to diene **48**

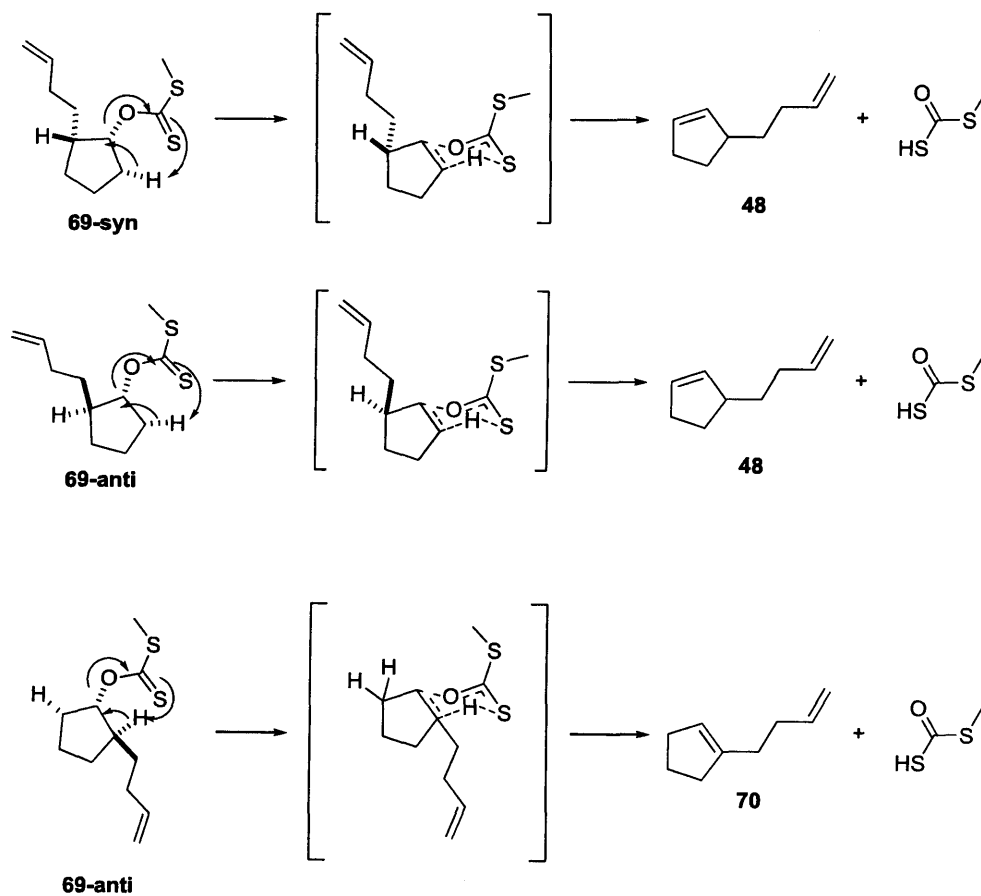
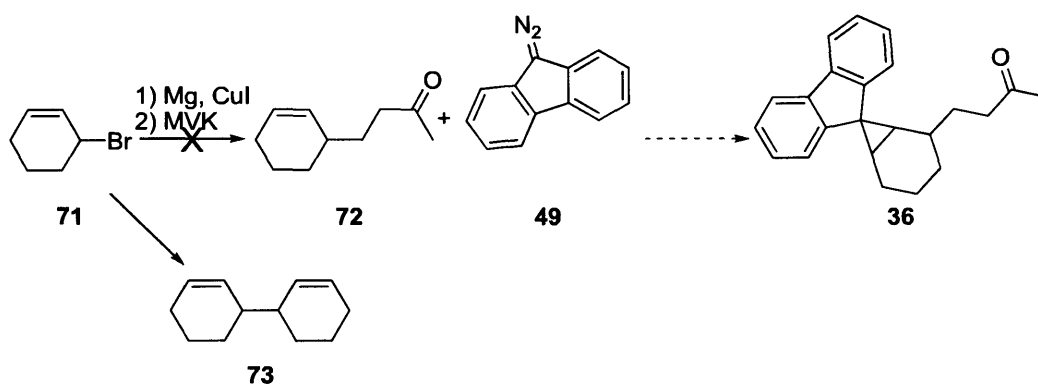


Figure 2.27. Mechanism of the Chugaev elimination

Because of the selectivity problems forming alcohol **68**, this route was abandoned. Additionally, because of the many problems with synthesising ketone intermediate **47**, and the fact that none of the cyclopropanations had as yet worked, it was decided to try to either cyclopropanate earlier in the synthesis (Section 2.8.2), or adapt the previously described syntheses to make ketone **36** (*vide infra*).

Whereas 3-bromocyclopentene was very unstable, 3-bromocyclohexene (**71**) is commercially available. Thus, it was decided to retry the initial route (Figure 2.17) again, but starting with 3-bromocyclohexene. This route is summarised in Figure 2.28. The retrosynthesis is the same as Figure 2.16, with the exception that the commercially available starting material was 3-bromocyclohexene **71**, rather than cyclohexene.



**Figure 2.28.** Attempted route to ketone **36**

Unfortunately this route had problems as well. Attempts to form the Grignard reagent from bromide **71** were unsuccessful. Instead of the Grignard adding to MVK to form ketone **72**, Wurtz coupling product **73** was formed exclusively.<sup>41</sup> Attempts to minimise the formation of **73** by varying the solvent, temperature, addition rates, and other factors were unsuccessful. Similar problems were seen when trying to form the organolithium or organocopper species. As the organometallic reagents could not be formed, this route was not continued.

### 2.8.2 Attempted Synthesis of Ketones 30 and 36 Using Early Cyclopropanations

In view of the earlier problems, new routes were designed which had the cyclopropanation early in the synthesis. These routes sought to make ketone 74 (shown in Figure 2.29) which would be functionalised to give final ketone 30. The endgame for this route will be discussed in more depth later (Figure 2.39). The simplest cyclopropanation is shown in Figure 2.24, reacting diazofluorene (49) and cyclopentenone (75) to form ketone 74 which could be functionalised to form ketone 30.

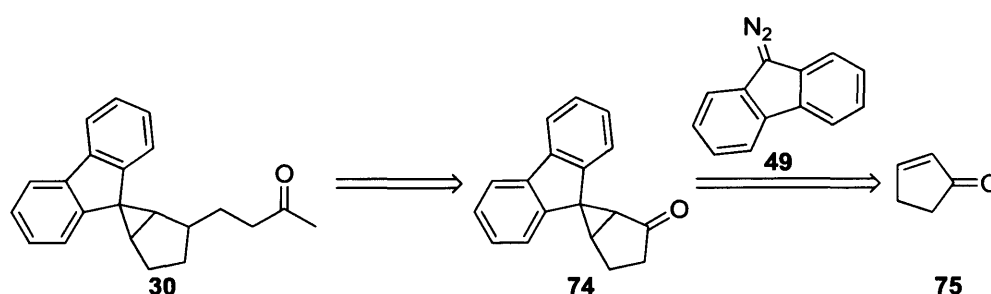
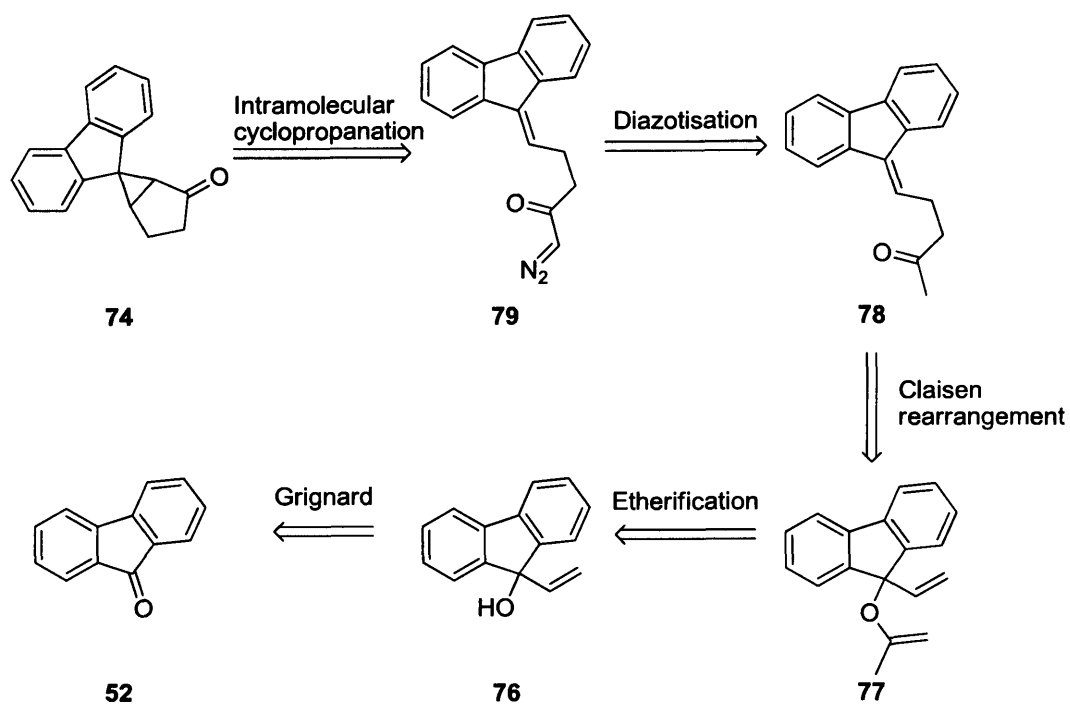


Figure 2.29. Initial proposed route to ketone 74 and then ketone 30

The cyclopropanation was initially unsuccessful, however subsequent optimisations (*vide infra* and Figure 2.38) were successful in forming ketone 74. For this reason, several other routes to ketone 74 were also developed. In the first of these routes (Figure 2.30), 9-fluorenone 52 could be reacted with vinyl magnesium bromide to form alcohol 76. This could then be alkylated with a propenyl ether to give allyl vinyl ether 77, which is poised to undergo a Claisen rearrangement<sup>42</sup> to give ketone 78. Diazotisation<sup>43</sup> on the less hindered side could give diazoketone 79 which could undergo an intramolecular cyclopropanation to give ketone 74.

Unfortunately, the reaction with the propenyl ether was unsuccessful in giving the Claisen precursor, instead yielding an intractably complex mixture (Figure 2.31).



**Figure 2.30.** First alternative proposed route to ketone **74**

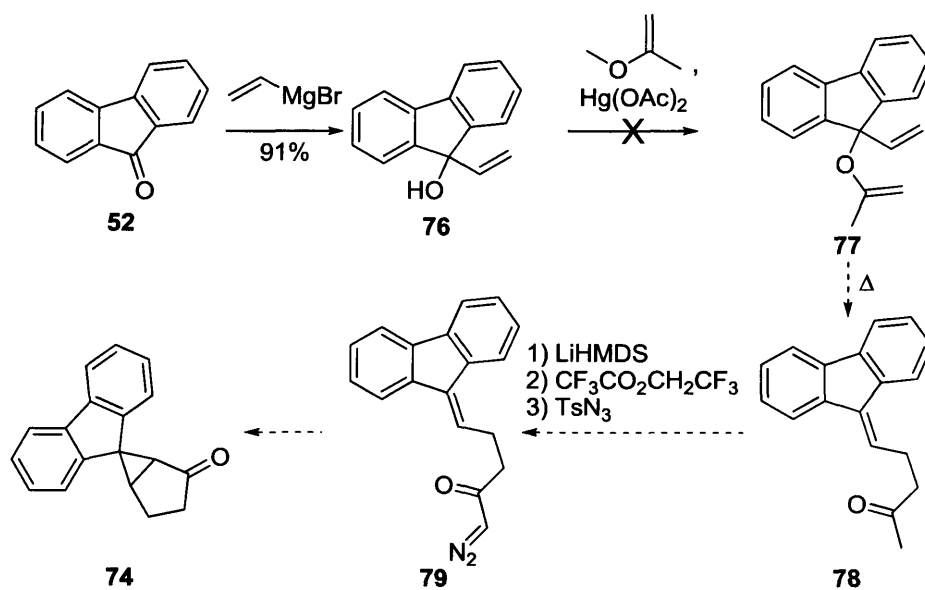


**Figure 2.31.** Attempted alternative route to ketone **74**

In the next proposed route to form ketone **74** (Figure 2.32), a Grignard reaction between magnesium bromide **80** and 9-fluorenone could give alcohol **81** which could be dehydrated to diene **82**. Wacker oxidation could give ketone **78** which could then be taken through the remainder of the route shown above in Figure 2.30. Alternatively, a Wittig reaction between ylide **83** and 9-fluorenone could give diene **82** directly.

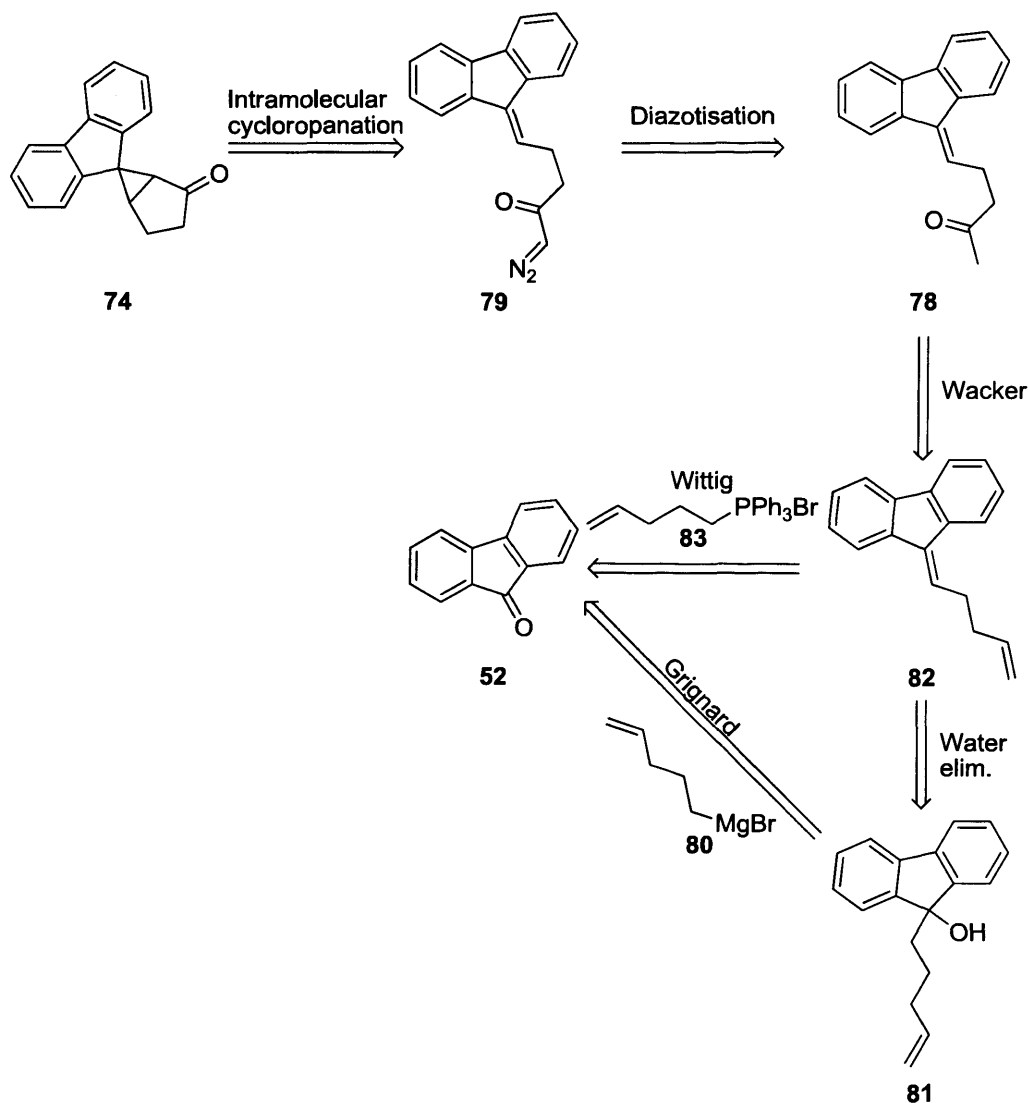


**Figure 2.32.** Next proposed route to ketone **74** *via* ketone **78**

Surprisingly (Figure 2.33), the Grignard reaction gave the 1,4 addition product **84**, as confirmed by NMR. It is not without precedent for Grignard reagents to

undergo conjugate additions on aromatic systems<sup>44</sup>, but ketone **84** was of no synthetic utility. The Wittig route, however, was successful in producing ketone **78**. The diazotisation of ketone **78** was unsuccessful, as NMR evidence suggested that LiHMDS, a hindered base, was not hindered enough to selectively deprotonate at the methyl position rather than the more thermodynamically acidic methylene position. The mixture of enolate anions gave rise to a complex product mixture, which did not appear to contain either diazoketone **79** or ketone **74**.

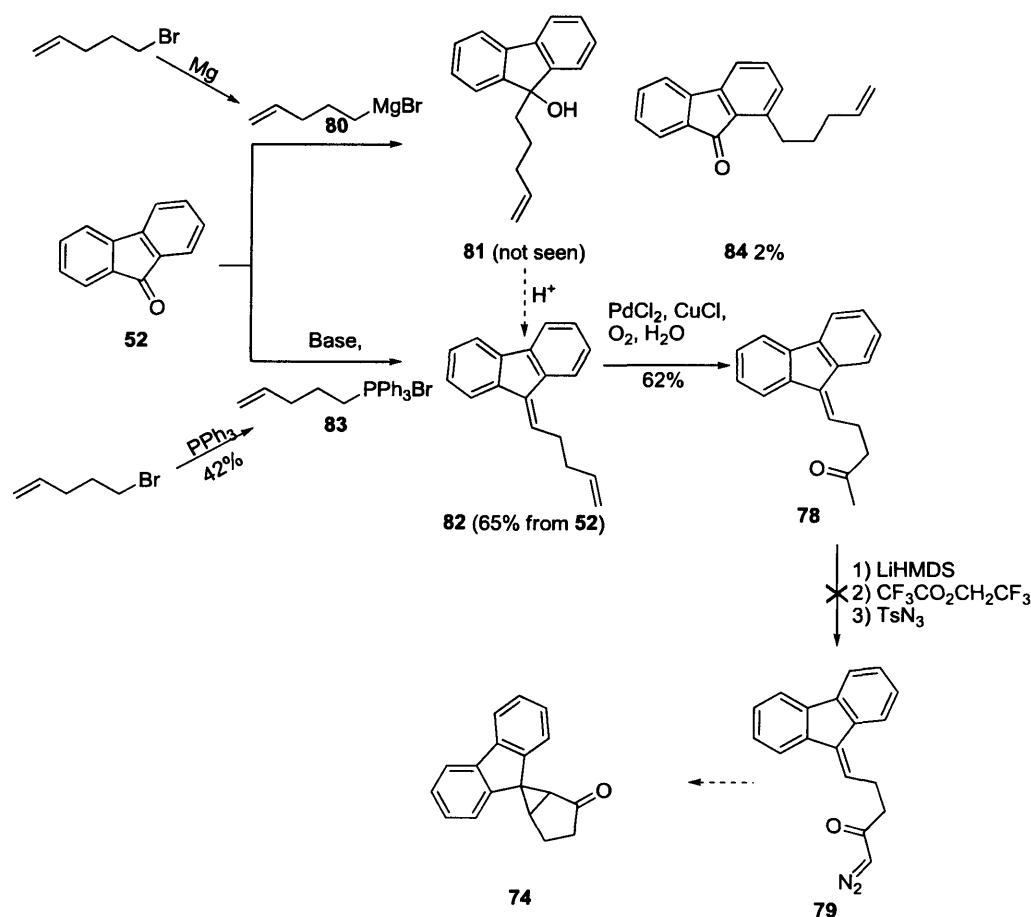


**Figure 2.33.** Next attempted route to ketone **74** via ketone **78**

The next proposed route to ketone **74** is shown in Figure 2.34 and again starts with 9-fluorenone (**52**). A Wittig reaction with ylide **85 c** could give alkene **86**. Deprotonation with a strong base such as Schlosser's base<sup>45</sup> could give a resonance-stabilised anion. It was hoped that the exocyclic anion of **86** would react with

epichlorohydrin to give epoxide **87**. Lithiation with LTMP could give a carbenoid intermediate which could cyclise to ketone **74**.<sup>46</sup>

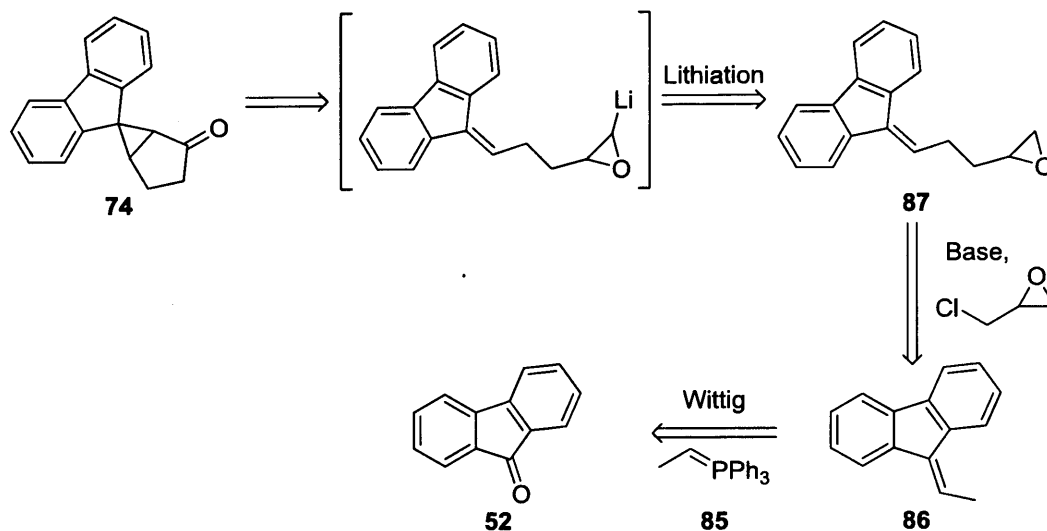


**Figure 2.34.** Alternative proposed route to ketone **74**

The results of this route are shown in Figure 2.35. The Wittig reaction was successful, however the alkylation using Schlosser's base gave only black tar. Efforts to clean up the reaction, or even determine what products were being formed were unsuccessful. Other bases such as *n*-BuLi showed some evidence of nucleophilic attack on the terminal vinyl carbon of alkene **86** to give a fluorenyl anion which was highly stabilised by resonance, although there were several other products which could not be identified.

The previous routes all involved a cyclopropanation with a carbene and an alkene. Instead, the next proposed route shown in Figure 2.26 tried the different tactic of a di- $\pi$ -methane rearrangement<sup>47</sup> to give a related ketone **88**. Following the procedure of Plieninger<sup>48</sup>, fluorene could be formylated to give aldehyde **89** which could undergo a Robinson annulations with MVK to give enone **91** (*via* dione **90**).<sup>48</sup> From here, DDQ could oxidise enone **91** to dienone **92**. Dienone could then undergo the di- $\pi$ -methane rearrangement to form ketone **88**, which could then be hydrogenated to form ketone **74**.

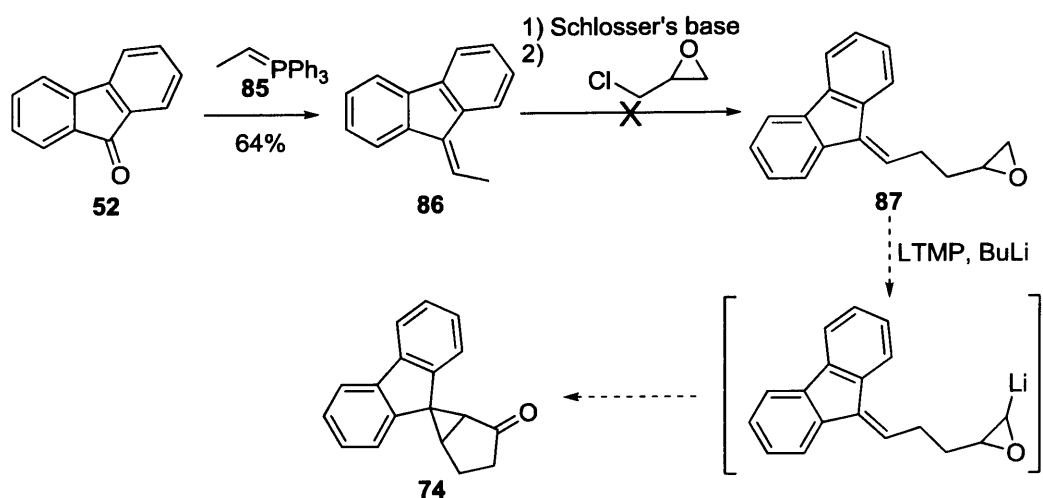


Figure 2.35. Alternative attempted route to ketone 74

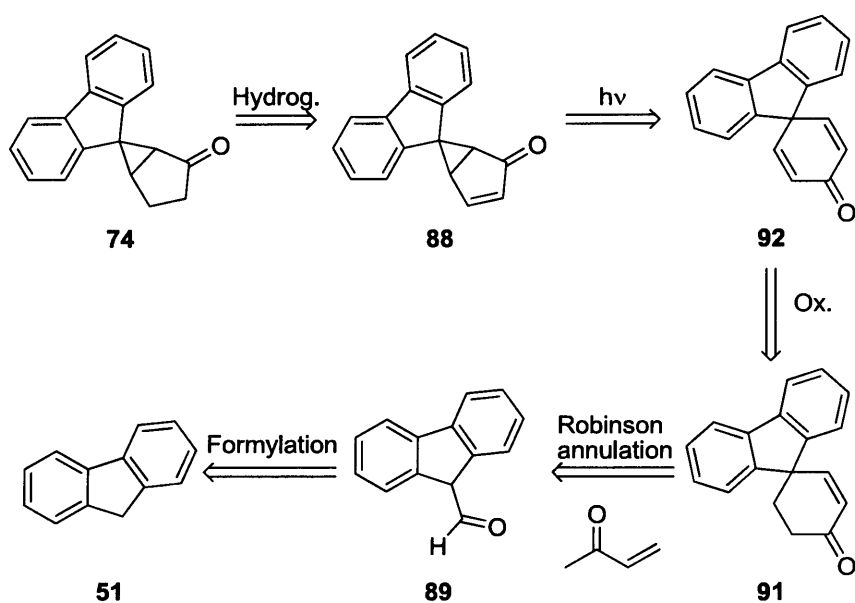
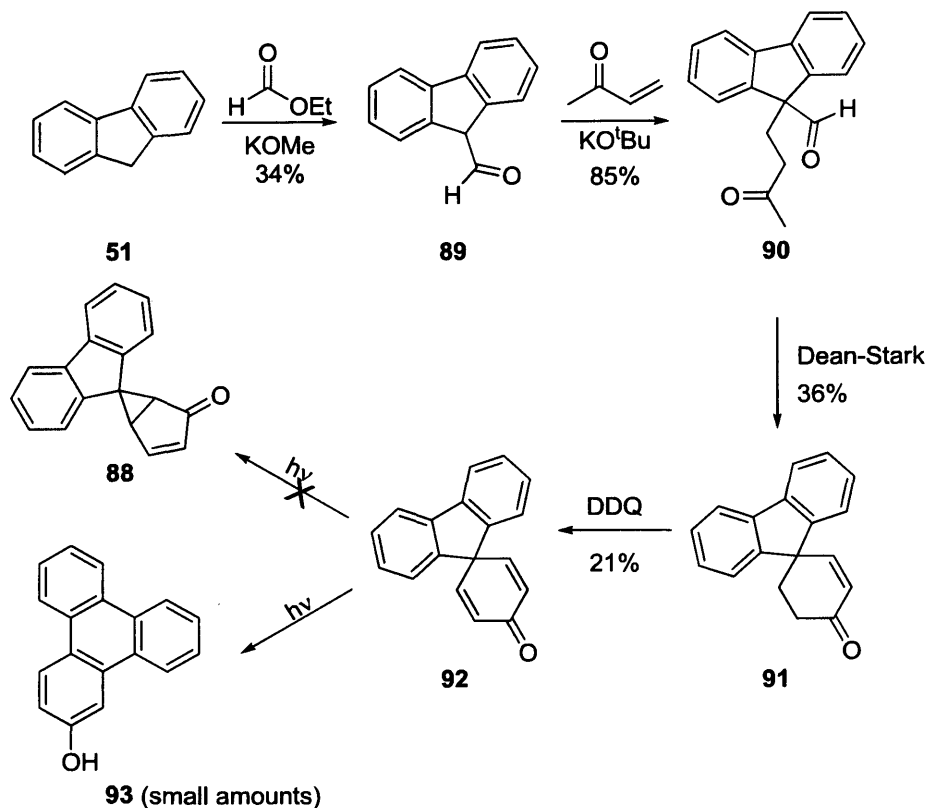


Figure 2.36. Proposed rearrangement route to ketone 74 via ketone 88

The initial steps of this route worked well, up to enone 91. The DDQ oxidation did form dienone 91, albeit very sluggishly. In fact, a mixture of 91 and 92 was obtained, but could not be separated by any chromatographic technique. Other oxidants such as IBX were unsuccessful in forming dienone 92. Rather than ketone 88 being formed upon irradiation of dienone 92, phenol 93 was formed instead amidst

a large number of unidentified products. This type of rearrangement is also known<sup>47</sup> and it was unlikely that the reaction could be modified to lead selectively to enone **88**.



**Figure 2.37.** Attempted rearrangement route to ketone **88**

At this stage, the syntheses were becoming more and more complicated with significantly more crucial intermediates. The decision was made to go back to the simple cyclopropanation between 9-diazo fluorene and 2-cyclopentenone or 2-cyclohexenone and to try and optimise it. While most reaction conditions gave the usual carbene byproducts **51** – **53**, eventually it was found that by using cyclopentenone **75** and cyclohexenone **95** respectively as solvent, the desired cyclopropanation occurred in moderate yield to give cyclopropanes **74** and **94** (Figure 2.38). Proposed syntheses of final ketones **30** and **36** are shown in Figures 2.39.

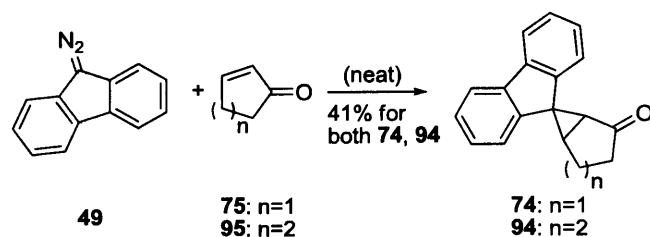


**Figure 2.38.** Optimised synthesis of ketones **74** and **94**

Ketones **74** and **94** could undergo a Wittig reaction with phosphonium bromide **96** (from the bromide and triphenylphosphine) to give dienes **97** and **98**. Wacker oxidation is selective for terminal alkenes<sup>30</sup> and could be used on dienes **97** and **98** followed by hydrogenation of the remaining double bond to give ketones **30** and **36**. If the Wittig reaction failed, a Horner-Wittig reaction<sup>49</sup> could be tried using phosphine oxide **99** (from phosphonium bromide **96**). Additionally, a Julia olefination<sup>50</sup> using sulfone **100** (from sulfinate **101**) could also be used. This reaction can be more suitable for hindered ketones, but requires more aggressive methods to remove the phosphorus and sulphur groups from intermediates **102a/b** and **103a/b** to form dienes **97** and **98**. If all of those reactions are unsuccessful, a Tebbe reaction could be done on ketones **74** and **94**.<sup>51</sup> The Tebbe reagent (Figure 2.40) is more reactive than phosphonium ylides and in fact is the method of choice for methylenating ketones.<sup>52</sup> The Tebbe reaction could lead to alkenes **104** and **105**. From here, there are several options. Olefin metathesis<sup>53</sup> could lead to dienes **97** and **98** followed by the same plan as described above. If the metathesis using 1,4-pentadiene failed, olefin metathesis on a mono-alkene-alcohol could lead to alcohols **106** and **107**. From here, alcohol oxidation could lead to final ketones **30** and **36**. If both metatheses failed, alkenes **104** and **105** could be hydroborated to give alcohols **108** and **109**. Conversion of the alcohols to leaving groups followed by alkylation with acetone could lead to final ketones **30** and **36**. And finally, ketones **74** and **94** could undergo Grignard reactions with 4-butenyl magnesium bromide to give alcohols **110** and **111**. Barton deoxygenation<sup>54</sup> would not be feasible because it proceeds through a radical pathway, which would most likely open the cyclopropane extremely rapidly. Instead, the alcohol could presumably be tosylated, followed by reduction with lithium aluminium hydride to give the monoalkene version of **97** and

98 where the unwanted internal bond has effectively already been hydrogenated.<sup>55</sup> Wacker oxidation could then lead to final ketones 30 and 36.

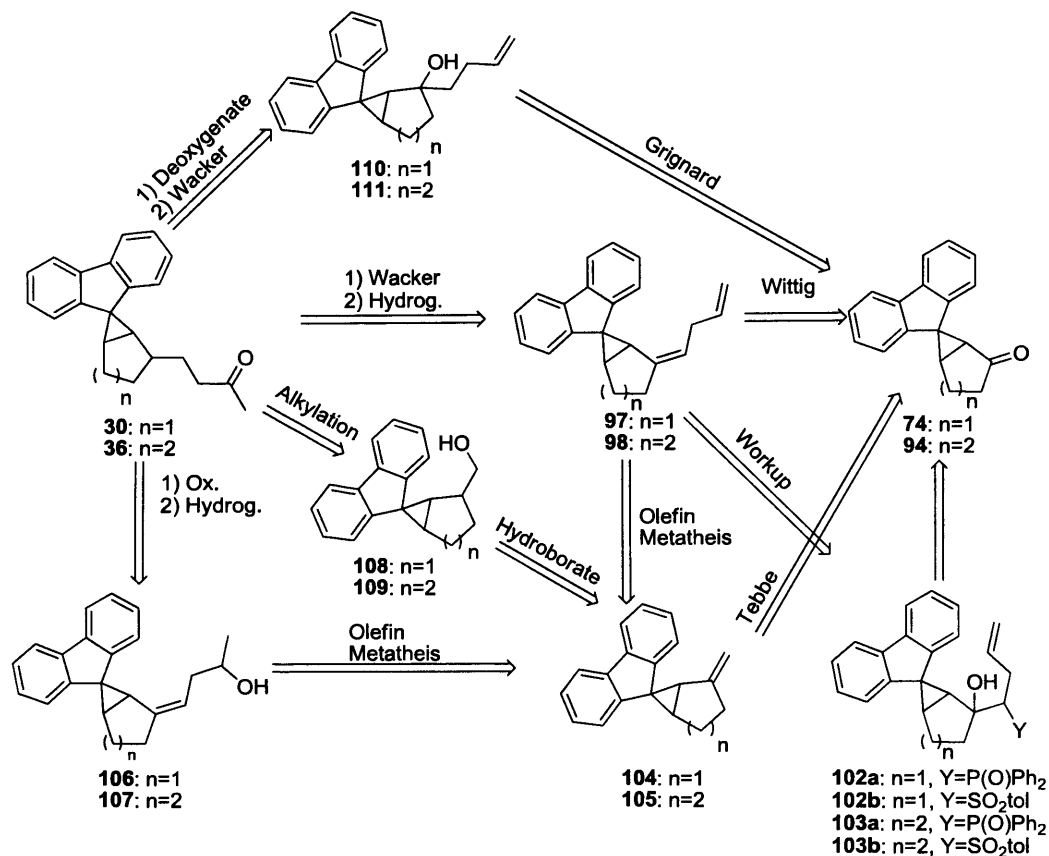


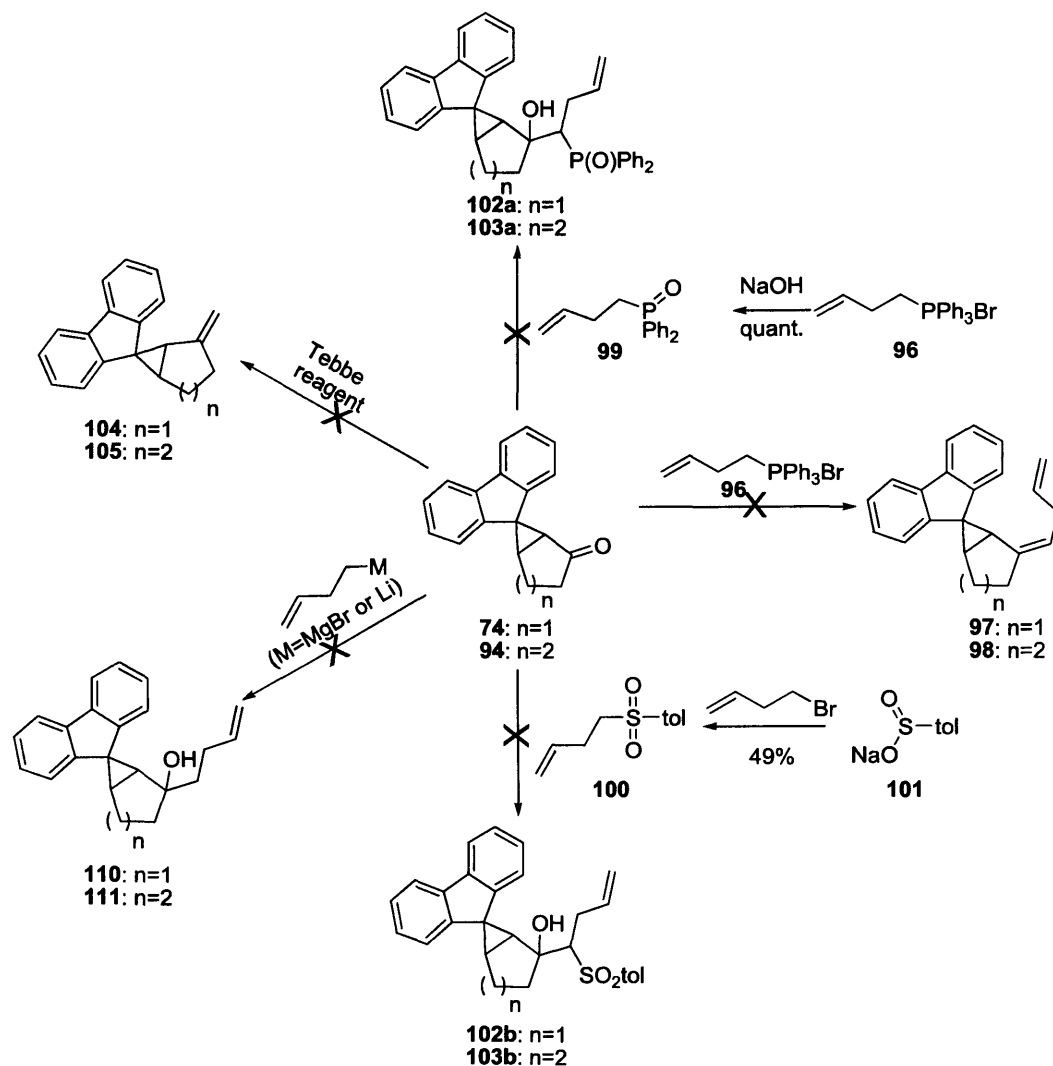
Figure 2.39. Proposed endgame from ketones 74 and 94 to final ketones 30 and 36



Figure 2.40. Tebbe reagent

In fact (Figure 2.41), all of the initial reactions on ketones 74 and 94 were unsuccessful. This included the Wittig, Horner-Wittig, Julia, Tebbe, and Grignard reactions. At this point, it was unclear what reagents were capable of reacting with 74 and 94. The remarkable unreactivity of ketones 74 and 94 were tested by adding them directly into 2.5M *n*-butyllithium in hexanes in which the only observable product was a black tar that slowly formed over several days, presumably through formation

of the enolate, rather than nucleophilic attack. A possible explanation for this unreactivity was seen in the X-ray structure for ketone **74** (Figure 2.42).



**Figure 2.41.** Attempted reactions of ketones **74** and **94**

The fluorene rings are perpendicular to the cyclopropane ring and the fluorene group clearly blocks the upper Bürgi-Dunitz<sup>56</sup> trajectory to attack the carbonyl. The lower trajectory appears unhindered, except any nucleophile attacking the carbonyl would push the newly formed O-Metal (Li or MgBr) group towards the fluorenyl rings, causing a large steric clash. That is what presumably makes addition onto

either face of the ketone unfavourable and explains the surprising stability of ketones **74** and **94**.

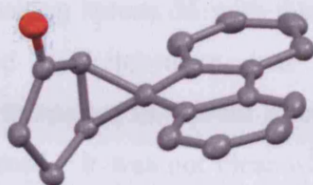


Figure 2.42. X-ray structure of ketone **74**

Since functionalisation of ketones **74** and **94** appeared impossible, a final route was proposed that both allowed for a similar cyclopropanation to the one that formed ketones **74** and **94**, and had the butyl chain already built into the molecule (Figure 2.43). Enol ethers **112** and **113** can be alkylated by 4-iodobutene **114** (from 4-bromobutene) to form enol ethers **115** and **116**. Reduction and then acidic workup could give ketones **117** and **118**.<sup>57</sup> These ketones could hopefully be cyclopropanated by 9-diazo fluorene (**49**) to yield ketones **119** and **120**. The endgame for this route would be deoxygenation and then Wacker oxidation to give final ketones **30** and **36**.

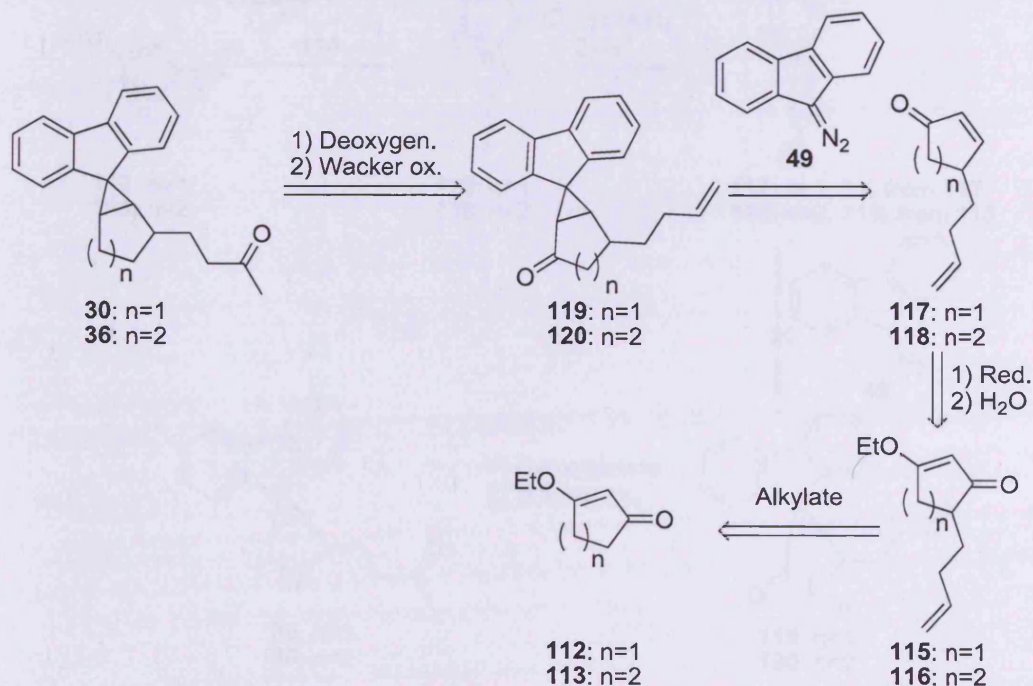
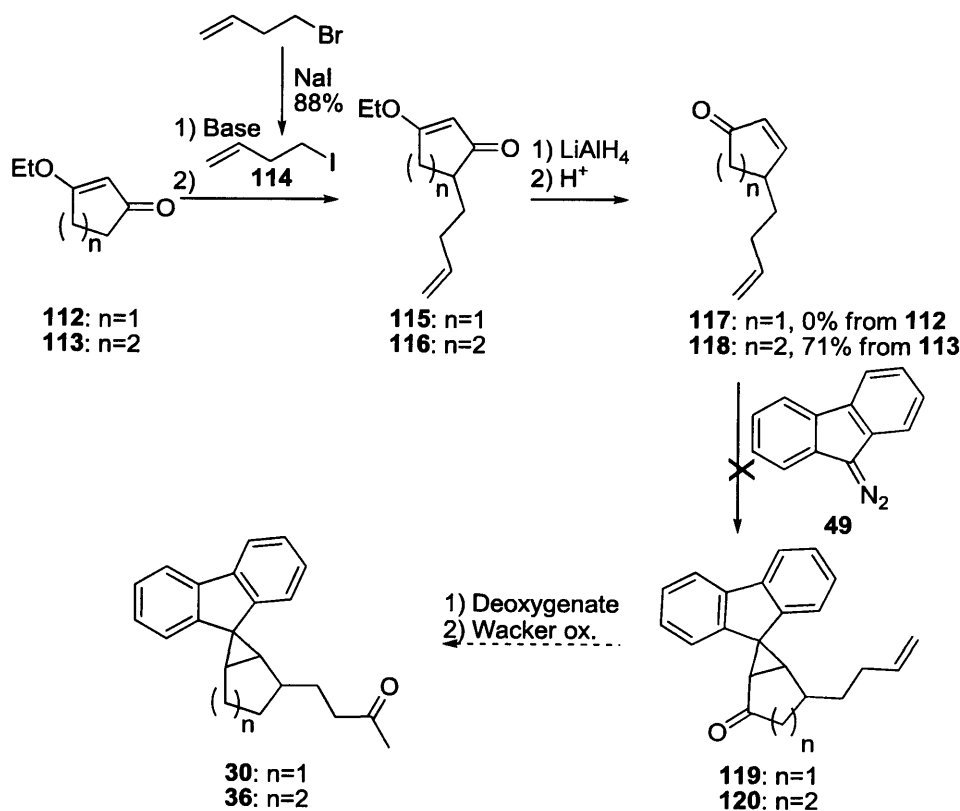


Figure 2.43. Proposed alternative route to ketones **30** and **36**

This route had mixed results. For  $n=2$ , the synthesis of ketone **118** was successful; for  $n=1$  the alkylation gave a complicated mixture of products instead of ketone **117** cleanly. Due to the large cost of vinyl enol ether **112**, the decision was made to focus entirely on making ketone **36** with this route. The cyclopropanation between diazofluorene and cyclohexenone was optimised and found that cyclohexenone did not have to be used as solvent if one equivalent of an amine such as pyridine or DMAP was used. It was not clear what purpose the amine served. Disappointingly, the cyclopropanation on enone **117** did not work at all, with or without the amine additives, only giving only black tar. As the differences between 2-cyclohexenone and enone **117** towards cyclopropanation were not expected to be large, we did not understand why the latter behaved so differently. Attempts to improve the cyclopropanation of **120** were unsuccessful. At this point, all synthetic routes to ketones **30** and **36** were exhausted, and the decision was made to focus on the computational work, as well as the cyclopentadiene project discussed in Chapters 4 – 5.



**Figure 2.44.** Alternative attempted route to ketones **30** and **36**

## 2.9 Summary and Conclusions

A mixture of synthetic and computational chemistry was used to probe the behaviour of biradicals **31** and **37**. Unfortunately the synthetic work was unsuccessful in producing ketones **30** and **36**, so the work on product distributions as a function of supercritical fluid pressure could not be carried out.

The computational results were more promising. Some of the key results were that a) DFT was a cheap and fairly accurate method for investigating these singlet biradicals and their reactivities, b) regardless of the conformation the biradicals are formed in, the Norrish and clock reactions appear to be competitive, and c) IVR from the OH (or OD) stretching mode to other vibrational modes of the biradicals is surprisingly slow which may be the source of any nonstatistical effects. If the synthesis of ketones **30** and **36** can be completed, it would provide a good chance to test for nonstatistical dynamics in systems that have potential biological applications.

## 2.10 References for Chapter 2

1. Owrutsky, J. C.; Raftery, D.; Hochstrasser, R. M. *Annu. Rev. Phys. Chem.* **1994**, *45*, 519 – 555.
2. Griller, D.; Ingold, K. U. *Acc. Chem. Res.* **1980**, *13*, 317 – 323.
3. Martin-Esker – A. A.; Johnson, C. C.; Horner, J. H. Newcomb, M. *J. Am. Chem. Soc.* **1994**, *116*, 9174 – 9181.
4. Oritz, P. R. Ed., *Cytochrome P450: Structure, Mechanism, and Biochemistry*, Plenum, New York, 2, **1995**.
5. (a) Groves, J. T.; McClusky, G. A.; White, R. E.; Coon, M. *J. Biochem. Biophys. Res. Commun.* **1978**, *81*, 154 – 160. (b) Schlichting, I.; Berendzen, J.; Chu, K.; Stock, A. M.; Maves, S. A.; Benson, D. E.; Sweet, R. M.; Ringe, D.; Petsko, G. A.; Sligar, S. G. *Science* **2000**, *287*, 1615 – 1622.
6. For compounds **11b**, **11c**, **11f**, **11g**, **11h** see: Atkinson, J. K., Ingold, K. U. *Biochemistry* **1993**, *32*, 9209 – 9214. For compound **11i**, see: Newcomb, M.; Le Tadic, M; Putt, D. A.; Hollenberg, P. F. *J. Am. Chem. Soc.* **1995**, *117*, 3312 – 3313.
7. Newcomb, M.; Chestney, D. L. *J. Am. Chem. Soc.* **1994**, *116*, 9753 – 9754.

8. (a) Meunier, B.; de Visser, S. P.; Shaik, S. *Chem. Rev.* **2004**, *104*, 3947 – 3980.  
(b) Shaik, S.; Cohen, S.; Wang, Y.; Chen, H.; Kumar, D.; Thiel, W. *Chem. Rev.* **2010**, *110*, 949 – 1017.
9. (a) Overview of nonstatistical dynamics: Carpenter, B. K. *Annu. Rev. Phys. Chem.* **2005**, *56*, 57 – 89. (b) IVR rate results: Rynbrandt, J. D.; Rabinovitch, B. S. *J. Phys. Chem.* **1971**, *75*, 2164 – 2175.
10. Carpenter, B. K. *Am. Sci.* **1997**, *85*, 138 – 149.
11. Salem, L.; Rowland, C. *Angew. Chem. Int. Ed. Engl.* **1972**, *11*, 92 – 111.
12. Wagner, P. *Chemistry of Excited Triplet Organic Carbonyl Compounds*, Topics in Current Chemistry, Springer Berlin: Heidelberg, **1976**, *66*, 1 – 52.
13. (a) Norrish, R. G. W. *Trans. Faraday Soc.* **1937**, *33*, 1521 – 1528. (b) Wagner, P. *J. Acc. Chem. Res.* **1971**, *4*, 168 – 177.
14. Broyles, D. A.; Carpenter, B. K. *Org. Biomol. Chem.* **2005**, *3*, 1757 – 1767.
15. Compare this to the systems discussed in Sections **1.4.1-3**
16. (a) For general use of supercritical fluids for kinetics, see: Dutton, M. L.; Bunker, D. L.; Harris, H. H. *J. Phys. Chem.* **1972**, *76*, 2614 – 2617. (b) For supercritical fluids in the DBH reaction, see: Reyes, M. B.; Carpenter, B. K. *J. Am. Chem. Soc.* **2000**, *122*, 10163 – 10176.
17. Cremer, D. *Mol. Phys.* **2001**, *99*, 1899–1940.
18. (a) U – unrestricted Hartree-Fock, see Section **1.5.1** (b) Becke exchange: Becke, A. D. *Phys. Rev. A* **1988**, *38*, 3098 – 3100. (c) Lee, Yang, and Parr correlation: Lee, C.; Yang, W.; Parr, R. G. *Phys. Rev. B* **1988**, *37*, 785 – 789. (d) Hybridisation: Becke, A. D. *J. Chem. Phys.* **1993**, *98*, 5648 – 5652.
19. Doubleday Jr., C. *J. Am. Chem. Soc.* **1993**, *115*, 11968 – 11983.
20. Obviously a reaction should not have a negative activation barrier. What is more likely happening is that either the reaction is barrierless and the energies are within the margin of error of the computational method, or alternatively, when entropy is taken into account, then there presumably be a very slight Gibbs energy barrier for the reaction.
21. Bernardi, F.; Olivucci, M.; Robb, M. A. *Chem. Soc. Rev.* **1996**, *25*, 321 – 328.
22. (a) Werner, H.-J. *Mol. Phys.* **1996**, *25*, 645 – 661. (b) Celani, P.; Werner, H.-J. *J. Chem. Phys.* **2000**, *112*, 5546 – 5557.

23. Some common semiempirical methods include (a) AM1: Dewar, M. J. S.; Zoebisch, E. G.; Healy, E. F. *J. Am. Chem. Soc.* **1985**, *107*, 3902 – 3909. (b): PM3 Stewart, J. J. P. *J. Comp. Chem.* **1989**, *10*, 209 – 264.
24. Cohen, A. J.; Handy, N. C. *Mol. Phys.* **2001**, *99*, 607 – 615.
25. Perdew, J. P.; Burke, K.; Ernzerhof, M. *Phys. Rev. Lett.* **1996**, *77*, 3865 – 3868.
26. Perdew, Wang exchange and correlation: (a) Perdew, J. P.; Chevary, J. A.; Vosko, S. H.; Jackson, K. A.; Pederson, M. D.; Singh, D. J.; Fiolhais, C. *Phys. Rev. B* **1992**, *46*, 6671 – 6687. (b) Perdew, J. P.; Wang, Y. *Phys. Rev. B* **1992**, *45*, 13244 – 13249. Hybridisation: (c) Adamo, C.; Barone, V. *J. Chem. Phys.* **1998**, *108*, 664 – 675.
27. Dondas, H. A.; Grigg, R.; Thibault, S. *Tetrahedron* **2001**, *57*, 7035-7045.
28. Bal, S. A.; Marfat, A.; Helquist, P. *J. Org. Chem.* **1982**, *47*, 5045 – 5050.
29. Tsuji, J.; Nagashima, H.; Nemoto, H. *Org. Synth.* **1984**, *62*, 9 – 13.
30. Morrison, H.; Danishefsky, S.; Yates, P. *J. Org. Chem.* **1961**, *26*, 2617-2618.
31. Kostitsyn, A. B.; Shulishov, E. V.; Tomilov, Y. V.; Nefedov, O. M. *Synlett* **1990**, , 713 – 714.
32. The reaction smelled strongly of bromobenzene, suggesting that the reaction worked, but under these conditions the halides decomposed.
33. (a) Corey, E. J.; Seebach, D. *Angew. Chem. Int. Ed. Engl.* **1965**, *4*, 1075 – 1077. (b) Corey, E. J.; Seebach, D. *J. Org. Chem.* **1975**, *40*, 231 – 237.
34. Appel, R. *Angew. Chem. Int. Ed. Engl.* **1975**, *14*, 801 – 811.
35. The cyclopropanation was not attempted directly with acid **57** because presumably the acid would react with diazofluorene by either protonating the carbene, or undergoing an O-H insertion reaction.
36. Belotti, D.; Cossy, J.; Pete, J. P.; Portella, C. *J. Org. Chem.* **1986**, *51*, 4196 – 4200.
37. (a) Tschugaeff, L. *Ber. Dtsch. Chem. Ges.* **1900**, *33*, 3118 – 3126. (b) Barton, D. H. R. *J. Chem. Soc.* **1949**, 2174 – 2178.
38. Kosicki, G. W.; Lipovac, S. N.; Annett, R. G. *Can. J. Chem.* **1964**, *42*, 2806 – 2810.
39. Brown, H. C.; Krishnamurthy, S. *J. Am. Chem. Soc.* **1972**, *94*, 7159 – 7161.

40. (a) For the Grignard-Wurtz reaction in general, see: Anteunis, M.; van Schoote, J. *Bull. des Soc. Chim. Belg.* **1963**, *72*, 787 – 796. (b) For the specific reaction of **73** to **75**, see: Leber, P. A.; Bogdan, A., R.; Powers, D., C.; Baldwin, J. E. *Tetrahedron* **2007**, *63*, 6331 – 6338.
41. (a) For the original Claisen reaction, see: Claisen, L. *Chem. Ber.* **1912**, *45*, 3157 – 3166. (b) For a similar reaction to **77** to **78**, see: Takanami, T.; Hayashi, M.; Iso, K.; Nakamoto, H.; Suda, K. *Tetrahedron* **2006**, *62*, 9467 – 9474.
42. Abad, A.; Agullo, C.; Cunat, A. C.; de Alfonso Marzal, I.; Navarro, I.; Gris, A. *Tetrahedron* **2006**, *62*, 3266 – 3283.
43. The conjugate addition of Grignard reagents to ketones is uncommon, but can occur when the ketone is in a strange electronic environment, such as being near several aromatic rings. For instance, see (a) Cooke, R. G.; Edwards, J. M. *Aust. J. Chem.* **1975**, *28*, 1053 – 1057. (b) Wehbe, M.; Lepage, L.; Lepage, Y.; Platzer, N. *Bull. Soc. Chim. Fr.* **1987**, 309 – 317.
44. Schlosser, M.; Strunk, S. *Tetrahedron Lett.* **1984**, *25*, 741 – 744.
45. Hodgson, D. M.; Chung, Y. K.; Paris, J. M. *Pract. Synth. Proc.* **2005**, *13*, 2264 – 2266.
46. Hixson, S. S.; Mariano, P. S.; Zimmerman, H. E. *Chem. Rev.* **1973**, *73*, 531 – 551.
47. Plieninger, H.; Ege, G.; Ullah, M. I. *Chem. Ber.* **1961**, *96*, 1610 – 1617.
48. Not to be confused with the Wittig or Horner-Wadsworth-Emmons reactions, which involve phosphonium salts and phosphonates respectively. The latter is confusingly sometimes called the Horner-Wittig reaction. Horner, L.; Hoffmann, H.; Wippel, H. G.; Klahre, G. *Chem. Ber.* **1959**, *92*, 581 – 601.
49. Julia, M.; Paris, J. M. *Tetrahedron Lett.* **1973**, *14*, 4833 – 4836.
50. Tebbe, F. N.; Parshall, G. W.; Reddy, G. S. *J. Am. Chem. Soc.* **1978**, *100*, 3611 – 3613.
51. A drawback of the Tebbe reagent is that it is considerably more air-sensitive than phosphonium ylides. In this case, it was confirmed that the Tebbe reagent was active by the vigorous way the reaction quenched at the end, suggesting that it simply did not react with ketones **74** and **94**.
52. Scholl, M.; Ding, S.; Lee, C. W.; Grubbs, R. H. *Org. Lett.* **1999**, *1*, 953 – 956.

53. Barton, D. H. R.; McCombie, S. W. *J. Chem. Soc. Perkin Trans. 1* **1975**, 1574 – 1585.
54. That structure has simply been omitted from Figures 3.20 and 3.21 for lack of space
55. Bürgi, H.-B.; Dunitz, J. D.; Lehn, J. M.; Wipff, G. *Tetrahedron* **1974**, *30*, 1563 – 1572.
56. Schinzer, D.; Solyom, S.; Becker, M. *Tetrahedron Lett.* **1985**, *26*, 1831 – 1834.

## CHAPTER 3

### EXPERIMENTAL SECTION FOR CHAPTER 2

#### 3.1 General Experimental

Moisture-sensitive and oxygen-sensitive reactions were carried out in glassware that was oven-dried and if necessary dried with a heat gun under reduced pressure. These reactions were performed either on a Schlenk line, bubbler, or under a balloon, depending on the sensitivity. All reactions were performed under a nitrogen atmosphere unless otherwise stated. Sensitive reagents were added using standard syringe techniques. Unless otherwise stated, all reactions were done with magnetic stirring and solvents were removed using a rotary evaporator at the automatically selected pressure, and if necessary under a high vacuum (<1 mbar). Solvents were degassed by the freeze-pump-thaw method using three cycles.

Reagents and solvents. Ether refers to diethylether, petrol refers to petroleum ether fraction 40° C–60° C. All reagents were purchased from Aldrich, Acros, or Alfa Aesar. THF, diethylether, and DCM were used from an MBraun SPS-800 solvent purification system. Other anhydrous solvents were purchased anhydrous from Acros over molecular sieves. Diisopropylamine was distilled from potassium hydroxide and used immediately. Triethylamine was distilled from calcium hydride and stored over potassium hydroxide. Pyridine was distilled from calcium hydride and stored under nitrogen. DMPU was distilled under reduced pressure from calcium hydride and stored away from light. The following reagents were bought as solutions: *n*-BuLi (2.6 M / hexane), lithium aluminium hydride (1.0 M / THF), vinyl magnesium bromide (0.7 M / THF), K-selectride (1.0 M / THF), and KHMDS (0.5 M / toluene). NMR solvents were used as bought. All aqueous solutions were saturated unless otherwise stated. Brine refers to saturated sodium chloride.

#### 3.2 Instrumentation

<sup>1</sup>H NMR and <sup>13</sup>C NMR spectra were obtained from a Bruker DPX 400 or DPX 500 spectrometer operating at the appropriate frequencies. <sup>1</sup>H NMR and <sup>13</sup>C NMR spectra were referenced to the internal solvent lock for chloroform-*d* (<sup>1</sup>H 7.26 ppm downfield from TMS, <sup>13</sup>C 77.2 ppm downfield from TMS). DEPT, COSY, NOESY, HSQC, and HMBC experiments were used to confirm assignments when necessary. All *J* values are in Hz.  $\delta$  values are reported in ppm downfield from TMS.

Infrared spectra were obtained using either a Perkin-Elmer 1600 Series IR or a Smiths Detection IdentifyIR. Samples were prepared as thin films on sodium chloride plates or applied directly to the diamond tip respectively. IR frequencies are reported in  $\text{cm}^{-1}$ .

Low-resolution GC/MS was obtained on a Perkin-Elmer Autosystem XL-GC / TurboMass GC/MS using a Supelco SLB fused silica capillary column (30m x 0.32 mm x 0.3  $\mu\text{m}$ ). High resolution MS was obtained on a Water LCT Premier XE MS. MS  $m/z$  is reported in  $\text{g mol}^{-1}$ .

X-ray crystallography was obtained from Dr Benson Kariuki at Cardiff University.

Thin-layer chromatography was performed using Merck 60 F<sub>254</sub> aluminium-backed plates. Plates were visualised by visual inspection, UV light (254 nm), anisaldehyde stain, permanganate stain, or ceric ammonium molybdate stain. Anisaldehyde stain was prepared from anisaldehyde (15 mL), ethanol (250 mL), and sulphuric acid (2.5 mL). Permanganate stain was prepared from potassium permanganate (1 g), sodium carbonate (2 g) and water (100 mL). Ceric ammonium molybdate stain was prepared from ceric ammonium molybdate (4 g), ammonium molybdate (10 g), sulphuric acid (40 mL) and water (360 mL).

Column chromatography was done as flash chromatography using silica gel (60 Å, 35–70  $\mu\text{m}$  particle size). Columns were packed as slurries in eluent and run using positive pressure from bellows, except for those mixtures not soluble in the eluent, in which case the mixture was preloaded on dry silica gel and poured into the column.

Melting points were determined using a Stuart Scientific SMP1 melting point apparatus and are uncorrected.

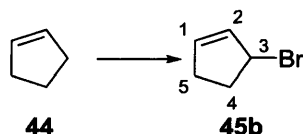
Photochemical reactions were performed with a Photochemical Reactors Ltd 400W water-jacket-cooled medium pressure mercury vapour lamp.

Chemical names were generated using ChemDraw.

Calculations were run using either the Gaussian03 suite of programmes<sup>1</sup>, GAMESS-US<sup>2</sup> or MOLPRO<sup>3</sup>. Pertinent information such as Cartesian coordinates and energies can be found at the end of this chapter.

### 3.3 Experimental Procedures

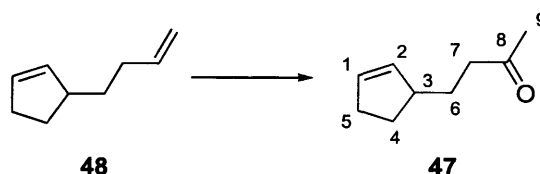
#### 3-Bromocyclopentene **45b**<sup>5</sup>



A solution of cyclopentene (0.65 mL, 7.35 mmol), NBS (1.4 g, 7.70 mmol), benzoyl peroxide (90 mg, 0.367 mmol) in cyclohexane (30 mL) was heated to 80 °C for 1 h and then allowed to cool. Most of the solvent and unreacted cyclopentene were removed by rotary evaporation and the product was filtered through glass wool. The solution of bromide **45b** in cyclohexane was immediately used in the next step and was found to degrade rapidly even if stored at -20 °C. Because of this instability, further characterisation could not be carried out. Spectroscopic data agreed with literature values.<sup>5</sup>

<sup>1</sup>H NMR (400 MHz, CDCl<sub>3</sub>): δ 6.05 (2H, m, H1,H2), 5.17 (1H, m, H3), 2.68 – 2.57 (1H, m, one of H4',H5'), 2.41 – 2.32 (3H, m, three of H4,H4',H5,H5').

#### 4-(Cyclopent-2-enyl)butan-2-one **47**



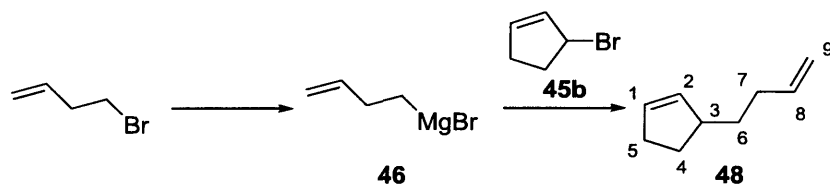
Diene **48** (170 mg, 1.39 mmol), copper (I) chloride (150 mg, 1.52 mmol) and palladium (II) chloride (50 mg, 0.282 mmol) were dissolved DMF (2.2 mL) and water (0.3 mL) at RT. The solution was stirred for 18 hours while exposed to the air. When the reaction was deemed complete by TLC, it was quenched by adding 2M hydrochloric acid (30 mL) and ether (30 mL). The organic layer was washed with water (50 mL) and brine (50 mL). The organic layer was then dried with magnesium sulphate and concentrated to yield a clear oil. Flash chromatography on silica gel (1 : 9 diethyl ether : hexane) gave enone **47** (110 mg, 57%).

<sup>1</sup>H NMR (400 MHz, CDCl<sub>3</sub>) δ 5.75 – 5.61 (2H, m, H1,H2), 2.70 – 2.58 (1H, m, H3), 2.44 (2H, t, *J* = 7.8, H7,H7'), 2.36 – 2.20 (2H, m, H5,H5'), 2.15 (3H, s, H9,H9',H9''), 2.09 – 1.98 (1H, m, H4 or H6), 1.74 – 1.58 (2H, m, two of H4,H4',H6,H6'), 1.44 – 1.32 (1H, m, H4 or H6).

$^{13}\text{C}$  NMR (125 MHz,  $\text{CDCl}_3$ )  $\delta$  209.5 (C8), 134.4 (C1 or C2), 131.2 (C1 or C2), [45.0, 42.1, 32.2, 30.1, 29.9, 29.6, comprised of C3,C4,C5,C6,C7,C9].

IR 3051 (w, C=C-H), 2928 (m, C-H), 2854 (m, C-H), 1712 (s, C=O), 1410 (m), 1358 (s), 1165 (m).

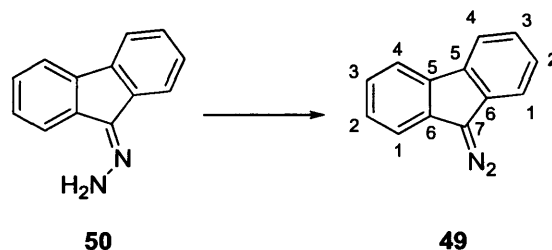
### 3-(But-3-enyl)cyclopent-1-ene **48**



Magnesium turnings (230 mg, 9.56 mmol) and iodine (1 crystal) were added to THF (9 mL). A solution of 4-bromo-1-butene (0.97 mL, 9.56 mmol) in THF (3 mL) was added dropwise at RT. The solution turned clear and spontaneously warmed over the course of a few minutes. After the exothermic reaction was over, the reaction was stirred at RT until all of the magnesium was gone. Then, a solution of the crude bromide **45b** in THF (3 mL) was added dropwise. The solution again spontaneously warmed and a clear precipitate began to form. After this exothermic reaction was over, the solution was stirred at RT for 2 h and quenched by pouring it into water (50 mL) and ether (50 mL). The organic layer was collected and washed with aqueous ammonium chloride (50 mL), water (50 mL), and brine (50 mL). The combined organic layer was then dried with magnesium sulphate and concentrated to yield a slightly brown coloured oil. Flash chromatography on silica gel (pentane) gave diene **48** (50 mg, 6% from cyclopentene).

$^1\text{H}$  NMR (400 MHz,  $\text{CDCl}_3$ )  $\delta$  5.77 – 5.75 (1H, m, H8), 5.66 – 5.60 (2H, m, H1, H2), 4.90 (2H, dd,  $J = 17.1, 7.1$ , H9, H9'), 2.63 – 2.55 (1H, m, H3), 2.28 – 2.19 (2H, m, either H5, H5' or H7, H7'), 2.04 – 1.93 (2H, m, either H5, H5' or H7, H7'), 1.48 – 1.25 (4H, m, H4, H4', H6, H6').

### 9-Diazofluorene **49**<sup>4</sup>



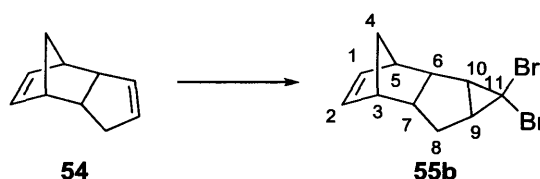
9-Diazofluorene (**49**) was prepared according to the method of Yates.<sup>4</sup> 9-fluorenone (500 mg, 2.58 mmol) and activated manganese dioxide (750 mg, 8.62 mmol) in chloroform (10 mL) was allowed to stand for 18 h. The reaction was monitored by IR. After 18 h, the remaining manganese dioxide was filtered out with glass wool and the filtrate was concentrated under reduced pressure by rotary evaporation to give 500 mg of 9-diazofluorene **49** (quantitative) as an orange powder. Some batches produced orange crystal plates.

<sup>1</sup>H NMR (500 MHz, CDCl<sub>3</sub>) δ 7.85 (2H, d, *J* = 7.8, 2x H1), 7.41 (2H, d, *J* = 7.6, 2x H4), 7.29 (2H, td, *J* = 7.7, 1.0, 2x H2), 7.23 (2H, td, *J* = 7.6, 1.0, 2x H3).

<sup>13</sup>C NMR (125 MHz, CDCl<sub>3</sub>) δ 133.0 (2x C6), 131.5 (2x C5), 126.4 (2x C2), 124.5 (2x C3), 121.0 (2x C1), 119.3 (2x C4), 67.0 (C7).

IR : 2064 (diazo stretch).

### 4,4-Dibromotetracyclo[6.2.1.0<sup>2,7</sup>.0<sup>3,5</sup>]undec-9-ene **55b**<sup>5</sup>

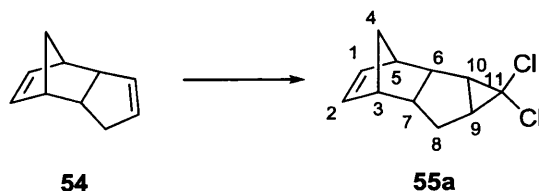


Dibromide **55b** was synthesised according to the method of Nefedov.<sup>5</sup> Dicyclopentadiene (1.5 mL, 11.2 mmol) and 50% sodium hydroxide solution (10 mL) were added to DCM (150 mL) at RT. Benzyltriethylammonium chloride (25 mg) and bromoform (1.5 mL, 17.1 mmol) were added and the solution was refluxed for 60 hours while being monitored by TLC. After cooling to RT, the solution was washed with water (2x 100 mL, dried with magnesium sulphate, and concentrated. Flash chromatography on silica gel (pentane) gave dibromide **55b** (2.44 g, 72%).

<sup>1</sup>H NMR (400 MHz, CDCl<sub>3</sub>) δ 6.00 – 5.90 (2H, m, H1,H2), [3.64 – 3.62 (1H, m), 3.23 – 3.18 (2H, m), 2.95 – 2.92 (1H, m), 2.80 – 2.67 (2H, m), 2.22 – 2.13 (1H, m), 1.44 (1H,

d, 7.8 Hz), these are comprised of H3,H4,H4',H5,H6,H7,H8,H8'], 1.32 – 1.20 (2H, m, H9,H10).

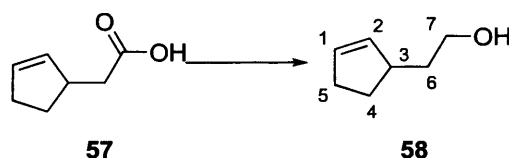
#### 4,4-Dichlorotetracyclo[6.2.1.0<sup>2,7</sup>.0<sup>3,5</sup>]undec-9-ene **55a**<sup>5</sup>



This compound was synthesised analogously to dibromide **55b** by adding chloroform (1.3 mL, 16.8 mmol) instead of bromoform, and by using the same amounts of all other reagents. Flash chromatography on silica gel (pentane) gave dichloride **55a** (2.13 g, 89%). Spectroscopic data agreed with literature values.<sup>5</sup>

<sup>1</sup>H NMR (400 MHz, CDCl<sub>3</sub>) δ 6.19 – 6.12 (2H, m, H1,H2), [2.98 – 2.96 (1H, m), 2.88 – 2.79 (1H, m), 2.74 – 2.72 (1H, m), 2.58 – 2.49 (1H, m), 1.94 – 1.83 (1H, m), 1.74 (1H, d, 7.6 Hz), these are comprised of all but two of H3,H4,H4',H5,H6,H7,H8,H8'], 1.59 – 1.49 (3H, m, H9, H10, and one of H3,H4,H4',H5,H6,H7,H8,H8'), 1.36 (1H, d, 8.2 Hz, one of H3,H4,H4',H5,H6,H7,H8,H8').

#### 2-(Cyclopent-2-enyl)ethanol **58**<sup>6</sup>



2-(Cyclopent-2-enyl)ethanol **58** was synthesised according to the method of Salomon.<sup>6</sup> A solution of 2-(cyclopent-2-enyl)acetic acid **57** (5 mL, 41.55 mmol) in THF (90 mL) was added to a solution of lithium aluminium hydride in THF (36 mL, 36 mmol) at 0 °C. Once bubbling ceased (after ~5 – 10 minutes), the solution was allowed to warm to RT and then refluxed for 2.5 h. The reaction was cooled to RT and quenched by carefully adding water (15 mL). The organic layer was separated and then washed with 10% sodium hydroxide (15 mL) and then brine (15 mL). The organic layer was dried with magnesium sulphate and concentrated. Flash chromatography on silica gel (1 : 1 ether : petrol) afforded alcohol **58** (2.99 g, 68%) as a pale yellow oil with an odour reminiscent of potatoes.

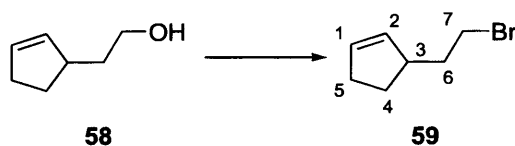
<sup>1</sup>H NMR (400 MHz, CDCl<sub>3</sub>) δ 5.69 – 5.65 (1H, m, H1 or H2), 5.64 – 5.60 (1H, m, H1 or H2), 3.71 – 3.58 (2H, m, H7,H7'), 2.76 – 2.65 (1H, m, H3), 2.34 – 2.16 (2H, m,

H<sub>5</sub>,H<sub>5'</sub>), 2.00 (1H, dtd, *J* = 12.8, 8.5, 4.5, H<sub>4</sub>), 1.68 – 1.59 (1H, m, H<sub>6</sub>), 1.56 – 1.47 (1H, m, H<sub>6'</sub>), 1.41 – 1.33 (1H, m, H<sub>4'</sub>), 1.23 – 1.18 (1H, broad s, OH).

<sup>13</sup>C NMR (125 MHz, CDCl<sub>3</sub>) δ 134.7 (C1 or C2), 130.7 (C1 or C2), 61.9 (C7), 42.2 (C3), 38.9 (C6), 32.0 (C5), 29.8 (C4).

IR: 3330 (br, C–H), 2928 (s, C–H) 2850 (s, C–H), 1057 (s).

### 3-(2-Bromoethyl)cyclopent-1-ene **59**<sup>6</sup>

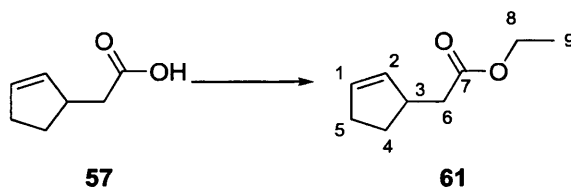


A solution of alcohol **58** (250 mg, 2.24 mmol) and triphenylphosphine (650 mg, 2.45 mmol) was dissolved in DCM (5 mL) at –30 °C. NBS (440 mg, 2.45 mmol) was added in 3 portions over 20 min. The solution was slowly warmed to RT and stirred for 21 h. The reaction was monitored by NMR and appeared to be ~90% complete by the end of the reaction time. The solution was then diluted with ether (15 mL) and the suspended material (triphenylphosphine oxide) was filtered off and the filtrate was concentrated. Purification of the crude material by flash chromatography on silica gel (petroleum ether) was attempted, but bromide **59** was unable to be satisfactorily separated from solvents under reduced pressure. Spectroscopic data agreed with literature values.<sup>6</sup>

<sup>1</sup>H NMR (400 MHz, CDCl<sub>3</sub>) δ 4.65 – 4.62 (1H, m, H<sub>1</sub> or H<sub>2</sub>), 4.54 – 4.51 (1H, m, H<sub>1</sub> or H<sub>2</sub>), 3.40 – 3.33 (2H, m, H<sub>7</sub>,H<sub>7'</sub>), 3.30 – 3.02 (3H, m, H<sub>5</sub>,H<sub>5'</sub>,H<sub>4</sub>), 2.88 – 2.64 (2H, m, H<sub>3</sub>,H<sub>4'</sub>), 1.58 – 1.33 (2H, m, H<sub>6</sub>,H<sub>6'</sub>).

IR: 2958 (m, C–H), 2936 (m, C–H), 2869 (m, C–H), 1436 (m), 1265 (s), 1165 (s)

### Ethyl 2-(cyclopent-2-enyl)acetate **61**<sup>8</sup>



2-(Cyclopent-2-enyl)acetic acid **57** (8.38 g, 66.3 mmol) and sulphuric acid (0.5 mL) in absolute ethanol (100 mL) were refluxed (90 °C) for 24 hours. After cooling down to RT, the reaction was diluted with water(40 mL) and ether (100 mL). The aqueous layer was extracted with ether (50 mL), and the combined organic layers

were washed with aqueous sodium bicarbonate until the aqueous layer was neutral (50 mL). The organic layer was then washed with brine (80 mL), dried over magnesium sulphate and concentrated. Flash chromatography on silica gel (1 : 19 ether : petroleum ether) yielded ester **61** as an extremely fruity smelling yellow oil (7.87 g, 76.8%). Spectroscopic data agreed with literature values.<sup>8</sup>

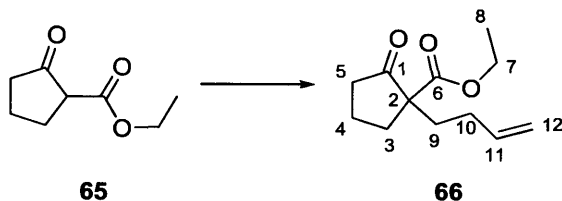
<sup>1</sup>H NMR (400 MHz, CDCl<sub>3</sub>) δ 5.75 – 5.72 (1H, m, H1 or H2), 5.65 – 5.62 (1H, m, H1 or H2), 4.11 (2H, q, *J*=7.1, H8,H8'), 3.05 (1H, dtt, *J* = 12.6, 8.3, 2.2, H3), 2.37 – 2.21 (4H, m, H5,H5',H6,H6'), 2.13 – 2.04 (1H, m, H4), 1.49 – 1.39 (1H, m, H4'), 1.21 (3H, t, *J* = 7.1, H9,H9',H9'').

<sup>13</sup>C NMR (125 MHz, CDCl<sub>3</sub>) δ 172.9 (C7), 133.7 (C1 or C2), 131.4 (C1 or C2), 60.1 (C8), 42.1 (C3), 40.4 (C4 or C6), 31.8 (C4 or C6), 29.6 (C5), 14.2 (C9).

IR: 2981 (w, C–H), 2940 (w, C–H), 1734 (s, C=O), 1258 (m), 1172 (s), 1031 (m)

HRMS (EI) for C<sub>9</sub>H<sub>14</sub>O<sub>2</sub> *m/z* Found: 155.1069, Required: 155.1072

#### Ethyl 1-(but-3-enyl)-2-oxocyclopentanecarboxylate **66**<sup>9</sup>

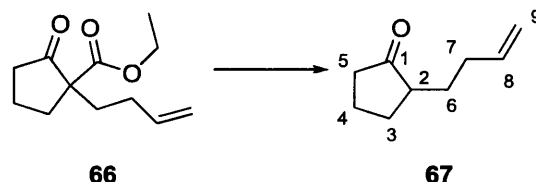


Oxo-ester **66** was synthesised according to the method of Portella<sup>9</sup>. Ethyl 2-oxocyclopentanecarboxylate **65** (5.0 mL, 33.7 mmol) was added to a solution of <sup>t</sup>BuOK (3.9 g, 34.8 mmol) in anhydrous DMSO (125 mL) at RT. After 1 h, 4-bromo-1-butene (3.75 mL, 36.9 mmol) was added and the solution was stirred at RT for 20 h. The reaction was then diluted with water (100 mL) and extracted with ethyl acetate (3 x 50 mL). The organic layer was dried over magnesium sulphate and concentrated. Flash chromatography on silica gel (1 : 9 ethyl acetate : hexane) yielded oxo-ester **66** as a yellow fruity-smelling oil (3.16 g, 49%). Subsequent batches of crude material were deemed pure enough to use without chromatography. Spectroscopic data agreed with literature values.<sup>9</sup>

<sup>1</sup>H NMR (400 MHz, CDCl<sub>3</sub>) δ 5.73 – 5.63 (1H, m, H11), 4.97 – 4.86 (2H, m, H12,H12'), 4.14 – 4.03 (2H, m, H7,H7'), 2.51 – 2.42 (1H, m, H5), 2.41 – 2.30 (1H, m, H4) 2.26 – 2.18 (1H, m, H4'), 2.11 – 1.99 (1H, m, H10), 1.97 – 1.70 (5H, m, H3,H3',H5',H9,H10'), 1.62 – 1.52 (1H, m, H9'), 1.19 (3H, td, *J* = 7.2, 1.8, H8,H8',H8''),

$^{13}\text{C}$  NMR (125 MHz,  $\text{CDCl}_3$ )  $\delta$  214.8 (C1), 170.8 (C6), 137.6 (C11), 115.0 (C12), 61.3 (C7), 60.2 (C2) 37.9 (C4), 33.0 (C5), 32.8 (C9), 29.1 (C10), 19.6 (C3), 14.1 (C8).

### 2-(But-3-enyl)cyclopentenone **67**<sup>9</sup>



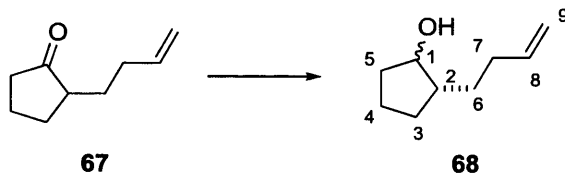
A solution of ethyl 1-(but-3-enyl)-2-oxocyclopentanecarboxylate **66** (10 g, 47.2 mmol) in ethanol (20 mL) and water (100 mL) was basified to pH 12 with 15% sodium hydroxide solution and stirred for 16 h at RT. Then the solution was acidified to pH 2 with 2M hydrochloric acid and the solution was heated at 65 °C for 5 d. In some cases, bubbles were seen at this point. The reaction mixture was basified with sodium bicarbonate to pH 8 and extracted with ether (3 x 75 mL). The combined organic layers were dried over magnesium sulphate and concentrated. Flash chromatography on silica gel (3 : 17 ether : hexane) yielded ketone **67** as a pale yellow oil (1.70 g, 26%). Spectroscopic data agreed with literature values.<sup>9</sup>

$^1\text{H}$  NMR (400 MHz,  $\text{CDCl}_3$ )  $\delta$  5.84 – 5.68 (1H, m, H8), 5.03 – 4.86 (2H, m, H9,H9'), 2.39 – 2.23 (2H, m, two of H4,H4',H5,H5'), 2.21 – 1.98 (4H, m, H2,H3, and two of H4,H4',H5,H5'), 1.96 – 1.87 (1H, m, H7), 1.84 – 1.76 (1H, m, H7'), 1.61 – 1.50 (1H, m, H6), 1.43 – 1.33 (1H, m, H3'), 1.32 – 1.26 (1H, m, H6'),

$^{13}\text{C}$  NMR (125 MHz,  $\text{CDCl}_3$ )  $\delta$  138.1 (C8), 115.1 (C9), 48.5 (C2), 38.2 (C4 or C5), 31.7 (C4 or C5), 29.6 (C3), 28.8 (C6), 20.8 (C7), C1 not seen.

IR 2951 (w, C–H), 1735 (s, C=O), 1437 (w), 1168 (w).

### 2-(But-3-enyl)cyclopentanol **68**<sup>10</sup>

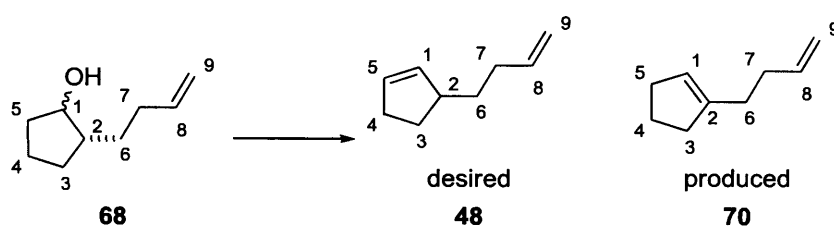


A solution of K-selectride solution in THF (20 mL, 20.0 mmol) was added dropwise to a solution of 2-(but-3-enyl)cyclopentenone **67** (1.7 g, 12.3 mmol) in anhydrous THF (100 mL) at 0 °C. After 1 h the reaction was warmed to RT and 30% hydrogen peroxide (15 mL) was added carefully. The mixture was poured into aqueous

ammonium chloride and extracted with ether, then washed with saturated sodium thiosulphate, and brine. The organic layer was dried over magnesium sulphate and concentrated under reduced pressure. Flash chromatography on silica gel (1 : 3 ether : hexane) yielded alcohol **68** as a colourless oil (297 mg, 17%). Crystallisation attempts (after esterifying with triphenylacetic acid) to determine the stereochemistry were unsuccessful. Subsequent chemistry (see below) implied that the reaction was either not stereoselective or was selective for the undesired *anti*-diastereomer, and further analysis was not carried out.

$^1\text{H}$  NMR (400 MHz,  $\text{CDCl}_3$ )  $\delta$  5.84 – 5.72 (1H, m, H8), 4.95 (1H, dd,  $J=18.7, 1.7$ , H9<sub>cis</sub>), 4.88 (1H, dd,  $J=10.2, 1.7$ , H9<sub>trans</sub>), 4.12 – 4.08 (1H, m, H1), 2.22 – 2.15 (1H, m, H2), 1.68 – 1.10 (10H, m, H3,H3',H4,H4',H5,H5',H6,H6',H7,H7'), the OH was not seen but was possibly underneath the HOD signal.

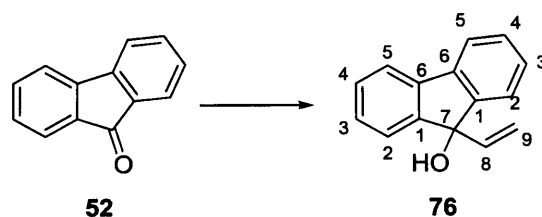
#### 1-(But-3-enyl)cyclopent-1-ene **70**.



DBU (600  $\mu\text{L}$ , 4.02 mmol) was added to a solution of 2-(But-3-enyl)cyclopentanol (500 mg, 3.57 mmol) in anhydrous DMSO (10 mL), resulting in a pale yellow solution. After 1 h carbon disulphide (230  $\mu\text{L}$ , 4.02 mmol) was added, resulting in a purple solution. After 1.5 h, methyl iodide (475  $\mu\text{L}$ , 7.63 mmol) was added, resulting in a light brown solution. After 1 h, DCM (10 mL) was added and the mixture was washed with brine. The organic layer was dried over magnesium sulphate and concentrated under reduced pressure. The crude material was then heated to 190  $^\circ\text{C}$  for 3.5 h. After cooling down, the residue was dissolved in hexane for flash chromatography on silica gel (hexane) to yield a colourless oil (48 mg, 11%). NMR analysis showed the product had four vinyl protons rather than five, indicating this was the undesired regioisomer for the double bond. No further characterisation was undertaken.

$^1\text{H}$  NMR (400 MHz,  $\text{CDCl}_3$ )  $\delta$  5.86 (1H, t,  $J=4.5$ , H1), 5.76 – 5.69 (1H, m, H8), 4.95 (1H, dd,  $J=17, 1.7$ , H9<sub>cis</sub>), 4.87 (1H, dd,  $J=10.2, 0.8$ , H9<sub>trans</sub>), 2.05 – 1.40 (10H, m, H3,H3',H4,H4',H5,H5',H6,H6',H7,H7').

### 9-Vinyl-9H-fluoren-9-ol **76**<sup>11</sup>



Vinyl magnesium bromide solution in THF (5 mL, 7.5 mmol) was added to a solution of 9-fluorenone **52** (900 mg, 5.0 mmol) in THF (10 mL) at 0 °C. After 3 h, saturated ammonium chloride was added and the mixture was extracted with ether. The organic layer was dried over magnesium sulphate and concentrated. Flash chromatography on silica gel (1 : 19 ethyl acetate : hexane) gave alcohol **76** as a pale yellow powder (945 mg, 91%). Spectroscopic data agreed with literature values.<sup>11</sup>

<sup>1</sup>H NMR (400 MHz, CDCl<sub>3</sub>) δ 7.55 (d, 2H, *J* = 7.4, 2x H4), 7.43 (d, 2H, *J* = 7.4, 2x H1), 7.31 (t, 2H, *J* = 7.4, 2x H3), 7.25 (t, 2H, *J* = 7.4, 2x H2), 5.96 (dd, 1H, *J* = 17.1, 10.6, H8), 5.49 (dd, 1H, *J* = 17.1, 1.3, H<sub>9cis</sub>), 5.18 (dd, 1H, *J* = 10.6, 1.3, H<sub>9trans</sub>), 2.10 (br s, 1H, OH).

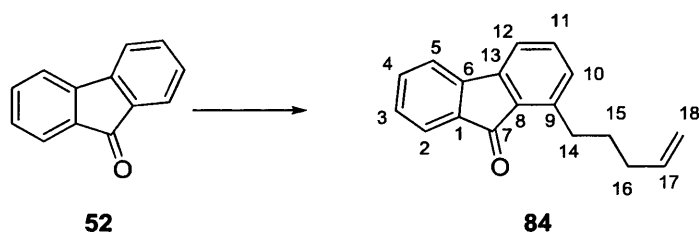
<sup>13</sup>C NMR (125 MHz, CDCl<sub>3</sub>) δ 148.0 (C1), 139.5 (C6), 139.1 (C8), 129.2 (C4), 128.2 (C3), 124.5 (C2), 120.2 (C5), 113.5 (C9), 82.5 (C7).

Melting point: 90 – 92 °C (lit. 90 – 91 °C).

IR 3278 (br, O–H), 3050 (w, C–H), 1448 (m), 1031 (s).

HRMS (EI) for C<sub>15</sub>H<sub>12</sub>O *m/z* Found: 208.0882, Required: 208.0888.

### 1-(Pent-4-enyl)-9H-fluoren-9-one **84**



Magnesium turnings (100 mg, 4.17 mmol) and iodine (1 crystal) were added to THF (5 mL). A solution of 5-bromo-1-butene (500 μL, 4.17 mmol) in THF (5 mL) was added dropwise at RT. The solution turned clear and spontaneously warmed over the course of a few minutes. After the exothermic reaction was over, the reaction was stirred at RT until all of the magnesium was gone (30 m). Then, a solution of the crude fluorenone **52** (500 mg, 2.78 mmol) in THF (5 mL) was added dropwise. The solution again spontaneously warmed and a clear precipitate began to form. After this

exothermic reaction was over, the solution was stirred at RT for 16 h and quenched by adding ammonium chloride solution (20 mL) and ether (20 mL). The organic layer was washed with brine (50 mL). The organic layer was then dried with magnesium sulphate and concentrated to yield a slightly brown coloured oil. Flash chromatography on silica gel (pentane) gave a white residue that was subsequently identified as ketone **84** (10 mg, 2%). The remainder of the material was comprised of unreacted fluorenone. The formation of the Grignard reagent was confirmed by titration against anisaldehyde.

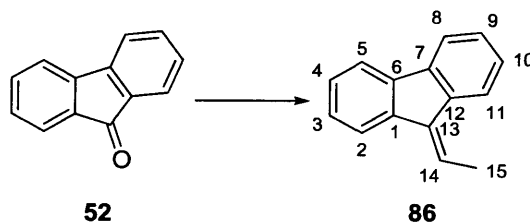
$^1\text{H}$  NMR (500 MHz,  $\text{CDCl}_3$ )  $\delta$  7.65 (1H, dt,  $J = 7.3, 0.8$ , H2), 7.51 (1H, d,  $J = 7.3$ , H5), 7.47 (1H, td,  $J = 7.4, 1.1$ , H4), 7.38 – 7.34 (2H, m, C11(H), C12(H)), 7.29 (1H, dd,  $J = 7.4, 1.1$ , H3), 7.07 (1H, dd,  $J = 6.0, 2.7$ , H10), 5.90 (1H, ddt,  $J = 17.1, 10.2, 6.3$ , H17), 5.07 (1H, dq,  $J = 17.1, 1.6$ , H18<sub>cis</sub>), 5.02 (1H, d quin,  $J = 10.2, 1.2$ , H18<sub>trans</sub>), 3.08 (2H, t,  $J = 7.8$ , H14, H14'), 2.20 (2H, tdt,  $J = 7.4, 6.3, 1.1$ , H16, H16''), 1.77 (2H, tt,  $J = 7.8, 7.4$ , H15, H15').

$^{13}\text{C}$  NMR (125 MHz,  $\text{CDCl}_3$ )  $\delta$  195.8 (C7), 145.6 (C13), 144.6 (C1), 144.2 (C9), 138.6 (C17), 135.1 (C8), 134.4 (C4), 134.1 (C11 or C12), 131.1 (C10), 128.9 (C3), 125.1 (C6), 123.9 (C2), 120.0 (C5), 118.1 (C11 or C12), 114.7 (C18), 33.6 (C16), 30.9 (14), 29.9 (C15).

IR 2923 (w, C–H), 1705 (s, C=O). 1608 (m), 1453 (m).

HRMS (EI) for  $\text{C}_{18}\text{H}_{16}\text{O}$   $m/z$  Found: 248.1201, Required: 248.1201.

### 9-Ethylidene-9H-fluorene **86**<sup>12</sup>



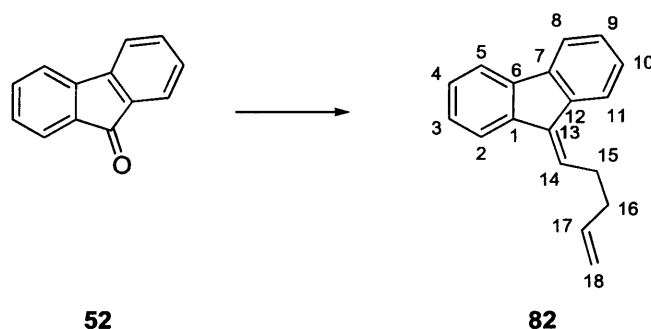
A solution of *n*-BuLi in hexanes (13.3 mL, 33.3 mmol) was added to ethyltriphenylphosphonium bromide (15.0g, 40.4 mmol) in THF (100 mL) at 0 °C. After 30 m, a solution of 9-fluorenone **52** (5.0 g, 27.8 mmol) in THF (100 mL) was added at 0 °C and the solution was warmed to RT. After 24 h, the mixture was diluted with saturated ammonium chloride (200 mL) and extracted with ether (200 mL). The organic layer was dried over magnesium sulphate and concentrated. Flash chromatography on silica gel (hexane) yielded alkene **86** as a white powder (3.44 g, 64%). Spectroscopic data agreed with literature values.<sup>12</sup>

$^1\text{H}$  NMR (400 MHz,  $\text{CDCl}_3$ )  $\delta$  7.82 (1H, d,  $J = 7.2$ , H11), 7.70 (1H, d,  $J = 6.4$ , H5), 7.63 (1H, d,  $J = 6.4$ , H8), 7.56 (1H, d,  $J = 8.8$ , H2), 7.32 – 7.17 (4H, m, H3,H4,H9,H10), 6.81 (1H, q,  $J = 7.6$ , H14), 2.55 (3H, d,  $J = 7.6$ , H15,H15',H15'').

$^{13}\text{C}$  NMR (125 MHz,  $\text{CDCl}_3$ )  $\delta$  140.8 (C12), 139.4 (C7), 138.5 (C1), 137.7 (C6), 136.6 (C13), 127.6 (C10), 127.3 (C3), 126.9 (C4), 126.9 (C9), 125.1 (C11), 124.8 (C14), 119.8 (C5), 119.6 (C2), 119.5 (C8), 15.3 (C15).

Melting point: 51 – 53 °C (lit. 53 – 54 °C).

### 9-(Pent-4-enylidene)-9H-fluorene **82**



9-(Pent-4-enylidene)-9H-fluorene **82** was prepared similarly to **86**, except using the following amounts of reagents: Pent-4-enyltriphenylphosphonium bromide **83** (4.8 g, 11.7 mmol) in THF (30 mL), BuLi solution (4 mL, 10.0 mmol), 9-fluorenone (1.5 g, 8.0 mmol) in THF (30 mL). Extraction amounts were scaled down by a factor of 3. Flash chromatography on silica gel (1 : 19 ether : hexane) yielded diene **82** as a yellow powder (1.37 g, 65%).

$^1\text{H}$  NMR (400 MHz,  $\text{CDCl}_3$ )  $\delta$  7.86 (1H, d,  $J = 7.5$ , H11), 7.75 (1H, d,  $J = 7.3$ , H5), 7.65 (1H, d,  $J = 7.3$ , H8), 7.59 (1H, d,  $J = 7.4$ , H2), 7.35 – 7.25 (4H, m, H3,H4,H9,H10), 6.85 (1H, t,  $J = 7.2$ , H14), 5.95 – 5.85 (1H, m, H17), 5.12 (1H, dd,  $J = 17.8, 1.3$ , H18<sub>cis</sub>), 5.01 (1H, dd,  $J = 11.5, 1.3$ , H18<sub>trans</sub>), 2.90 (2H, q,  $J = 7.4$ , H15,H15'), 2.40 (2H, m, H16,H16').

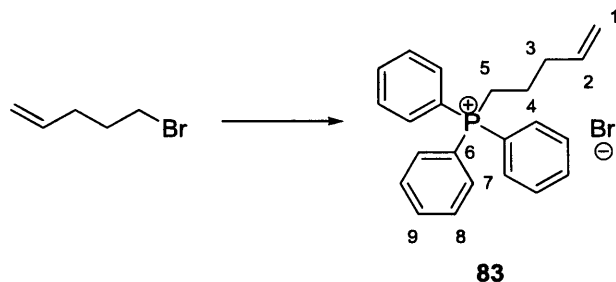
$^{13}\text{C}$  NMR (125 MHz,  $\text{CDCl}_3$ )  $\delta$  140.8 (C12), 139.3 (C7), 138.6 (C1), 137.7 (C17), 137.4 (C6), 135.7 (C13), 130.0 (C14), 127.8 (C3), 127.5 (C10), 126.9 (C4), 126.9 (C9), 125.0 (C11), 119.8 (C5), 119.7 (C2), 119.5 (C8), 115.6 (C18), 33.5 (C16), 28.5 (C15).

IR 3059 (m, C–H), 2977 (w, C–H), 2921 (m, C–H), 1640 (m), 1448 (s), 1198 (m), 912 (s), 729 (s).

HRMS (EI) for  $\text{C}_{18}\text{H}_{16}$   $m/z$  Found: 232.1252, Required: 232.1252.

Melting point: 65 – 66 °C.

### Pent-4-enyltriphenylphosphonium bromide **83**<sup>13</sup>



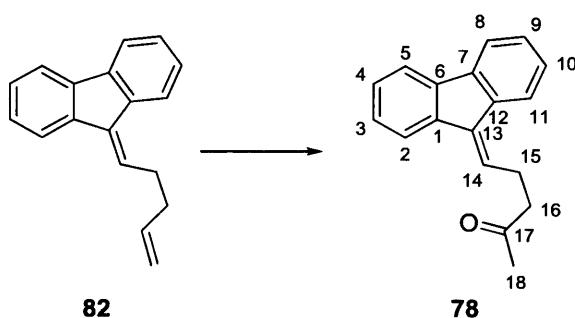
A solution of 5-bromo-1-pentene (3.3 mL, 27.8 mmol) and triphenylphosphine (7.5 g, 28.6 mmol) in toluene (50 mL) was heated to 95 °C for 3 d. Upon reaching that temperature, a precipitate of phosphonium salt **83** slowly formed. The solution was cooled and poured into petrol, and the precipitate was filtered out and dried to give a phosphonium salt **83** white powder (4.82 g, 42%) that was used immediately in the next step. Spectroscopic data agreed with literature values.<sup>13</sup>

<sup>1</sup>H NMR (400 MHz, CDCl<sub>3</sub>) δ 8.00 – 7.80 (9H, m, 6x H7, 3x H9), 7.72 – 7.65 (6H, m, 6x H8), 5.71 (1H, ddt, *J* = 17.0, 10.2, 6.7, H2), 5.05 (1H, dd, *J* = 17.1, 1.5, H1<sub>cis</sub>), 5.00 (1H, d, *J* = 10.2, H1<sub>trans</sub>), 3.89 – 3.80 (2H, m, H5, H5'), 2.44 (2H, q, *J* = 7.0, H3, H3'), 1.74 (2H, sextet, *J* = 7.0, H4, H4').

<sup>13</sup>C NMR (125 MHz, CDCl<sub>3</sub>) δ 136.4 (s, C2), 135.0 (d, *J* = 3, C9), 133.7 (d, *J* = 10, C7), 130.5 (d, *J* = 13, C8), 118.3 (d, *J* = 85, C6), 116.9 (s, C1), 33.8 (d, *J* = 16, C3), 21.9 (d, *J* = 50, C5), 21.8 (d, *J* = 4, C4).

Melting point: 191 – 193 °C (lit. 191 – 192 °C).

### 5-(9H-Fluoren-9-ylidene)pentan-2-one **78**



Diene **82** (1.75 g, 7.5 mmol), copper (I) chloride (1.0 g, 10.1 mmol), and palladium (II) chloride (300 mg, 1.69 mmol) were dissolved in DMF (30 mL) and water (5 mL). The solution was exposed to the air for 24 hours. When the reaction was deemed complete by TLC, it was quenched by adding 2M hydrochloric acid (250 mL) and ether (250 mL). The organic layer was washed with water (200 mL) and brine

(200 mL). The organic layer was dried over magnesium sulphate and concentrated. Flash chromatography on silica gel (1 : 3 ether hexane) yielded ketone **78** as a yellow powder (1.15 g, 62%).

$^1\text{H}$  NMR (400 MHz,  $\text{CDCl}_3$ )  $\delta$  7.88 (1H, d,  $J = 7.3$ , H11), 7.80 (1H, d,  $J = 7.0$ , H8), 7.75 (1H, d,  $J = 6.9$ , H2), 7.70 (1H, d,  $J = 7.2$ , H5), 7.44 – 7.28 (4H, m, H3,H4,H9,H10), 6.71 (1H, t,  $J = 7.3$ , H14), 3.09 (2H, q,  $J = 7.4$ , H15,H15'), 2.86 – 2.76 (2H, m, H16,H16'), 2.21 (3H, s, H18,H18',H18'').

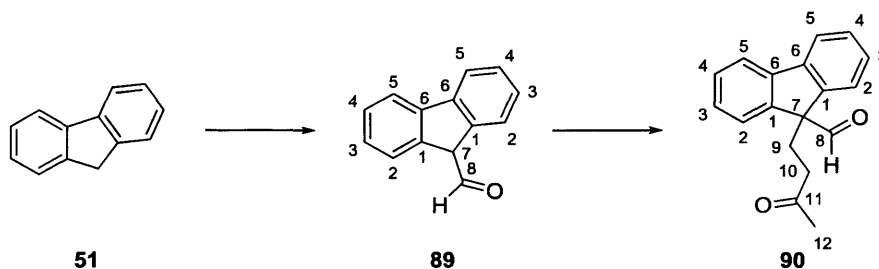
$^{13}\text{C}$  NMR (125 MHz,  $\text{CDCl}_3$ )  $\delta$  207.7 (C17), 140.9 (C12), 139.1 (C1), 138.9 (C6), 137.1 (C7), 136.2 (C13), 128.4 (C14), 128.0 (C10), 127.6 (C4), 127.1 (C9), 126.9 (C3), 125.0 (C11), 119.9 (C8), 119.8 (C5), 119.5 (C2), 43.1 (C16), 30.1 (C18), 23.3 (C15).

IR 3036 (w, C–H), 2991 (w, C–H), 1719 (s, C=O), 1428 (m), 1373 (m).

HRMS (EI) for  $\text{C}_{18}\text{H}_{16}\text{O}$   $m/z$  Found: 248.1200, Required: 248.1201.

Melting point: 120 – 123 °C.

### 9H-Fluorene-9-carbaldehyde **89** and 9-(3-oxobutyl)-9H-fluorene-9-carbaldehyde **90**<sup>14</sup>



According to the method of Pleininger,<sup>14</sup> ethyl formate (6.70 g, 90.0 mmol), fluorene **51** (15.0 g, 90.0 mmol) and potassium methoxide (6.30 g, 90.0 mmol) were refluxed in ether (75 mL) for 4 h. The yellow solution was cooled to RT and extracted with water (150 mL). The water was extracted into ether (150 mL) and acidified to pH 2 with dilute sulphuric acid. An oil formed above the water which was extracted with ether (150 mL). The organic later was dried over magnesium sulphate and concentrated to give a dark green oil that was vacuum distilled (170 °C, 2 mbar) to give aldehyde **89** as a green oil (5.94 g, 34%) that was used immediately due to stability problems. The structure was confirmed by low resolution GC-MS ( $m/z = 194$ ).

Aldehyde **89** (5.94 g, 30.6 mmol) and *t*-BuOK (342 mg, 3.06 mmol) were dissolved in *t*-BuOH (30 mL). MVK (2.5 mL, 30.6 mmol) was added dropwise through a dropping funnel. The temperature spontaneously rose to 35 °C and turned a brilliant

red. After the exotherm, the reaction was stirred at RT for 18 h. The solution was then diluted with ether (100 mL), cooled to 0 °C and washed with ice cold 1M sodium hydroxide (3x 30 mL). The organic layer was then warmed to RT and washed with water (30 mL), brine (30 mL), dried over magnesium sulphate and concentrated. Dione **90** was obtained as a white powder (6.83 g, 85%) was deemed pure enough to use in the next step without further purification.

<sup>1</sup>H NMR (500 MHz, CDCl<sub>3</sub>) δ 8.90 (1H, s, H8), 7.89 (2H, d, *J* = 7.5, 2x H5), 7.58 – 7.53 (2H, m, 2x H4), 7.47 – 7.28 (4H, m, 2x H2, 2x H3), 2.68 (2H, td, *J* = 6.2, 2.8, H9,H9'), 1.88 (3H, s, H12,H12',H12''), 1.82 (2H, td, *J* = 8.1, 2.8, H10,H10').

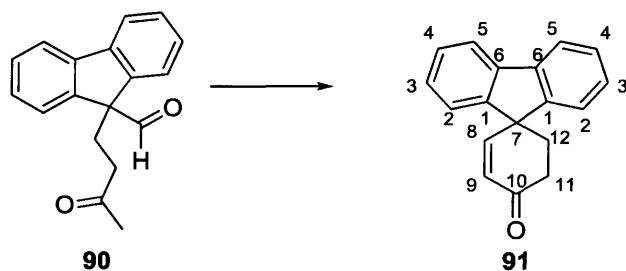
<sup>13</sup>C NMR (125 MHz, CDCl<sub>3</sub>) δ 208.0 (C11), 196.5 (C8), 142.5 (C6) 141.4 (C1), 129.1 (C4), 128.2 (C2), 125.0 (C3), 120.5 (C5), 66.7 (C7), 37.5 (C10), 29.8 (C12), 24.7 (C9).

IR 3063 (w, C–H), 2934 (w, C–H), 2813 (w, C–H), 2714 (w, O=C–H), 1715 (br s, appears to be two peaks overlapping, C=O), 1448 (s), 1366 (m), 1162 (m).

HRMS (EI) for C<sub>18</sub>H<sub>16</sub>O<sub>2</sub> *m/z* Found: 264.1159, Required: 264.1150.

Melting point: 132 – 135 °C.

#### Spiro[2-cyclohexene-1,9'-[9H]fluoren]-4-one **91**<sup>14</sup>



Dione **90** (6.83 g, 25.9 mmol), piperidine (250 μL, 2.59 mmol), and acetic acid (400 μL, 2.59 mmol) were dissolved in toluene (25 mL) and refluxed in a Dean-Stark trap for 4.5 h. Solvent was removed and the residue was dissolved in ether (50 mL). The organic layer was washed with 1M hydrochloric acid (50 mL), 1M sodium carbonate (50 mL) and brine (50 mL) and then dried over magnesium sulphate and concentrated. The residue was crystallised from EtOH to give enone **91** as a white powder (2.28 g, 36%). Spectroscopic data agreed with literature values.<sup>14</sup>

<sup>1</sup>H NMR (500 MHz, CDCl<sub>3</sub>) δ 7.81 (2H, d, *J* = 7.5, 2x H5), 7.56 – 7.45 (2H, m, 2x H2), 7.41 – 7.32 (2H, m, 2x H4), 7.21 – 7.17 (2H, m, 2x H3), 6.54 (1H, d, *J* = 10.1, H9), 6.30 (1H, d, *J* = 10.1, H8), 2.88 (2H, t, *J* = 7.0, H12,H12'), 2.36 (2H, t, *J* = 6.9, H11,H11')

<sup>13</sup>C NMR (125 MHz, CDCl<sub>3</sub>) δ 199.1 (C11), 152.7 (C9), 148.3 (C1), 140.3 (C6), 129.9 (C8), 128.4 (C4), 127.7 (C3), 124.4 (C2), 120.5 (C5), 52.0 (C7), 35.1 (C12), 34.1 (C11).

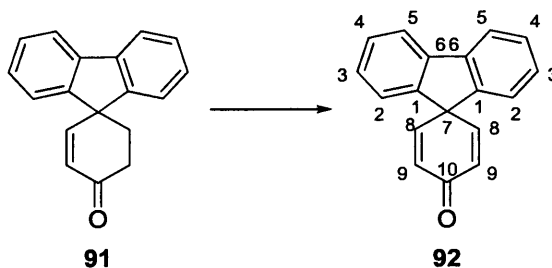


IR 3062 (m, C–H), 2938 (m, C–H), 1676 (s, C=O), 1447 (s)

HRMS (EI) for C<sub>18</sub>H<sub>14</sub>O *m/z* Found: 246.1053, Required: 246.1045

Melting point: 156 – 158 °C (lit. 160 – 161 °C)

**Spiro[2,5-cyclohexadiene-1,9'-[9H]fluoren]-4-one **92****<sup>14</sup>



IBX (5.2 g, 18.6 mmol) and NMO (1.65 g, 14.1 mmol) were mixed in DMSO (10 mL) at 60 °C for 1 h. Then, a solution of enone **92** (2.28 g, 9.3 mmol) in fluorobenzene (15 mL) was added at 60 °C and the mixture maintained at that temperature while being monitored by TLC. After 8 days, the mixture was cooled and ether (75 mL) was added. The organic layer was washed with sodium bicarbonate (3 x 50mL) and then brine (50 mL), dried over magnesium sulphate, and concentrated. Flash chromatography on silica gel (1 : 3 ether : petrol) yielded dienone **92** as a white powder (487 mg, 21%) slightly contaminated with enone **91** which could not be separated by any means. Spectroscopic data agreed with literature values.<sup>14</sup>

<sup>1</sup>H NMR (500 MHz, CDCl<sub>3</sub>) δ 7.82 (2H, d, *J* = 7.5, 2x H2), 7.47 (2H, td, *J* = 7.6, 0.8, 2x H4), 7.34 (2H, t, *J* = 7.4, 0.7, 2x H3), 7.28 – 7.25 (2H, m, 2x H5), 6.53 (2H, d, *J* = 10.3, 2x H8 or 2x H9), 6.50 (2H, d, *J* = 10.3, 2x H8 or 2x H9).

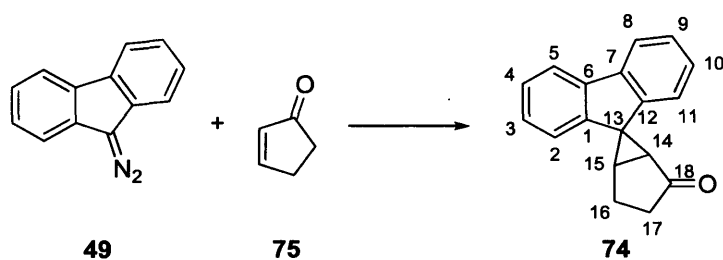
<sup>13</sup>C NMR (125 MHz, CDCl<sub>3</sub>) δ 186.4 (C10), 149.8 (C8 or C9), 143.1 (C1), 142.8 (C6), 129.2 (C8 or C9), 129.0 (C4), 128.2 (C3), 125.0 (C5), 121.0 (C2), 57.6 (C7).

IR 3073 (w, C–H), 3029 (w, C–H), 1663 (s, C=O), 1446 (w), 1396 (w).

HRMS (EI) for C<sub>18</sub>H<sub>12</sub>O *m/z* Found: 244.0897, Required: 244.0888.

Melting point: 172 – 174 °C (lit. 173 – 174 °C).

## 2-Oxo-spiro[bicyclo[3.1.0]hexane-6,9'-[9H]fluorene] 74



**Caution!** Diazofluorene (**49**) is potentially explosive. All work should be carried out using appropriate protections. Diazofluorene (**49**) (1 g, 5.21 mmol) was dissolved in cyclopent-2-enone (**75**) (10 mL) in a microwave tube. The cap was sealed on and the mixture was degassed three times by the freeze-pump-thaw method. The tube was warmed to RT and placed on a Schlenk line. The dark orange mixture was heated at 60 °C for 12 h and then cooled down to RT. Most of the cyclopentenone was removed by Kugelrohr distillation (65 °C, 19 mbar) and some pale yellow crystals (plates) precipitated. The crystals were filtered out and confirmed to be ketone **74**. The remainder of the material was subjected to flash chromatography on silica gel (1 : 1 DCM : petrol) to yield another pale yellow solid which had identical properties as the first batch. The batches were combined to yield ketone **74** (530 mg, 41%). Subsequent reactions yielded solids ranging in colour from pale yellow to medium orange, but showed identical spectral characteristics.

<sup>1</sup>H NMR (500 MHz, CDCl<sub>3</sub>) δ 7.80 (1H, d, *J* = 7.6, H5), 7.72 (1H, d, *J* = 7.6, H8), 7.38 (1H, t, *J* = 7.6, H4), 7.32 (1H, t, *J* = 7.5, H9), 7.26 (1H, t, *J* = 7.6, H10), 7.22 (1H, t, *J* = 7.5, H3), 6.88 (1H, d, *J* = 7.7, H2), 6.76 (1H, d, *J* = 7.6, H11), 2.93 (1H, q, *J* = 6.4, H15), 2.85 (1H, d, *J* = 5.7, H14), 2.70 – 2.65 (1H, m, H17), 2.62 – 2.56 (1H, m, H17'), 2.54 – 2.51 (1H, m, H16), 2.24 (1H, quin., H16').

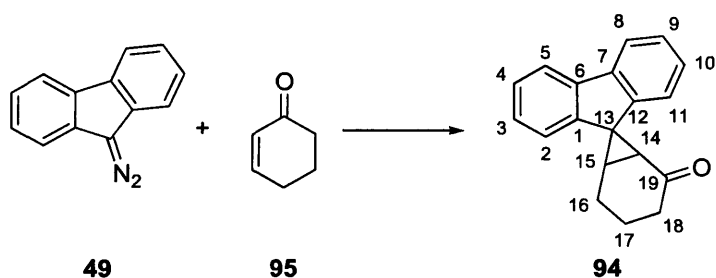
<sup>13</sup>C NMR (125 MHz, CDCl<sub>3</sub>) δ 212.4 (C18), 146.3 (C7), 142.3 (C1), 140.7 (C6), 138.2 (C12), 127.5 (C10), 127.2 (C4), 127.0 (C9), 126.9 (C3), 126.0 (C8), 122.0 (C2), 120.7 (C5), 118.9 (C11), 43.6 (C14), 41.3 (C13), 40.8 (C17), 37.9 (C15), 19.8 (C16).

IR 3040 (w, C–H), 2955 (w, C–H), 1726 (s, C=O), 1448 (m).

HRMS (EI) for C<sub>18</sub>H<sub>14</sub>O *m/z* Found: 246.1040, Required: 246.1045.

Melting point: 165 – 166 °C.

## 2-Oxo-spiro[bicyclo[3.1.0]heptane-7,9'-[9H]fluorene] **94**



**Caution!** Diazofluorene (**49**) is potentially explosive. All work should be carried out using appropriate protections. Ketone **94** was prepared similarly to ketone **74** using 9-Diazafluorene (**49**) (1 g, 5.21 mmol) and cyclohex-2-enone (**95**) (10 mL). Most of the cyclohexenone was removed by Kugelrohr distillation (75 °C, 12 mm Hg). The material was subjected to flash chromatography on silica gel (1 : 1 DCM : petrol) to yield ketone **94** (570 mg, 41%) as a pale yellow oil. Subsequent reactions yielded solids ranging in colour from pale yellow to light orange, but showed identical spectral characteristics.

$^1\text{H}$  NMR (500 MHz,  $\text{CDCl}_3$ )  $\delta$  7.78 (1H, d,  $J = 7.5$ , H8), 7.68 (1H, d,  $J = 7.4$ , H5), 7.31 (1H, t,  $J = 7.4$ , H3), 7.28 (1H, t,  $J = 7.4$ , H10), 7.20 (1H, t,  $J = 7.4$ , H4), 7.16 (1H, t,  $J = 7.4$ , H9), 7.13 (1H, d,  $J = 7.7$ , H2), 6.86 (1H, d,  $J = 7.6$ , H11), 2.65 – 2.61 (1H, m, H18), 2.60 – 2.56 (2H, m, H14, H15), 2.55 – 2.50 (1H, m, H18'), 2.19 – 2.08 (2H, m, H16, H17), 2.06 – 1.96 (1H, m, H17'), 1.91 (1H, tt,  $J = 13.7, 3.7$ , H16').

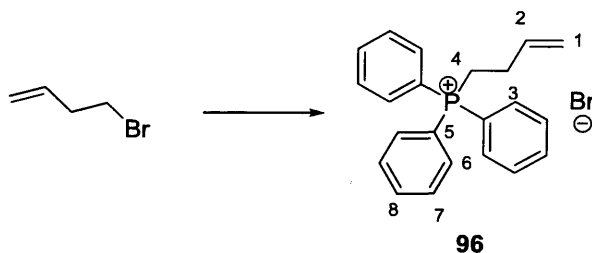
$^{13}\text{C}$  NMR (125 MHz,  $\text{CDCl}_3$ )  $\delta$  206.3 (C19), 148.0 (C6), 142.3 (C1), 140.8 (C7), 138.6 (C12), 127.4 (C4), 126.9 (C3), 126.8 (C10), 126.3 (C9), 123.4 (C2), 120.6 (C8), 119.6 (C5), 118.2 (C11), 41.4 (C13), 39.7 (C18), 35.6 (C14), 32.1 (C15), 24.4 (C17), 18.2 (C16).

IR 3032 (w, C–H), 2970 (w, C–H), 1716 (s, C=O), 1444 (m).

HRMS (EI) for  $\text{C}_{19}\text{H}_{16}\text{O}$   $m/z$  Found: 260.1194, Required: 260.1201.

Melting point: 172 – 174 °C.

## But-3-enyltriphenylphosphonium bromide **96**<sup>15</sup>



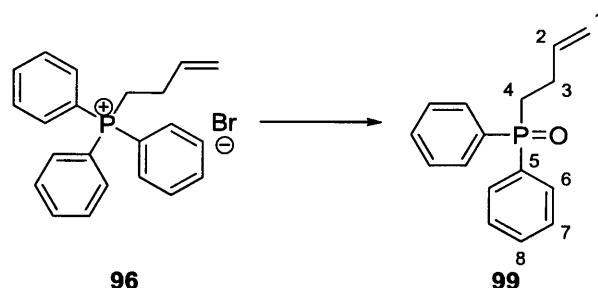
Phosphonium salt **96** was prepared similarly to **83** using the following amounts: 4-bromo-1-butene (1.0 mL, 9.85 mmol), triphenylphosphine (2.84 g, 10.8 mmol), and toluene (15 mL). The resulting precipitate was filtered out and dried to give phosphonium salt **96** white powder (3.00 g, 77%) that was used immediately in the next step. Spectroscopic data agreed with literature values.<sup>15</sup>

<sup>1</sup>H NMR (400 MHz, CDCl<sub>3</sub>) δ 7.82 – 7.52 (15H, m, 6x H6, 6x H7, 3x H8), 5.93 (1H, ddt, *J* = 17.0, 10.1, 6.5, H2), 5.03 (1H, dd, *J* = 17.0, 1.2, H1<sub>cis</sub>), 4.91 (1H, d, *J* = 10.1, H1<sub>trans</sub>), 3.74 (2H, dt, *J* = 12.4, 8.0, H4,H4'), 2.38 (2H, td, *J* = 7.7, 6.5, H3,H3').

<sup>13</sup>C NMR (125 MHz, CDCl<sub>3</sub>) δ 135.2 (d, *J* = 2.5, C8), 134.8 (d, *J* = 15, C2 or C6 or C7), 133.6 (d, *J* = 10, C2 or C6 or C7), 130.6 (d, *J* = 12.5, C2 or C6 or C7), 118.0 (d, *J* = 85, C5), 117.4 (s, C1), 26.6 (d, *J* = 3.75, C3), 22.3 (d, *J* = 51, C4).

Melting point: 214 – 215 °C (lit. 216 – 217 °C).

#### But-4-enyldiphenylphosphine oxide **99**<sup>16</sup>

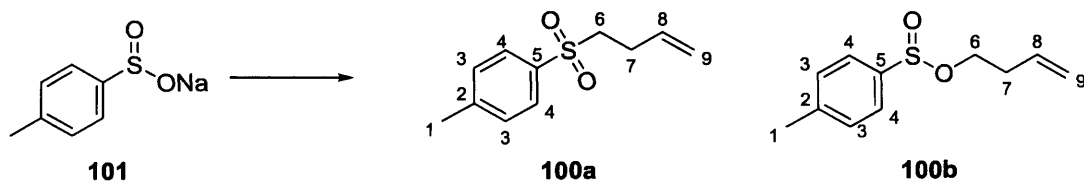


But-3-enyldiphenylphosphonium bromide **96** (3.0 g, 7.6 mmol) was refluxed in 40% sodium hydroxide (20 mL) for 2 h and then cooled. A solid precipitated out which was filtered, dried, and identified as pure phosphine oxide **99** (2.7 g, 100 %). Spectroscopic data agreed with literature values.<sup>16</sup>

<sup>1</sup>H NMR (500 MHz, CDCl<sub>3</sub>) δ 7.73 – 7.68 (m, 4H, 4x H7), 7.50 – 7.37 (6H, m, 4x H6, 2x H8), 5.80 (ddt, *J* = 17.1, 10.3, 5.6, H2), 4.98 (1H, dd, *J* = 17.1, 1.1, H1<sub>cis</sub>), 4.91 (1H, dd, *J* = 9.3, 1.1, H1<sub>trans</sub>), 2.30 (4H, s, H3,H3',H4,H4').

<sup>13</sup>C NMR (125 MHz, CDCl<sub>3</sub>) δ 137.3 (C2), 132.9 (C5), 131.8 (C8), 130.8 (C7), 128.7 (C6), 115.2 (C1), 29.0 (C4), 25.5 (C3).

**1-(But-3-enylsulfonyl)-4-methylbenzene 100a and but-3-enyl 4-methylbenzenesulfinate 100b**



Sodium 4-methylbenzenesulfinate (**101**) (5.0 g, 28.1 mmol) and 4-bromobutene (1.9 mL, 18.7 mmol) were dissolved in DMF (100 mL) and stirred at RT for 18 h. Then water (150 mL) was added and the mixture was extracted with ether (3 x 100 mL). The combined organic layers were washed with brine (100 mL), dried over magnesium sulphate and concentrated. Flash chromatography on silica gel (1 : 19 ethyl acetate : petrol) yielded two colourless oils. The high Rf spot was the *O*-alkylated sulfinate **100b** (0.37 g, 9%) and the low Rf spot was the *S*-alkylated sulfone **100a** (1.94 g, 49%).

1-(But-3-enylsulfonyl)-4-methylbenzene **100a** (*S*-alkylated):

$^1\text{H NMR}$  (500 MHz,  $\text{CDCl}_3$ )  $\delta$  7.72 (2H, d,  $J = 8.0$ , 2x H3), 7.30 (2H, d,  $J = 8.0$ , 2x H4), 5.65 (1H, ddt,  $J = 17.0, 10.2, 6.5$ , H8), 4.98 (1H, dd,  $J = 17.0, 1.1$ , H9<sub>cis</sub>), 4.96 (1H, dd,  $J = 10.2, 1.3$ , H9<sub>trans</sub>), 3.12 – 3.05 (2H, m, H6, H6'), 2.50 – 2.45 (2H, m, H7, H7'), 2.44 (3H, s, H1, H1', H1'').

$^{13}\text{C NMR}$  (125 MHz,  $\text{CDCl}_3$ )  $\delta$  144.8 (C2), 136.1 (C5), 136.1 (C8), 129.9 (C4), 128.2 (C3), 117.1 (C9), 55.5 (C6), 26.9 (C7), 21.6 (C1).

IR 3080 (w, C–H), 2978 (w, C–H), 2922 (w, C–H), 1642 (w), 1596 (m), 1315 (s), 1144 (s), 1087 (s).

HRMS (EI) for  $\text{C}_{11}\text{H}_{14}\text{O}_2\text{S}$   $m/z$  Found: 210.0714, Required: 210.0715.

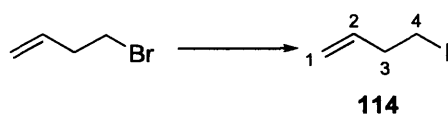
But-3-enyl 4-methylbenzenesulfinate **100b** (*O*-alkylated):

$^1\text{H NMR}$  (500 MHz,  $\text{CDCl}_3$ )  $\delta$  7.53 (2H, d,  $J = 8.2$ , 2x H3), 7.27 (2H, d,  $J = 8.2$ , 2x H2), 5.65 (1H, ddt,  $J = 17.1, 10.3, 3.2$ , H8), 5.03 (1H, dd,  $J = 14.9, 1.3$ , H9<sub>cis</sub>), 5.00 (1H, dd,  $J = 10.2, 1.3$ , H9<sub>trans</sub>), 4.01 (1H, dt,  $J = 9.9, 6.7$ , H6), 3.55 (1H, dt,  $J = 9.9, 6.7$ , H6'), 2.37 (3H, s, H1, H1', H1''), 2.32 (2H, qd,  $J = 6.7, 1.2$ , H7, H7').

$^{13}\text{C NMR}$  (125 MHz,  $\text{CDCl}_3$ )  $\delta$  144.7 (C2), 141.8 (C5), 133.6 (C8), 129.7 (C4), 125.3 (C3), 117.5 (C9), 63.4 (C6), 34.1 (C7), 21.5 (C1).

HRMS (ES) for  $\text{C}_{11}\text{H}_{15}\text{O}_2\text{S}$  ( $\text{M}+\text{H}^+$ )  $m/z$  Found: 211.0797, Required: 211.0793.

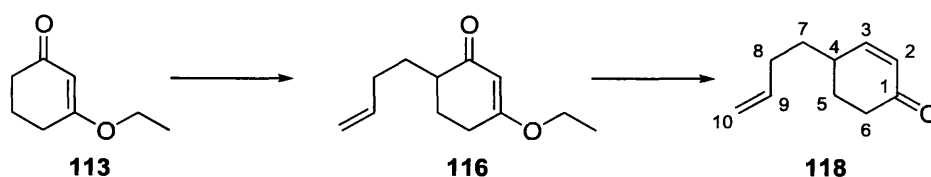
#### 4-Iodobutene **114**<sup>17</sup>



4-Bromobutene (9.0 mL, 88.8 mmol) and sodium iodide (13.3 g, 88.8 mmol) were added to acetone (500 mL). The mixture was refluxed for 3 h and all solid material dissolved upon the initial heating. After 3 h, a different solid coated the flask. The solid was filtered out and most of the acetone was distilled off (55 – 60 °C). Brine (300 mL) and ether (300 mL) were added to the residue and the organic layer was dried over magnesium sulphate. Most of the ether was distilled off (35 – 40 °C) and then THF (500 mL) was added. Most of the THF was distilled off (65 – 70 °C) and the remaining solution was cooled and tested by GC-MS ( $m/z = 182$ ) and NMR (against mesitylene). The product was a yellow solution of 4-iodobutene **114** (30 mL, 2.6 M, 78.0 mmol, 88%, ~7 mmol acetone by NMR) that was stable while protected from light. Different batches had iodobutene concentrations ranging from 0.8 M to 2.6 M with 4 – 10% acetone. Spectroscopic data agreed with literature values.<sup>17</sup>

<sup>1</sup>H NMR (400 MHz, CDCl<sub>3</sub>)  $\delta$  5.65 (1H, ddt,  $J = 17.6, 9.7, 6.6$ , H<sub>2</sub>,H<sub>2</sub>'), 5.05 – 5.01 (2H, m, H<sub>1</sub>,H<sub>1</sub>'), 3.09 (2H, t,  $J = 7.2$ , H<sub>4</sub>,H<sub>4</sub>'), 2.53 (2H,  $J = 7.0$ , H<sub>3</sub>,H<sub>3</sub>').

#### 4-(But-3-enyl)-cyclohex-2-enone **118**<sup>18</sup>



Ketone **118** was prepared according to the method of Schinzer.<sup>18</sup> A solution of KHMDS in toluene (120 mL, 60.0 mmol) was cooled to -78 °C. A solution of 3-ethoxycyclohex-2-enone **113** (5 g, 39.7 mmol) in THF (50 mL) was added dropwise over 15 m at -78 °C. Meanwhile, 4-iodobutene (a 2.6 M solution in THF, 23 mL, 60.0 mmol) and DMPU (4.8 mL, 39.7 mmol) were mixed at RT. The ketone solution was warmed to -40 °C and the iodide/DMPU solution was added dropwise over 5 m. The solution was allowed to slowly warm to RT over 18 h. The reaction was quenched by adding water (250 mL) and ether (250 mL). The aqueous layer was extracted with ether (3 x 75 mL). The combined organic layers were washed with water (200 mL) and brine (200 mL) and then dried over magnesium sulphate and concentrated to yield a light brown oil. GC-MS confirmed the presence of vinyl enol ether **116** ( $m/z = 194$ ) and

the crude NMR yield (based on mesitylene) was approximately 50%. Because of difficulty purifying the product at this stage, the entire mixture was carried through the next step.

The residue was dissolved in THF (50 mL). In another flask, LiAlH<sub>4</sub> (1.8 g, 48.0 mmol) was dissolved in THF (150 mL) at 0 °C. **Caution!** This step is highly exothermic and a reflux condenser should be used if ether is chosen as the solvent. The solution of ketone **116** was then added to the lithium aluminium hydride dropwise at 0 °C. The reaction was stirred at 0 °C for 2 h and then water (5 mL) was added carefully until fizzing ceased. The aluminium salts were filtered out and washed with ether (5 x 100 mL). The combined organic layers were concentrated and the residue was dissolved in THF (70 mL) and 2M hydrochloric acid (30 mL) and stirred at RT for 15 min. The solution was neutralised with potassium carbonate and diluted with ether (200 mL), washed with brine (200 mL), dried over magnesium sulphate and concentrated. Flash chromatography on silica gel (1 : 9 ether petrol) yielded ketone **118** a pale yellow oil (3.8 g, 71% over two steps). Spectroscopic data agreed with literature values.<sup>18</sup>

<sup>1</sup>H NMR (400 MHz, CDCl<sub>3</sub>) δ 6.78 (1H, dq, *J* = 10.2, 1.3, H2), 5.92 (1H, dd, *J* = 10.2, 2.4, H3), 5.75 (1H, ddt, *J* = 16.9, 10.2, 6.7, H9), 5.00 (1H, dq, *J* = 17.1, 1.6, H10<sub>cis</sub>), 4.95 (1H, dd, *J* = 10.2, 1.4, H10<sub>trans</sub>), [2.49 – 2.25 (3H, m), 2.18 – 2.03 (3H, m), 1.69 – 1.42 (3H, m) comprised of H4,H5,H5',H6,H6',H7,H7',H8,H8'].

HRMS (EI) for C<sub>10</sub>H<sub>14</sub>O *m/z* Found: 150.1043, Required: 150.1045.

### 3.4 References for Chapter 3

1. Gaussian 03, Revision E.01, Frisch, M. J.; Trucks, G. W.; Schlegel, H. B.; Scuseria, G. E.; Robb, M. A.; Cheeseman, J. R.; Montgomery, Jr., J. A.; Vreven, T.; Kudin, K. N.; Burant, J. C.; Millam, J. M.; Iyengar, S. S.; Tomasi, J.; Barone, V.; Mennucci, B.; Cossi, M.; Scalmani, G.; Rega, N.; Petersson, G. A.; Nakatsuji, H.; Hada, M.; Ehara, M.; Toyota, K.; Fukuda, R.; Hasegawa, J.; Ishida, M.; Nakajima, T.; Honda, Y.; Kitao, O.; Nakai, H.; Klene, M.; Li, X.; Knox, J. E.; Hratchian, H. P.; Cross, J. B.; Bakken, V.; Adamo, C.; Jaramillo, J.; Gomperts, R.; Stratmann, R. E.; Yazyev, O.; Austin, A. J.; Cammi, R.; Pomelli, C.; Ochterski, J. W.; Ayala, P. Y.; Morokuma, K.; Voth, G. A.; Salvador, P.; Dannenberg, J. J.; Zakrzewski, V. G.; Dapprich, S.; Daniels, A. D.; Strain, M. C.; Farkas, O.; Malick, D. K.; Rabuck, A.

- D.; Raghavachari, K.; Foresman, J. B.; Ortiz, J. V.; Cui, Q.; Baboul, A. G.; Clifford, S.; Cioslowski, J.; Stefanov, B. B.; Liu, G.; Liashenko, A.; Piskorz, P.; Komaromi, I.; Martin, R. L.; Fox, D. J.; Keith, T.; Al-Laham, M. A.; Peng, C. Y.; Nanayakkara, A.; Challacombe, M.; Gill, P. M. W.; Johnson, B.; Chen, W.; Wong, M. W.; Gonzalez, C.; and Pople, J. A.; Gaussian, Inc., Wallingford CT, 2004.
2. (a) GAMESS US, Version "April 11 2008": Schmidt, M. W.; Baldridge, K. K.; Boatz, J. A.; Elbert, S. T.; Gordon, M. S.; Jensen, J. H.; Koseki, S.; Matsunaga, N.; Nguyen, K. A.; Su, S.; Windus, T. L.; M. Dupuis, Montgomery, J. A. *J. Comput. Chem.* **1993**, *14*, 1347 – 1363. (b) DRC: Taketsugu, T.; Yanai, T.; Hirao, K.; Gordon, M. S. *Theochem* **1998**, *451*, 163 – 177.
  3. (a) MOLPRO, version 2008.1, a package of *ab initio* programs: Werner, H.-J.; Knowles, P. J.; Lindh, R.; Manby, R. R.; Schütz, M.; Celani, P.; Korona, T.; Mitrushenkov, A.; Rauhut, G.; Adler, T. B.; Amos, R. D.; Bernhardsson, A.; Berning, A.; Cooper, D. L.; Deegan, M. J. O.; Dobbyn, A. J.; Eckert, F.; Goll, E.; Hampel, C.; Hetzer, G.; Hrenar, T.; Knizia, G.; Köppl, C.; Liu, Y.; Lloyd, A. W.; Mata, R. A.; May, A. J.; McNicholas, S. J.; Meyer, W.; Mura, M. E.; Nicklass, A.; Palmieri, P.; Pflüger, K.; Pitzer, R.; Reiher, M.; Schumann, U.; Stoll, H.; Stone, A. J.; Tarroni, R.; Thorsteinsson, T.; Wang, M.; Wold, A. see <http://www.molpro.net>. (b) MCSCF/CASSCF: Werner, H.-J.; Knowles, P. J. *J. Chem. Phys.* **1985**, *82*, 5053 – 5063; and Knowles, P. J.; Werner, H.-J. *Phys. Lett.* **1985**, *115*, 259 – 266.. c) RS2C / MRMP2: Werner, H.-J. *Mol. Phys.* **1996**, *89*, 645 – 661; and Celani, P.; Werner, H.-J. *J. Chem. Phys.* **2000**, *112*, 5546 – 5557.
  4. Morrison, H.; Danishefsky, S.; Yates, P. *J. Org. Chem.* **1961**, *26*, 2617-2618.
  5. Kostitsyn, A. B.; Shulishov, E. V.; Tomilov, Y. V.; Nefedov, O. M. *Synlett* **1990**, 713 – 714.
  6. Salomon, R. G.; Ghosh, S.; Zagorski, M. G.; Reitz, M. *J. Am. Chem. Soc.* **1982**, *47*, 829 – 836.
  7. Oppolzer, W.; Roberts, D. A.; Bird, T. G. C. *Helv. Chim. Acta* **2004**, *62*, 2017 – 2021.
  8. Motherwell, W. B.; Begis, G.; Cladingboel, D. E.; Jerome, L.; Sheppard, T. D. *Tetrahedron* **2007**, *63*, 6462 – 6476.
  9. Belotti, D.; Cossy, J.; Pete, J. P.; Portella, C. *J. Org. Chem.* **1986**, *51*, 4196 – 4200.
  10. Clive, D. L. J.; Pham, M. P.; Subedi, R. *J. Am. Chem. Soc.* **2007**, *129*, 2713 – 2717.
  11. Albrecht, U.; Langer, P. *Tetrahedron* **2007**, *63*, 4648 – 4654.

12. Subba-Reddy, K.; Sola, L.; Moyano, A.; Pericas, M. A.; Riera, A. *Synthesis* **2000**, 165 – 176.
13. Shih, C.; Fritzen, E. L.; Swenton, J. S. *J. Org. Chem.* **1980**, *45*, 4462 – 4471.
14. Plieninger, H.; Ege, G.; Ullah, M. I. *Chem. Ber.* **1961**, *96*, 1610 – 1617.
15. White, J. D.; Jensen, M. S. *Tetrahedron* **1995**, *51*, 5743 – 5756.
16. Nelson, A.; Warren, S. *J. Chem. Soc., Perkin Trans. 1* **1999**, 3425 – 3433.
17. Hoarau, S.; Fauchere, J-L.; Pappalardo, L.; Roumestant, M-L.; Viallefont, P. *Tetrahedron: Asymmetry* **1996**, *7*, 2585 – 2593.
18. Schinzer, D.; Solyom, S.; Becker, M. *Tetrahedron Lett.* **1985**, *26*, 1831 – 1834.

# CHAPTER 4

## NONSTATISTICAL EFFECTS IN CYCLOPENTADIENE

### 4.1 Introduction to Chapter 4

This chapter gives an overview of the cyclopentadiene project. It begins by summarising important chemistry of cyclopentadiene (CP) applicable to this work, including the isomerisation to and from bicyclo[2.1.0]pent-2-ene (BCP). From here, there is a discussion of how nonstatistical dynamics may play a role in the ring-opening reaction from BCP to CP and the subsequent [1,5]-hydrogen-migration of CP. The computational and experimental work to test for nonstatistical effects is then discussed. Computational details are found in the appendix.

### 4.2 Cyclopentadiene and Bicyclopentene

Cyclopentadiene (**123**) is one of the simplest cyclic hydrocarbons. Although stable at room temperature for short periods of time, within a few days as a neat liquid it will undergo Diels-Alder dimerisation to form dicyclopentadiene (**124**) (Figure 4.1). For this reason, CP (**123**) is usually formed by cracking dicyclopentadiene at high temperatures to force the retro-Diels-Alder reaction, followed by distillation of the more volatile CP. As shown by its dimerisation, cyclopentadiene can act as both a diene and a dienophile in Diels-Alder reactions. In synthetic chemistry, however, it is mainly used as the diene. Additional important reactions of CP are discussed below.



**Figure 4.1.** Formation of dicyclopentadiene

CP is known to be relatively acidic for a hydrocarbon, with an aqueous pKa of 18.0.<sup>1</sup> This acidity is unusual for a hydrocarbon and is due to the aromaticity of the cyclopentadienyl anion. A use for this acidity will be described later in this chapter (Section 4.4).

The CP anion is also commonly used as a ligand for metals. While the cyclopentadienyl anion has numerous uses as a ligand, full coverage of the topic is beyond the scope of this work and so only a broad overview will be given.<sup>2</sup> Three types of bonds can be formed between metals and the cyclopentadienyl anion: covalent bonds,

ionic bonds, and  $\pi$ -complexes. Covalent bonds are formed with soft metals such as tin. Ionic bonds are formed with alkali metals such as sodium and potassium. Of more importance for organometallic chemistry are the  $\pi$ -complexes. These are formed with transition metals. Cyclopentadienyl ligands are common in organometallic compounds. Examples include the Tebbe reagent<sup>3</sup> (Figure 2.40) and ferrocene. The former includes a titanium cyclopentadienyl complex and is used to methylenate carbonyl compounds; the latter has many uses, including as a fuel additive to reduce knocking<sup>4</sup>.

Two final reactions of cyclopentadiene lead into the core of the nonstatistical dynamics project. The first is the photoisomerisation of CP to form BCP (Figure 4.2)<sup>5</sup>. The preparation of BCP was optimised by Baldwin.<sup>6</sup> The isomerisation of BCP to reform CP is very exothermic ( $\sim 200 \text{ kJ mol}^{-1}$ )<sup>7</sup>, but the reaction is thermally forbidden by the Woodward-Hoffmann rules<sup>8</sup>. Being forbidden in this case simply means the reaction has a large activation barrier ( $\sim 100 \text{ kJ mol}^{-1}$ )<sup>7</sup> and can occur slowly at room temperature or rapidly if BCP is heated to about  $60^\circ\text{C}$ . The second key reaction is the degenerate [1,5]-hydrogen-shift of CP, which also has a large barrier ( $\sim 100 \text{ kJ mol}^{-1}$ )<sup>9</sup>.

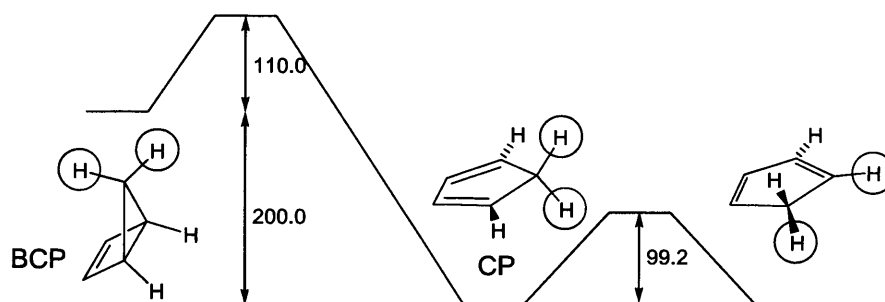


**Figure 4.2.** Reactions involving bicyclopentene and their energetics (in  $\text{kJ mol}^{-1}$ )

When BCP was first discovered, there was a vigorous debate as to the mechanisms for the ring-opening and hydrogen-shift reactions. For reasons of experimental utility, various methylcyclopentadienes were used rather than cyclopentadiene itself. It was assumed that the mechanisms and kinetics for methylcyclopentadienes would be the essentially the same as for cyclopentadiene. This discussion will cover both sets of molecules.

One proposed mechanism for the ring-opening in 2-methylbicyclopentene (2-MeBCP, **126**) has the central cyclopropyl bond homolysing to form a biradical, which is effectively an excited state of 2-methylcyclopentadiene (2-MeCP, **127**).<sup>10</sup> A second proposed mechanism involves a retro-ene reaction of 2-MeBCP that leads to 1-methylcyclopentadiene (1-MeCP, **128**) instead (Figure 4.3). Work by Baldwin<sup>11</sup>

suggested the major product was **128**, which favoured the retro-ene mechanism. However, further work by Baldwin<sup>12</sup> appeared to rule out the retro-ene mechanism. This was based on studies of BCP-5-*d* (*i.e.* the unmethylated, but singly deuterated, compound). The deuterium ended up in positions that would have been predicted by the “biradical” mechanism, but not the “retro-ene” mechanism. Additionally, there was not a large primary H/D isotope effect which would have been expected for the “retro-ene” mechanism. At this point in time, the results for methyl-BCP and BCP appeared to contradict each other.

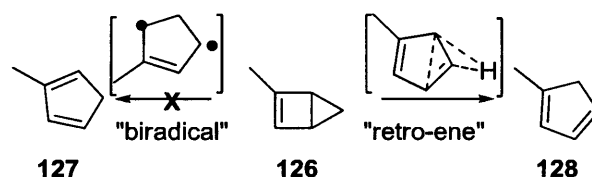


**Figure 4.3.** Possible mechanisms of the thermal opening

McLean<sup>13</sup> provided evidence that Baldwin’s early results<sup>11</sup> shown in Figure 4.3 were incorrect. 2-MeBCP **126** was shown to give *predominantly* 2-MeCP **127** rather than 1-MeCP **128** as Baldwin had found, despite both this and Baldwin’s earlier work being carried out under the same conditions. Based on McLean’s newer results, the BCP and MeBCP results would now agree with each other and both point towards the “biradical” mechanism for ring-opening. Needless to say, at this point there was considerable confusion into the mechanism of the ring-opening, let alone how the hydrogen shift.<sup>9</sup> An additional complexity is that there is the potential for [1,5] hydrogen shifts to interconvert 1-MeCP and 2-MeCP. Around this time though, experimental results began to point more conclusively towards the “biradical” mechanism. Additional evidence came from RRKM calculations by Flowers<sup>14</sup> which supported McLean’s experimental results on 2-MeBCP<sup>13</sup> as well as computational work by Dewar<sup>16</sup> at the semiempirical level for both BCP and MeBCP. <sup>13</sup>C isotope labelling led to the same conclusions<sup>17</sup> as did subsequent DFT calculations.<sup>18</sup> Our proposal for the specific mechanism based on MD calculations will be seen in Section 4.5.3.

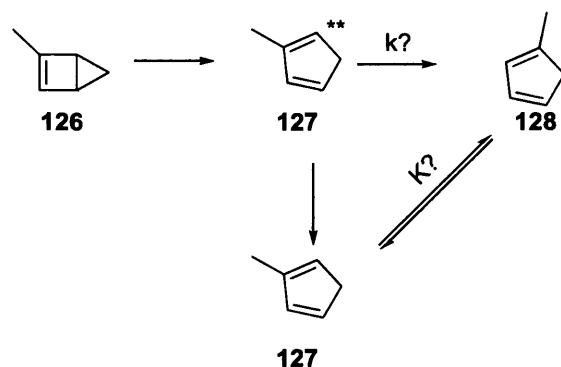


**Figure 4.4.** Revised mechanism of ring-opening

### 4.3 Nonstatistical Effects in the CP/BCP System

Two commonly observed conditions for nonstatistical dynamics to occur are shallow intermediate wells and obviously similar reaction coordinates<sup>19</sup>. When two reaction coordinates are similar, it is easy to see how vibrational coupling could allow energy from the first reaction coordinate to carry over to the second reaction coordinate. Shallow wells are important because they are believed to increase the rate of IVR as follows. The density of vibrational states increases with energy. For this reason, the area near the top of a deep well will have more vibrational states than the area near the top of a shallow well. Having more states available increases the number of ways vibrational energy can redistribute, effectively increasing the rate of IVR which is normally antithetical to nonstatistical behaviour. This would explain why nonstatistical dynamics is usually seen in systems with high-energy, shallow-well intermediates. (See the examples in Chapter 1 and the singlet biradical in Chapter 2). An example of a system that shows nonstatistical dynamics despite having a deep well intermediate is the acetone radical cation (Section 1.4.1). Possible explanations for this seeming discrepancy are that either mode coupling in the acetone system compensates for the deep well, or that the deep well assumption might not be as necessary as previously thought.

Based on these common requirements for nonstatistical dynamics, it is not obvious that nonstatistical dynamics would play a role in the CP-BCP system because it does not seem to meet either criterion. The primary vibrational modes involved in the ring-opening from BCP to CP are the C-C stretching mode (“C-C stretch”) for the central bond, and a ring-bending mode (“ring-bend”) that brings the methylene carbon into the same plane as the other carbons. The primary vibrational modes involved in the hydrogen-shift reaction are the C-C-H bending modes (“methylene bends” based on the

plane that includes the methylene CH<sub>2</sub>, not the plane that includes the CP ring) that move the methylene hydrogens closer to the neighbouring carbons. Figure 4.5 shows all of these vibrational modes. A more detailed discussion of important vibrational modes is in section 4.5.2. The modes involved in the ring-opening reaction (C-C stretch and ring-bend) and the modes involved in the hydrogen shift (symmetrical and antisymmetrical methylene bends) do not appear to be related to each other. In fact, they are of different symmetry and should not interact with each other. For the well-depth criterion, both the ring-opening to form CP, and the hydrogen-migration have barriers of approximately 100 kJ mol<sup>-1</sup>. One might think that this should be deep enough to not see nonstatistical effects, although it is comparable to the well depth of the acetone radical cation which does show them. Regardless of the well depth, the lack of comparable vibrational modes would predict that nonstatistical effects should not be present<sup>7,9</sup>. As will be seen later in this work, this is not the case.

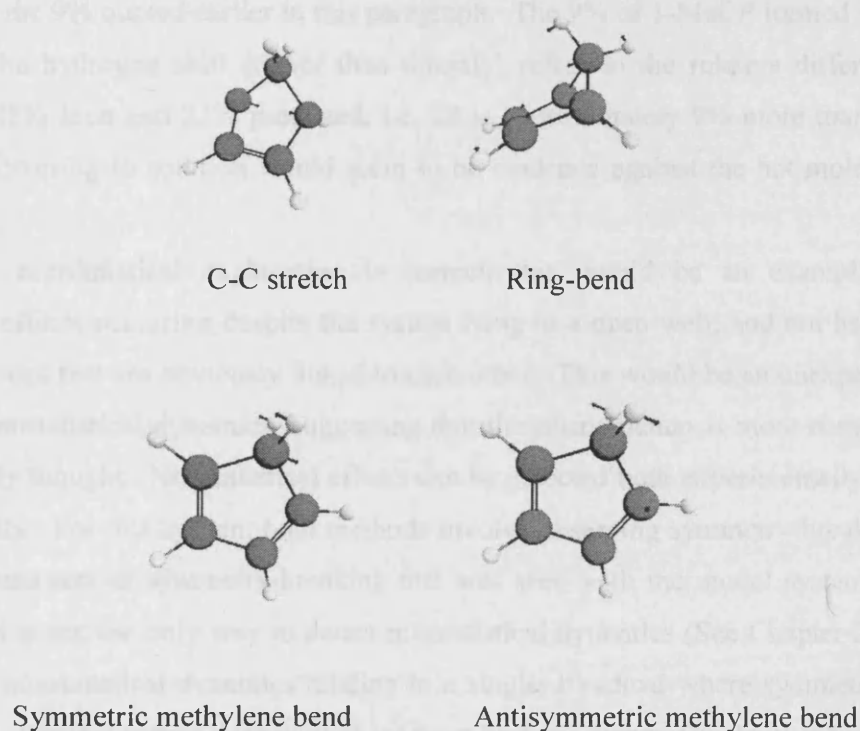


**Figure 4.5.** Important vibrational modes

Despite this, there are signs of nonstatistical dynamics in the system. One of these puzzles involves the amount of 1-MeCP formed from 2-MeBCP via 2-MeCP (*vide supra*)<sup>13b</sup>. A kinetic analysis showed that the hydrogen-shift occurred in roughly 9% of

2-MeCP 127 that was formed from 2-MeBCP 126 in THF. This could either be caused by a “hot molecule” effect or a nonstatistical effect. In the former, the molecule has an excess of energy because it just underwent an exothermic reaction. Until that energy is removed by molecular collisions, it can cause the molecule to undergo unexpected chemistry. In solution, those collisions would usually happen sufficiently fast to remove the excess energy, which would prevent the hydrogen shift from taking place. To explain this, Brauman proposed that the solvent cooling was only 20% effective. In contrast, if the hydrogen shift is the sign of a nonstatistical effect, this would be the result of vibrational mode coupling between the ring-opening and hydrogen-shift reactions. This mode coupling could effectively accelerate the hydrogen shift reaction to the point where it would compete with IVR / vibrational cooling, despite it taking place in solution. Both the “hot molecule with inefficient cooling” and “nonstatistical dynamics” explanations would explain why more 1-MeCP is being formed than Brauman predicted (28% seen vs. 25% predicted). Note that these numbers are different than the 9% quoted earlier in this paragraph. The 9% of 1-MeCP formed from 2-MeCP by the hydrogen shift (rather than directly) refers to the relative difference between the 28% seen and 25% predicted, i.e. 28 is approximately 9% more than 25. That this is occurring in solution would seem to be evidence against the hot molecule effect.

If the nonstatistical explanation is correct, this would be an example of nonstatistical effects occurring despite the system lying in a deep well, and not having vibrational modes that are obviously linked to each other. This would be an unexpected example of nonstatistical dynamics, suggesting that the phenomenon is more common than previously thought. Nonstatistical effects can be detected both experimentally and computationally. For this system, both methods involve observing symmetry-breaking. This is the same sort of symmetry-breaking that was seen with the model systems in Chapter 1, but is not the only way to detect nonstatistical dynamics (See Chapter 2 for discussion of nonstatistical dynamics relating to a singlet biradical where symmetry is not involved). For this approach to work there must be some symmetry element present in CP that was not present in BCP. Statistical theories would require that the product distribution conform to this new symmetry element, while nonstatistical theories would not require this. In this case, that symmetry element relates to the methylene hydrogens. In CP they are equivalent, while in BCP one is *endo* and the other is *exo* to the cyclobutene ring. Statistically, the hydrogens in CP should undergo the H shift with

equal frequency. If nonstatistical behaviour is observed, one H might undergo the shift more frequently than the other. This is analogous to the acetone radical cation system where one methyl group was seen to fragment more than the other methyl group (Section 1.4.1). The experimental and computational methods to look for this will be described in the next sections.

#### 4.4 Proposed Experimental Tests for Nonstatistical Dynamics

In the acetone radical cation, the symmetrical methyl groups were distinguished with isotopic labels. A similar approach could also be used for the CP/BCP system. Figure 4.6 shows the labelling necessary to do this.

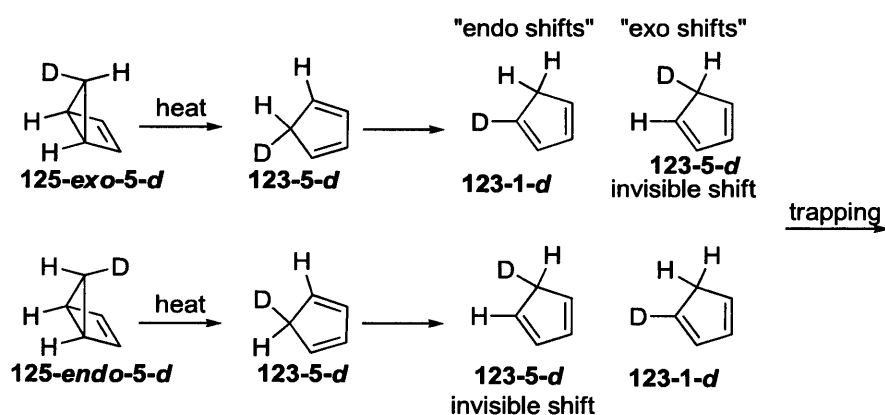


Figure 4.6. Isotopic labelling to study CP/BCP

The synthetic details of the isotopic labelling will be discussed below. In the ideal case, isotopically pure *endo* and *exo* labelled **125** would be prepared separately. Each isotopomer of **125-5-d** would be heated to cause it to isomerise to **123-5-d**. If the system were behaving statistically, both isotopomers of **125-5-d** would lead to identical molecules of **123-5-d**, which would undergo the H shift at the exact same rate regardless of which isotopomer the **123-5-d** came from. But if CP retained memory of coming from BCP, the D atoms in the upper and lower **123-5-d** would effectively be different (“formerly *endo*” vs “formerly *exo*”) and could thus migrate at different rates. For each isotopomer, deuterium shifts would be invisible because they are degenerate. For the *exo-d* isotopomer, only the “*endo*” shift is visible and *vice versa*. (While CP no longer has *endo* or *exo* hydrogens, the names of the shifts refer to the hydrogen’s positions in the original BCP) This would allow a way to measure the rate of both *endo* and *exo* shifts. If the *endo* and *exo* shifts occurred at different rates,

then this would be evidence for nonstatistical effects. One might be concerned that isotope effects may make the system appear to be behaving nonstatistically when it is in fact behaving statistically. However, this synthetic scheme would eliminate primary isotope effects as follows. In both reactions in Figure 4.6, D-shifts are degenerate, hence invisible. Since the D-shift is not being observed, there is no H/D primary isotope effect. This would leave only secondary isotope effects such as for the *endo* or *exo* hydrogen that is not shifting. This isotope effect should be essentially the same for both isotopomers. The secondary isotope effects would effectively cancel each other out and so a difference in *endo* and *exo* rates would be indicative of nonstatistical effects.

The proposed method for selectively isotopically labelling BCP is given in Figure 4.7. Computational work by Carpenter<sup>20</sup> suggests that the *exo* position is 1.6 pKa units more acidic than the *endo* position. With an appropriate base, that position could be selectively deprotonated. The phenyl anion has approximately the right pKa and can be prepared by treating benzene with Schlosser's base<sup>21</sup>. Treatment of protiated BCP with deuteriophenyl anion, or deuterated BCP with protiophenyl anion would hopefully distinguish between the *endo* and *exo* sites. There are some potential problems. It is possible that the methylene sites are not the most acidic. If the bridgehead and vinyl sites are more acidic, they would be isotopically labelled first (the latter products in Figure 4.7). This is not relevant to the study because whereas in Figure 4.3 only H shifts were visible, in that case only D shifts would be visible, and *endo* and *exo* shifts could still be distinguished. Primary H/D isotope effects would still not be a problem for the same reason as described above.

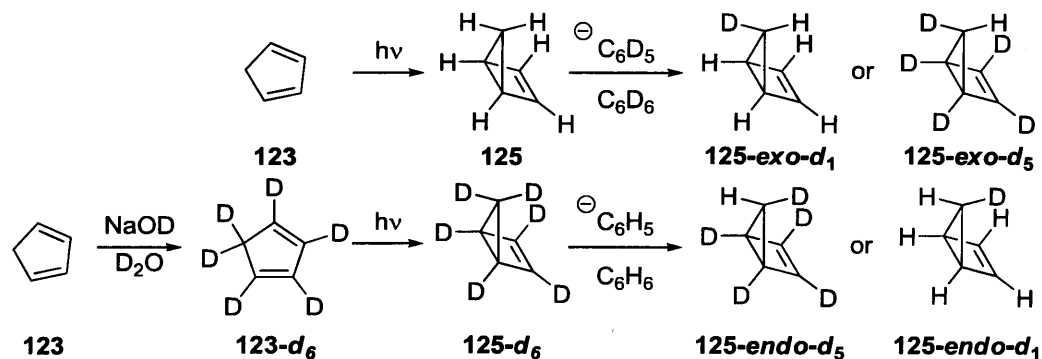


Figure 4.7. Isotopically labelled syntheses.

It will presumably be very difficult to separate a mixture of the two isotopomeric BCPs. Therefore, this approach was designed so that each route would form only one of the isotopomers. If both isotopomers are formed by the above chemistry, then the kinetic work can still be carried out as long as the ratio of isotopomers is not 50:50. Any difference between the shift rates in 50:50 *endo:exo* labelled isotopomers and non-50:50 labelled isotopomers would be attributable to nonstatistical effects, though the effects would be smaller than if the isotopomers had been fully separated. Rather than trying to detect relatively unstable molecules such as BCP and CP, the product CP would be trapped through a Diels-Alder reaction with a dienophile such as tetracyanoethylene. This would afford a stable product that can be analysed by NMR to see in which positions the deuterium lies.

Whilst this experimental work has not been carried out, it is available as an experimental method to test for the nonstatistical dynamics predicted by the computational work described below.

#### 4.5 Computational Work

The computational work on cyclopentadiene falls into two categories. Firstly, an appropriate level of theory had to be chosen so that the calculation was both accurate and tractable for molecular dynamics. In the past, molecular dynamics simulations on small organic systems were done at semiempirical levels of theory.<sup>24</sup> This project used a DFT method to give presumably more accurate results. As CP and BCP have been studied experimentally, various DFT models could be benchmarked against experimental properties, rather than very high level computational methods such as CASSCF or MRMP2. Secondly, once an appropriate level of theory was chosen, molecular dynamics had to be performed on the system and the results analysed. The ideal starting point is the highest point on the reaction coordinate. In this case (Figure 4.2), it was the TS between BCP and CP, which could be found easily using DFT methods.

##### 4.5.1 DFT Benchmarks

Cyclopentadiene and bicyclopentene are both well-known compounds, and many of their physical properties are known<sup>7,9,32</sup>. For the purposes of benchmarking a method, their relative energies, and the relative energies of the two TSs were compared as well as the vibrational spectrum of CP. A broad range of DFT methods was

surveyed. Unrestricted broken symmetry methods were used (see Chapter 1). Table 4.1 lists the calculated energies for the varying methods and the experimental values. In each method, the relative energies are referenced to cyclopentadiene.

<i>Method</i>	<i>E(CP-TS)<sup>a</sup></i>	<i>E(BCP)<sup>a</sup></i>	<i>E(BCP-TS)<sup>a</sup></i>	<i>RMS Error</i>
Experimental <sup>7,9</sup>	99	200	310	-
<b>UB97-2/6-31+G(d)<sup>26</sup></b>	<b>104</b>	<b>194</b>	<b>300</b>	<b>7</b>
<b>UB1B95/6-31+G(d)<sup>27</sup></b>	<b>99</b>	<b>177</b>	<b>302</b>	<b>8</b>
<b>UO3LYP/6-31+G(d)<sup>28</sup></b>	<b>99</b>	<b>183</b>	<b>294</b>	<b>9</b>
<b>UB3LYP/6-31+G(d)<sup>29</sup></b>	<b>110</b>	<b>201</b>	<b>297</b>	<b>10</b>
<b>UMPWPW91/3-21G<sup>30</sup></b>	<b>112</b>	<b>212</b>	<b>304</b>	<b>11</b>
<b>UO3LYP/3-21G</b>	<b>119</b>	<b>209</b>	<b>308</b>	<b>11</b>
UB1B95/3-21G	122	207	316	14
UVSXC/3-21G <sup>31</sup>	118	217	305	15
UB97-2/3-21G	122	215	315	16
UB3LYP/3-21G	127	228	313	23

<sup>a</sup>: All energies are in kJ mol<sup>-1</sup> and referenced to CP at 0 kJ mol<sup>-1</sup>

**Table 4.1.** DFT Energy benchmarks

The six DFT methods that performed the best for energies were then tested on how well they calculated the experimental vibrational frequencies of CP<sup>32</sup>. The frequencies were not initially scaled by their “normal” scaling factors<sup>33</sup>. Instead, the optimum scaling factor was determined for each level of theory, which would hopefully show which method would be the most accurate. Most of the optimised scaling factors were close to the literature values. The analysis is shown in Table 4.2.

Finally, the overall goodnesses of the methods were compared. Table 4.3 shows the methods, their energy RMS errors, frequency RMS errors, and relative computational cost (the amount of time in hours required to run one trajectory). The (somewhat arbitrary) method for determining the best method is (“Golf Score” = Energy RMS Error + Frequency RMS Error + Relative cost). As in its namesake, a lower golf score was therefore indicative of a better overall method for the BCP-CP system.

<i>Method</i>	<i>Literature Freq.</i> <i>Scale Factor</i>	<i>Optimised Freq.</i> <i>Scale Factor</i>	<i>Frequency</i> <i>RMS (cm<sup>-1</sup>)</i>
UB1B95/6-31+G(d)	0.9535 <sup>33c</sup>	0.9552	22
UO3LYP/6-31+G(d)	0.9625 <sup>33a</sup> 0.9648 <sup>33c</sup>	0.9560	24
UB97-2/6-31+G(d)	0.9538 <sup>33a</sup> 0.9543 <sup>33c</sup>	0.9500	20
UMPWPW91/3-21G	0.9534 <sup>33b</sup>	0.9750	27
UO3LYP/3-21G	0.9704 <sup>33a</sup>	0.9510	21
UB3LYP/6-31+G(d)	0.9611 <sup>33b</sup> 0.9648 <sup>33c</sup>	0.9569	20

**Table 4.2.** DFT Frequency benchmarks

<i>Method</i>	<i>Energy RMS</i> <i>Error</i>	<i>Frequency RMS</i> <i>Error</i>	<i>Relative cost</i>	<i>“Golf</i> <i>Score”</i>
UB1B95/6-31+G(d)	8	22	27	57
UO3LYP/6-31+G(d)	9	24	17	50
UB97-2/6-31+G(d)	7	20	27	54
UMPWPW91/3-21G	11	27	6	44
<b>UO3LYP/3-21G</b>	<b>11</b>	<b>21</b>	<b>6</b>	<b>38</b>
UB3LYP/6-31+G(d)	10	20	21	51

**Table 4.3.** DFT method comparisons

From this benchmarking, UO3LYP/3-21G was chosen for the MD on the BCP-CP system. While there may of course be criticisms as to how the method was chosen, this was a semi-quantitative approach that sought to include computational cost, energy accuracy, and frequency accuracy. Also of note is that UB3LYP, one of the most commonly used methods, actually did quite poorly in the benchmark test, suggesting that B3LYP should not simply be used as a default method in general computational work. Follow-up work on the system may choose to use another of the methods that performed well, e.g. UMPWPW91/3-21G and confirm that it gives substantially the same results as UO3LYP/3-21G. Table 4.4 summarises some of the important bond distances and dihedrals for the BCP-CP system at the O3LYP/3-21G level of theory. Figure 4.9 shows the BCP and CP with numbered hydrogen atoms.

<i>Structure</i>	<i>R (C1-C5) / Å</i>	<i>R (H7-C2) / Å</i>	<i>R (H7-C1) / Å</i>	<i>D (Ring-bend) / °</i>
BCP (125)	1.55	1.08	2.27/2.24	56
BCP-TS	2.12	1.09	2.20	33
CP (123)	2.36	1.10	2.16	0
CP-TS	2.34	1.34	1.34	0

**Table 4.4.** Summary of important geometric parameters

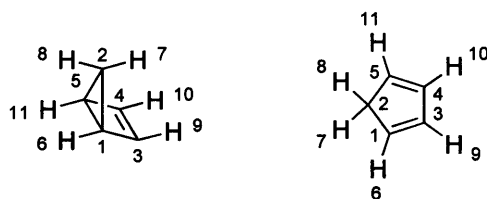


**Figure 4.8.** Atom numbering used in Gaussian calculations

The DFT calculations also allow for the calculation of isotope effects. Isotope effects are given next to the labels for both the ring opening and hydrogen shift reactions, and were determined at the UO3LYP/3-21G level of theory. The bridgehead hydrogens appear to have a very large secondary isotope effect. The most likely explanation is because of the hybridisation change that occurs in the ring-opening. The bridgehead site begins in a cyclopropyl system and ends as a vinyl site. Cyclopropyl bonds are known for behaving strangely and it has been postulated that they contain bent “banana” bonds, unlike other cyclic hydrocarbon bonds.<sup>34</sup> The surprisingly large secondary H/D isotope effect for the ring-opening reaction is essentially unimportant because it will only effect how quickly CP is formed, not how quickly *endo* or *exo* shifts occur. For the hydrogen shift reaction, it is arbitrary which H is chosen to shift because of the symmetry of the system. The important result is that the migrating hydrogen is expected to have a large KIE and other hydrogens are predicted to have small secondary isotope effects which would hopefully not interfere with any experimental work. In fact, the primary KIE is invisible because of the specific labelling used, and the secondary KIEs should cancel out for each of the isotopomers (See section 4.4).

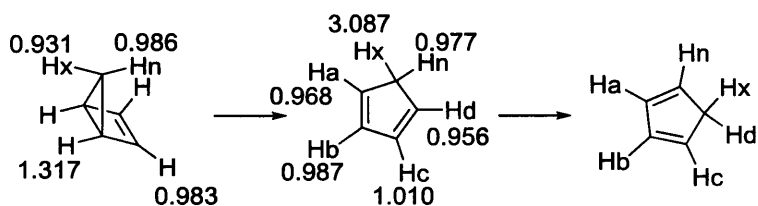


**Figure 4.9.** Isotope effects for cyclopentadiene chemistry

#### 4.5.2 Molecular Dynamics

Molecular dynamics calculations were performed using Gaussian03 and begun from the TS for the ring-opening of BCP to CP. Atom numbering is as given in Figure 4.9 and is the same numbering used in the Gaussian calculations. The first approach was to simply run some trajectories to see if any underwent a hydrogen shift. These trajectories were initiated with quasiclassical normal mode sampling from a canonical ensemble at 333 K (the temperature at which bicyclopentene was experimentally reacted). Of the first 57 trajectories, 45 went to CP and 12 went to BCP. None showed a hydrogen shift. While some shifts might have been observed if more trajectories were carried out, the very low shifting rate would have required a prohibitively large number of trajectories to obtain a mathematically meaningful number of trajectories that showed a hydrogen-shift. A possible explanation is that according to Borden<sup>35</sup>, the hydrogen shift reaction involves large amount of quantum tunnelling. The exact amount of tunnelling varies with the temperature, ranging from 97% at 260 K to 84% at 320 K. Presumably the percent of tunnelling at 333 K would be slightly lower than at 320 K, but would still account for the majority of the reactivity. The MD calculations do not include tunnelling at all, so would ignore that contribution and would show a significantly smaller number of shifts. That the reaction involves tunnelling would not affect the conclusions drawn from any observed symmetry-breaking.

It was necessary to excite the molecules in order to force a shift. This could be done either by raising the temperature (and exciting all atoms / vibrational modes) or by exciting specific vibrational modes. The former would be a “brute force” way of accelerating the H-shift reaction, while if the vibrational modes were chosen well, the latter would more effectively encourage the hydrogen shift reaction. The latter would also be a way of probing the reaction mechanism, while both methods would find any evidence for the expected symmetry being broken. It would not be feasible to test all vibrational modes individually in order to determine which ones should be excited. The important modes could either be guessed or determined more methodically.

Experimental design (also called design of experiment) was used as a screen for which vibrational modes were important and is discussed in more detail in the next section.

#### 4.5.2.1 Experimental Design to study the CP/BCP System

Experimental design provides a way for screening many variables efficiently to determine which variables are the most important in affecting the results of a process and in predicting the values of those variables.<sup>36</sup> The general process is A) identify important variables and their possible values, B) design experiments to probe these variables, and C) statistically analyse the experiments to determine the effect of the variables. The process of experimental design is demonstrated with a hypothetical example below. The application of the technique to the MD simulations is then described.

In order to carry out an experimental design, all of the variables must be clearly defined. For example, an experiment to optimise an industrial chemical process might include the temperature, amount of catalyst, stirring rate, time, etc. The possible values for each variable must also be decided. In general, when variables are allowed  $n$  values (also known as an  $n$ -level system), this gives  $(n-1)^{\text{th}}$  order information about variable coupling. This means that allowing variables two values would only allow first-order information, *i.e.*, linear behaviour of each variable to be obtained. Three values for each variable would give second-order information, that is, quadratic variable behaviour and first order coupling between variables. Methods commonly allow 2 – 4 values for each variable. For a small set of variables and values, a full factorial method can be used to design the experiments, *i.e.*, every possible combination of variables is tested. If there are  $x$  variables that can each take  $y$  values, there will be  $y^x$  total experiments. Needless to say, this quickly becomes intractable, but it gives complete information about the system. For larger systems, there are specially designed algorithms for designing the experiments. These include Plackett-Burman<sup>37</sup> (for variables with two values) and Box-Behnken<sup>38</sup> (for variables with three values). Full-factorial designs for two and three level systems would normally require  $2^x$  and  $3^x$  experiments. Plackett-Burman and Box-Behnken designs only require on the order of  $x$  and  $x^2$  experiments respectively, for considerable savings, but at the cost of knowledge of higher order couplings.

The hypothetical example involves optimising a chemical reaction for the highest yield. The chemist has identified six potential variables that might affect the yield: reaction temperature; amount of catalyst added; whether the reaction is stirred; stoichiometry of the two reagents; the atmosphere the reaction is conducted in; and the time before the reaction is worked up. Each of these variables is assigned two values (Table 4.5). If every variable was tested independently, that would require  $2^6 = 64$  experiments. However, a Plackett-Burman design only requires 8 experiments to be performed (Table 4.6). This design is not unique, but it is one of many possible sets of experiments. The experiments are chosen so that every variable is tested with an equal number of “high” and “low” values. In contrast, the simplest set of experiments would allow one variable at a time to take their “high” value. This would cluster all of the variables around their “low” values and tend to bias the results in that direction. The Plackett-Burman design cuts out most of the experiments, but at the cost of higher-order information. If two variables interact with each other, for instance catalyst loading and temperature, this would not be seen in a Plackett-Burman design. The hypothetical yields of these chemical reactions are also shown in Table 4.6.

<i>Variable</i>	<i>“Low” Value</i>	<i>“High” Value</i>
Temperature	Room temperature	Reflux
Amount of catalyst	5 mol%	20 mol%
Stirring?	No	Yes
Amount of reagent B	1 equivalent	2 equivalents
Atmosphere	Air	Nitrogen
Reaction time	1 hour	6 hours

**Table 4.5.** Summary of hypothetical variables

<i>Expt.</i>	<i>Temp.</i>	<i>Catalyst</i>	<i>Stirring</i>	<i>Reagent B</i>	<i>Atm.</i>	<i>Time</i>	<i>Yield</i>
1	Reflux	20%	Yes	1 eq.	N <sub>2</sub>	1 h	55
2	RT	20%	Yes	2 eq.	Air	6 h	90
3	RT	5%	Yes	2 eq.	N <sub>2</sub>	1 h	80
4	Reflux	5%	No	2 eq.	N <sub>2</sub>	6 h	40
5	RT	20%	No	1 eq.	N <sub>2</sub>	6 h	88
6	Reflux	5%	Yes	1 eq.	Air	6 h	30
7	Reflux	20%	No	2 eq.	Air	1 h	40
8	RT	5%	No	1 eq.	Air	1 h	80

**Table 4.6.** Design of experiments and results for the experiments

The final phase of the experimental design is to analyse the results. At first glance, Table 4.6 might seem hopelessly complicated. But there exist statistical programs that will analyse common experimental designs. Additionally for full-factorial designs, linear algebra can be used to determine the quantitative effect of each variable. For a full-factorial method, the data can be fit exactly to an  $(n-1)$ th order polynomial, where  $n$  is the number of possible values for each variable. The results of the hypothetical chemical experiment are given in Table 4.7. Positive values favour the “high” variable values in Table 4.5, negative values favour the “low” variable values. The contributions show the quantitative effect each of the variables has on the yield (*i.e.*, stirring the reaction improves the yield by 3% on average). From only eight experiments, it can be concluded that A) increasing the temperature has a strongly deleterious effect on the product yield, B) increasing the catalyst loading and running the reaction under a protective atmosphere improve the yield, C) stirring the reaction improves the yield slightly, and D) the amount of reagent B and the reaction time have very little effect on the yield. This is a very large amount of information that can be taken from a small number of experiments, highlighting the utility of experimental design.

<i>Variable</i>	<i>Contribution to yield</i>	<i>Result</i>
Temperature	-42	Strongly favours room temperature
Amount of catalyst	12	Favours 20 mol% over 5 mol%
Stirring?	3	Little difference, stirring preferred
Amount of reagent B	0.5	Little difference
Atmosphere	7	Favours nitrogen over air
Reaction time	-0.5	Little difference

**Table 4.7.** Results of the hypothetical experimental design.

Experimental design was also used to screen the vibrational modes in CP to see which of them were important to the hydrogen-migration reaction. As before, the main stages were A) identifying the variables, B) designing experiments, and C) analysing the results. The variables were the 27 vibrational modes in CP and possible values were the number of quanta of additional energy that would be placed into those modes. Either a Plackett-Burman, Box-Behnken, or full factorial design would provide the trajectories that had to be run in order to determine the effect of additional energy in those vibrational modes.

The next step was to rate these trajectories. For the previous hypothetical chemical reaction, the experiments were rated based on their yield. It was less obvious how to rate a trajectory. None of the trajectories underwent a hydrogen shift, however even if some trajectories showed a shift, a binary rating scale would be undesirable. Such a scale would ignore those trajectories where the system was close to, but did not undergo an H-shift. Instead, the trajectories were graded on how close they approached one of the four possible TSs. These correspond to shifting either of the methylene Hs to either of the neighbouring Cs. Based on the atom numbering in Figure 4.8 (reproduced below), these were called the “17”, “18”, “57”, and “58” shifts. Note that the *endo* hydrogen is H7 and the *exo* hydrogen is H8. They are initially bonded to C2. A “17” shift means that H7 (*endo*) shifts from C2 to C1.

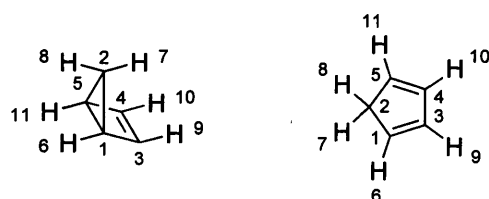


**Figure 4.8.** Atom numbering used in Gaussian calculations

The quality of each trajectory was rated on two components, one positional and one based on velocity. The positional component compared how much the structure at every point looked like each of the four possible TSs, based on comparison of the distance matrices. At each point in a trajectory, the positional “quality” was found by finding the RMS difference between every element the trajectory’s distance matrix and each of the four TS distance matrices. The distance matrix was chosen rather than the Cartesian coordinates to account for the molecules’ orientation in space. Rotation would change the Cartesian coordinate matrix, but not the distance matrix. The velocity component compared the direction of motion of the atoms at each point in the trajectory. The ideal velocity for each TS was the one that directly connected CP with that TS. This did not take into account the shape of the PES, but was simple to code. The hydrogen-shift TS structure was numbered to correspond to one of the four possible hydrogen shifts. For each of the atoms, their CP Cartesian coordinates were subtracted from their coordinates in the TS. This gives the effective “velocity” that would connect CP to that particular hydrogen-shift product. This was repeated for each of the other possible hydrogen shifts. The velocity “quality” at each point was found by finding the RMS difference between the atomic velocities at that point and the velocity necessary linking the reactant and one of the four TSs. These positional and velocity “qualities” were determined for each of the four possible hydrogen shifts. The positional and velocity “qualities” for each of the four TSs were normalised over the whole trajectory and then multiplied together to give the overall quality for each of the four TSs<sup>39</sup>. In addition to qualities for the 17, 18, 57, and 58 shifts (dubbed 17Q, 18Q, 57Q, and 58Q, respectively), additional combinations of them were considered. These were the average quality for both possible *endo* shifts (*i.e.*  $(17Q + 57Q) / 2$ ), the maximum quality for both of the *endo* shifts (*i.e.*  $\text{Max}(17Q, 57Q)$ ), and the corresponding values for the *exo* shifts. This generated eight sets of quality values, which could be analysed to determine the ideal energy in the bending modes. Finally, these “quality” values were used to determine the ideal quanta of energy in each of the vibrational modes to encourage each of the four possible hydrogen migrations.

The initial approach was to use a Plackett-Burman design to screen all 27 vibrational modes. Several Plackett-Burman designs were generated, all similar to the experiments given in Table 4.6. Overall, this approach was unsuccessful because each time the design was carried out, it suggested a different set of “important” vibrational modes. Further, the modes that were assumed to be important for chemical reasons (the

methylene bending modes) were usually not included as important modes in the screening results. It is possible that the chemical reasoning was incorrect and that there were numerous additional vibrational modes were important. Alternatively, it was possible that there were higher order effects taking place that the Plackett-Burman design would have overlooked. And it was possible that the “quality” criterion was inappropriate for this system. This could be because the trajectories did not actually pass through the TS, but only near it. The positional and velocity “qualities” based on the TS would not be accurate for those trajectories.

To compensate for this, chemical intuition was used to limit the vibrational modes tested to two modes assumed to be important to the reaction (See Section 4.3). These modes were the two methylene bending modes that brought the methylene hydrogens closer to the neighbouring carbons. A full factorial design for two variables would therefore have  $y^2$  experiments, where  $y$  is the number of energy values for each mode. Since this is small, six values were chosen for each variable, and a full-factorial design was chosen which required 36 trajectories to be run. Each vibrational mode was given initial energies of  $-5.5$ ,  $-3.5$ ,  $-1.5$ ,  $0.5$ ,  $2.5$ , or  $4.5$  quanta (including ZPE), while all other modes were only allowed their ZPEs. It was important that the values be evenly spaced and physically meaningful, which had the consequence of their not being centred about 0 energy. While a negative value of kinetic vibrational energy might seem strange, the sign simply indicated the corresponding momentum direction. For a given TS, the forward and reverse directions correspond to the two possible directions along the intrinsic reaction coordinate. The forward direction is defined as the direction that shows the steepest descent from the TS; in the case of the BCP-CP system the forward direction from the ring-opening TS is towards CP. For each vibrational mode, a positive number of quanta indicates the orientation that moves the system closer to CP, and a negative number of quanta indicates the orientation that moves the system closer to BCP. The resulting 36 trajectories were run, completing the first two phases of the statistical analysis. The “quality” of each of these trajectories was also found. A small subset of this data is in Table 4.8 (for 7 of the 36 trajectories and 2 of the 8 quality sets). Given these results, a set of matrix equations can be set up to determine the 5<sup>th</sup> order polynomial that best fits each set of data. Determining the global minimum for this polynomial is equivalent to finding the optimum values for of quanta in the two bending modes. Table 4.9 shows the optimised values of quanta for the two out-of-plane bending modes that should encourage the various possible hydrogen-shifts.

<i>Symmetrical Quanta</i>	<i>Antisymmetrical Quanta</i>	<i>"17 TS" Quality</i>	<i>"18 TS Quality"</i>
-3.5	-5.5	0.458	0.478
-1.5	-5.5	0.354	0.52
0.5	-5.5	0.527	0.449
2.5	-5.5	0.077	0.035
4.5	-5.5	0.036	0.028
-5.5	-3.5	0.439	0.475

**Table 4.8.** A small subset of data from the experimental trajectories

<i>Quality set</i>	<i>Symmetrical Quanta</i>	<i>Antisymmetrical Quanta</i>
17Q	4.5	3.5
18Q	-4.5	1.5
57Q	1.5	-2.5
58Q	-2.5	1.5
<i>Endo average (17Q+57Q)/2</i>	-4.5	-5.5
<i>Endo maximum [Max(17Q,57Q)]</i>	0.5	-2.5
<i>Exo average (18Q+58Q)/2</i>	4.5	3.5
<i>Exo maximum [Max(18Q,58Q)]</i>	-2.5	1.5

**Table 4.9.** Optimum quanta of energy according to the statistical analysis

The next step in the MD was to take these sets of quanta and simulate many trajectories. 99 trajectories on each of the sets of quanta in Table 4.9 were run<sup>40</sup>. These 99 trajectories differed in how the thermal energy at 333 K was randomly distributed amongst all of the vibrational modes, both as potential energy and kinetic energy. The results of this are shown in Table 4.10. Of the eight sets of optimum quanta shown in Table 4.9, there were two identical pairs, so only six sets of trajectories were run. In Table 4.10, "Correct H" refers to how many of the shifts involved the predicted (formerly) *endo* or *exo* hydrogen atom. "Correct shift" refers to how many of the shifts were exactly what was predicted, for instance a 17 shift or a 58 shift. The significances are binomial probabilities that show how likely the distribution of shifts would have been if the system was random (*i.e.* a 50% chance of getting the right hydrogen, and a 25% chance of getting the exact shift right). Our threshold was 95% significance.

Several conclusions were taken from these results. Firstly, the experimental design did a poor job of predicting which shift(s) would occur for a given input of vibrational energy. This might be because the BCP-CP system is more complicated than thought and could not be simplified to giving two vibrational modes extra amounts of energy. Secondly, the *endo* and *exo* sites are not distinguished from each other in this approach. Only one of the six inputs has a significant preference for shifting either the *endo* or *exo* hydrogens over the other, but it is subject to a possible small sample effect. Thirdly, and possibly the most basic conclusion, the approach of giving selected vibrational modes extra energy was successful in causing shifts to occur. While exciting only the two described methylene bending modes was not successful in understanding the system or finding nonstatistical effects, it suggested that giving the system more energy by increasing the temperature might also be successful.

<i>Optimisation Set (Table 4.9)</i>	17	18	57	58	<i>Endo avg</i>	<i>Endo max</i>
# BCP	20	27	23	29	23	19
# CP	72	62	68	64	67	75
# 17 shift ( <i>endo</i> )	4	2	3	2	3	2
# 18 shift ( <i>exo</i> )	2	0	2	1	1	0
# 57 shift ( <i>endo</i> )	0	5	0	2	2	3
# 58 shift ( <i>exo</i> )	1	3	3	1	3	0
% Correct H	57	30	38	33	56	100
Significance of <i>endo/exo</i>	50	83	64	66	50	97
% Correct shift	57	0	0	17		
Significance of exact shift	93	94	90	47		

**Table 4.10.** Summary of the statistically designed trajectories

#### 4.5.2.2 High-temperature MD studies of the BCP/CP system

The ring-opening of BCP to CP occurs at 333 K experimentally with roughly 8% of the molecules undergoing a hydrogen shift<sup>15b,41</sup>. Simulations at that temperature were unsuccessful in causing hydrogen shifts. Instead, trajectories were run at elevated temperatures to see if a) that would lead to more shifts and b) the shifts would show a preference between the *endo* and *exo* hydrogens. Table 4.11 shows the results for trajectories run at 1000 K, 1500 K, and 2000 K. Note that some of the trajectories

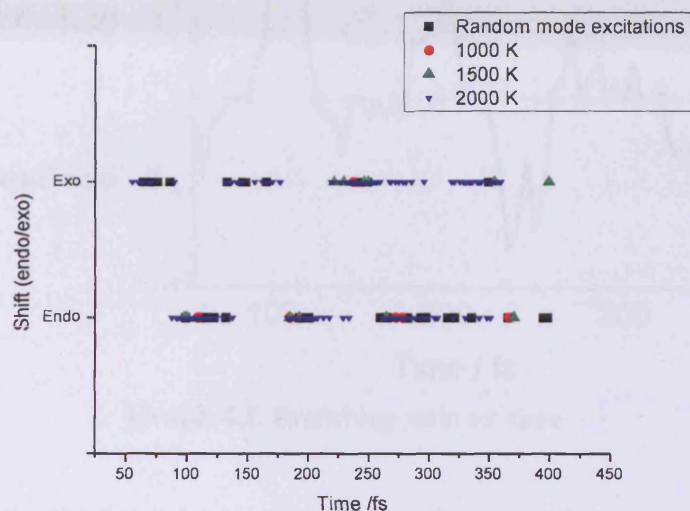
failed, usually because of SCF failure that led to energy not being conserved. These runs were ignored for the subsequent analysis.

<i>Temperature</i>	<i>1000 K</i>	<i>1500 K</i>	<i>2000 K</i>
# Trajectories	642	200	1998
Average Thermal Energy (kJ mol <sup>-1</sup> )	75	137	281
% SCF Failure	5.0	5.5	9.7
% BCP	0.9	1.5	1.6
% CP	92.1	87.0	77.6
% Endo shift	1.2	3.0	5.9
% Exo shift	0.8	3.0	5.3
Binomial Significance of shift (%)	71	39	75
MD rate constant (s <sup>-1</sup> )	5.44*10 <sup>11</sup>	1.67*10 <sup>12</sup>	3.42*10 <sup>12</sup>
RRKM rate constant (s <sup>-1</sup> )	4.10*10 <sup>11</sup>	9.00*10 <sup>11</sup>	3.17*10 <sup>12</sup>

**Table 4.11.** Summary of trajectories at various temperatures

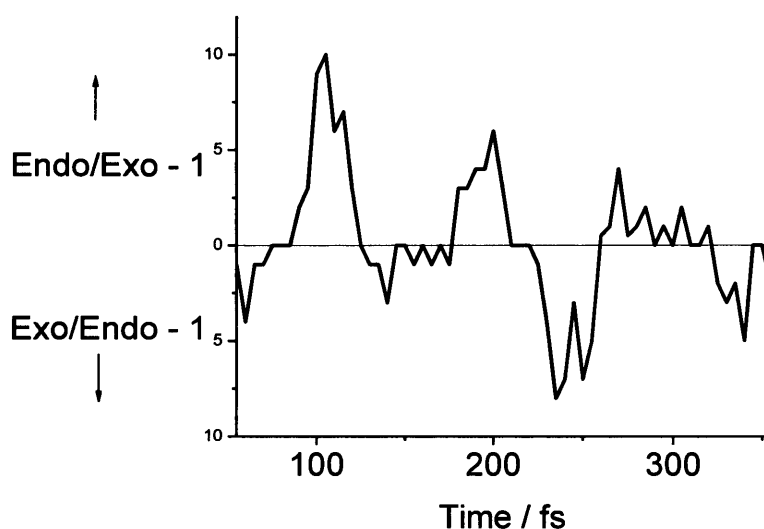
Again, several things stand out. The selectivity was not significant at any temperature. In contrast, the percentage of trajectories showing a shift increased with temperature. Because the trajectories at 2000 K gave the highest percentage of shifts, a larger number of trajectories were run at that temperature. There was a slight preference for the endo hydrogen to shift, but this was not statistically significant so that particular test for nonstatistical dynamics was inconclusive. The shift rate was compared to the rate predicted by RRKM theory using the MESMER program.<sup>23</sup> The shift rate constant was calculated based on how many shifts had occurred amongst all of the trajectories in the 500 fs the trajectories were run for. This was turned into a rate constant assuming first order behaviour. The RRKM calculations incorporated the energies and vibrational frequencies for both CP and the hydrogen shift transition state, the energy of BCP, and the average thermal energy gained by running the trajectories at 2000K. There were not enough observed hydrogen shifts to estimate the MD rate constant for the trajectories at 1000 or 1500 K, so the results are shown for 2000 K. The molecular dynamics had the hydrogen shift occurring at essentially the same rate as RRKM predicted. At this point, all of the tests for nonstatistical dynamics were essentially inconclusive.

The time-dependence of the hydrogen shift was also investigated. Graph 4.1 plots all of the observed hydrogen shifts from both the trajectories with extra energy in the bending modes (*vide infra*), and the trajectories run at higher temperature.



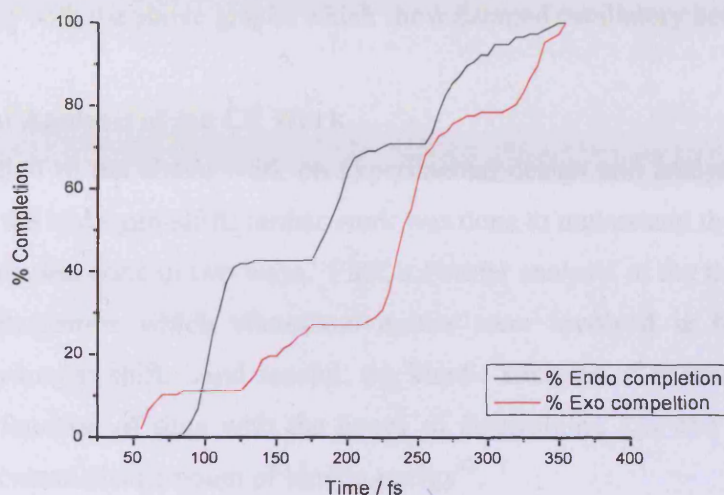
**Graph 4.1.** Shift vs. time

If the system was showing statistical behaviour, the time of the shift would be irrelevant and there would be no preference at any time for either the *endo* or *exo* hydrogen. Instead, not only was there a clear preference, but that preference appeared to oscillate. The period of the oscillation matched up with the vibrational period for the ring-bending mode of the BCP-CP TS, which suggested a way that the ring-opening and hydrogen shift reactions might be coupled to each other and might allow for nonstatistical effects (See Section 4.3). The preference seemed to die out after 300 fs, possibly because IVR had completed and the vibrational modes were no exchanging significant amounts of energy. In effect, at this point, CP had lost any “memory” it had of where it came from, so the system was now behaving statistically. Graph 4.2 shows the *endo/exo* branching ratio as a function of time. Conventional theory would predict a selectivity of 1 for all times, larger values indicate *endo* selectivity and smaller values indicate *exo* selectivity.



**Graph 4.2.** Branching ratio vs. time

This graph also showed a large oscillatory divergence from statistical behaviour, though the specific vibrational dependence is more difficult to see. The data predicted that if the reaction terminated before 250 fs, there would be a statistically significant excess of *endo* shifts over *exo* shifts, something that could be seen experimentally (See section 4.4) if solvent collisions were successful in deactivating vibrationally excited CP in that timeframe. A more clear way of seeing the time-dependence of the product distribution is shown in Graph 4.3. This shows the “reaction completion” for the molecules that either shift their *endo* (black) or *exo* (red) hydrogens (*i.e.*, the number of observed shifts to occur by that time divided by the total number of shifts observed at all times). This sort of graph should either be linear (0<sup>th</sup> order kinetics), a decaying exponential (1<sup>st</sup> order kinetics), or a similar decay for higher order kinetics. Instead, the reaction rate appeared to oscillate, yet another way of showing the oscillatory behaviour of this system. This was not consistent with any simple kinetic behaviour or in fact statistical behaviour in general. It also showed that the largest selectivity would be observed if the reaction was quenched after approximately 220 fs.



**Graph 4.3.** Reaction “completion” vs. time

#### 4.5.3 Reaction Mechanism

Based on the molecular dynamics results, we provide a prospective mechanism for the hydrogen shift that explains the oscillatory behaviour (Figure 4.10).

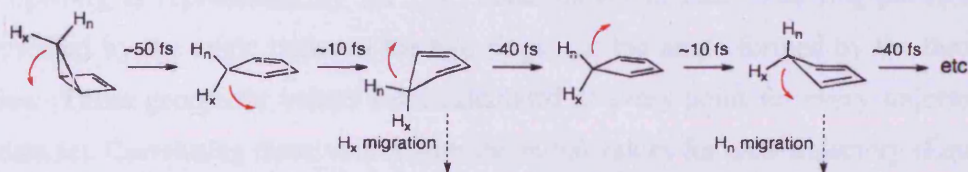


**Figure 4.10.** Proposed mechanism for the hydrogen shift

Calculations on the PES of bicyclopentene and cyclopentadiene suggest that the hydrogen shift is more facile from the *endo* face of cyclopentadiene than the *exo* face. This is possibly because of better orbital overlap between the *endo* C–H bond and the the CP  $\pi$  orbitals. That would suggest that initially, the hydrogen labelled  $H_n$  is in position to shift. However, the carbon framework is unsuitable for a shift at that time. Rather, the first opportunity for a hydrogen shift comes after the ring flattens out (the second structure). Conservation of momentum means that when the atom movement involved in flattening the 5-membered ring will continue to pucker the ring in the opposite direction (the third structure). It is at this point that the first shifts are seen. As Graphs 4.1 – 4.2 show, this is the hydrogen labelled  $H_x$ . From here, the ring flips again to form the fifth structure, where now  $H_n$  is again in position to shift. This time, the carbon framework is suitable, so the shift occurs. This oscillation can continue several

more times until eventually this oscillation damps out at approximately 250 fs. Again, this is consistent with the above graphs which show damped oscillatory behaviour.

#### 4.5.4 Statistical Analysis of the CP Work

In addition to the above work on experimental design and analysing the time-dependence of the hydrogen-shift, further work was done to understand the dynamics of the system. This was done in two ways. First, a Fourier analysis of the trajectories was performed to determine which vibrational modes were involved in both the ring-opening and hydrogen shift. And second, the kinetic energies of various bonds were analysed as a function of time with the hopes of determining  $k_{IVR}$  and seeing which bonds have a nonstatistical amount of kinetic energy<sup>42</sup>.

A Fourier transform interconverts data between the time and frequency domains. The MD trajectories gave a wealth of data as a function of time, transforming this data to the frequency domain allowed comparisons with vibrational modes. To do this, two geometrical coordinates (Figure 4.11) were chosen that represent the ring-opening and puckering that were predicted to be important to the mechanism (Figure 4.10). The ring-opening is represented by the C-C bond shown in red. The ring-puckering is represented by the angle between the two rings, *i.e.* the angle formed by the three red circles. These geometric values were calculated at every point for every trajectory in the data set. Correlating these values with the initial values for each trajectory (Equation 4.1) gave a time-dependent correlation function. Here,  $f(x,t)$  was either the distance or angle parameter at time  $t$  in the  $x^{th}$  trajectory that was correlated with  $f(x,1)$  - the first point in the distance/angle function of the  $x^{th}$  trajectory. Each step in the trajectories was sorted into 1 fs time bins and ensemble averaged to give a single function of time (Equation 4.2). Here,  $N$  was the number of points in a given time bin. This was then Fourier transformed to give a data set that was a function of frequency (Equation 4.3). Here,  $i$  was the imaginary number, and  $\nu$  was the frequency. The results of the FT are shown in Graph 4.4.

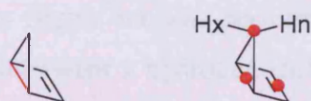
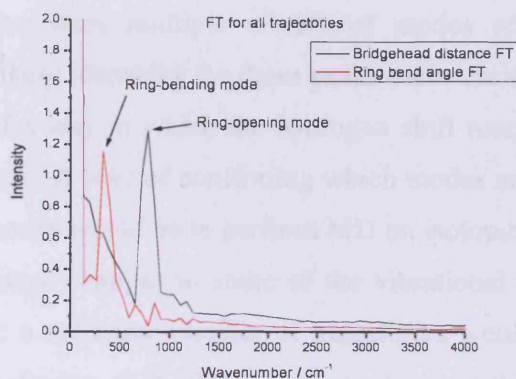


**Figure 4.11.** Geometric coordinates important to the Fourier analysis

$$\text{Corr}(x,t) = f(x,1) * f(x,t) \quad \text{Equation 4.1}$$

$$\text{AvgCorr}(t) = \frac{1}{N} \sum_{x=1}^N \text{Corr}(x,t) \quad \text{Equation 4.2}$$

$$\text{FT}(\nu) = \frac{1}{N} \sum_{t=1}^N \text{AvgCorr}(t) * e^{-2\pi i t \nu / N} \quad \text{Equation 4.3}$$



**Graph 4.4.** Fourier Transform of the geometrical data

This result can be likened to an IR spectrum where rather than representing dipolar transitions, the peaks represent vibrational mode coupling. In Graph 4.4, the black curve shows the C-C distance FT, and the red curve shows the ring-bend angle FT. Each of these would naturally show a strong correlation with themselves (the large black peak at  $\sim 700 \text{ cm}^{-1}$  and red peak at  $300 \text{ cm}^{-1}$ ). Note also that there appears to be a small red peak at  $700 \text{ cm}^{-1}$  and a small black peak at  $300 \text{ cm}^{-1}$  that overlap the larger ones. This suggested that the ring-opening and ring-puckering modes were strongly coupled to each other, as would be expected since both molecular motions were involved in the ring-opening reaction. There are additional peaks in the graph, which may also be important, but it was difficult to determine what vibrational modes they corresponded to, or in fact if the peaks were statistically significant rather than simply noise in the spectrum.

The Fourier analysis in Graph 4.4 was performed on all of the trajectories at 2000 K, whether the system underwent a hydrogen shift or remained at CP (those that went to BCP were ignored). In order to investigate a possible relation between the ring-opening and hydrogen-migration reactions, the Fourier analysis was also performed on only those trajectories that underwent a hydrogen shift. The shift names and atom numbering are the same as before and Figure 4.9 is reprinted for convenience. Those

results are shown in Graphs 4.5 – 4.8, with each graph analysing one of the four possible H-shifts. All of these graphs looked very similar to each other, and also qualitatively similar to the full set of trajectories analysed in Graph 4.4. They showed the self-correlational peaks, and the correlational peak between the ring-opening and ring-puckering. However, all four graphs showed new peaks at approximately 1000, 1300, and 1500  $\text{cm}^{-1}$  that appeared to be correlated to both the ring-opening and ring-puckering. While there were multiple vibrational modes with those approximate frequencies, the most likely identities for these peaks were the methylene out of plane bends, which suggested a way in which the hydrogen shift reaction was coupled with the ring-opening reaction. A way of confirming which modes are coupling to the ring-opening and bending modes would be to perform MD on isotopically labelled CP as the isotopes would cause large changes to some of the vibrational modes and effectively spread them out. Once a sufficient number of trajectories would be run in which the system underwent a hydrogen shift, the Fourier analysis could be performed and it would be seen if a peak appears that corresponds to the methylene bending. Some initial MD on the isotopomers was performed; however there was not enough time to run the number of trajectories that would have been required to obtain hundreds of hydrogen shifts. The vibrational coupling seen here could either be a direct coupling through energy transfer, or an indirect coupling. An indirect coupling could occur if the extra energy in the ring-bending mode caused the ring to pucker more than it otherwise would have, which in turn would allow a greater chance for the H-shift to occur (see the mechanism in Figure 4.10).

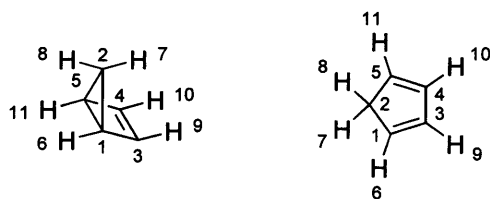
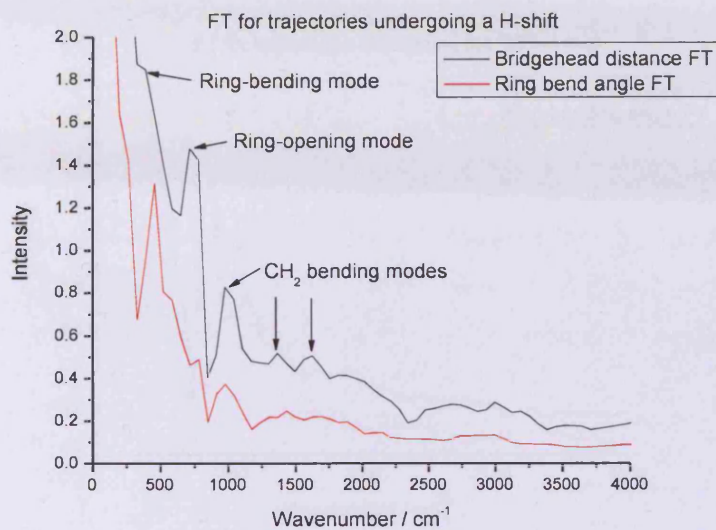
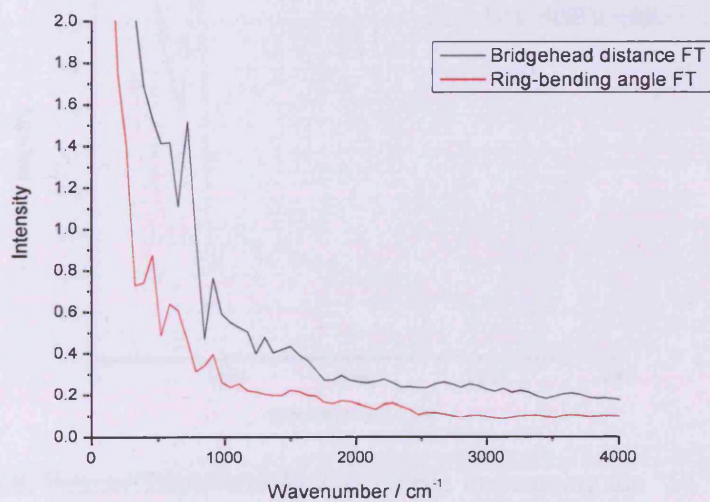


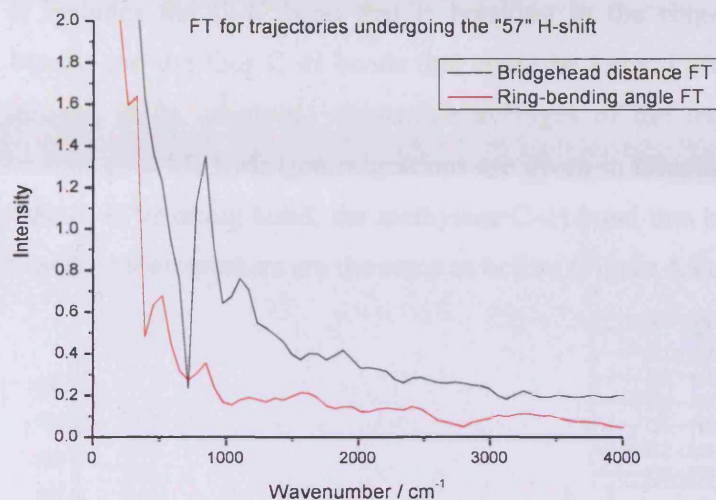
**Figure 4.8.** Atom numbering used in Gaussian calculations



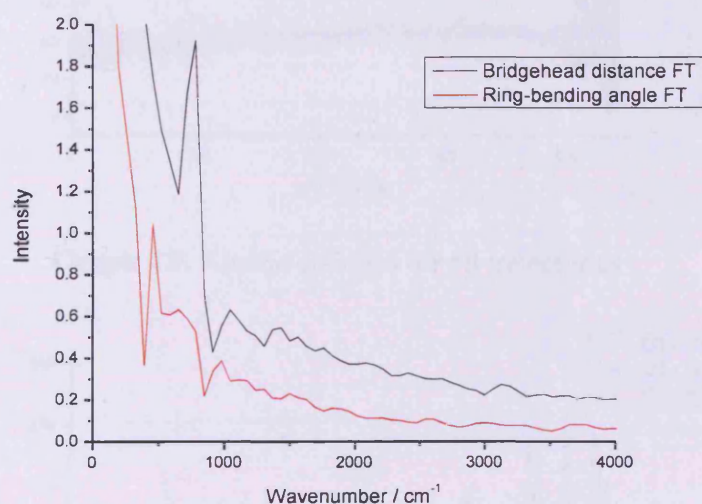
**Graph 4.5.** Fourier Transform for trajectories undergoing the “17” H-shift



**Graph 4.6.** Fourier Transform for trajectories undergoing the “18” H-shift



**Graph 4.7.** Fourier Transform for trajectories undergoing the “57” H-shift

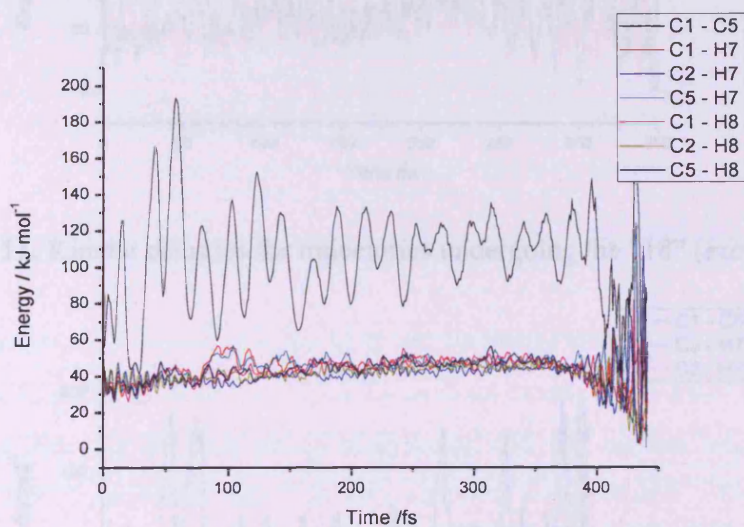


**Graph 4.8.** Fourier Transform for trajectories undergoing the “58” H-shift

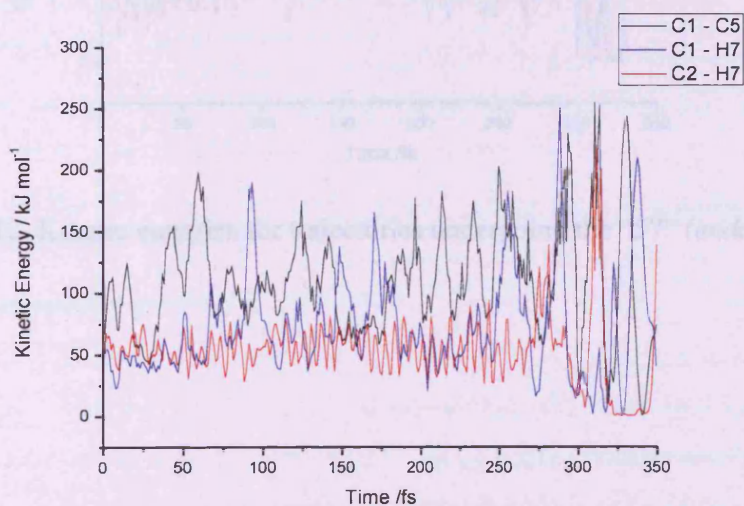
The second approach was to investigate the kinetic energy between various pairs of atoms as a function of time. If CP is formed in a nonstatistical vibrational state, certain atoms will have significantly more or less energy than others. As IVR occurs, this energy discrepancy will decay. Plotting the kinetic energy in various modes as a function of time would hopefully allow the “ $k_{IVR}$ ” to be determined (see Section 1.3).

The kinetic energy was calculated between any two atoms by comparing the atoms’ relative mass, position, and velocity for each step in the trajectory, with some algebra yielding the kinetic energy. As with the Fourier analysis, the kinetic energies

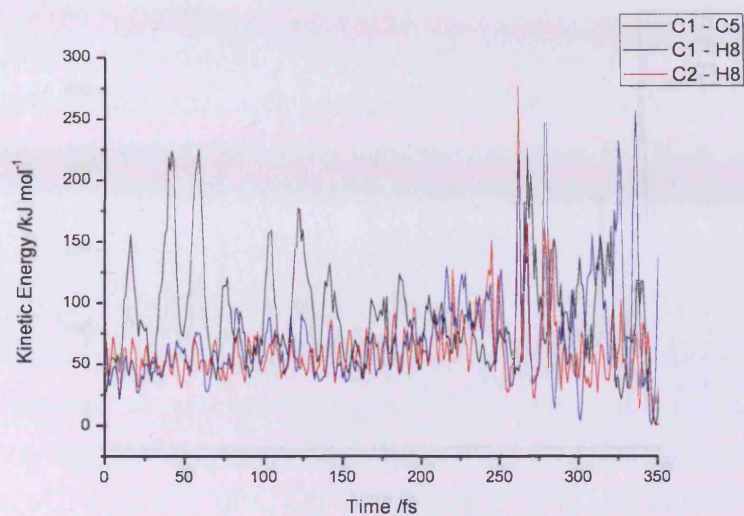
were ensemble averaged. The average for all trajectories that pass through CP is shown in Graph 4.9. It includes the C–C bond that is breaking in the ring-opening, the methylene C–H bonds, and the four C–H bonds that could be formed after any of the four possible hydrogen shifts occurred. Ensemble averages of the trajectories that showed one of the four possible hydrogen migrations are given in Graphs 4.10 – 4.13. These show only the C–C breaking bond, the methylene C–H bond that broke, and the C–H bond that formed. Atom numbers are the same as before (Figure 4.9).



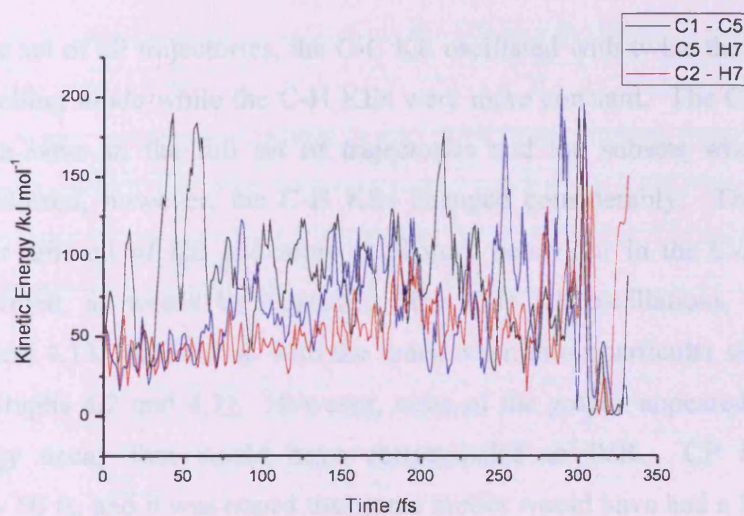
**Graph 4.9.** Kinetic energies for all trajectories



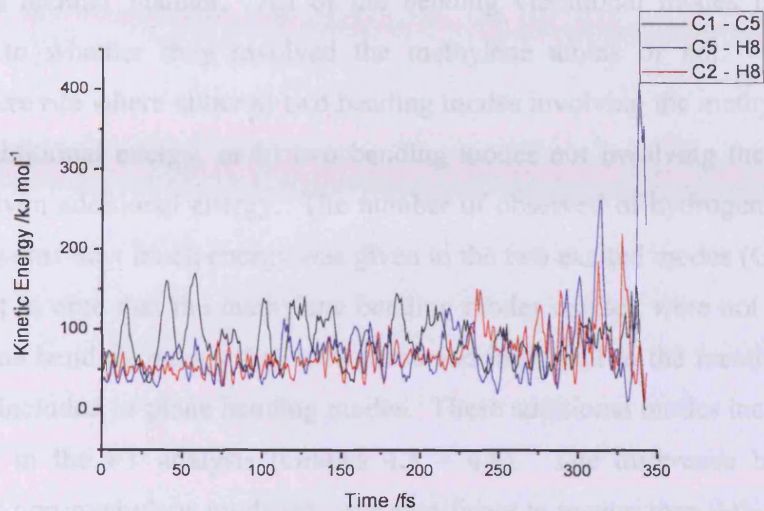
**Graph 4.10.** Kinetic energies for trajectories undergoing the “17” (*endo*) H-shift



**Graph 4.11.** Kinetic energies for trajectories undergoing the “18” (*exo*) H-shift



**Graph 4.12.** Kinetic energies for trajectories undergoing the “57” (*endo*) H-shift

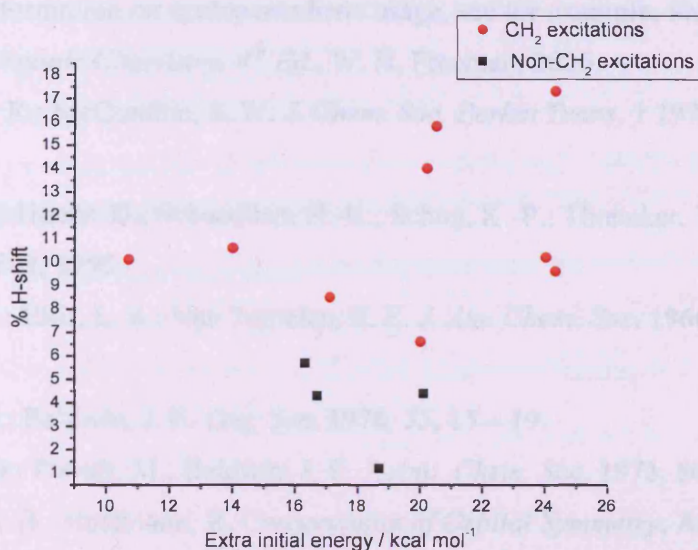


**Graph 4.13.** Kinetic energies for trajectories undergoing the “58” (*exo*) H-shift

For the set of all trajectories, the C-C KE oscillated with twice the frequency of that C-C stretching mode while the C-H KEs were more constant. The C-C KEs were essentially the same in the full set of trajectories and the subsets where hydrogen migrations occurred, however, the C-H KEs changed considerably. They tended to have a greater amount of KE and more oscillatory behaviour in the C-H bonds that broke and formed, as would be expected. The C-H KE oscillations, especially in Graphs 4.11 and 4.13, matched up with the times when those particular shifts are most favourable (Graphs 4.2 and 4.3). However, none of the graphs appeared to show the desired energy decay that would have corresponded to IVR. CP is formed at approximately 50 fs, and it was hoped that some modes would have had a large increase of energy around that time that would subsequently decay according to  $k_{IVR}$ . A possible explanation for the lack of decay is that because the reactions were intramolecular, all atoms were indirectly connected to each other at all times. As such, there was never a time when a large amount of KE was introduced or removed from the atoms. As such, this system is not ideal to determine  $k_{IVR}$ . Contrast that with work by Glowacki on the reaction between cyclopentyne and ethylene<sup>42</sup>. As an intermolecular reaction, there was a much clearer change in the kinetic energies between certain pairs of atoms as the two fragments were coupled together that allowed them to estimate  $k_{IVR}$  for that particular reaction.

While the kinetic energy analysis did not yield the desired information about which bonds showed a nonstatistical energy distribution, this information was

determined in another manner. All of the bending vibrational modes in CP were classified as to whether they involved the methylene atoms or not. Sets of 99 trajectories were run where either a) two bending modes involving the methylene group were given additional energy, or b) two bending modes not involving the methylene group were given additional energy. The number of observed of hydrogen migrations was plotted against how much energy was given to the two excited modes (Graph 4.14). It is important to note that the methylene bending modes excited were not necessarily the out-of-plane bending modes that were presumed important to the reaction (Section 4.2), but also included in-plane bending modes. These additional modes included those that appeared in the FT analysis (Graphs 4.5 – 4.8). The difference between the methylene and non-methylene mode sets was significant to greater than 99% confidence using Welch's t-test, which suggested that there were vibrational mode couplings. When extra energy was given to any bending modes involving the methylene group, that energy was eventually used to promote the hydrogen-migration. Energy given to modes involving other atoms was not used to promote the hydrogen-migration to any great extent. When energy is provided to the methylene bending modes, be it from selective mode excitations or as a consequence of raising the temperature to 2000 K, this energy is transferred to modes important for the hydrogen-migration through unexpected vibrational mode coupling, allowing for significant nonstatistical effects to take place.



**Graph 4.14.** Relative number of shifts seen from exciting methylene or non-methylene bending modes.

#### 4.6 Summary and Conclusions

DFT calculations with a small basis set gave reasonably accurate results for the CP-BCP system. MD simulations on the BCP-CP system showed significant evidence of nonstatistical effects. There was a very large time-dependence on when either the *endo* or *exo* shifts occurred, breaking the expected symmetry. There was also evidence for coupling between modes involved in the ring-opening reaction and modes involved in the hydrogen-migration reaction, either directly or indirectly. Giving additional energy to the methylene group through any bending modes was effective in promoting the hydrogen-migration, whereas according to conventional theory it should have been no more effective than giving energy to any other vibrational modes. All of this evidence together implies that there are significant nonstatistical effects that might be seen in the CP-BCP system using experimental techniques. This is all the more surprising because the CP-BCP system is not the sort of chemical system where nonstatistical behaviour would be expected. This suggests that nonstatistical dynamics may be more common than previously thought and should encourage more chemists to search for where it may appear.

#### 4.7 References for Chapter 4

1. Bordwell, F. G.; Drucker, G. E.; Fried, H. E. *J. Org. Chem.* **1981**, *46*, 632 – 635.
2. For further information on cyclopentadiene usage, see for example, Shriver, D.; Atkins, P. *Inorganic Chemistry*, 4<sup>th</sup> Ed., W. H. Freeman, 2006.
3. Barton, D. H. R.; McCombie, S. W. *J. Chem. Soc. Perkin Trans. 1* **1975**, *16*, 1574 – 1585.
4. Guttman, H.; Hoehr, D.; Schaedlich, H.-K.; Schug, K.-P.; Thuenker, W. U.S. Patent 5,386,804, **1995**.
5. Brauman, J. I.; Ellis, L. E.; Van Tamelen, E. E. *J. Am. Chem. Soc.* **1966**, *88*, 846 – 848.
6. Andrist, A. H.; Baldwin, J. E. *Org. Syn.* **1976**, *55*, 15 – 19.
7. Andrews, G.D.; Davalt, M.; Baldwin, J. E. *J. Am. Chem. Soc.* **1973**, 5044 – 5046.
8. Woodward, R. B.; Hoffmann, R. *Conservation of Orbital Symmetry*; Academic Press, Inc., 1970.
9. Roth, W. R. *Tetrahedron Lett.* **1964**, *17*, 1009 – 1013.
10. Brauman, J. I.; Golden, D. M. *J. Am. Chem. Soc.* **1968**, *90*, 1920 – 1921.

11. Andrist, A. H.; Baldwin, J. E. *Chem. Comm.* **1970**, *22*, 1561 - 1562.
12. Baldwin, J. E.; Pinschmidt, R. K., Jr.; Andrist, A. H. *J. Am. Chem. Soc.* **1970**, *92*, 5249 – 5250.
13. McLean, S.; Findlay, D. M.; Dmitrienko, G. I. *J. Am. Chem. Soc.* **1972**, *94*, 1380 – 1381.
14. Flowers, M. C.; Frey, H. M. *J. Am. Chem. Soc.* **1972**, *94*, 8636 – 8637.
15. (a) Brauman, J. I.; Farneth, W. E.; D'Amore, M. B. *J. Am. Chem. Soc.* **1973**, *95*, 5043 – 5044. (b) Farneth, W. E.; D'Amore, M. B.; Brauman, J. I. *J. Am. Chem. Soc.* **1976**, *98*, 5546 – 5552.
16. Dewar, M. J. S.; Kirschner, S. *J. Chem. Soc. Chem. Commun.* **1975**, *12*, 461 – 462.
17. Andrews, G. D.; Baldwin, J. E. *J. Am. Chem. Soc.* **1977**, *99*, 4853 – 4854.
18. Oezkan, I; Kinal, A.; Balci, M. *J. Phys. Chem. A* **2004**, *108*, 507 – 514.
19. (a) Carpenter, B. K. *Annu. Rev. Phys. Chem.* **2004**, *56*, 57 – 89. (b) Carpenter, B. K. *J. Phys. Org. Chem.* **2003**, *16*, 858 – 868.
20. Carpenter, B.K. Unpublished results
21. Schlosser, M. *J. Organomet. Chem.* **1967**, *8*, 9 – 16.
22. Cohen, A. J.; Handy, N. C. *Mol. Phys.* **2001**, *99*, 607 – 615.
23. MESMER: Robertson, S. H., Glowacki, D. R., Liang, C.-H.; Morley, C., Pilling, M. J., MESMER (Master Equation Solver for Multi-Energy Well Reactions), 2008; an object oriented C++ program for carrying out ME calculations and eigenvalue-eigenvector analysis on arbitrary multiple well systems.  
<http://sourceforge.net/projects/mesmer>
24. Common semiempirical methods include a) AM1: Dewar, M. J. S; Zoebisch, E. G.; Healy, E. F. *J. Am. Chem. Soc.* **1985**, *107*, 3902 – 3909. and b) PM3: Stewart, J. J. *P. J. Comp. Chem.* **1989**, *10*, 209 – 264.
25. Hegarty, D.; Robb, M. A. *Mol. Phys.* **1979**, *38*, 1795 – 1812.
26. Grimme's exchange and correlation: Grimme, S. *J. Comp. Chem.* **2006**, *27*, 1787 – 1799. Wilson, Bradley, and Tozer modification to above: Wilson, P. J.; Bradley, T. J.; Tozer, D. J. *J. Chem. Phys.* **2001**, *115*, 9233 – 9242.
27. Becke exchange, correlation, and hybridisation: Becke, A. D. *J. Chem. Phys.* **1996**, *104*, 1040 – 1046.
28. Cohen, A. J.; Handy, N. C. *Mol. Phys.* **2001**, *99*, 607 – 615.

29. Becke exchange: (a) Becke, A. D. *Phys. Rev. A* **1988**, *38*, 3098 – 3100. Lee, Yang, and Parr correlation: (b) Lee, C.; Yang, W.; Parr, R. G. *Phys. Rev. B* **1988**, *37*, 785 – 789. Hybridisation: (c) Becke, A. D. *J. Chem. Phys.* **1993**, *98*, 5648 – 5652
30. Perdew, Wang exchange and correlation: (a) Perdew, J. P.; Chevary, J. A.; Vosko, S. H.; Jackson, K. A.; Pederson, M. D.; Singh, D. J.; Fiolhais, C. *Phys. Rev. B* **1992**, *46*, 6671 – 6687. (b) Perdew, J. P.; Wang, Y. *Phys. Rev. B* **1992**, *45*, 13244 – 13249. Hybridisation: (c) Adamo, C.; Barone, V. *J. Chem. Phys.* **1998**, *108*, 664 – 675.
31. van Voorhis exchange and correlation: Van Voorhis, T.; Scuseria, G. E.; *J. Chem. Phys.* **1998**, *109*, 400 – 410.
32. Gallinella, E.; Fortunato, B.; Mirone, P. *J. Mol. Spect.* **1967**, *24*, 345 – 362.
33. Vibrational scaling frequencies: (a) Tantirungrotechai, Y.; Panasant, K.; Roddecha, S.; Surawatanawong, P.; Sutthikhum, V.; Limtrakul, J. *Theochem* **2006**, *760*, 189 – 192. (b) Irikura, K. K.; Johnson, R. D., III; Kacker, R. N. *J. Phys. Chem. A* **2005**, *109*, 8430 – 8437. (c) Merrick, J. P.; Moran, D.; Radom, L. *J. Phys. Chem. A* **2007**, *111*, 11683 – 11700.
34. Wiberg, K. B. *Acc. Chem. Res.* **1996**, *29*, 229 – 234.
35. Shelton, G. C.; Hrovat, D. A.; Borden, W. T. *J. Am. Chem. Soc.* **2007**, *129*, 164 – 168.
36. For general information about design of experiments and mathematical algorithms, see: Montgomery, D. C. *Design and Analysis of Experiments*, 7<sup>th</sup> Ed., John Wiley and Sons, 2009.
37. Plackett, R. L.; Burman, J. P. *Biometrika* **1946**, *33*, 305 – 325.
38. Box, G.; Behnken, D. *Technometrics* **1960**, *2*, 455 – 475.
39. There is not a unique way for the positional and velocity “quality” components to be combined. Several approaches were benchmarked against trajectories that underwent the shift. These were of the form  $p^x v^{4-x}$ . It was found that  $p^2 v^2$  gave the best results for trajectories that did undergo a shift (e.g. those run at 2000 K)..
40. 99 trajectories were chosen because of a limitation of the FORTRAN program used to write the input files that required a 2 digit number.
41. Carpenter, B. K. Unpublished results.
42. Glowacki, D. R.; Marsden, S. P.; Pilling, M. J. *J. Am. Chem. Soc.* **2009**, *131*, 13896 – 13897.

## Appendix

### A.1 X-ray Structure for Compound 74

Table 1. Crystal data and structure refinement for bc0901.

Identification code	bc0901	
Empirical formula	C <sub>36</sub> H <sub>28</sub> O <sub>2</sub>	
Formula weight	492.58	
Temperature	293(2) K	
Wavelength	0.71073 Å	
Crystal system	Monoclinic	
Space group	P21/c	
Unit cell dimensions	a = 7.6680(3) Å	α = 90°.
	b = 18.9390(7) Å	β = 90.13°.
	c = 17.2520(7) Å	γ = 90°.
Volume	2505.40(17) Å <sup>3</sup>	
Z	4	
Density (calculated)	1.306 Mg/m <sup>3</sup>	
Absorption coefficient	0.079 mm <sup>-1</sup>	
F(000)	1040	
Crystal size	0.40 x 0.30 x 0.20 mm <sup>3</sup>	
Theta range for data collection	2.66 to 27.49°.	
Index ranges	-9<=h<=9, -24<=k<=22, -22<=l<=22	
Reflections collected	9466	
Independent reflections	5715 [R(int) = 0.0680]	
Completeness to theta = 27.49°	99.5 %	
Max. and min. transmission	0.9843 and 0.9690	
Refinement method	Full-matrix least-squares on F <sup>2</sup>	
Data / restraints / parameters	5715 / 0 / 343	
Goodness-of-fit on F <sup>2</sup>	1.022	
Final R indices [I>2σ(I)]	R1 = 0.0728, wR2 = 0.1368	
R indices (all data)	R1 = 0.1378, wR2 = 0.1618	
Largest diff. peak and hole	0.201 and -0.219 e.Å <sup>-3</sup>	

Table 2. Atomic coordinates ( $\times 10^4$ ) and equivalent isotropic displacement parameters ( $\text{\AA}^2 \times 10^3$ ) for bc0901.  $U(\text{eq})$  is defined as one third of the trace of the orthogonalized  $U^{ij}$  tensor.

	x	y	z	$U(\text{eq})$
C(1)	9219(3)	2556(1)	1548(1)	28(1)
C(2)	8390(4)	1917(1)	1425(1)	34(1)
C(3)	8979(4)	1328(1)	1824(1)	38(1)
C(4)	10366(4)	1375(1)	2341(2)	42(1)
C(5)	11195(4)	2011(1)	2460(1)	36(1)
C(6)	10641(3)	2604(1)	2056(1)	29(1)
C(7)	11276(3)	3334(1)	2057(1)	28(1)
C(8)	12681(3)	3634(1)	2440(1)	36(1)
C(9)	13029(4)	4345(2)	2335(1)	39(1)
C(10)	11981(3)	4747(1)	1853(1)	34(1)
C(11)	10576(3)	4452(1)	1458(1)	30(1)
C(12)	10219(3)	3738(1)	1553(1)	26(1)
C(13)	8859(3)	3266(1)	1206(1)	26(1)
C(14)	8264(3)	3261(1)	348(1)	27(1)
C(15)	8585(3)	3916(1)	-108(1)	29(1)
C(16)	7331(3)	4481(1)	150(1)	31(1)
C(17)	6454(3)	4212(1)	898(1)	31(1)
C(18)	6988(3)	3438(1)	979(1)	27(1)
C(19)	5913(3)	1500(1)	-338(1)	31(1)
C(20)	6193(4)	863(1)	39(1)	36(1)
C(21)	5196(4)	695(2)	687(1)	42(1)
C(22)	3922(4)	1151(2)	956(2)	45(1)
C(23)	3610(4)	1783(2)	578(1)	42(1)
C(24)	4599(3)	1955(1)	-67(1)	32(1)
C(25)	4550(3)	2585(1)	-565(1)	33(1)
C(26)	3501(4)	3184(1)	-540(2)	42(1)
C(27)	3773(4)	3707(1)	-1088(2)	45(1)
C(28)	5042(4)	3636(1)	-1653(2)	42(1)
C(29)	6092(4)	3040(1)	-1682(2)	37(1)
C(30)	5836(3)	2514(1)	-1137(1)	31(1)
C(31)	6800(3)	1838(1)	-1017(1)	31(1)
C(32)	7537(3)	1472(1)	-1745(1)	31(1)
C(33)	7922(3)	702(1)	-1706(1)	32(1)
C(34)	9503(4)	584(1)	-1195(1)	40(1)

C(35)	9904(4)	1292(1)	-794(2)	42(1)
C(36)	8737(3)	1838(1)	-1187(1)	34(1)
O(1)	9631(2)	3969(1)	-630(1)	40(1)
O(2)	7161(3)	244(1)	-2064(1)	41(1)

Table 4. Anisotropic displacement parameters ( $\text{\AA}^2 \times 10^3$ ) for bc0901. The anisotropic displacement factor exponent takes the form:  $-2\pi^2 [ h^2 a^{*2} U^{11} + \dots + 2 h k a^* b^* U^{12} ]$

	$U^{11}$	$U^{22}$	$U^{33}$	$U^{23}$	$U^{13}$	$U^{12}$
C(1)	32(2)	29(1)	22(1)	-1(1)	7(1)	3(1)
C(2)	44(2)	29(1)	29(1)	1(1)	2(1)	2(1)
C(3)	52(2)	28(1)	35(1)	-3(1)	13(1)	5(1)
C(4)	52(2)	34(1)	39(2)	8(1)	13(1)	16(1)
C(5)	38(2)	42(2)	29(1)	5(1)	4(1)	14(1)
C(6)	30(2)	34(1)	24(1)	-1(1)	5(1)	9(1)
C(7)	24(1)	38(1)	22(1)	1(1)	4(1)	6(1)
C(8)	26(2)	54(2)	26(1)	3(1)	0(1)	5(1)
C(9)	29(2)	58(2)	30(1)	-7(1)	2(1)	-9(1)
C(10)	32(2)	38(1)	30(1)	-5(1)	7(1)	-9(1)
C(11)	30(2)	34(1)	25(1)	2(1)	2(1)	-2(1)
C(12)	26(1)	32(1)	21(1)	-2(1)	6(1)	1(1)
C(13)	29(2)	26(1)	22(1)	1(1)	-1(1)	1(1)
C(14)	31(2)	26(1)	23(1)	-1(1)	0(1)	1(1)
C(15)	29(2)	35(1)	22(1)	-2(1)	-2(1)	-1(1)
C(16)	33(2)	34(1)	27(1)	3(1)	-1(1)	4(1)
C(17)	26(2)	34(1)	32(1)	0(1)	2(1)	4(1)
C(18)	27(1)	29(1)	24(1)	-2(1)	2(1)	-3(1)
C(19)	30(2)	38(1)	24(1)	-8(1)	6(1)	-7(1)
C(20)	41(2)	37(1)	31(1)	-8(1)	8(1)	-4(1)
C(21)	51(2)	43(2)	32(1)	-4(1)	11(1)	-17(1)
C(22)	48(2)	59(2)	30(1)	-3(1)	16(1)	-18(2)
C(23)	33(2)	61(2)	33(1)	-15(1)	11(1)	-5(1)
C(24)	28(2)	45(2)	25(1)	-10(1)	6(1)	-8(1)
C(25)	23(1)	43(1)	33(1)	-12(1)	-2(1)	-4(1)
C(26)	37(2)	48(2)	39(2)	-14(1)	-1(1)	1(1)
C(27)	41(2)	42(2)	52(2)	-16(1)	-12(2)	2(1)
C(28)	42(2)	35(1)	49(2)	-3(1)	-11(1)	-11(1)
C(29)	35(2)	39(2)	38(1)	-6(1)	3(1)	-10(1)

C(30)	28(1)	34(1)	30(1)	-7(1)	2(1)	-7(1)
C(31)	27(2)	36(1)	28(1)	-7(1)	8(1)	-5(1)
C(32)	32(2)	38(1)	23(1)	-3(1)	9(1)	-2(1)
C(33)	32(2)	43(1)	22(1)	-3(1)	12(1)	1(1)
C(34)	33(2)	51(2)	35(1)	-3(1)	7(1)	6(1)
C(35)	30(2)	59(2)	36(1)	-7(1)	6(1)	-1(1)
C(36)	27(2)	43(1)	31(1)	-5(1)	8(1)	-6(1)
O(1)	42(1)	44(1)	34(1)	8(1)	10(1)	6(1)
O(2)	45(1)	41(1)	38(1)	-7(1)	2(1)	-1(1)

Table 5. Hydrogen coordinates ( $\times 10^4$ ) and isotropic displacement parameters ( $\text{\AA}^2 \times 10^3$ ) for bc0901.

	x	y	z	U(eq)
H(2)	7459	1883	1081	41
H(3)	8437	894	1745	46
H(4)	10736	975	2609	50
H(5)	12120	2042	2808	43
H(8)	13381	3361	2764	43
H(9)	13970	4553	2589	47
H(10)	12221	5225	1792	40
H(11)	9886	4728	1134	36
H(14)	8156	2809	75	32
H(16A)	6461	4567	-249	38
H(16B)	7949	4919	250	38
H(17A)	6849	4482	1342	37
H(17B)	5196	4253	859	37
H(18)	6079	3092	1101	32
H(20)	7038	551	-140	43
H(21)	5389	270	943	51
H(22)	3275	1032	1392	54
H(23)	2748	2089	754	51
H(26)	2640	3233	-165	50
H(27)	3091	4113	-1077	54
H(28)	5193	3993	-2017	51
H(29)	6949	2994	-2059	45
H(32)	7327	1688	-2253	37

H(34A)	10491	434	-1504	47
H(34B)	9262	222	-812	47
H(35A)	9646	1264	-244	50
H(35B)	11123	1415	-856	50
H(36)	9272	2283	-1353	40

---

## A.2 Computational Details for Chapter 2

### A.2.1 Molecular Dynamics Details

Born-Oppenheimer direct dynamics were run at the BS-UO3LYP/3-21G level of theory using the Gaussian03 suite of programs. Trajectories were begun from the ring-opening TS. Initial kinetic energy distributions were selected by quasiclassical normal-mode sampling from a canonical ensemble with a rotational temperature of 273 K. This sampling also served to randomly perturb the structures slightly from the optimised TS. In some cases, additional energy was given to specific vibrational modes. Trajectories were run for approximately 500 fs, or until a termination criterion was reached. The possible terminating states were either reaching the retro-Norrish product, Norrish fragmentation product, Norrish cyclisation product, or clock ring-opening product. For the retro-Norrish product, the termination was the appropriate C–H bond length becoming less than 1.20 Å. For the Norrish cyclisation, the termination was the appropriate C–C bond length becoming less than 1.60 Å. For the Norrish fragmentation and clock ring-opening reactions, the termination was the appropriate C–C bond length becoming greater than 2.00 Å. The timestep was chosen automatically by the program based on the energy gradient at each step. The program ensured that total energy was conserved.

### A.2.2 Computed Energies and Geometries

Note that geometries are in the form (Atomic Symbol:Atom Type:X:Y:Z) Cartesian coordinates are in Angstroms. Energies are in Hartrees. Electronic energy refers to the SCF single point energy. Frequencies are in  $\text{cm}^{-1}$ . Unless otherwise stated, calculations are performed with a simulated pressure and temperature of 1 atm and 298.15 K respectively.

Prop-1-en-2-ol (2)  
B3LYP/6-31+G(d)

C	0	-1.219764	-0.792205	-0.000197
C	0	-0.118515	-0.032654	-0.000059
C	0	1.293921	-0.547437	0.000093
O	0	-0.250270	1.341163	0.000547
H	0	-2.208684	-0.345590	-0.000472
H	0	-1.142201	-1.873052	0.000270
H	0	1.841337	-0.198461	-0.887252
H	0	1.313601	-1.640290	0.000065
H	0	1.841138	-0.198339	0.887475
H	0	0.623118	1.760206	-0.003481

Imaginary Frequency :	None
<S <sup>2</sup> >	0.0000
Electronic Energy	-193.137265757
Zero-point correction	0.084193
Thermal correction to Energy	0.089327
Thermal correction to Enthalpy	0.090271
Thermal correction to Gibbs Free Energy	0.057028

UMP2/6-31+G(d)

<S <sup>2</sup> >	0.0000
Electronic Energy	-192.505343

Biradical 31a

UB3LYP/6-31+G(d)

C	0	4.66495	-2.08956	-1.11739
C	0	4.03261	-3.0074	-0.26751
C	0	2.87223	-2.65227	0.43151
C	0	2.34889	-1.36834	0.27108
C	0	2.98922	-0.4434	-0.58344
C	0	4.14667	-0.80098	-1.27907
C	0	2.23329	0.81029	-0.54698
C	0	1.12451	0.65385	0.32702
C	0	0.25752	1.73217	0.52119
C	0	0.49540	2.94186	-0.14336
C	0	1.59034	3.08745	-1.00335
C	0	2.46525	2.01781	-1.20901
C	0	1.13740	-0.73825	0.87327
C	0	0.65137	-1.24926	2.21525
C	0	-0.13412	-1.71896	1.02417
C	0	-0.27818	-0.3977	3.08989
C	0	-1.66979	-0.39425	2.38511
C	0	-1.49672	-1.20864	1.12627
C	0	-2.55920	-1.42556	0.12665
C	0	-2.79017	-0.17371	-0.85234
C	0	-3.84135	-0.42455	-1.86177

C	0	-3.60695	-1.27535	-3.07054
O	0	-5.11104	-0.46984	-1.30675
H	0	5.56537	-2.38098	-1.6522
H	0	4.44732	-4.00523	-0.14784
H	0	2.39535	-3.37747	1.08761
H	0	4.64277	-0.09052	-1.93633
H	0	-0.60247	1.6558	1.17434
H	0	-0.18275	3.77714	0.01331
H	0	1.75994	4.03367	-1.51087
H	0	3.31778	2.12736	-1.8754
H	0	1.33991	-1.9185	2.72823
H	0	0.04479	-2.67871	0.54285
H	0	0.11528	0.61423	3.23751
H	0	-0.34591	-0.85643	4.08229
H	0	-2.03308	0.62650	2.18778
H	0	-2.44213	-0.84375	3.03189
H	0	-3.52935	-1.61107	0.60748
H	0	-2.32402	-2.29593	-0.49962
H	0	-1.84259	0.05817	-1.34716
H	0	-3.06622	0.68419	-0.22842
H	0	-4.35251	-1.0794	-3.85505
H	0	-3.65625	-2.35789	-2.84179
H	0	-2.61990	-1.07458	-3.49987
H	0	-5.75584	-0.74557	-1.97708

Imaginary Frequency :	None
<S <sup>2</sup> >	0.8664
Electronic Energy	-926.731177124
Zero-point correction	0.376718
Thermal correction to Energy	0.396978
Thermal correction to Enthalpy	0.397922
Thermal correction to Gibbs Free Energy	0.326740

UMP2/6-31+G(d)	
<S <sup>2</sup> >	1.08
Electronic Energy	-923.69399

**Biradical 31b**  
UB3LYP/6-31+G(d)

C	0	4.9218872733	-0.5282938936	-1.0628352596
C	0	4.3850730999	-1.796148406	-0.8014433685
C	0	3.086581756	-1.9309615111	-0.2937379308
C	0	2.3291550888	-0.7842817632	-0.0539328871
C	0	2.8713527404	0.4931770778	-0.3169746517
C	0	4.1677131191	0.6242767732	-0.8209991945
C	0	1.8620294302	1.498027963	0.0273508392
C	0	0.6975314762	0.8374006982	0.499876025
C	0	-0.4204422064	1.5944849269	0.8567489118
C	0	-0.3650371088	2.9909280819	0.7600812994

C	0	0.7920451001	3.6375927949	0.3102661351
C	0	1.9124089233	2.8905197265	-0.0634014621
C	0	0.9418662647	-0.6385451106	0.4805799602
C	0	0.4452627915	-1.6976109829	1.4512487802
C	0	-0.1025512857	-1.7641967132	0.0516274109
C	0	-0.7147586596	-1.3973968647	2.4065801078
C	0	-2.0098648361	-1.3953333617	1.5383840623
C	0	-1.5484722528	-1.5390073337	0.1069045847
C	0	-2.439727633	-1.6060295166	-1.0746684761
C	0	-2.9318586652	-0.2071607218	-1.6902934215
C	0	-4.1306177762	0.4018935148	-1.0678861798
C	0	-5.4859217117	-0.2240132583	-1.1701672403
O	0	-3.866707807	1.125257312	0.0874690679
H	0	5.9319812905	-0.4406053849	-1.4550611321
H	0	4.9821012295	-2.6843479673	-0.9929608832
H	0	2.685844241	-2.9226486731	-0.093991652
H	0	4.5893532584	1.6062590219	-1.0228845878
H	0	-1.3426390436	1.130731398	1.1823648741
H	0	-1.2403294111	3.5755277815	1.0316383937
H	0	0.8163014179	4.7224541256	0.2431923378
H	0	2.8089564682	3.3893787131	-0.4243969436
H	0	1.2037435816	-2.4024858586	1.7858701286
H	0	0.3035268204	-2.4335216263	-0.7056468894
H	0	-0.571214654	-0.4436481517	2.9270409782
H	0	-0.7564972596	-2.1743161391	3.1776137503
H	0	-2.6207951529	-0.4991318556	1.7007683014
H	0	-2.6621666401	-2.2452581242	1.8105323615
H	0	-3.3414885	-2.1967260101	-0.8527860111
H	0	-1.9156660861	-2.1220275988	-1.8897937593
H	0	-3.1638921953	-0.406118002	-2.7441917129
H	0	-2.0927569778	0.4953230557	-1.6648909752
H	0	-6.2869418893	0.5043511586	-0.9750606673
H	0	-5.626014285	-1.0549130339	-0.4511153672
H	0	-5.652093911	-0.629621652	-2.1739049934
H	0	-4.6975794147	1.4733536082	0.4480636381

Imaginary Frequency :	None
<S <sup>2</sup> >	0.9290
Electronic Energy	-926.726700400
Zero-point correction	0.376607
Thermal correction to Energy	0.396872
Thermal correction to Enthalpy	0.397816
Thermal correction to Gibbs Free Energy	0.326887

UMP2/6-31+G(d)	
<S <sup>2</sup> >	1.02
Electronic Energy	-923.694477

**Biradical 31c**  
UB3LYP/6-31+G(d)

C	0	4.6176374474	-0.1718880456	-1.7615285239
C	0	4.0956869574	-1.409479027	-1.3614314364
C	0	2.9371611381	-1.4759779153	-0.5771817839
C	0	2.3048727897	-0.2911908389	-0.1995496841
C	0	2.8325033099	0.9557506707	-0.6017788236
C	0	3.9890107835	1.0185194003	-1.3828512822
C	0	1.9730785282	2.0120626533	-0.0604734586
C	0	0.9158138096	1.4135244559	0.6738643401
C	0	-0.0468225424	2.230847759	1.2711828053
C	0	0.0536824171	3.6224386566	1.1454746307
C	0	1.1030694508	4.2057536319	0.4259208915
C	0	2.0682417926	3.3997861933	-0.1834851038
C	0	1.0742607254	-0.0729882418	0.6176023533
C	0	0.7155021497	-1.1126359301	1.6658897948
C	0	-0.1070848881	-1.1277820877	0.4081389105
C	0	-0.2057536123	-0.7515616129	2.8375283193
C	0	-1.6439976847	-0.6427804895	2.2442405632
C	0	-1.4826222139	-0.7696072156	0.7500770516
C	0	-2.6133963286	-0.6854918832	-0.2261315142
C	0	-3.4574832036	-1.9872269052	-0.3149245331
C	0	-4.6323066019	-1.8976093964	-1.2404107729
C	0	-4.4775924871	-1.6015308076	-2.7001593824
O	0	-5.6167546523	-2.8138610127	-0.8982491307
H	0	5.5183500205	-0.1373907112	-2.3691445222
H	0	4.5951408446	-2.327486215	-1.6609107989
H	0	2.5461638137	-2.4447869099	-0.2732170286
H	0	4.3999214358	1.976458526	-1.6931758125
H	0	-0.8771661069	1.8135479398	1.8272975536
H	0	-0.6965809186	4.2549007483	1.6136525204
H	0	1.1656290521	5.2875310319	0.3389017373
H	0	2.881433656	3.8505146304	-0.7476407352
H	0	1.4797790528	-1.8668410036	1.84258478
H	0	0.0907222827	-1.8088638548	-0.4183261996
H	0	0.1076789168	0.1782559687	3.3252973212
H	0	-0.150364143	-1.5395730056	3.5960399198
H	0	-2.1525436399	0.2888297304	2.5373946676
H	0	-2.2858514946	-1.4502656548	2.638335919
H	0	-2.2158282739	-0.4426935715	-1.2199742693
H	0	-3.2899381704	0.1372056921	0.0509782851
H	0	-3.8341723828	-2.2484238921	0.681477121
H	0	-2.7914229096	-2.8192638416	-0.6170901669
H	0	-5.4412556347	-1.3537471306	-3.1677874925
H	0	-4.0569084203	-2.4627810539	-3.255644434
H	0	-3.8113497135	-0.7488820721	-2.8651873029
H	0	-6.3281704694	-2.7909553951	-1.5579481844

Imaginary Frequency :

<S<sup>2</sup>>

Electronic Energy

Zero-point correction

None

1.0093

-926.726219057

0.376453

Thermal correction to Energy	0.396897
Thermal correction to Enthalpy	0.397841
Thermal correction to Gibbs Free Energy	0.325024

UMP2/6-31+G(d)	
<S <sup>2</sup> >	1.07
Electronic Energy	-923.692186

**Biradical 31d**  
UB3LYP/6-31+G(d)

C	0	4.5787211857	-2.182031333	-0.6544968937
C	0	3.5454828047	-3.0339800614	-0.2413777966
C	0	2.3068667229	-2.5144656847	0.155715938
C	0	2.1118121247	-1.1331542732	0.133099952
C	0	3.1542164372	-0.2753971617	-0.2823892056
C	0	4.3888872841	-0.7967834814	-0.6765814717
C	0	2.6700698569	1.1050348712	-0.2007765071
C	0	1.3290366765	1.0954401964	0.2651626947
C	0	0.6497104667	2.3077040656	0.4093225587
C	0	1.3040986013	3.5076414502	0.1018806409
C	0	2.6282793638	3.5094136967	-0.3517043551
C	0	3.3175308839	2.3038404886	-0.506659623
C	0	0.910836216	-0.3224506051	0.493590066
C	0	-0.0462036303	-0.8828187261	1.5326230712
C	0	-0.5036974742	-0.9529450162	0.102250153
C	0	-1.0009253595	0.0426017865	2.2957348148
C	0	-2.1057442063	0.4630787496	1.2788884554
C	0	-1.678784509	-0.0964423474	-0.0511180214
C	0	-2.4809805533	0.0217220458	-1.3009193817
C	0	-3.7725923351	-0.8711788884	-1.3389009167
C	0	-4.8893591177	-0.4227375944	-0.4576388339
C	0	-5.7377096772	0.7624479732	-0.7961197125
O	0	-5.513246231	-1.4763737457	0.1969703579
H	0	5.5344224753	-2.6013221509	-0.9587449531
H	0	3.7062847328	-4.1090984408	-0.22758501
H	0	1.5161818102	-3.1903344768	0.4748336195
H	0	5.1944858609	-0.1393850239	-0.9953908062
H	0	-0.3775600446	2.3429513922	0.7502535743
H	0	0.7723565155	4.4490211733	0.2172801971
H	0	3.1205297565	4.4500187385	-0.5856586867
H	0	4.3453161639	2.302210687	-0.8623614822
H	0	0.3090237457	-1.7727914271	2.0480983378
H	0	-0.4001430924	-1.8497247826	-0.5067054084
H	0	-0.4766386953	0.9084798575	2.7155877877
H	0	-1.4322765234	-0.5049494605	3.1405798861
H	0	-2.264986036	1.5523311969	1.2539335149
H	0	-3.0889376046	0.0438419672	1.5604091053
H	0	-1.8624195854	-0.2600199194	-2.1622895081
H	0	-2.7856984406	1.0663881938	-1.4691978604

H	0	-3.5076748165	-1.8999335048	-1.0693919214
H	0	-4.1078991299	-0.8976168326	-2.3923797428
H	0	-6.293619089	1.1355032646	0.0763417725
H	0	-6.4815665854	0.5303743854	-1.5831131926
H	0	-5.1230606252	1.5904105062	-1.1663118304
H	0	-6.2674615154	-1.1426062822	0.7085359882

Imaginary Frequency :	None
<S <sup>2</sup> >	0.9653
Electronic Energy	-926.726164803
Zero-point correction	0.376396
Thermal correction to Energy	0.396694
Thermal correction to Enthalpy	0.397638
Thermal correction to Gibbs Free Energy	0.325865

UMP2/6-31+G(d)	
<S <sup>2</sup> >	1.07
Electronic Energy	-923.692045

### Rot TS 31ab

UB3LYP/6-31+G(d)

C	0	4.7948571235	-0.4968345314	-1.3942074994
C	0	4.2993854959	-1.7683147634	-1.0743835204
C	0	3.0635000663	-1.9123960126	-0.4315053183
C	0	2.326983825	-0.7708976203	-0.111923853
C	0	2.8294335067	0.5101288886	-0.4310764026
C	0	4.0623165507	0.6501812329	-1.0731839133
C	0	1.861792657	1.5076072641	0.0310727341
C	0	0.7621545875	0.8387506624	0.631759297
C	0	-0.2896709739	1.5959419357	1.1537415293
C	0	-0.2424604017	2.9935739797	1.0759598462
C	0	0.8444134207	3.6451200237	0.4813851086
C	0	1.903435342	2.9014057621	-0.0452171841
C	0	0.9979136235	-0.6365127859	0.5543988713
C	0	0.5603738576	-1.7313980411	1.5069408502
C	0	-0.0803998647	-1.763812521	0.1474000239
C	0	-0.5413117616	-1.478876965	2.5440109274
C	0	-1.8807338792	-1.371568383	1.7522635635
C	0	-1.5160115524	-1.5549704242	0.299192358
C	0	-2.4880488683	-1.5044810692	-0.8114513922
C	0	-2.7981596496	-0.0126113261	-1.3771482976
C	0	-4.2040312549	0.4132889415	-1.2059686703
C	0	-5.3204469525	-0.1828198154	-2.005613775
O	0	-4.5011451069	0.7519856999	0.1073029904
H	0	5.7559882231	-0.4019677274	-1.8931834624
H	0	4.8800609626	-2.6522605184	-1.3262546937
H	0	2.6946688578	-2.9069933126	-0.1894903103
H	0	4.4528020801	1.6348807043	-1.3196853504
H	0	-1.151225005	1.1281656853	1.6125245901

H	0	-1.0658021838	3.5759223354	1.4819754127
H	0	0.8640940264	4.7307718135	0.429067891
H	0	2.7499576359	3.4042845112	-0.50714301
H	0	1.3380551211	-2.4453664555	1.7722300134
H	0	0.2873139707	-2.3932031118	-0.6610479241
H	0	-0.3403938196	-0.5845114186	3.1446695383
H	0	-0.5672268225	-2.3247161625	3.2397960427
H	0	-2.4071761414	-0.4246518229	1.9383844687
H	0	-2.5930100651	-2.1524984062	2.0696131565
H	0	-3.4441610179	-1.9405915414	-0.4935295044
H	0	-2.1261136831	-2.0991058128	-1.6592544448
H	0	-2.5440871707	0.0006191486	-2.4422274273
H	0	-2.1315826535	0.6926797044	-0.8745733256
H	0	-6.2252928055	0.4412677239	-1.9696770942
H	0	-5.6081432067	-1.1888196307	-1.6413932726
H	0	-5.0342776778	-0.2838077465	-3.0578078995
H	0	-5.446997157	0.950989849	0.1899109837

Imaginary Frequency :	34.9773i
<S <sup>2</sup> >	0.8959
Electronic Energy	-926.725789278
Zero-point correction	0.376620
Thermal correction to Energy	0.396021
Thermal correction to Enthalpy	0.396965
Thermal correction to Gibbs Free Energy	0.328562

UMP2/6-31+G(d)	
<S <sup>2</sup> >	1.09
Electronic Energy	-923.689849

### Rot TS 31cd

UB3LYP/6-31+G(d)

C	0	4.6140252398	-1.8975712143	-1.1416110965
C	0	3.6889150694	-2.840013322	-0.6724467861
C	0	2.4822584537	-2.4289001532	-0.0922531471
C	0	2.2095347113	-1.064601879	0.0113904695
C	0	3.1435421118	-0.1154572918	-0.4598541262
C	0	4.3466664281	-0.5289799884	-1.0368490114
C	0	2.597815735	1.222540829	-0.2170815095
C	0	1.3269182416	1.0950750341	0.4025305837
C	0	0.6026458143	2.2481559999	0.7140279379
C	0	1.1454717866	3.5059429265	0.4212783937
C	0	2.4026579085	3.6239886263	-0.1828174139
C	0	3.1344946723	2.478649296	-0.507132709
C	0	1.0192635713	-0.358896057	0.5724228101
C	0	0.2263566924	-1.0479884236	1.6695642787
C	0	-0.398493498	-1.0474905678	0.3024427152
C	0	-0.6759488652	-0.2381355929	2.609193477
C	0	-1.9165328562	0.1872658759	1.7659209433

C	0	-1.6229128716	-0.2512709688	0.3533706796
C	0	-2.5652338352	-0.0509987961	-0.7873577307
C	0	-3.7834259459	-1.0521648275	-0.781810597
C	0	-5.1240754019	-0.3976855509	-0.7266039492
C	0	-5.6139533007	0.4976760709	-1.8218769127
O	0	-6.0723299678	-1.2027001428	-0.111802935
H	0	5.5463406761	-2.2331882969	-1.5886529493
H	0	3.9096452073	-3.9010511666	-0.7582718933
H	0	1.7758238776	-3.1737911271	0.2682519113
H	0	5.0692402963	0.1985810378	-1.3992324979
H	0	-0.3767391587	2.1934491369	1.1726901696
H	0	0.5789828454	4.4007665808	0.6674165247
H	0	2.809002015	4.6080672695	-0.4023625242
H	0	4.1093922054	2.5674586902	-0.980965876
H	0	0.6886151686	-1.9474263394	2.071592049
H	0	-0.3220469589	-1.8908677052	-0.3821033732
H	0	-0.1500542485	0.6258950638	3.0310640539
H	0	-0.9715984969	-0.8695698924	3.4538853035
H	0	-2.1270134694	1.2654167016	1.8388176202
H	0	-2.8323629788	-0.3023316294	2.1416735479
H	0	-2.0209362609	-0.1467678251	-1.7341967155
H	0	-2.9568414657	0.9753555123	-0.7578363682
H	0	-3.7073662429	-1.7287098383	0.0773411658
H	0	-3.7060145041	-1.6975545063	-1.6769930886
H	0	-6.4747015471	1.1034354984	-1.5033965777
H	0	-5.9307413055	-0.078065755	-2.7134127766
H	0	-4.830283588	1.1908767326	-2.1451360962
H	0	-6.9416414916	-0.7732171524	-0.1524319254

Imaginary Frequency :	49.4617i
<S <sup>2</sup> >	0.9921
Electronic Energy	-926.722423910
Zero-point correction	0.376363
Thermal correction to Energy	0.395882
Thermal correction to Enthalpy	0.396826
Thermal correction to Gibbs Free Energy	0.327331

UMP2/6-31+G(d)	
<S <sup>2</sup> >	1.07
Electronic Energy	-923.687975

**Clock TS 31a**  
UB3LYP/6-31+G(d)

C	0	4.4143206553	-0.5838105595	-1.9877449038
C	0	4.0011356007	-1.8404374111	-1.5229180961
C	0	2.9287354899	-1.9555916211	-0.6305083648
C	0	2.2704449355	-0.7983885116	-0.2060744796
C	0	2.6920456174	0.4694407485	-0.6729925192
C	0	3.7619373628	0.5784819135	-1.5634403402

C	0	1.8439311797	1.4862729218	-0.049771075
C	0	0.9027702803	0.8402525883	0.7998389566
C	0	-0.0058974394	1.6216956679	1.5211178766
C	0	0.0224625807	3.0152444541	1.3913252863
C	0	0.9476557562	3.6420738911	0.5476141483
C	0	1.8647924605	2.8761364855	-0.1769282418
C	0	1.1164173967	-0.6278631288	0.7095925745
C	0	0.7359063643	-1.7399709384	1.6447358137
C	0	-0.1333288641	-1.7690116844	0.4232056588
C	0	-0.186294013	-1.4801373298	2.8465704477
C	0	-1.6254452475	-1.3020869719	2.270200746
C	0	-1.4897060493	-1.4778451699	0.7773068292
C	0	-2.641200886	-1.4187273453	-0.1767592543
C	0	-3.252739686	-0.001543212	-0.3459813093
C	0	-4.4131272417	0.0498770736	-1.2939376276
C	0	-4.2572846605	-0.2423139711	-2.7547250362
O	0	-5.2967795726	1.0670998728	-0.9613672526
H	0	5.249754478	-0.5125732336	-2.6795596907
H	0	4.5201204906	-2.7355062999	-1.8567803036
H	0	2.6232415812	-2.9389944669	-0.2795811519
H	0	4.0905713533	1.5513798579	-1.9216845986
H	0	-0.7364330259	1.1753088469	2.1837130326
H	0	-0.6863668805	3.6161290519	1.9556971125
H	0	0.9540069537	4.7254071397	0.4587495042
H	0	2.5888636003	3.360001353	-0.828471937
H	0	1.5047940968	-2.4997041766	1.7846029249
H	0	0.1139611997	-2.3267389065	-0.4753012518
H	0	0.1393256337	-0.6146397091	3.4332363426
H	0	-0.1429221212	-2.3472262262	3.514208149
H	0	-2.0695575248	-0.3350670724	2.5482260198
H	0	-2.3148901369	-2.0576298653	2.6832379828
H	0	-3.4459918488	-2.0890518229	0.1662217453
H	0	-2.3166308865	-1.7936165548	-1.1559187612
H	0	-2.4547204211	0.6920510015	-0.6700893597
H	0	-3.6004058588	0.3660021841	0.6266373861
H	0	-5.2291082298	-0.3991652957	-3.2444682585
H	0	-3.6645893828	-1.1481544423	-2.9180635552
H	0	-3.7500138991	0.5845029586	-3.2892241061
H	0	-5.9839621442	1.1399993593	-1.6428117434

Imaginary Frequency :	333.1882i
$\langle S^2 \rangle$	1.0154
Electronic Energy	-926.725605788
Zero-point correction	0.375769
Thermal correction to Energy	0.395846
Thermal correction to Enthalpy	0.396790
Thermal correction to Gibbs Free Energy	0.324910

UMP2/6-31+G(d)	
$\langle S^2 \rangle$	1.64
Electronic Energy	-923.6383

**Clock product 32a**  
UB3LYP/6-31+G(d)

C	0	5.2496	-1.76833	-1.45358
C	0	4.56719	-2.94938	-1.12303
C	0	3.29074	-2.9023	-0.55634
C	0	2.69168	-1.65322	-0.31866
C	0	3.39509	-0.45348	-0.65865
C	0	4.66408	-0.513	-1.22218
C	0	2.53159	0.67508	-0.2998
C	0	1.32243	0.13692	0.24773
C	0	0.30746	1.01	0.6776
C	0	0.50156	2.38969	0.56454
C	0	1.68972	2.90758	0.0277
C	0	2.71137	2.04909	-0.40829
C	0	1.40962	-1.3064	0.24428
C	0	0.39563	-2.28217	0.76057
C	0	-1.04285	-2.06715	0.31235
C	0	0.24365	-2.29795	2.31987
C	0	-1.23218	-2.68102	2.57847
C	0	-1.93527	-2.29316	1.2875
C	0	-3.43408	-2.26628	1.15319
C	0	-4.11303	-1.17982	2.01852
C	0	-5.60818	-1.1588	1.91407
C	0	-6.3112	-0.86916	0.62368
O	0	-6.18765	-0.63477	3.06061
H	0	6.24181	-1.82552	-1.89376
H	0	5.03726	-3.91138	-1.31074
H	0	2.77404	-3.82599	-0.30703
H	0	5.20341	0.3949	-1.48293
H	0	-0.62031	0.62111	1.08583
H	0	-0.27914	3.07002	0.89544
H	0	1.82082	3.98367	-0.05256
H	0	3.62848	2.46144	-0.82307
H	0	0.70782	-3.28529	0.42997
H	0	-1.29393	-1.82169	-0.71729
H	0	0.43876	-1.2921	2.70764
H	0	0.95953	-2.97684	2.79448
H	0	-1.64245	-2.17955	3.4642
H	0	-1.34788	-3.76261	2.75582
H	0	-3.84572	-3.24445	1.44469
H	0	-3.694	-2.11756	0.09792
H	0	-3.69486	-0.1931	1.73813
H	0	-3.85647	-1.32945	3.07377
H	0	-7.38043	-1.11879	0.67897
H	0	-5.8871	-1.45098	-0.20082
H	0	-6.23862	0.20049	0.34523
H	0	-7.14588	-0.5489	2.93362

Imaginary Frequency :

None

<S <sup>2</sup> >	1.0248
Electronic Energy	-926.765881776
Zero-point correction	0.377315
Thermal correction to Energy	0.397903
Thermal correction to Enthalpy	0.398847
Thermal correction to Gibbs Free Energy	0.325581

UMP2/6-31+G(d)

<S <sup>2</sup> >	1.9766
Electronic Energy	-923.659588

### Clock TS 31b

UB3LYP/6-31+G(d)

C	0	4.8490643024	-0.5260206442	-1.1977599258
C	0	4.3674525506	-1.7843227404	-0.8090351147
C	0	3.113251225	-1.9130382804	-0.2009439837
C	0	2.3405698591	-0.7681847303	0.0139915335
C	0	2.8312240001	0.5021569189	-0.3744216055
C	0	4.0832990637	0.6242889569	-0.9802491894
C	0	1.8289455165	1.5036531541	-0.0097835371
C	0	0.7240263094	0.8447085058	0.6004583578
C	0	-0.3671028677	1.606503214	1.0318599248
C	0	-0.3492278515	2.9956409658	0.8629951981
C	0	0.7440548158	3.6373071168	0.267594009
C	0	1.8393609532	2.8897083496	-0.1736216002
C	0	0.9994290957	-0.6132182038	0.6223323591
C	0	0.4406663023	-1.7156280497	1.4728714132
C	0	-0.1286536036	-1.8274752605	0.0914274411
C	0	-0.7396325601	-1.4623423258	2.4250154623
C	0	-2.0170893257	-1.3757337591	1.5334749562
C	0	-1.5390302621	-1.5965681284	0.1160983773
C	0	-2.4114603968	-1.6132944011	-1.0836116404
C	0	-2.8482908772	-0.1833021018	-1.6660122657
C	0	-4.0759301884	0.417606318	-1.0928333275
C	0	-5.4302569598	-0.1834816636	-1.3002662264
O	0	-3.8757830003	1.1029325411	0.0967236943
H	0	5.8258550946	-0.4438832938	-1.6677534063
H	0	4.9749302009	-2.6697770319	-0.9794123401
H	0	2.7566522539	-2.8972837893	0.0952721182
H	0	4.4648696124	1.598674221	-1.2768955267
H	0	-1.2388806581	1.1472964713	1.4790273021
H	0	-1.203394072	3.5802611791	1.1951280411
H	0	0.7391880886	4.7175740752	0.1457346978
H	0	2.6894215955	3.3845728404	-0.637958559
H	0	1.1812118456	-2.4399415429	1.8129909928
H	0	0.3474110382	-2.3870354162	-0.708238443
H	0	-0.5904455285	-0.5609939173	3.0290336374
H	0	-0.8102128733	-2.3026351987	3.1240224509
H	0	-2.5501692227	-0.4249901344	1.6505466839

H	0	-2.7482691733	-2.1533298124	1.8139158336
H	0	-3.3312656554	-2.1842227813	-0.889143502
H	0	-1.8860210436	-2.1262562178	-1.8991231601
H	0	-3.0180326496	-0.3333437827	-2.7396264408
H	0	-2.0043653801	0.5057026877	-1.5603709346
H	0	-6.2317552875	0.5532025115	-1.141383430035
H	0	-5.6304984444	-1.027738396	-0.6118227096
H	0	-5.5346409698	-0.5634126935	-2.3221750172
H	0	-4.7233393736	1.4503204271	0.4169584664

Imaginary Frequency :	382.6233i
<S <sup>2</sup> >	0.9336
Electronic Energy	-926.725768745
Zero-point correction	0.375870
Thermal correction to Energy	0.395825
Thermal correction to Enthalpy	0.396769
Thermal correction to Gibbs Free Energy	0.326305

UMP2/6-31+G(d)	
<S <sup>2</sup> >	1.87
Electronic Energy	-923.636215

**Clock product 32a**  
UB3LYP/6-31+G(d)

C	0	5.4339680944	-0.7967307827	0.1389806007
C	0	4.7201019705	-2.0047817449	0.1717447467
C	0	3.3229049263	-2.0098430856	0.1523706997
C	0	2.6329026895	-0.7862794934	0.1000130542
C	0	3.3692628338	0.4414241975	0.0667035532
C	0	4.7588225286	0.4336085288	0.086073243
C	0	2.3938640096	1.5340825165	0.0148494194
C	0	1.0869964693	0.9481302087	0.0170521193
C	0	-0.0475738223	1.7784653041	-0.0267847481
C	0	0.1280589322	3.1648324491	-0.0716868478
C	0	1.4119198139	3.7306079199	-0.0751188144
C	0	2.5531209506	2.914191547	-0.031658249
C	0	1.2215629889	-0.4912711265	0.0712327847
C	0	0.1168786074	-1.5047358841	0.109762105
C	0	-0.9358554618	-1.3750058462	-0.9820832906
C	0	-0.7590057369	-1.4630889661	1.4087883629
C	0	-2.1840871333	-1.8564333978	0.9558331151
C	0	-2.1862049961	-1.5584951019	-0.5337421105
C	0	-3.4413570778	-1.5481046885	-1.3642997229
C	0	-4.1712725951	-0.1638235429	-1.4555264881
C	0	-4.7445319132	0.3992936046	-0.1979229183
C	0	-5.9096930621	-0.2134355665	0.512437567
O	0	-3.8120438041	1.0763153469	0.5765303528
H	0	6.5207536747	-0.8132792148	0.1543450906
H	0	5.2608528543	-2.9469685923	0.2120501128

H	0	2.7840577478	-2.9539367606	0.1769480452
H	0	5.3234350805	1.3630226432	0.0608030127
H	0	-1.0490015266	1.3594216405	-0.0287590335
H	0	-0.7445538213	3.8122856874	-0.1068519026
H	0	1.525073794	4.8112171782	-0.1121731268
H	0	3.5442817413	3.3624069641	-0.0344309187
H	0	0.5798524617	-2.5002689985	0.0255692926
H	0	-0.6635891691	-1.2006783498	-2.0209663821
H	0	-0.7683744335	-0.4413097449	1.8017798224
H	0	-0.3559509359	-2.1131341282	2.192466376
H	0	-2.9575679582	-1.3035830429	1.5011686272
H	0	-2.3845846799	-2.927779408	1.1207314051
H	0	-4.1481404104	-2.2968185875	-0.9790790577
H	0	-3.2006624411	-1.8455920352	-2.393414551
H	0	-4.9887213993	-0.2831950926	-2.1803138035
H	0	-3.4690364056	0.5648706951	-1.8791959238
H	0	-6.4201310664	0.5151324652	1.160332312
H	0	-5.6232929801	-1.0669362067	1.1563752499
H	0	-6.6490112772	-0.5818884015	-0.2073196527
H	0	-4.2440365157	1.4408462206	1.3655830973

Imaginary Frequency :	None
$\langle S^2 \rangle$	1.0243
Electronic Energy	-926.764449301
Zero-point correction	0.377337
Thermal correction to Energy	0.397851
Thermal correction to Enthalpy	0.398796
Thermal correction to Gibbs Free Energy	0.326015

UMP2/6-31+G(d)	
$\langle S^2 \rangle$	1.98
Electronic Energy	-923.659588

**Clock TS 31c**  
UB3LYP/6-31+G(d)

C	0	4.3520246088	-2.2484554201	-1.1101683855
C	0	3.547570098	-3.0285169821	-0.2673167034
C	0	2.4627651245	-2.4614652656	0.4118022464
C	0	2.1880740136	-1.1021792868	0.2389077097
C	0	3.0039797661	-0.3156594039	-0.6090877876
C	0	4.0847868983	-0.8865269973	-1.2840471607
C	0	2.4960567214	1.0563478902	-0.5802300976
C	0	1.3687451713	1.1095377209	0.2866987153
C	0	0.7218217764	2.3346066451	0.481363212
C	0	1.1897116246	3.4780580579	-0.1767463358
C	0	2.2973192681	3.4154789944	-1.031340758
C	0	2.955958957	2.2000262991	-1.2350791618
C	0	1.1165153811	-0.2558859781	0.8159079984
C	0	0.37622507	-0.7204891809	2.0377726926

C	0	-0.4232113386	-1.0253765157	0.8080663317
C	0	-0.4495019411	0.2670437071	2.8776120119
C	0	-1.7439572728	0.5692635049	2.0597535238
C	0	-1.6272700066	-0.2519345513	0.7977410291
C	0	-2.590642227	-0.1739108367	-0.3455739827
C	0	-4.0656240841	-0.36041199	0.0671771335
C	0	-5.0441491313	-0.2172460519	-1.0593878185
C	0	-4.9406590291	-1.0173272235	-2.321337016
O	0	-6.3260768671	0.003521956	-0.5772837411
H	0	5.1908620752	-2.7049883445	-1.6293623658
H	0	3.769290593	-4.0848817922	-0.137395393
H	0	1.850166147	-3.0822654998	1.0620945502
H	0	4.7159471625	-0.2844038667	-1.933651494
H	0	-0.1381903417	2.4227751406	1.1329630368
H	0	0.6834542927	4.4271762227	-0.0185047739
H	0	2.6464530571	4.3137260233	-1.5341695823
H	0	3.8196751499	2.1489817099	-1.8940727554
H	0	0.8650549042	-1.5259348773	2.5858796026
H	0	-0.3317237679	-1.9494410057	0.2449342711
H	0	0.1168186872	1.1738134721	3.114710842
H	0	-0.6989974156	-0.2078139218	3.8323392367
H	0	-1.8709459028	1.6423417434	1.8487840176
H	0	-2.6408806451	0.287415247	2.6333898198
H	0	-2.312551254	-0.9238144053	-1.0968071453
H	0	-2.4991929846	0.8069971841	-0.8475502743
H	0	-4.331943225	0.377025997	0.834492442
H	0	-4.1801836746	-1.35199825	0.5498955289
H	0	-5.6196993964	-0.6350679497	-3.0966987115
H	0	-5.1969434196	-2.0828651298	-2.1590977319
H	0	-3.9283849419	-0.9828538848	-2.7358142208
H	0	-6.9587068546	-0.0019622755	-1.3130133512

Imaginary Frequency :	346.9389i
<S <sup>2</sup> >	1.0073
Electronic Energy	-926.725992026
Zero-point correction	0.375819
Thermal correction to Energy	0.395815
Thermal correction to Enthalpy	0.396759
Thermal correction to Gibbs Free Energy	0.325875

UMP2/6-31+G(d)	
<S <sup>2</sup> >	1.85
Electronic Energy	-923.637216

**Clock Prod 32c**  
UB3LYP/6-31+G(d)

C	0	5.1751578978	-2.1150266577	-0.403799047
C	0	4.0973626491	-2.980161218	-0.15951264
C	0	2.8093704161	-2.4775365742	0.0430679208

C	0	2.6006806091	-1.0882663383	-0.0000597704
C	0	3.7059982518	-0.2129659003	-0.2494686427
C	0	4.9824315462	-0.72471096	-0.4497250333
C	0	3.1886237585	1.1582660453	-0.2359137413
C	0	1.7809610763	1.0860450548	0.0188059944
C	0	1.0262995782	2.2705986504	0.0840874565
C	0	1.6680633111	3.4989928333	-0.0977380067
C	0	3.0475399527	3.5600538848	-0.3459655139
C	0	3.8143265048	2.3861735872	-0.417134856
C	0	1.4035826536	-0.3016902685	0.1698152124
C	0	0.0429494416	-0.8453810443	0.4858134638
C	0	-1.1121987636	-0.3019786585	-0.343893097
C	0	-0.451576027	-0.5531390904	1.9437709844
C	0	-1.99169897	-0.4662250343	1.8350049834
C	0	-2.2255370443	-0.1051380754	0.377183137
C	0	-3.5596620795	0.3627880851	-0.13676291
C	0	-4.6798499595	-0.688197337	0.0330871778
C	0	-6.0275163742	-0.2345195936	-0.4406103755
C	0	-6.2825944348	0.158003931	-1.8633163963
O	0	-7.0449711257	-0.9294336975	0.1972928297
H	0	6.1697102639	-2.5251158675	-0.5593101135
H	0	4.2669347633	-4.0534096341	-0.1279648431
H	0	1.9843662533	-3.1606448535	0.2299494115
H	0	5.8260213596	-0.064877364	-0.6396778292
H	0	-0.043477671	2.2351245356	0.2654801309
H	0	1.0904825278	4.4186557605	-0.0483437135
H	0	3.5277814397	4.5251740901	-0.4857185668
H	0	4.8829771879	2.445427723	-0.6111306467
H	0	0.0826197452	-1.9367194026	0.3430951822
H	0	-1.0290566689	-0.1493523136	-1.4177256198
H	0	-0.0481003281	0.4120981106	2.2690985523
H	0	-0.1057769614	-1.3108466261	2.6543929126
H	0	-2.4227094879	0.2694776743	2.5280170756
H	0	-2.4660130663	-1.4308041436	2.0737491665
H	0	-3.4591014045	0.6361798611	-1.1943635813
H	0	-3.86109694	1.2752402622	0.4000635014
H	0	-4.7747271826	-0.9616985276	1.0908021429
H	0	-4.3778577626	-1.6136091468	-0.4959188978
H	0	-7.2522272912	0.6635306569	-1.9764647569
H	0	-6.2901129131	-0.7192043667	-2.5397249735
H	0	-5.515839283	0.8474970253	-2.2304756185
H	0	-7.901311539	-0.6825658012	-0.1865893542

Imaginary Frequency :	None
<S <sup>2</sup> >	1.0246
Electronic Energy	-926.766234672
Zero-point correction	0.377326
Thermal correction to Energy	0.397896
Thermal correction to Enthalpy	0.398840
Thermal correction to Gibbs Free Energy	0.325938

UMP2/6-31+G(d)

<S<sup>2</sup>>

Electronic Energy

1.98

-923.659588

**Clock TS 31d**

UB3LYP/6-31+G(d)

C	0	4.6871053149	-1.9720954361	-0.8082712138
C	0	3.7734683333	-2.8935146778	-0.2767574448
C	0	2.5378799564	-2.4677979989	0.2246334325
C	0	2.2218341106	-1.1068115812	0.1882052871
C	0	3.1472648488	-0.1779096952	-0.3453145163
C	0	4.378490756	-0.6083026875	-0.8437191689
C	0	2.5606541255	1.1580456665	-0.2358337178
C	0	1.2765309993	1.0464108458	0.3680615405
C	0	0.5292701592	2.2084929896	0.5890398621
C	0	1.0517840353	3.4509009787	0.2106763332
C	0	2.3136087248	3.5505497555	-0.3886881102
C	0	3.0740952662	2.3999137955	-0.6131196904
C	0	1.0033088735	-0.389436955	0.6317668831
C	0	0.0458611413	-1.0584215389	1.5766555189
C	0	-0.44914371	-1.1910686847	0.1689712729
C	0	-1.0035091202	-0.24113102	2.3463475682
C	0	-2.1018672497	0.1544415351	1.3104204834
C	0	-1.6637518114	-0.4524627013	0.0022372605
C	0	-2.4106829311	-0.3140692652	-1.2831027167
C	0	-3.839146805	-0.944952699	-1.2860782042
C	0	-4.87204472	-0.2006977436	-0.5056673613
C	0	-5.3927392752	1.131743348	-0.944038336
O	0	-5.7747195269	-1.0490118006	0.120575711
H	0	5.6426096593	-2.320106863	-1.1923792421
H	0	4.0274886397	-3.9503230308	-0.2513787458
H	0	1.8425712229	-3.1973707809	0.6344234724
H	0	5.0932417359	0.1031532067	-1.2510705971
H	0	-0.44976937	2.1717899041	1.0497854478
H	0	0.4667597901	4.3501560904	0.388083545
H	0	2.7028109944	4.5238742523	-0.6764426851
H	0	4.0566172673	2.4741115029	-1.0736332826
H	0	0.4537549111	-1.9260493645	2.0951521054
H	0	-0.1833996982	-2.0147753132	-0.4870354503
H	0	-0.5609476639	0.6304504755	2.8403968003
H	0	-1.4270257855	-0.870718458	3.1361292839
H	0	-2.2444894981	1.2435625236	1.2417595415
H	0	-3.0907222009	-0.2368402832	1.6005540628
H	0	-1.8329514088	-0.7861817411	-2.0873376229
H	0	-2.5038395652	0.7485733095	-1.5633762617
H	0	-3.7842073719	-1.9691681751	-0.8989337333
H	0	-4.1520893094	-1.0284004205	-2.3443386652
H	0	-5.9114437688	1.6583717229	-0.12973051
H	0	-6.1092714321	1.0420244292	-1.7838123912

H	0	-4.578349934	1.7814134428	-1.2823847892
H	0	-6.4692171354	-0.5264094066	0.5524142568

Imaginary Frequency :	339.1254i
<S <sup>2</sup> >	0.9781
Electronic Energy	-926.725551103
Zero-point correction	0.375712
Thermal correction to Energy	0.395643
Thermal correction to Enthalpy	0.396587
Thermal correction to Gibbs Free Energy	0.325805

UMP2/6-31+G(d)	
<S <sup>2</sup> >	1.87
Electronic Energy	-923.636215

### Cyclisation Prod 33b

UB3LYP/6-31+G(d)

C	0	3.86512	-2.23106	-0.80899
C	0	2.95956	-3.19286	-0.34137
C	0	1.69271	-2.81661	0.12162
C	0	1.33952	-1.4674	0.1139
C	0	2.25338	-0.5017	-0.35277
C	0	3.51683	-0.87789	-0.81653
C	0	1.62901	0.81592	-0.2279
C	0	0.32693	0.66362	0.32002
C	0	-0.43437	1.81124	0.56109
C	0	0.08238	3.07563	0.24401
C	0	1.35936	3.21071	-0.30962
C	0	2.13997	2.07646	-0.54439
C	0	0.06406	-0.80164	0.54268
C	0	-0.70917	-1.46853	1.68689
C	0	-1.2122	-1.63342	0.28453
C	0	-1.73593	-0.67289	2.48753
C	0	-2.8883	-0.31476	1.50454
C	0	-2.6191	-1.05249	0.1634
C	0	-3.63009	-2.18134	-0.23142
C	0	-3.56418	-1.71977	-1.70643
C	0	-2.95476	-0.37809	-1.24129
C	0	-3.97969	0.75477	-1.17451
O	0	-1.8567	-0.01079	-2.06357
H	0	4.84418	-2.53957	-1.16645
H	0	3.2422	-4.24258	-0.3377
H	0	1.00382	-3.578	0.48078
H	0	4.2223	-0.13337	-1.17795
H	0	-1.42081	1.75259	1.00075
H	0	-0.52047	3.95943	0.43736
H	0	1.74565	4.19725	-0.55224
H	0	3.13686	2.17578	-0.96716
H	0	-0.17494	-2.26401	2.20291

H	0	-1.01584	-2.53987	-0.28298
H	0	-1.30012	0.21566	2.96068
H	0	-2.10593	-1.30891	3.30022
H	0	-2.97192	0.76554	1.35983
H	0	-3.85523	-0.6265	1.91606
H	0	-4.61588	-2.01118	0.21613
H	0	-3.32434	-3.2107	-0.0121
H	0	-4.50485	-1.66719	-2.26534
H	0	-2.83211	-2.28384	-2.29209
H	0	-3.54704	1.66572	-0.74193
H	0	-4.85428	0.47928	-0.57266
H	0	-4.31858	0.99195	-2.18936
H	0	-1.37704	0.72987	-1.65478

Imaginary Frequency :	None
<S <sup>2</sup> >	0.0000
Electronic Energy	-926.797061253
Zero-point correction	0.381908
Thermal correction to Energy	0.400285
Thermal correction to Enthalpy	0.401229
Thermal correction to Gibbs Free Energy	0.336624

UMP2/6-31+G(d)	
<S <sup>2</sup> >	1.14
Electronic Energy	-923.886454

### Cyclisation product 33d

UB3LYP/6-31+G(d)

C	0	4.3455485074	-1.426651157	-1.0435203954
C	0	3.4614779258	-2.4410954123	-0.6526766491
C	0	2.191957179	-2.1274261168	-0.150615975
C	0	1.8152572979	-0.7888661291	-0.0446697547
C	0	2.7079433653	0.2311480543	-0.433763569
C	0	3.9740267365	-0.0834704214	-0.9349111721
C	0	2.0570181431	1.5227460313	-0.2016445465
C	0	0.7574881645	1.2995332884	0.3225161675
C	0	-0.0442167797	2.4006630689	0.6311995644
C	0	0.4422145418	3.6968586995	0.4195647306
C	0	1.724403248	3.9073132052	-0.1002215594
C	0	2.5385064199	2.8168513904	-0.4138724765
C	0	0.53598122	-0.1825824652	0.4517496706
C	0	-0.1797518515	-0.9131001815	1.5990347079
C	0	-0.7440782095	-1.0113011562	0.2180396264
C	0	-1.1593880082	-0.1441993814	2.4793649384
C	0	-2.4104111395	0.1419067972	1.5983479596
C	0	-2.1384220677	-0.3814948713	0.1582892969
C	0	-3.208645505	-1.3639085516	-0.5096339348
C	0	-2.9471020422	-0.6588307198	-1.8644456425
C	0	-2.3575301723	0.5422829761	-1.0856388817

C	0	-4.637229724	-1.1542256236	-0.0174371821
O	0	-2.9979501405	-2.7689426549	-0.4289488979
H	0	5.3271467313	-1.6862809143	-1.4316804098
H	0	3.7632028239	-3.4820001294	-0.7380464651
H	0	1.5213997445	-2.9282584735	0.1545570813
H	0	4.6642081803	0.700935152	-1.236606571
H	0	-1.0453828443	2.2771709389	1.0235340656
H	0	-0.1890902822	4.5482507511	0.6616398842
H	0	2.0864720887	4.9197760596	-0.2596701459
H	0	3.5359998305	2.9753849426	-0.8169293814
H	0	0.3776406795	-1.7330111847	2.0470286762
H	0	-0.5570200554	-1.8980416415	-0.3827395051
H	0	-0.7143730824	0.7738623962	2.8812116524
H	0	-1.4243372479	-0.7660229232	3.3417320989
H	0	-2.674755953	1.2053572773	1.5898772797
H	0	-3.2772107867	-0.375365499	2.0212550673
H	0	-3.8153672452	-0.4873996505	-2.5105921089
H	0	-2.1754139665	-1.1762872354	-2.4484267089
H	0	-1.4643749093	1.0125068461	-1.5026245706
H	0	-3.1057732546	1.3198548062	-0.89501023
H	0	-4.7774425804	-1.5908456385	0.9770900864
H	0	-5.3282588207	-1.6548388328	-0.7046685372
H	0	-4.8997399867	-0.0922229875	0.0272794567
H	0	-2.1942114351	-3.0038907645	-0.9169490721

Imaginary Frequency :	None
<S <sup>2</sup> >	0.0000
Electronic Energy	-926.795538370
Zero-point correction	0.381880
Thermal correction to Energy	0.400346
Thermal correction to Enthalpy	0.401291
Thermal correction to Gibbs Free Energy	0.336429

UMP2/6-31+G(d)	
<S <sup>2</sup> >	1.15
Electronic Energy	-923.71888

**Frag TS 31a**  
UB3LYP/6-31+G(d)

C	0	4.4052712179	-0.5168539583	-1.935334338
C	0	3.919520045	-1.793726316	-1.6216476743
C	0	2.8026563965	-1.9495824411	-0.791304181
C	0	2.17455736	-0.8141547322	-0.2769045313
C	0	2.6673354086	0.471766713	-0.5915803923
C	0	3.7816015875	0.6237539496	-1.4206852131
C	0	1.8295617048	1.4604035296	0.0899387009
C	0	0.8179118384	0.7813176833	0.8205442018
C	0	-0.0963462483	1.5300372081	1.5659858573
C	0	-0.003492943	2.9273520009	1.5780471754
C	0	0.9932593909	3.5887430876	0.85076439

C	0	1.9159563166	2.8543834873	0.101845532
C	0	0.9772837311	-0.6910650921	0.606662419
C	0	0.6652873915	-1.8370288863	1.5541013276
C	0	-0.1841283668	-1.7578296539	0.3193310779
C	0	-0.2419497627	-1.6231598424	2.771648036
C	0	-1.6880083176	-1.4294966401	2.2209831161
C	0	-1.5780124541	-1.534389982	0.7151785322
C	0	-2.6638667661	-1.352876283	-0.188666027
C	0	-3.0329897871	0.390622862	-0.4867990138
C	0	-4.0969642388	0.5164408658	-1.4246564681
C	0	-3.9263809569	0.3932498713	-2.9043736753
O	0	-5.3514676854	0.2345239609	-0.9190741469
H	0	5.2739425196	-0.4133716099	-2.5806711611
H	0	4.4153851543	-2.6730225393	-2.0253576747
H	0	2.4402041185	-2.9484300053	-0.5575486272
H	0	4.1641780748	1.6125901875	-1.6630928058
H	0	-0.8830209023	1.0541220597	2.1375137078
H	0	-0.7181559683	3.5030625666	2.1611284436
H	0	1.0500702974	4.6741567611	0.870480919
H	0	2.6941458402	3.3642401216	-0.4615303633
H	0	1.4521561105	-2.5835123469	1.6458890381
H	0	0.0244888885	-2.3490045888	-0.5704496611
H	0	0.087557326	-0.7762470934	3.3842911826
H	0	-0.1859327448	-2.5118925702	3.4098422208
H	0	-2.1291187303	-0.4742332385	2.5466394358
H	0	-2.3676465541	-2.2009925476	2.6166662334
H	0	-3.6376602221	-1.6856544715	0.1814683902
H	0	-2.4734914561	-1.736259443	-1.1945743078
H	0	-2.0910196603	0.8100928914	-0.8352008431
H	0	-3.2862777012	0.7403420616	0.5148198546
H	0	-4.6562267129	1.0084513424	-3.4510639708
H	0	-4.0586775641	-0.6495505972	-3.2505113796
H	0	-2.9270923956	0.7184218532	-3.2087470289
H	0	-6.0044415193	0.2130549317	-1.6358715397

Imaginary Frequency :	699.9771i
<S <sup>2</sup> >	0.4966
Electronic Energy	-926.728226836
Zero-point correction	0.375449
Thermal correction to Energy	0.395478
Thermal correction to Enthalpy	0.396422
Thermal correction to Gibbs Free Energy	0.325966

UMP2/6-31+G(d)	
<S <sup>2</sup> >	1.04
Electronic Energy	-923.684113

**Frag Prod 34**  
UB3LYP/6-31+G(d)

C	0	3.45983	-2.16643	-1.67765
C	0	2.57284	-3.13601	-1.22056
C	0	1.28358	-2.78849	-0.78919
C	0	0.90437	-1.45906	-0.82842
C	0	1.81295	-0.46289	-1.30079
C	0	3.08865	-0.81512	-1.72189
C	0	1.13966	0.83127	-1.23724
C	0	-0.18614	0.63035	-0.72864
C	0	-1.0343	1.71464	-0.59494
C	0	-0.57495	2.99301	-0.94768
C	0	0.71418	3.1837	-1.43118
C	0	1.58657	2.09359	-1.58479
C	0	-0.38787	-0.81635	-0.42727
C	0	-1.10879	-1.40403	0.76983
C	0	-1.66096	-1.61923	-0.62956
C	0	-2.09079	-0.56081	1.54456
C	0	-3.34478	-0.44492	0.66608
C	0	-2.97296	-0.93594	-0.70301
C	0	-3.7254	-0.8154	-1.79383
H	0	4.46669	-2.45922	-2.01018
H	0	2.88141	-4.19157	-1.19461
H	0	0.5914	-3.56267	-0.42863
H	0	3.79386	-0.05444	-2.08513
H	0	-2.06292	1.58691	-0.22805
H	0	-1.25174	3.85353	-0.83913
H	0	1.05695	4.19329	-1.70121
H	0	2.60348	2.24294	-1.97411
H	0	-0.59585	-2.19767	1.33725
H	0	-1.57943	-2.57695	-1.17146
H	0	-1.66182	0.4504	1.75939
H	0	-2.33614	-1.04657	2.52096
H	0	-3.72238	0.60705	0.63155
H	0	-4.16737	-1.08246	x1.08214
H	0	-4.70476	-0.32066	-1.77692
H	0	-3.40708	-1.20009	-2.77103

Imaginary Frequency :	None
<S <sup>2</sup> >	0.0000
Electronic Energy	-733.645954484
Zero-point correction	0.291015
Thermal correction to Energy	0.305174
Thermal correction to Enthalpy	0.306118
Thermal correction to Gibbs Free Energy	0.250222

UMP2/6-31+G(d)	
<S <sup>2</sup> >	0.94
Electronic Energy	-731.170033

**Frag TS 31a**  
UB3LYP/6-31+G(d)

C	0	4.8485792554	-0.335815782	-1.2357872093
C	0	4.3827647626	-1.6333081017	-0.9832992467
C	0	3.1186294501	-1.8409238796	-0.4169785351
C	0	2.3228917933	-0.7371500613	-0.1079038503
C	0	2.7944151128	0.5697523483	-0.3611427043
C	0	4.0564799283	0.773697476	-0.9248379439
C	0	1.7624995847	1.5180572325	0.0641247413
C	0	0.653810324	0.7935113505	0.576790875
C	0	-0.4671632146	1.494808317	1.0267910212
C	0	-0.4731870043	2.8944768734	0.9749449016
C	0	0.6275429607	3.6023783972	0.4786068347
C	0	1.7521223763	2.9136686631	0.0168033616
C	0	0.9566069001	-0.6703691282	0.4939480994
C	0	0.5551134245	-1.7835544446	1.448193944
C	0	-0.0418174973	-1.8364976458	0.0698431136
C	0	-0.5792834795	-1.5783905308	2.4578490383
C	0	-1.9055294404	-1.5649022811	1.6385366182
C	0	-1.5007172967	-1.7103338437	0.1846447842
C	0	-2.401253531	-1.7205708397	-0.9241595343
C	0	-2.7964624602	-0.0873392867	-1.6217900438
C	0	-4.0245284199	0.4566736363	-1.1401085548
C	0	-5.3701363951	-0.047928101	-1.5523628166
O	0	-3.9573349443	1.0919351616	0.0881516242
H	0	5.8326400458	-0.1914519962	-1.6746610905
H	0	5.0086829564	-2.488026604	-1.2277056625
H	0	2.7741527938	-2.8551540737	-0.225902092
H	0	4.4228970908	1.7790807997	-1.1193633431
H	0	-1.3472048649	0.9848193612	1.3957830412
H	0	-1.3525881229	3.4328563352	1.3189206973
H	0	0.6048578774	4.6888445098	0.4461931003
H	0	2.6063824421	3.4596734376	-0.3770776405
H	0	1.3623997798	-2.4552840362	1.7336223146
H	0	0.3720359235	-2.4614600503	-0.7197130976
H	0	-0.4441051075	-0.6594151725	3.0397729394
H	0	-0.5688886952	-2.407931549	3.1733892569
H	0	-2.4957823844	-0.6589839825	1.8223358393
H	0	-2.5582548308	-2.4018645305	1.9386391954
H	0	-3.3918171024	-2.1249945178	-0.698029159
H	0	-1.9863553233	-2.2086295733	-1.8098816553
H	0	-2.8423336367	-0.3131635016	-2.6879942134
H	0	-1.9185868935	0.5112473173	-1.3848194554
H	0	-6.1351905261	0.7412689386	-1.5061282122
H	0	-5.7188107764	-0.8734109796	-0.9019679652
H	0	-5.3492907142	-0.4245818874	-2.5795995844
H	0	-4.8444231807	1.3714382546	0.3627324292

Imaginary Frequency :	687.4807i
<S <sup>2</sup> >	0.5820
Electronic Energy	-926.723430075
Zero-point correction	0.375245
Thermal correction to Energy	0.395368

Thermal correction to Enthalpy	0.396312
Thermal correction to Gibbs Free Energy	0.325648
UMP2/6-31+G(d)	
<S <sup>2</sup> >	1.04
Electronic Energy	-923.682211

### Biradical 42

UB3LYP/6-31+G(d)

C	0	3.1679517977	-0.3105176807	-0.4592697295
C	0	3.5181185653	0.943024864	-0.8552338093
C	0	2.6398118126	1.9062185042	-0.1952749231
C	0	1.7556501652	1.2381838105	0.594522081
C	0	2.0283627075	-0.2103782263	0.475943536
C	0	1.7860010804	-1.2727962383	1.5361565737
C	0	0.8868537564	-1.3382410364	0.3456319694
C	0	0.9241012594	-0.9193786993	2.7515912293
C	0	-0.4765909592	-0.5363667044	2.1885897758
C	0	-0.4757948474	-1.0117590152	0.7559496054
C	0	-1.6213894464	-0.8736419658	-0.1596806964
C	0	-1.8322780369	0.6359617223	-0.6831549075
C	0	-2.9709280477	0.7637300458	-1.6125342211
C	0	-2.902827828	0.3100798441	-3.0370571139
O	0	-4.1964838439	0.6354350373	-0.9774821672
H	0	3.6217436243	-1.2472076528	-0.7662912676
H	0	4.313290653	1.1991715458	-1.5476038813
H	0	2.6907431629	2.9825285793	-0.3249232818
H	0	0.983969657	1.6816048069	1.2106940429
H	0	2.5872591863	-1.9952897043	1.6715963384
H	0	1.0593613579	-2.0165483153	-0.485861857
H	0	1.3656185517	-0.1235730115	3.3617538674
H	0	0.846448597	-1.8099789394	3.3869731678
H	0	-0.6487828585	0.551703555	2.2555071603
H	0	-1.2920543394	-0.9921590697	2.7696933379
H	0	-2.5628007803	-1.1570122468	0.3282699433
H	0	-1.4919335596	-1.5127385881	-1.042595248
H	0	-0.9074243299	0.9608080144	-1.169299839
H	0	-1.9943439049	1.2656675624	0.1994404404
H	0	-3.6798451532	0.7867815591	-3.6524962503
H	0	-3.0378576464	-0.7844282268	-3.1385077818
H	0	-1.9338069627	0.564287145	-3.4790302361
H	0	-4.9099663779	0.6181873424	-1.6345375377

Imaginary Frequency :	None
<S <sup>2</sup> >	0.8441
Electronic Energy	-619.408835754
Zero-point correction	0.281891
Thermal correction to Energy	0.297011
Thermal correction to Enthalpy	0.297956

Thermal correction to Gibbs Free Energy	0.238616
CASSCF/6-31+G(d) Electronic Energy	-615.422402
RS2C/6-31+G(d) Electronic Energy	-616.616097

**Clock Prod 43**  
UB3LYP/6-31+G(d)

C	0	4.2739152644	-0.4755587669	-0.2158003585
C	0	4.9933007985	0.7099127011	-0.2454665395
C	0	4.058179212	1.8288451209	-0.0398796144
C	0	2.8052341968	1.3076552629	0.1109934265
C	0	2.9075914778	-0.1502198862	0.0060549946
C	0	1.7695256449	-1.1130941689	0.1339501715
C	0	0.5369252309	-0.7648430496	-0.6868918351
C	0	1.1731538059	-1.1931320894	1.5815077001
C	0	-0.337576002	-1.4584699514	1.3865967997
C	0	-0.6114625783	-0.9498979423	-0.0187191948
C	0	-2.0039157499	-0.7754994925	-0.5621114724
C	0	-2.7959505137	0.3565553004	0.1325790241
C	0	-4.203418912	0.5119919152	-0.3588981255
C	0	-4.5170109928	0.87674494	-1.7771840279
O	0	-5.0198304825	1.0700981151	0.614418531
H	0	4.6682910447	-1.477853741	-0.3365668235
H	0	6.0632063818	0.8121517973	-0.3936776112
H	0	4.3366715725	2.8763868551	-0.0185685965
H	0	1.8834001234	1.8532246287	0.2740582018
H	0	2.135131736	-2.1087249965	-0.1642535784
H	0	0.6084885927	-0.454648851	-1.7270695063
H	0	1.315257857	-0.2270562992	2.0788114833
H	0	1.6766546245	-1.9521638187	2.1887373304
H	0	-0.9464453961	-0.9646368132	2.1542247636
H	0	-0.5755247094	-2.5326877235	1.4476227763
H	0	-2.5656317186	-1.7137484073	-0.4395690316
H	0	-1.9451719864	-0.5809490845	-1.6401173475
H	0	-2.2367308154	1.304118856	0.007644558
H	0	-2.8415226483	0.1709740172	1.2120549128
H	0	-5.5796820452	0.7197936495	-2.0111958825
H	0	-3.9396350011	0.2695109249	-2.4814878271
H	0	-4.2881678687	1.9391759978	-1.991425998
H	0	-5.9008911776	1.2404087266	0.2450442371

Imaginary Frequency :	None
<S <sup>2</sup> >	1.0185
Electronic Energy	-619.437061307
Zero-point correction	0.281349
Thermal correction to Energy	0.297010

Thermal correction to Enthalpy	0.297954
Thermal correction to Gibbs Free Energy	0.236113

CASSCF/6-31+G(d)	
Electronic Energy	-615.465467

RS2C/6-31+G(d)	
Electronic Energy	-616.65421

**Clock TS 42**

UB3LYP/6-31+G(d)

C	0	-2.7749220732	-1.3063058881	-0.9004783236
C	0	-2.9396889132	-2.3247334717	-0.0177195058
C	0	-2.2878678499	-1.9661352479	1.2410298784
C	0	-1.724838812	-0.7357789931	1.1197389153
C	0	-1.9988643354	-0.2266918838	-0.2454990173
C	0	-2.287174149	1.2327390141	-0.6066168663
C	0	-1.0213372708	0.6256127731	-1.1223794572
C	0	-1.9148434265	2.333743451	0.3877223766
C	0	-0.383671886	2.1942211663	0.6310055275
C	0	0.1190382252	1.2951028442	-0.4724316728
C	0	1.5237678515	0.8784473044	-0.6169261784
C	0	1.9311675861	-0.332981469	0.3693201694
C	0	3.3558946816	-0.6999778503	0.2654441733
C	0	3.9040953488	-1.4441803749	-0.9120212987
O	0	4.1934049404	0.2356878747	0.8541207448
H	0	-3.1287334822	-1.2617141571	-1.925390748
H	0	-3.4622123454	-3.2574717613	-0.2031459752
H	0	-2.2582958025	-2.5955333931	2.1247331762
H	0	-1.1645757056	-0.2100807037	1.8821594877
H	0	-3.1424530293	1.3959969274	-1.2567622214
H	0	-0.9220107101	0.2739086447	-2.1468506023
H	0	-2.4979981239	2.2834477533	1.3140753742
H	0	-2.1347415077	3.3009486038	-0.0811714498
H	0	-0.1767951413	1.7682358691	1.6284047603
H	0	0.1232808401	3.1706169915	0.6269586494
H	0	2.2094379671	1.7025372152	-0.3835996494
H	0	1.7305821759	0.5444228128	-1.6423802374
H	0	1.2982407176	-1.1928303681	0.1299030359
H	0	1.6996856854	-0.0118552072	1.3911705111
H	0	4.8949893109	-1.8700708404	-0.697828487
H	0	4.0163005929	-0.7984790343	-1.8048432953
H	0	3.2439547493	-2.2735302957	-1.1873390494
H	0	5.1195744215	0.0074596993	0.6778084385

Imaginary Frequency :	None
<S <sup>2</sup> >	0.8450
Electronic Energy	-619.407733231
Zero-point correction	0.282129

Thermal correction to Energy	0.297154
Thermal correction to Enthalpy	0.298098
Thermal correction to Gibbs Free Energy	0.238876

CASSCF/6-31+G(d)	
Electronic Energy	-615.419626

RS2C/6-31+G(d)	
Electronic Energy	-616.614098

**Biradical 37a**

UB3LYP/6-31+G(d)

C	0	-4.37151	-1.09085	-1.84992
C	0	-3.78802	-0.04984	-2.58494
C	0	-2.66679	0.6307	-2.09436
C	0	-2.12742	0.25611	-0.86266
C	0	-2.71413	-0.79579	-0.12719
C	0	-3.83723	-1.46925	-0.615
C	0	-0.96244	0.8159	-0.10737
C	0	-0.87071	-0.04327	1.11852
C	0	-1.93716	-0.98214	1.09864
C	0	0.05526	-0.10684	2.16242
C	0	-0.1061	-1.04921	3.18539
C	0	-1.18279	-1.94332	3.1763
C	0	-2.09937	-1.91769	2.12307
C	0	-0.70506	2.31452	-0.29892
C	0	0.25414	1.37842	-0.96742
C	0	-0.21308	3.31262	0.74558
C	0	1.2003	3.07239	1.31165
C	0	2.18788	2.52028	0.26653
C	0	1.66179	1.36852	-0.55105
C	0	2.60169	0.36913	-1.11265
C	0	2.97064	-0.8101	-0.09614
C	0	3.90869	-1.79967	-0.67674
C	0	3.46996	-2.82669	-1.67316
O	0	5.18796	-1.2879	-0.83432
H	0	-5.24382	-1.6068	-2.24303
H	0	-4.21031	0.2342	-3.54564
H	0	-2.23106	1.43748	-2.68009
H	0	-4.29182	-2.2773	-0.04645
H	0	0.9175	0.54554	2.18657
H	0	0.62138	-1.08689	3.99254
H	0	-1.297	-2.66561	3.98062
H	0	-2.92446	-2.62569	2.09714
H	0	-1.4639	2.75554	-0.94381
H	0	0.09049	1.15197	-2.02377
H	0	-0.93794	3.38916	1.56667
H	0	-0.21953	4.29059	0.24345
H	0	1.15051	2.39249	2.1654

H	0	1.58539	4.02005	1.70979
H	0	3.1286	2.2403	0.76062
H	0	2.45935	3.34338	-0.42502
H	0	3.55783	0.83426	-1.39194
H	0	2.17878	-0.09282	-2.01489
H	0	2.04562	-1.3081	0.20803
H	0	3.41663	-0.35239	0.79488
H	0	4.18296	-3.66184	-1.73644
H	0	3.37059	-2.40898	-2.69398
H	0	2.498	-3.24619	-1.39366
H	0	5.74114	-1.92282	-1.31601

Imaginary Frequency :	None
<S <sup>2</sup> >	0.8896
Electronic Energy	-966.043798803
Zero-point correction	0.406426
Thermal correction to Energy	0.427755
Thermal correction to Enthalpy	0.428699
Thermal correction to Gibbs Free Energy	0.355105

**Biradical 37b**

UB3LYP/6-31+G(d)

C	0	-3.16599	3.19229	-2.16624
C	0	-2.929	2.00471	-2.87143
C	0	-1.90454	1.13371	-2.47934
C	0	-1.12278	1.45722	-1.36991
C	0	-1.3658	2.65196	-0.65908
C	0	-2.38413	3.52293	-1.05557
C	0	0.03492	0.73022	-0.75734
C	0	0.41099	1.56799	0.42819
C	0	-0.41603	2.72222	0.45287
C	0	1.33636	1.37812	1.45574
C	0	1.4656	2.3458	2.46009
C	0	0.67533	3.50091	2.45462
C	0	-0.27909	3.68851	1.452
C	0	0.94024	-0.0255	-1.73921
C	0	0.04338	-0.84437	-0.85929
C	0	2.45921	-0.1669	-1.65613
C	0	3.00399	-1.03803	-0.50354
C	0	2.06739	-2.20399	-0.14098
C	0	0.6486	-1.76941	0.11639
C	0	-0.21443	-2.48673	1.09169
C	0	-0.17905	-1.96479	2.60478
C	0	1.0112	-2.33738	3.40408
C	0	1.28622	-3.74701	3.82472
O	0	2.11498	-1.52594	3.18029
H	0	-3.96278	3.8597	-2.48483
H	0	-3.54487	1.75632	-3.73227
H	0	-1.73386	0.21837	-3.04251
H	0	-2.57024	4.44561	-0.51069

H	0	1.93078	0.47727	1.52069
H	0	2.18399	2.18494	3.26
H	0	0.79164	4.24348	3.24018
H	0	-0.9148	4.57102	1.45754
H	0	0.60198	0.11265	-2.76508
H	0	-0.89975	-1.19383	-1.28849
H	0	2.93193	0.82385	-1.63572
H	0	2.76538	-0.62849	-2.60517
H	0	3.17431	-0.43101	0.38907
H	0	3.98663	-1.43205	-0.795
H	0	2.46949	-2.74248	0.72413
H	0	2.07026	-2.92838	-0.98159
H	0	0.03093	-3.55968	1.11761
H	0	-1.26487	-2.40642	0.78062
H	0	-1.06445	-2.39278	3.09204
H	0	-0.30214	-0.8773	2.59397
H	0	1.97407	-3.79002	4.68223
H	0	1.74156	-4.35286	3.01719
H	0	0.36024	-4.24871	4.12549
H	0	2.86476	-1.84427	3.70777

Imaginary Frequency :	None
<S <sup>2</sup> >	0.9234
Electronic Energy	-966.040480962
Zero-point correction	0.406295
Thermal correction to Energy	0.427522
Thermal correction to Enthalpy	0.428466
Thermal correction to Gibbs Free Energy	0.355944

**Biradical 37c**  
UB3LYP/6-31+G(d)

C	0	-4.36291	-1.1008	-1.86347
C	0	-3.78229	-0.05352	-2.59184
C	0	-2.66532	0.62955	-2.0951
C	0	-2.12729	0.25121	-0.86396
C	0	-2.71109	-0.80697	-0.1352
C	0	-3.82996	-1.48299	-0.62914
C	0	-0.96667	0.81236	-0.10303
C	0	-0.87412	-0.05245	1.11881
C	0	-1.9363	-0.99597	1.0916
C	0	0.0495	-0.11703	2.16473
C	0	-0.11018	-1.06518	3.18261
C	0	-1.1828	-1.96407	3.16637
C	0	-2.09686	-1.93731	2.11098
C	0	-0.71535	2.31304	-0.28647
C	0	0.24955	1.38448	-0.95726
C	0	-0.23032	3.30799	0.76427
C	0	1.18285	3.0713	1.33237
C	0	2.17526	2.52874	0.28681

C	0	1.65617	1.37855	-0.53741
C	0	2.60188	0.38591	-1.10158
C	0	2.97432	-0.79541	-0.09007
C	0	3.91829	-1.77813	-0.67303
C	0	3.48639	-2.80303	-1.67461
O	0	5.1953	-1.2594	-0.82617
H	0	-5.23194	-1.61866	-2.26131
H	0	-4.2035	0.23344	-3.55215
H	0	-2.23177	1.44119	-2.67572
H	0	-4.28231	-2.2959	-0.06576
H	0	0.90871	0.53912	2.19432
H	0	0.61543	-1.10359	3.99141
H	0	-1.29577	-2.69084	3.96681
H	0	-2.9187	-2.64886	2.07947
H	0	-1.47452	2.75396	-0.93104
H	0	0.08944	1.16257	-2.01511
H	0	-0.95739	3.37702	1.58406
H	0	-0.24007	4.28849	0.26714
H	0	1.13421	2.38699	2.18265
H	0	1.5628	4.0187	1.73603
H	0	3.11615	2.25066	0.78164
H	0	2.44447	3.35637	-0.40019
H	0	3.5562	0.85697	-1.37725
H	0	2.18274	-0.07382	-2.00673
H	0	2.05121	-1.29933	0.21022
H	0	3.41641	-0.33976	0.80398
H	0	4.2035	-3.63449	-1.74001
H	0	3.38697	-2.38152	-2.69386
H	0	2.51592	-3.22835	-1.39874
H	0	5.75255	-1.88968	-1.30925

Imaginary Frequency :	None
<S <sup>2</sup> >	0.8902
Electronic Energy	-966.043799557
Zero-point correction	0.406426
Thermal correction to Energy	0.427758
Thermal correction to Enthalpy	0.428702
Thermal correction to Gibbs Free Energy	0.355075

**Biradical 37d**  
UB3LYP/6-31+G(d)

C	0	4.94424	-0.45823	-1.17887
C	0	4.35398	-1.72726	-1.10849
C	0	3.04737	-1.8814	-0.62797
C	0	2.3323	-0.75321	-0.22486
C	0	2.92754	0.52418	-0.30028
C	0	4.23354	0.67539	-0.77386
C	0	0.95082	-0.63534	0.34246
C	0	0.75309	0.83954	0.52828

C	0	1.95156	1.51034	0.16706
C	0	-0.35296	1.59614	0.91873
C	0	-0.24767	2.99084	0.99328
C	0	0.94994	3.64169	0.67555
C	0	2.05501	2.90073	0.24991
C	0	0.49951	-1.79686	1.2382
C	0	-0.1215	-1.69472	-0.12315
C	0	-0.35817	-1.69864	2.49865
C	0	-1.83476	-1.29774	2.29228
C	0	-2.41498	-1.81877	0.96564
C	0	-1.57362	-1.46241	-0.23154
C	0	-2.188	-1.22146	-1.56385
C	0	-2.62999	0.28176	-1.89235
C	0	-3.86928	0.76415	-1.23982
C	0	-5.22195	0.22909	-1.59121
O	0	-3.6866	1.19081	0.06836
H	0	5.96044	-0.3552	-1.55108
H	0	4.91505	-2.60176	-1.42861
H	0	2.6083	-2.87578	-0.57737
H	0	4.6946	1.65886	-0.82929
H	0	-1.30826	1.13402	1.12587
H	0	-1.11707	3.57152	1.29119
H	0	1.01496	4.72488	0.74265
H	0	2.97991	3.40297	-0.02449
H	0	1.29199	-2.53615	1.34456
H	0	0.2959	-2.32299	-0.91492
H	0	0.11571	-1.02996	3.22924
H	0	-0.3379	-2.70104	2.94847
H	0	-1.94556	-0.21103	2.32375
H	0	-2.42569	-1.68793	3.13153
H	0	-3.43893	-1.44953	0.84233
H	0	-2.49304	-2.92389	1.02892
H	0	-3.07748	-1.85451	-1.70639
H	0	-1.47273	-1.493	-2.35204
H	0	-2.77974	0.32078	-2.97893
H	0	-1.79283	0.94423	-1.65104
H	0	-6.02404	0.92095	-1.29413
H	0	-5.43803	-0.74144	-1.10342
H	0	-5.30869	0.07625	-2.6723
H	0	-4.5402	1.45642	0.44591

Imaginary Frequency :

<S<sup>2</sup>>

Electronic Energy

Zero-point correction

Thermal correction to Energy

Thermal correction to Enthalpy

Thermal correction to Gibbs Free Energy

None

0.9235

-966.040481043

0.406319

0.427532

0.428476

0.356055

Rot TS 37ab

## UB3LYP/6-31+G(d)

C	0	4.7074945475	-0.1945943087	-1.7393446352
C	0	4.1455569673	-1.4784753341	-1.7503362031
C	0	2.9335347216	-1.7335477485	-1.0968094877
C	0	2.2825019889	-0.6902439849	-0.4366665751
C	0	2.8485179379	0.602275236	-0.4309341749
C	0	4.0612724034	0.8537070913	-1.0781212026
C	0	1.0055235701	-0.6890535545	0.344862219
C	0	0.8320336502	0.7406257204	0.7659105991
C	0	1.9520114651	1.4882080084	0.3124111743
C	0	-0.1974567917	1.4144305397	1.4273468928
C	0	-0.0906488403	2.7892184452	1.6709871839
C	0	1.034788782	3.5086760358	1.253405781
C	0	2.0589905617	2.8584482065	0.5619572607
C	0	0.6779929026	-1.992668513	1.0793607687
C	0	-0.1365131436	-1.6880209075	-0.1407285528
C	0	0.0065012785	-2.1491792145	2.4399247529
C	0	-1.4407765608	-1.631688034	2.5529415789
C	0	-2.2703067799	-1.8507206247	1.2736712326
C	0	-1.5800538676	-1.4567979994	-0.0079921813
C	0	-2.3825684121	-1.0921462955	-1.2037274477
C	0	-2.563435732	0.4976639811	-1.4553131632
C	0	-3.9711479439	0.9560178488	-1.4203292011
C	0	-4.9495071447	0.6066410438	-2.4982938131
O	0	-4.4756126229	1.0271170261	-0.1283054364
H	0	5.6507281953	-0.0135158205	-2.2485180918
H	0	4.65543347	-2.2859379204	-2.2699972779
H	0	2.5163370309	-2.7383409946	-1.1146929793
H	0	4.4996708824	1.8489804474	-1.0709382916
H	0	-1.0973215594	0.9006354593	1.7366639814
H	0	-0.9004710091	3.3010665292	2.1849110966
H	0	1.104368119	4.5748256688	1.4539193663
H	0	2.9250721924	3.4160400448	0.2128320431
H	0	1.476242722	-2.7213660247	0.9443769913
H	0	0.1638646374	-2.1563255741	-1.0809294197
H	0	0.6292508205	-1.6972023405	3.2231808595
H	0	0.0012002263	-3.229871826	2.642295679
H	0	-1.4403038788	-0.5707905539	2.8132379597
H	0	-1.9313680116	-2.1408477741	3.3926119594
H	0	-3.2293480073	-1.3250706321	1.3622323555
H	0	-2.5283901504	-2.9279802264	1.2096265505
H	0	-3.3852132891	-1.5327793799	-1.1282584179
H	0	-1.9185165446	-1.5028739986	-2.1103756571
H	0	-2.1332819281	0.7356529084	-2.4340371036
H	0	-1.9804455835	1.0389537355	-0.7065947064
H	0	-5.8348713633	1.2586288232	-2.4723658278
H	0	-5.314479024	-0.4359199052	-2.4145437636
H	0	-4.4918494012	0.7155277861	-3.4872404401
H	0	-5.4172409228	1.2589215336	-0.1560502101

Imaginary Frequency :	41.3859i
<S <sup>2</sup> >	0.9136
Electronic Energy	-966.037927549
Zero-point correction	0.406249
Thermal correction to Energy	0.426774
Thermal correction to Enthalpy	0.427718
Thermal correction to Gibbs Free Energy	0.356537

**Clock TS 37a**  
UB3LYP/6-31+G(d)

C	0	-4.26906	-1.33221	-1.8165
C	0	-3.7569	-0.27351	-2.58029
C	0	-2.70536	0.51414	-2.09847
C	0	-2.15978	0.232	-0.8414
C	0	-2.67834	-0.83895	-0.07587
C	0	-3.7317	-1.61884	-0.55802
C	0	-1.06323	0.89619	-0.09422
C	0	-0.94405	0.13158	1.17598
C	0	-1.9253	-0.90289	1.17375
C	0	-0.06407	0.20481	2.26223
C	0	-0.18521	-0.69416	3.32732
C	0	-1.174	-1.68568	3.32692
C	0	-2.04405	-1.79599	2.24029
C	0	-0.67241	2.2899	-0.53386
C	0	0.31331	1.31818	-1.09082
C	0	-0.15893	3.43474	0.33816
C	0	1.1914	3.20591	1.03881
C	0	2.22041	2.44882	0.17635
C	0	1.67612	1.3147	-0.65986
C	0	2.61882	0.2748	-1.14529
C	0	2.92998	-0.85041	-0.05639
C	0	3.8666	-1.8866	-0.55094
C	0	3.44141	-2.98177	-1.47748
O	0	5.15736	-1.40652	-0.70347
H	0	-5.08895	-1.93119	-2.20461
H	0	-4.18234	-0.05945	-3.55767
H	0	-2.32631	1.32983	-2.71026
H	0	-4.13373	-2.43737	0.03471
H	0	0.73112	0.93562	2.29251
H	0	0.50549	-0.62045	4.16387
H	0	-1.25667	-2.37342	4.16461
H	0	-2.80376	-2.57417	2.22306
H	0	-1.39794	2.67024	-1.25412
H	0	0.09985	0.85459	-2.05209
H	0	-0.92161	3.71532	1.07581
H	0	-0.05661	4.29453	-0.33921
H	0	1.03131	2.67447	1.97878
H	0	1.60965	4.17983	1.32334
H	0	3.04046	2.0937	0.81749

H	0	2.69968	3.16728	-0.51607
H	0	3.58946	0.71307	-1.4166
H	0	2.21559	-0.22324	-2.03662
H	0	1.98606	-1.31449	0.24409
H	0	3.3563	-0.35401	0.82358
H	0	4.14149	-3.82981	-1.45124
H	0	3.37861	-2.62608	-2.5545
H	0	2.4507	-3.35442	-1.22746
H	0	5.71078	-2.07301	-1.14831

Imaginary Frequency :	397.4858 <i>i</i>
<S <sup>2</sup> >	0.8863
Electronic Energy	-966.041873945
Zero-point correction	0.405385
Thermal correction to Energy	0.426211
Thermal correction to Enthalpy	0.427155
Thermal correction to Gibbs Free Energy	0.354941

**Clock Product 38a**  
UB3LYP/6-31+G(d)

C	0	5.58197	-0.56023	-0.93055
C	0	4.8988	-1.77655	-1.08129
C	0	3.52482	-1.85903	-0.83821
C	0	2.8285	-0.70586	-0.43893
C	0	3.53292	0.52867	-0.2866
C	0	4.89935	0.60011	-0.53199
C	0	1.43158	-0.50094	-0.12529
C	0	1.27714	0.89429	0.22247
C	0	2.55672	1.53707	0.13138
C	0	0.15607	1.65397	0.60662
C	0	0.31272	3.01195	0.89595
C	0	1.56967	3.62816	0.80618
C	0	2.69885	2.88874	0.42143
C	0	0.41469	-1.61763	-0.13001
C	0	-0.96196	-1.2167	-0.62567
C	0	0.32841	-2.35713	1.24081
C	0	-0.71223	-1.72479	2.16905
C	0	-2.10494	-1.76731	1.52609
C	0	-2.10114	-1.30677	0.08083
C	0	-3.44084	-0.95183	-0.52554
C	0	-3.9776	0.44523	-0.07869
C	0	-5.34656	0.76288	-0.58791
C	0	-5.61213	1.10465	-2.02101
O	0	-6.33045	0.04491	0.07831
H	0	6.65053	-0.51538	-1.12466
H	0	5.44442	-2.66434	-1.39076
H	0	3.01026	-2.80908	-0.95994
H	0	5.43995	1.53722	-0.41906
H	0	-0.82403	1.19555	0.66948

H	0	-0.55298	3.59873	1.19297
H	0	1.67059	4.68599	1.03505
H	0	3.67011	3.37389	0.35429
H	0	0.79566	-2.35516	-0.85263
H	0	-1.00522	-0.86516	-1.65773
H	0	1.31622	-2.37697	1.71499
H	0	0.0444	-3.40156	1.04665
H	0	-0.43236	-0.68467	2.38112
H	0	-0.72699	-2.2491	3.13308
H	0	-2.80963	-1.15968	2.11044
H	0	-2.50488	-2.79412	1.56621
H	0	-4.18588	-1.70785	-0.24126
H	0	-3.36644	-0.96785	-1.62008
H	0	-3.27879	1.21626	-0.42664
H	0	-3.99302	0.49247	1.01797
H	0	-6.57501	1.62278	-2.14268
H	0	-5.64272	0.21162	-2.67466
H	0	-4.83357	1.76952	-2.4105
H	0	-7.1958	0.22183	-0.32294

Imaginary Frequency :	None
<S <sup>2</sup> >	1.0229
Electronic Energy	-966.082992651
Zero-point correction	0.406974
Thermal correction to Energy	0.428472
Thermal correction to Enthalpy	0.429417
Thermal correction to Gibbs Free Energy	0.354726

**Clock TS 37b**  
UB3LYP/6-31+G(d)

C	0	4.85718322	-0.3892284429	-1.3495571498
C	0	4.3203321834	-1.6741838698	-1.1854568195
C	0	3.0687347972	-1.8556345652	-0.5859743222
C	0	2.3480453031	-0.7366342309	-0.1552435565
C	0	2.893340482	0.5583455465	-0.324623435
C	0	4.1454816631	0.7341524644	-0.9169999919
C	0	1.0274668384	-0.6378598721	0.5115394657
C	0	0.7966968856	0.8172255475	0.7021117222
C	0	1.9332997171	1.5221684369	0.2075017892
C	0	-0.2856898827	1.5595459524	1.1874740711
C	0	-0.2152638563	2.9561592754	1.2239689019
C	0	0.9226362487	3.6358394161	0.7726591817
C	0	2.0000407457	2.9155658168	0.2516856484
C	0	0.4902326578	-1.8836328685	1.1750795273
C	0	-0.1862064395	-1.7459930934	-0.148780462
C	0	-0.3728773289	-1.9488379467	2.4372560734
C	0	-1.804181604	-1.396020192	2.314598954
C	0	-2.4687930898	-1.7107374999	0.9630833646
C	0	-1.5886312401	-1.5001166243	-0.2466964259

C	0	-2.2130605261	-1.2669620746	-1.5787484646
C	0	-2.5667499153	0.2513776184	-1.9330914012
C	0	-3.8020797135	0.8099077032	-1.3344775572
C	0	-5.1673338942	0.3100325277	-1.6872478835
O	0	-3.6325882455	1.331833299	-0.0609229154
H	0	5.8322162278	-0.2663814533	-1.8142745794
H	0	4.8822819989	-2.5404732643	-1.5258685007
H	0	2.6738933199	-2.8626455909	-0.4692766329
H	0	4.5665789003	1.729279922	-1.041161536
H	0	-1.2022926821	1.0819163025	1.5010844314
H	0	-1.067482474	3.5177668087	1.5982607877
H	0	0.9607366708	4.7215569744	0.8122126138
H	0	2.8785094043	3.4362445595	-0.1228540516
H	0	1.2658840926	-2.6499394961	1.2155700056
H	0	0.308870823	-2.1538110498	-1.0277897632
H	0	0.149451663	-1.4639382737	3.2718293841
H	0	-0.4388686541	-3.0152852926	2.6947227408
H	0	-1.8070131901	-0.3162667363	2.476081933
H	0	-2.4136902947	-1.8175724945	3.1245516787
H	0	-3.3925383467	-1.1288821129	0.8708569742
H	0	-2.7847590865	-2.7728466707	0.9627314628
H	0	-3.1381877635	-1.8529157386	-1.6860224284
H	0	-1.5276929032	-1.6035763601	-2.3677709773
H	0	-2.6743066333	0.2846184472	-3.025234915
H	0	-1.7073184824	0.8750173526	-1.6673090265
H	0	-5.943604188	1.0610846001	-1.4775273533
H	0	-5.447048679	-0.604095129	-1.1283619632
H	0	-5.227342474	0.0698317216	-2.7542280247
H	0	-4.4813107943	1.6697724324	0.266793682

Imaginary Frequency :	425.9791 <i>i</i>
<S <sup>2</sup> >	0.9317
Electronic Energy	-966.037944644
Zero-point correction	0.405163
Thermal correction to Energy	0.426266
Thermal correction to Enthalpy	0.427210
Thermal correction to Gibbs Free Energy	0.354201

**Clock product 38b**  
UB3LYP/6-31+G(d)

C	0	-1.89058	4.34099	-3.05113
C	0	-1.84777	3.09022	-3.68569
C	0	-1.32542	1.973	-3.02768
C	0	-0.84005	2.11338	-1.71666
C	0	-0.88727	3.39162	-1.07814
C	0	-1.40947	4.49621	-1.74127
C	0	-0.25592	1.14869	-0.81073
C	0	0.06336	1.85392	0.41058
C	0	-0.3196	3.22889	0.26186

C	0	0.64683	1.43108	1.62027
C	0	0.83668	2.3587	2.64823
C	0	0.45598	3.69968	2.4927
C	0	-0.12487	4.13986	1.29291
C	0	-0.02515	-0.29598	-1.18646
C	0	-0.27498	-1.28812	-0.06685
C	0	1.36539	-0.53519	-1.84915
C	0	2.44387	-0.86556	-0.81364
C	0	2.07465	-2.13221	-0.03007
C	0	0.63434	-2.13502	0.44307
C	0	0.24648	-3.15452	1.49521
C	0	0.42318	-2.70912	2.98769
C	0	1.81068	-2.52716	3.50651
C	0	2.76537	-3.66208	3.70108
O	0	2.35393	-1.28288	3.21354
H	0	-2.30059	5.19855	-3.57852
H	0	-2.22511	2.98923	-4.70017
H	0	-1.29962	1.01093	-3.53371
H	0	-1.44802	5.47082	-1.25971
H	0	0.9481	0.40129	1.76971
H	0	1.28434	2.02907	3.58234
H	0	0.61047	4.40409	3.30628
H	0	-0.41575	5.18184	1.17848
H	0	-0.77611	-0.51765	-1.9599
H	0	-1.29945	-1.3221	0.30772
H	0	1.64802	0.33955	-2.44607
H	0	1.26891	-1.38136	-2.54496
H	0	2.55845	-0.0246	-0.11796
H	0	3.41398	-1.00007	-1.3096
H	0	2.74349	-2.24449	0.83161
H	0	2.23976	-3.02395	-0.65848
H	0	0.81401	-4.08273	1.33473
H	0	-0.81309	-3.41302	1.37159
H	0	-0.06661	-3.47664	3.60347
H	0	-0.13592	-1.77667	3.13589
H	0	3.55234	-3.41077	4.42827
H	0	3.27847	-3.96195	2.76726
H	0	2.2412	-4.54556	4.08203
H	0	3.2451	-1.21623	3.59204

Imaginary Frequency :

<S<sup>2</sup>>

Electronic Energy

Zero-point correction

Thermal correction to Energy

Thermal correction to Enthalpy

Thermal correction to Gibbs Free Energy

None

1.0246

-966.0803877774

0.406965

0.428336

0.429280

0.356027

**Clock TS 37c**

UB3LYP/6-31+G(d)

C	0	-4.26901	-1.33238	-1.81642
C	0	-3.75686	-0.27373	-2.58029
C	0	-2.70533	0.51397	-2.09853
C	0	-2.15976	0.23194	-0.84143
C	0	-2.67832	-0.83895	-0.07582
C	0	-3.73167	-1.6189	-0.55791
C	0	-1.06322	0.89619	-0.0943
C	0	-0.94405	0.13169	1.17597
C	0	-1.92529	-0.90279	1.17381
C	0	-0.06409	0.20503	2.26223
C	0	-0.18523	-0.69385	3.32739
C	0	-1.17401	-1.68539	3.32706
C	0	-2.04404	-1.79579	2.24044
C	0	-0.6724	2.28987	-0.53404
C	0	0.31332	1.3181	-1.09091
C	0	-0.15893	3.43476	0.33793
C	0	1.19143	3.20602	1.03856
C	0	2.22043	2.44884	0.17616
C	0	1.67613	1.31466	-0.65995
C	0	2.61883	0.27471	-1.14531
C	0	2.92999	-0.85042	-0.05631
C	0	3.86656	-1.88668	-0.5508
C	0	3.44128	-2.98193	-1.4772
O	0	5.15732	-1.40666	-0.70344
H	0	-5.0889	-1.93139	-2.20449
H	0	-4.18229	-0.05975	-3.5577
H	0	-2.32628	1.32961	-2.71038
H	0	-4.13369	-2.43738	0.03488
H	0	0.73109	0.93586	2.29246
H	0	0.50545	-0.62005	4.16395
H	0	-1.25668	-2.37305	4.16481
H	0	-2.80374	-2.57398	2.22326
H	0	-1.39791	2.67017	-1.25433
H	0	0.09987	0.85445	-2.05215
H	0	-0.9216	3.71533	1.07559
H	0	-0.05667	4.29454	-0.33947
H	0	1.03138	2.67467	1.97859
H	0	1.60968	4.17997	1.32297
H	0	3.04048	2.09377	0.81733
H	0	2.69971	3.16724	-0.51633
H	0	3.58946	0.71295	-1.41665
H	0	2.21559	-0.22341	-2.03659
H	0	1.98607	-1.31443	0.24425
H	0	3.35636	-0.35394	0.8236
H	0	4.14133	-3.82998	-1.45092
H	0	3.38144	-2.64601	-2.53072
H	0	2.45391	-3.36329	-1.19741
H	0	5.71291	-2.07852	-1.1291

Imaginary Frequency :

411.5994i

<S <sup>2</sup> >	0.8874
Electronic Energy	-966.042399330
Zero-point correction	0.405331
Thermal correction to Energy	0.426454
Thermal correction to Enthalpy	0.427398
Thermal correction to Gibbs Free Energy	0.353892

**Clock product 38c**  
UB3LYP/6-31+G(d)

C	0	5.29756	-0.84064	-1.43209
C	0	4.5221	-2.01002	-1.43416
C	0	3.19757	-1.9899	-0.98772
C	0	2.64564	-0.78034	-0.53374
C	0	3.44291	0.40574	-0.53484
C	0	4.75901	0.37512	-0.98139
C	0	1.32753	-0.46966	-0.02483
C	0	1.31759	0.94154	0.28994
C	0	2.60762	1.49097	-0.01592
C	0	0.31975	1.78824	0.81008
C	0	0.60709	3.13957	1.01971
C	0	1.87248	3.66404	0.71767
C	0	2.87964	2.83693	0.19656
C	0	0.25093	-1.51364	0.15552
C	0	-1.15987	-1.0134	-0.09312
C	0	0.35879	-2.24995	1.52432
C	0	-0.42979	-1.52545	2.61813
C	0	-1.9164	-1.4481	2.24607
C	0	-2.1514	-1.00856	0.81222
C	0	-3.57281	-0.57846	0.51338
C	0	-3.89478	-0.1913	-0.9389
C	0	-5.3274	0.19198	-1.15012
C	0	-5.93829	0.17955	-2.5171
O	0	-5.72714	1.21632	-0.30272
H	0	6.32575	-0.87602	-1.783
H	0	4.95664	-2.94193	-1.7869
H	0	2.60997	-2.90475	-0.99604
H	0	5.36969	1.27522	-0.9845
H	0	-0.66735	1.40224	1.03782
H	0	-0.16364	3.79356	1.41986
H	0	2.07496	4.71851	0.88709
H	0	3.85874	3.25065	-0.03457
H	0	0.44723	-2.27117	-0.61894
H	0	-1.35064	-0.66586	-1.10684
H	0	1.4121	-2.36094	1.806
H	0	-0.0501	-3.26331	1.40042
H	0	-0.02732	-0.51283	2.75196
H	0	-0.30903	-2.04174	3.57909
H	0	-2.44105	-0.76081	2.92587
H	0	-2.39211	-2.43082	2.40045

H	0	-3.83113	0.26535	1.16889
H	0	-4.25027	-1.39163	0.81886
H	0	-3.65939	-1.02642	-1.61022
H	0	-3.24006	0.648	-1.24336
H	0	-5.58509	1.02503	-3.13916
H	0	-7.03512	0.24715	-2.47417
H	0	-5.68846	-0.7455	-3.04753
H	0	-6.64001	1.47194	-0.50751

Imaginary Frequency :	None
<S <sup>2</sup> >	1.0250
Electronic Energy	-966.082744174
Zero-point correction	0.406791
Thermal correction to Energy	0.428308
Thermal correction to Enthalpy	0.429252
Thermal correction to Gibbs Free Energy	0.354615

### Clock TS 37d

UB3LYP/6-31+G(d)

C	0	4.8569328558	-0.3901114855	-1.3504363885
C	0	4.3202496511	-1.6749581324	-1.1849398254
C	0	3.0688081079	-1.8559417682	-0.5849910702
C	0	2.3480988789	-0.7365872998	-0.1552127472
C	0	2.89322199	0.5582810277	-0.3260077623
C	0	4.1452135803	0.7336263344	-0.9188362649
C	0	1.0276814905	-0.637283314	0.5118013685
C	0	0.7967656721	0.8179677228	0.7008989829
C	0	1.933191016	1.5225365234	0.2053493295
C	0	-0.2856568327	1.5606568237	1.1856191455
C	0	-0.2153962658	2.957315481	1.2206542953
C	0	0.9223619908	3.6366662673	0.7684893551
C	0	1.9997706094	2.9159870116	0.2480849967
C	0	0.4907751756	-1.8824300518	1.1767756754
C	0	-0.1861251943	-1.7462361526	-0.1469957545
C	0	-0.3718863136	-1.9464088482	2.4393217339
C	0	-1.8032802598	-1.3938453769	2.3165859297
C	0	-2.4683204238	-1.7100257414	0.9656212669
C	0	-1.5885950973	-1.5005674178	-0.244681489
C	0	-2.2135008838	-1.2687791268	-1.5767480409
C	0	-2.5673562635	0.2491959671	-1.9324853926
C	0	-3.8024984437	0.8082880569	-1.3340083895
C	0	-5.1678597819	0.3080334449	-1.6858248174
O	0	-3.6325925895	1.3314888483	-0.0610310473
H	0	5.8318489127	-0.2676270134	-1.8154947942
H	0	4.8822100252	-2.5415273613	-1.5246209977
H	0	2.6740963033	-2.8628765964	-0.4672020455
H	0	4.5661810356	1.7286729801	-1.0440808839
H	0	-1.2021829076	1.0832414987	1.4997809061
H	0	-1.06764021	3.5192074457	1.594460522

H	0	0.9603357885	4.7224288414	0.80691438
H	0	2.8781088204	3.4363866704	-0.1271482444
H	0	1.2665171361	-2.6486167714	1.2177947367
H	0	0.3087104078	-2.1548793467	-1.0257577951
H	0	0.1506916731	-1.4605842253	3.2732007366
H	0	-0.4376850702	-3.0125922443	2.6979278821
H	0	-1.8061454203	-0.3139260576	2.4769604927
H	0	-2.4124774309	-1.8146171958	3.1271785866
H	0	-3.39216255	-1.1283687523	0.8731135874
H	0	-2.7841705867	-2.7721687706	0.9664763477
H	0	-3.1386468	-1.8548686954	-1.6831101098
H	0	-1.528398042	1.6061627898	-2.3656722299
H	0	-2.6752863069	0.2813458154	-3.0246247041
H	0	-1.7078526761	0.8731239192	-1.667615811
H	0	-5.9440759372	1.0592794314	-1.4765990071
H	0	-5.4473718007	-0.6055404477	-1.1259333874
H	0	-5.2282164339	0.0667646726	-2.7525442582
H	0	-4.4812187644	1.6697145339	0.2666396478

Imaginary Frequency :	426.0560i
<S <sup>2</sup> >	0.9317
Electronic Energy	-966.037944542
Zero-point correction	0.405164
Thermal correction to Energy	0.426266
Thermal correction to Enthalpy	0.427210
Thermal correction to Gibbs Free Energy	0.354203

**Clock product 38d**  
UB3LYP/6-31+G(d)

C	0	5.03808	-0.61818	-1.22428
C	0	4.30269	-1.79455	-1.43462
C	0	2.95853	-1.87378	-1.05944
C	0	2.34541	-0.75789	-0.46547
C	0	3.10237	0.43617	-0.25493
C	0	4.4385	0.5049	-0.63245
C	0	0.9954	-0.5597	0.01463
C	0	0.92462	0.79059	0.52744
C	0	2.20862	1.41203	0.37222
C	0	-0.12388	1.52502	1.11322
C	0	0.10841	2.83653	1.53574
C	0	1.36912	3.4322	1.38048
C	0	2.42584	2.71811	0.79467
C	0	-0.05422	-1.64589	-0.00493
C	0	-1.45903	-1.15682	-0.30835
C	0	-0.02111	-2.52954	1.27731
C	0	-0.90063	-1.94753	2.38688
C	0	-2.35926	-1.84675	1.91976
C	0	-2.50734	-1.2713	0.52209
C	0	-3.92717	-0.87182	0.1701

C	0	-4.26234	-0.44007	-1.28287
C	0	-3.79465	0.91066	-1.73443
C	0	-4.03071	2.15818	-0.94675
O	0	-2.67761	0.87486	-2.5569
H	0	6.0823	-0.57537	-1.52314
H	0	4.78385	-2.65358	-1.89524
H	0	2.40243	-2.79217	-1.23093
H	0	5.01862	1.41147	-0.47503
H	0	-1.10661	1.08191	1.22806
H	0	-0.70011	3.40344	1.99093
H	0	1.52937	4.45373	1.71584
H	0	3.40074	3.18641	0.67837
H	0	0.22385	-2.30391	-0.84202
H	0	-1.59067	-0.70974	-1.28997
H	0	1.01269	-2.65459	1.61945
H	0	-0.3949	-3.52913	1.01163
H	0	-0.52878	-0.95349	2.66692
H	0	-0.83793	-2.57103	3.28804
H	0	-2.93975	-1.23628	2.62803
H	0	-2.82872	-2.84433	1.94442
H	0	-4.24935	-0.07611	0.86157
H	0	-4.57806	-1.72725	0.41468
H	0	-5.3608	-0.46196	-1.35754
H	0	-3.89108	-1.19194	-1.98948
H	0	-3.99455	3.05424	-1.58442
H	0	-3.28499	2.3074	-0.14279
H	0	-5.02019	2.13648	-0.47568
H	0	-2.39904	1.77837	-2.77541

Imaginary Frequency :

<S<sup>2</sup>>

Electronic Energy

Zero-point correction

Thermal correction to Energy

Thermal correction to Enthalpy

Thermal correction to Gibbs Free Energy

None

1.0252

-966.079063958

0.406859

0.428280

0.429224

0.355621

### Cyclisation product 39b

UB3LYP/6-31+G(d)

C	0	-3.19966	3.23869	-1.52375
C	0	-3.00423	2.02464	-2.19608
C	0	-1.92682	1.192	-1.86973
C	0	-1.0431	1.58442	-0.86439
C	0	-1.23987	2.80766	-0.19262
C	0	-2.31688	3.63771	-0.51688
C	0	0.17589	0.89094	-0.32527
C	0	0.69308	1.83793	0.72584
C	0	-0.16349	2.96858	0.78555
C	0	1.81992	1.8106	1.55094

C	0	2.0761	2.87346	2.42577
C	0	1.21661	3.97592	2.48645
C	0	0.09156	4.02699	1.66136
C	0	1.03952	0.10761	-1.33241
C	0	0.14756	-0.65708	-0.39857
C	0	2.55917	-0.02274	-1.23857
C	0	3.07201	-1.02353	-0.17691
C	0	2.09025	-2.17274	0.07862
C	0	0.71539	-1.69917	0.57813
C	0	-0.3699	-2.85118	0.84394
C	0	-0.80607	-2.09199	2.10929
C	0	0.54836	-1.34136	2.0944
C	0	0.22307	-4.22597	1.15456
O	0	-1.43049	-2.99329	-0.09952
H	0	-4.04238	3.87278	-1.7874
H	0	-3.6969	1.72371	-2.97811
H	0	-1.79622	0.25171	-2.40076
H	0	-2.46926	4.58084	0.00283
H	0	2.50292	0.97206	1.53947
H	0	2.95476	2.83602	3.06505
H	0	1.42728	4.79331	3.17144
H	0	-0.57523	4.88537	1.69647
H	0	0.68503	0.22021	-2.35657
H	0	-0.79087	-0.99328	-0.82996
H	0	3.02649	0.96034	-1.09449
H	0	2.89601	-0.37382	-2.22263
H	0	3.28226	-0.52264	0.77437
H	0	4.03518	-1.43067	-0.51053
H	0	2.53519	-2.8717	0.7966
H	0	1.94678	-2.73317	-0.85943
H	0	-1.05957	-2.69604	2.98799
H	0	-1.64032	-1.42013	1.88445
H	0	0.51893	-0.28501	2.35879
H	0	1.3073	-1.83717	2.71205
H	0	0.69526	-4.67721	0.2711
H	0	-0.57978	-4.89047	1.49468
H	0	0.97937	-4.17875	1.94458
H	0	-1.16787	-3.62885	-0.78506

Imaginary Frequency :

<S<sup>2</sup>>

Electronic Energy

Zero-point correction

Thermal correction to Energy

Thermal correction to Enthalpy

Thermal correction to Gibbs Free Energy

None

0.0000

-966.107443798

0.411479

0.430917

0.431861

0.365264

**Cyclisation product 39d**

UB3LYP/6-31+G(d)

C	0	-3.21253	2.69124	-2.04507
C	0	-3.07541	1.42322	-2.62427
C	0	-2.00612	0.58936	-2.27195
C	0	-1.07522	1.0313	-1.33189
C	0	-1.21029	2.31201	-0.76029
C	0	-2.27707	3.14404	-1.11051
C	0	0.15734	0.35359	-0.79327
C	0	0.73667	1.37009	0.15659
C	0	-0.08462	2.52577	0.14942
C	0	1.88785	1.37927	0.94486
C	0	2.21007	2.5086	1.70543
C	0	1.38834	3.64173	1.69561
C	0	0.23212	3.65174	0.91444
C	0	0.95571	-0.48751	-1.80064
C	0	0.0871	-1.19772	-0.79479
C	0	2.47641	-0.63072	-1.74843
C	0	3.01398	-1.56333	-0.64089
C	0	2.05754	-2.72385	-0.36504
C	0	0.65615	-2.30664	0.12023
C	0	-0.35239	-3.5078	0.14978
C	0	-0.93771	-2.98598	1.4797
C	0	0.35898	-2.15454	1.6762
C	0	1.366	-2.84926	2.59586
O	0	0.18247	-0.80612	2.08184
H	0	-4.04783	3.32726	-2.32731
H	0	-3.80383	1.08174	-3.35561
H	0	-1.91679	-0.38823	-2.74142
H	0	-2.38006	4.13188	-0.66742
H	0	2.53016	0.513	1.00683
H	0	3.10901	2.4982	2.31737
H	0	1.65069	4.51101	2.29359
H	0	-0.41161	4.52824	0.89718
H	0	0.57012	-0.41561	-2.81726
H	0	-0.88797	-1.48808	-1.1782
H	0	2.95251	0.35655	-1.68405
H	0	2.78031	-1.05173	-2.71597
H	0	3.19799	-1.01847	0.29014
H	0	3.99104	-1.95502	-0.95243
H	0	2.51132	-3.42726	0.342
H	0	1.91106	-3.28726	-1.30007
H	0	0.17249	-4.46235	0.27363
H	0	-1.03155	-3.59745	-0.70471
H	0	-1.1864	-3.72208	2.25343
H	0	-1.79446	-2.32332	1.32102
H	0	2.34162	-2.3516	2.56522
H	0	1.50373	-3.90534	2.33927
H	0	0.99809	-2.81501	3.63104
H	0	-0.04649	-0.78704	3.02524

Imaginary Frequency :  
 $\langle S^2 \rangle$

None  
0.0000

Electronic Energy	-966.098585290
Zero-point correction	0.410895
Thermal correction to Energy	0.430461
Thermal correction to Enthalpy	0.431405
Thermal correction to Gibbs Free Energy	0.364276

**Fragmentation TS 37b**  
UB3LYP/6-31+G(d)

C	0	4.9063752349	-0.2437286105	-1.2461029237
C	0	4.3747630329	-1.540103003	-1.217220918
C	0	3.0855405374	-1.7724409801	-0.7218379654
C	0	2.3280443615	-0.6950719039	-0.260216162
C	0	2.8653473881	0.6093244105	-0.2917988217
C	0	4.15378076	0.8388923048	-0.7818878425
C	0	0.9500292394	-0.6634959049	0.3271188126
C	0	0.6981920324	0.7907547236	0.5947947186
C	0	1.8590155314	1.5290226342	0.2401438161
C	0	-0.4195401732	1.4808202068	1.0672634643
C	0	-0.3664681531	2.8725185514	1.2147893471
C	0	0.7921964045	3.588464292	0.8930157627
C	0	1.9106146595	2.9162114359	0.3949013518
C	0	0.555700011	-1.8821570667	1.1710888961
C	0	-0.0639727726	-1.757937981	-0.1895322658
C	0	-0.3117315188	-1.8618672047	2.4301503716
C	0	-1.812123609	-1.555466135	2.2254001886
C	0	-2.3455681371	-2.0863288432	0.8842310963
C	0	-1.5342600999	-1.6363268662	-0.3064300009
C	0	-2.1417770028	-1.29930475	-1.556093421
C	0	-2.5289416636	0.4564380613	-1.8236548171
C	0	-3.7532722424	0.8751331693	-1.228072327
C	0	-5.1038266008	0.5474038553	-1.7797809194
O	0	-3.6906637179	1.1625129765	0.1231857915
H	0	5.9097280866	-0.0797569019	-1.6311277761
H	0	4.9685190777	-2.3749611291	-1.5812949321
H	0	2.6929099462	-2.7870836597	-0.704379868
H	0	4.5695532663	1.8436584801	-0.8042969146
H	0	-1.3470314959	0.9707797059	1.286307365
H	0	-1.2465477118	3.3995050362	1.57459718
H	0	0.8170802227	4.6682794905	1.0171254933
H	0	2.807382661	3.4685247968	0.1233430316
H	0	1.3830150327	-2.5850607397	1.2582824536
H	0	0.4008902799	-2.3267326218	-0.9982954679
H	0	0.1156950955	-1.1764511379	3.1738462279
H	0	-0.2282152548	-2.8680310294	2.8636198895
H	0	-1.9993623309	-0.4804164867	2.2817961228
H	0	-2.3775684105	-2.0058391983	3.0522886675
H	0	-3.3964582672	-1.7994958139	0.7629804807
H	0	-2.3313156204	-3.1935526313	0.9254156669
H	0	-3.1167528348	-1.7635222928	-1.7308868039

H	0	-1.4835259173	-1.4565553437	-2.4154275733
H	0	-2.5697900882	0.4965274652	-2.9132261095
H	0	-1.6434341824	0.9608484664	-1.4416643712
H	0	-5.8397487989	1.3340222267	-1.5559227147
H	0	-5.5048008437	-0.3971165084	-1.3650156529
H	0	-5.063846997	0.4376604787	-2.8677325345
H	0	-4.5797684906	1.35013916	0.4625651596

Imaginary Frequency :	705.1397i
<S <sup>2</sup> >	0.5618
Electronic Energy	-966.036751737
Zero-point correction	0.404851
Thermal correction to Energy	0.425943
Thermal correction to Enthalpy	0.426887
Thermal correction to Gibbs Free Energy	0.354762

### Fragmentation product 40

UB3LYP/6-31+G(d)

C	0	-0.2848648156	1.6404474529	-2.2986291844
C	0	-0.2760882708	1.708899026	-0.7992968258
C	0	1.0484062957	1.675886546	-0.0952866223
C	0	2.3582069286	1.6084441888	-0.8823648766
C	0	2.2324098539	1.5636663636	-2.4266250373
C	0	0.947300955	2.2339422441	-2.9459458443
C	0	0.0589166151	0.5140479459	0.1184346275
C	0	-0.6145477084	0.4487009766	1.457612593
C	0	-0.7788490397	-0.8981605047	1.842547735
C	0	-0.2521963043	-1.7477829788	0.7714678367
C	0	0.2335542899	-0.9232015633	-0.2762436692
C	0	-1.3710998535	-1.2217139761	3.0662830738
C	0	-1.8029621549	-0.189596948	3.9043723749
C	0	-1.6427466288	1.1488714035	3.5219556931
C	0	-1.046094765	1.4745768372	2.2972248864
C	0	-0.2017806953	-3.1401038395	0.6755769619
C	0	0.3278051044	-3.7251548822	-0.477248765
C	0	0.7904339579	-2.9190985905	-1.5232388381
C	0	0.7426910718	-1.5221740007	-1.4291986022
C	0	-1.3172049685	1.1449584686	-2.9919530091
H	0	-2.2669645097	-0.4264471245	4.8584532802
H	0	-1.9847596188	1.9430229393	4.1808533418
H	0	-0.9299777641	2.5197873612	.0172649869
H	0	-1.4984987677	-2.2593096173	3.3661015412
H	0	1.084971048	-0.9273441079	-2.265356104
H	0	1.1874551059	-3.3788481423	-2.4248956945
H	0	0.3726853149	-4.8077615435	-0.5652156779
H	0	-0.5750213928	-3.7636266274	1.4846530574
H	0	1.1311707024	2.2937765316	0.7970239679
H	0	-1.0480356553	2.3557371237	-0.3822539762
H	0	2.9725597143	0.768939486	-0.531997153

H	0	2.9122679668	2.5175961056	-0.6147600247
H	0	2.2617806834	0.5301163905	-2.786087059
H	0	3.1076076656	2.057943652	-2.8667727488
H	0	0.8892885068	2.1472920273	-4.0373197693
H	0	0.987307881	3.3095909266	-2.709434391
H	0	-1.3232970961	1.1451033142	-4.0800405762
H	0	-2.1882789901	0.7217062878	-2.4968840487

Imaginary Frequency :	None
<S <sup>2</sup> >	0.0000
Electronic Energy	-772.960506635
Zero-point correction	0.320443
Thermal correction to Energy	0.335739
Thermal correction to Enthalpy	0.336684
Thermal correction to Gibbs Free Energy	0.278184

### Fragmentation TS 37d

UB3LYP/6-31+G(d)

C	0	4.889746338	-0.4044765891	-1.2693808739
C	0	4.3389798276	-1.6874221573	-1.1479759356
C	0	3.0512995107	-1.8654354079	-0.6267555335
C	0	2.3146528405	-0.7475348191	-0.2327134131
C	0	2.8712037704	0.5431412177	-0.3574067074
C	0	4.1581049812	0.7187618653	-0.873150677
C	0	0.9430654904	-0.6546529992	0.3631102207
C	0	0.715780137	0.8181547738	0.5336843146
C	0	1.8840738944	1.5124169002	0.1196581631
C	0	-0.3867693862	1.5560730648	0.9679692877
C	0	-0.3113082122	2.9535621061	1.0202641486
C	0	0.8548111579	3.6278159802	0.640570332
C	0	1.9580648536	2.9059200461	0.1794858369
C	0	0.5386791646	-1.8070364283	1.2912270521
C	0	-0.0922948244	-1.7655247995	-0.0692372472
C	0	-0.3160260655	-1.6879318285	2.5535179813
C	0	-1.8135621244	-1.3726103407	2.3415260691
C	0	-2.367993486	-1.9846341988	1.0441651231
C	0	-1.561654204	-1.6290607991	-0.1813063327
C	0	-2.1761835159	-1.3679352295	-1.4456200436
C	0	-2.5393892593	0.3715213888	-1.8283382779
C	0	-3.7514173381	0.8487720343	-1.251942341
C	0	-5.1120604386	0.5057081987	-1.7684144307
O	0	-3.6713534341	1.2259507096	0.076113053
H	0	5.8916501442	-0.2827082568	-1.6733722497
H	0	4.9165161621	-2.5542253121	-1.4597262928
H	0	2.6436234589	-2.8702840697	-0.5370741415
H	0	4.5887221816	1.7130596992	-0.9673030302
H	0	-1.3196543674	1.0766445388	1.2291888909
H	0	-1.1797985486	3.5174403541	1.3511452405
H	0	0.8971632345	4.7130328082	0.6909095412

H	0	2.8603559235	3.4244452921	-0.1367249105
H	0	1.3561248964	-2.5153150384	1.4187040009
H	0	0.3560396951	-2.3949965689	-0.8415612803
H	0	0.1289038848	-0.960512229	3.2452334435
H	0	-0.2434406727	-2.6636165156	3.0535248807
H	0	-1.9840376216	-0.2934058466	2.3264766721
H	0	-2.3776307993	-1.7570401644	3.2019610844
H	0	-3.4155798106	-1.6902276422	0.9128914302
H	0	-2.3700083621	-3.0866154614	1.1602557438
H	0	-3.1597124113	-1.8275442477	-1.5800021321
H	0	-1.52879738	-1.5933524752	-2.2980032507
H	0	-2.5902172086	0.338379583	-2.9177235308
H	0	-1.6427008961	0.8866651159	-1.4891517084
H	0	-5.833817203	1.3171461581	-1.5920678892
H	0	-5.5231965093	-0.4021452893	-1.2870634165
H	0	-5.0843132843	0.321944124	-2.8467193021
H	0	-4.5541857035	1.4500738915	0.409677489

Imaginary Frequency :	705.1266i
<S <sup>2</sup> >	0.5618
Electronic Energy	-966.036751736
Zero-point correction	0.404851
Thermal correction to Energy	0.425943
Thermal correction to Enthalpy	0.426887
Thermal correction to Gibbs Free Energy	0.354762

Triplet biradical **31** used in MD simulations (H/D isotopomers)  
 UO3LYP/3-21G

C	0	-1.8067	-1.38008	0.85394
C	0	-0.42374	-1.65094	0.4365
C	0	0.46516	-1.67299	1.68174
C	0	-0.41171	-1.37623	2.90128
C	0	-1.88545	-1.31538	2.37492
C	0	0.71205	-0.56118	0.66617
C	0	0.53481	0.91725	0.83519
C	0	1.54479	1.58531	0.08468
C	0	2.39058	0.58092	-0.57526
C	0	1.90542	-0.70358	-0.22967
C	0	3.50262	0.72042	-1.40798
C	0	4.13096	-0.43081	-1.89556
C	0	3.65345	-1.70244	-1.55218
C	0	2.53729	-1.84615	-0.71647
C	0	-0.3912	1.67386	1.55518
C	0	-0.31119	3.07336	1.52674
C	0	0.68464	3.7215	0.78932
C	0	1.61995	2.97808	0.06223
C	0	-2.98249	-1.90999	0.0637
C	0	-3.09074	-1.3933	-1.39789
C	0	-3.45962	0.06583	-1.47059
O	0	-2.66029	0.98412	-0.77487

C	0	-4.02572	0.64379	-2.7335
H	0	4.99563	-0.33895	-2.54398
H	0	4.15235	-2.5858	-1.93628
H	0	2.1799	-2.83767	-0.45836
H	0	3.8763	1.70323	-1.67382
H	0	-1.17712	1.20508	2.12865
H	0	-1.03741	3.65793	2.08103
H	0	0.72889	4.80508	0.77784
H	0	2.39162	3.47912	-0.51211
H	0	1.26236	-2.40152	1.78117
H	0	-0.23695	-2.28459	-0.423
H	0	-0.11083	-0.44172	3.38453
H	0	-0.30257	-2.18298	3.63389
H	0	-2.42659	-0.43097	2.73632
H	0	-2.44661	-2.1929	2.73649
H	0	-3.91554	-1.66118	0.58476
H	0	-2.91085	-3.01431	0.03762
H	0	-3.86393	-1.97281	-1.91706
H	0	-2.1345	-1.59517	-1.91939
H	0	-4.37411	1.66588	-2.54704
H	0	-4.86811	0.04035	-3.08947
H	0	-3.2743	0.69487	-3.54312
H/D	0	-2.12721	0.49287	-0.08594

Imaginary Frequency :  
<S<sup>2</sup>>

None  
2.0071

Electronic Energy

-921.256436863

Zero-point correction

0.377868 / 0.374699

Thermal correction to Energy

0.397907 / 0.394921

Thermal correction to Enthalpy

0.398851 / 0.395865

Thermal correction to Gibbs Free Energy

0.327417 / 0.324091

Conical intersection between ketone **30** and biradical **31**

CASSCF(6,5)/3-21G (GAMESS)

C	6.0	-1.86076188	-1.32726645	0.80516970
C	6.0	-0.47067142	-1.55698240	0.36022153
C	6.0	0.39139006	-1.60906923	1.60775161
C	6.0	-0.47141227	-1.25836766	2.82316065
C	6.0	-1.94351459	-1.25009131	2.31128216
C	6.0	0.65021592	-0.53051078	0.57031548
C	6.0	0.53888768	0.95603281	0.75345844
C	6.0	1.61226547	1.57825530	0.09790838
C	6.0	2.44166613	0.54723805	-0.54831761
C	6.0	1.87822998	-0.70054072	-0.28258595
C	6.0	3.58939338	0.65721172	-1.30731654
C	6.0	4.17657375	-0.49699795	-1.80342543
C	6.0	3.61957240	-1.73753226	-1.53863573
C	6.0	2.46557426	-1.84678626	-0.77417576
C	6.0	-0.38699263	1.73058426	1.42120600
C	6.0	-0.23353651	3.11090589	1.44257951
C	6.0	0.83177668	3.71581912	0.80192578

C	6.0	1.76355720	2.94788241	0.12008090
C	6.0	-2.98912120	-1.96206760	0.02843269
C	6.0	-3.14310646	-1.47068942	-1.42918074
C	6.0	-3.56122017	-0.02763893	-1.43550432
O	8.0	-2.89313364	0.88508070	-0.56796592
C	6.0	-3.99033499	0.65770382	-2.70654607
H	1.0	5.06716824	-0.42942736	-2.39589214
H	1.0	4.08280373	-2.62242770	-1.92762339
H	1.0	2.04522228	-2.81359291	-0.57628989
H	1.0	4.02228165	1.61592209	-1.51364803
H	1.0	-1.22608256	1.29586506	1.92031014
H	1.0	-0.95812303	3.71123648	1.95502412
H	1.0	0.93335223	4.78237057	0.82589221
H	1.0	2.58614755	3.41544747	-0.38383344
H	1.0	1.15153730	-2.35434651	1.72218621
H	1.0	-0.32298335	-2.22811651	-0.46090281
H	1.0	-0.18283074	-0.30417639	3.24032688
H	1.0	-0.34565857	-2.00738096	3.59351039
H	1.0	-2.52526021	-0.41068390	2.67499089
H	1.0	-2.44499993	-2.15239668	2.65314651
H	1.0	-3.92894006	-1.82847667	0.55103230
H	1.0	-2.78250933	-3.03273058	0.01398615
H	1.0	-3.91841984	-2.05529261	-1.91349959
H	1.0	-2.21737432	-1.64709067	-1.97640288
H	1.0	-4.34831810	1.64819658	-2.45523429
H	1.0	-4.79955339	0.10389866	-3.17145967
H	1.0	-3.18199039	0.75929528	-3.42880392
H	1.0	-2.36143756	0.51163501	0.02818927

State 1 MCSCF Energy: -915.5425733723

State 2 MCSCF Energy: -915.5423613884

### A.3 Computational Details for Chapter 4

#### A.3.1 Molecular Dynamics Details

Born-Oppenheimer direct dynamics were run at the BS-UO3LYP/3-21G level of theory using the Gaussian03 suite of programs. Trajectories were begun from the ring-opening TS. Initial kinetic energy distributions were selected by quasiclassical normal-mode sampling from a canonical ensemble with a rotational temperature of 2000 K (or other temperatures as described in the text). This sampling also served to randomly perturb the structures slightly from the optimized TS. In some cases, additional energy was given to specific vibrational modes. Trajectories were run for approximately 500 fs, or until a termination criterion was reached. The termination criteria were either reaching bicyclopentene (the bridgehead C-C bond length becoming less than 1.60 Å) or undergoing one of the possible hydrogen migrations (the forming C-H bond length becoming less than 1.20 Å). The timestep was chosen automatically by the program

based on the energy gradient at each step. The program ensured that total energy was conserved.

### A.3.2 Computed Energies and Geometries

Note that geometries are in the form (Atomic Symbol:Atom Type:X:Y:Z) Cartesian Coordinates are in Angstroms. Energies are in Hartrees. Electronic energy refers to the SCF single point energy. Frequencies are in  $\text{cm}^{-1}$ . Unless otherwise stated, calculations are performed with a simulated pressure and temperature of 1 atm and 298.15 K respectively.

#### 1,3-Cyclopentadiene (123) O3LYP/3-21G

C	0	1.187828	-0.282041	0.000000
C	0	-0.000015	-1.226859	0.000000
C	0	0.739212	0.995273	0.000000
C	0	-0.739188	0.995291	0.000000
C	0	-1.187835	-0.282013	0.000000
H	0	2.216935	-0.613987	-0.000001
H	0	-0.000023	-1.875293	0.888803
H	0	-0.000023	-1.875298	-0.888800
H	0	1.347217	1.890285	0.000001
H	0	-1.347171	1.890318	0.000000
H	0	-2.216950	-0.613933	-0.000001

Imaginary Frequency :	None
$\langle S^2 \rangle$	0.0000
Electronic Energy	-192.965439901
Zero-point correction	0.093064
Thermal correction to Energy	0.097198
Thermal correction to Enthalpy	0.098142
Thermal correction to Gibbs Free Energy	0.066456

#### O3LYP/6-31+G(d)

C	0	-0.284741	-1.179510	-0.000001
C	0	-1.215129	-0.000004	0.000000
C	0	0.993161	-0.732587	0.000000
C	0	0.993156	0.732594	0.000000
C	0	-0.284749	1.179508	-0.000001
H	0	-0.614142	-2.213373	-0.000003
H	0	-1.879453	-0.000006	0.878326
H	0	-1.879475	-0.000006	-0.878308
H	0	1.888528	-1.347639	0.000001
H	0	1.888518	1.347652	0.000001
H	0	-0.614157	2.213368	-0.000003

Imaginary Frequency :	None
<S <sup>2</sup> >	0.0000
Electronic Energy	-194.041317771
Zero-point correction	0.092431
Thermal correction to Energy	0.096616
Thermal correction to Enthalpy	0.097560
Thermal correction to Gibbs Free Energy	0.065814

#### B1B95/3-21G

C	0	-0.7324342773	-0.96081255	0.1354181968
C	0	0.7784048955	-0.9408324251	0.0642609695
C	0	-1.1984056929	0.2981114856	0.0231407259
C	0	-0.0633464667	1.2269366721	-0.1272662782
C	0	1.0890827564	0.5297390079	-0.1059829671
H	0	-1.3122201177	-1.8628969417	0.2576270462
H	0	1.1499802101	-1.5321126893	-0.7828793542
H	0	1.2306540721	-1.3453243843	0.9792219423
H	0	-2.2342663579	0.6030864879	0.0381036715
H	0	-0.1647721397	2.2965639905	-0.2361282722
H	0	2.090817043	0.9218303942	-0.1933689152

Imaginary Frequency :	None
<S <sup>2</sup> >	0.0000
Electronic Energy	-192.936179745
Zero-point correction	0.093752
Thermal correction to Energy	0.097857
Thermal correction to Enthalpy	0.098802
Thermal correction to Gibbs Free Energy	0.067163

#### B1B95/6-31+G(d)

C	0	-0.7241833696	-0.9582391997	0.1347587197
C	0	0.7706551492	-0.9314672412	0.0636226131
C	0	-1.1922125349	0.3007357753	0.0225840861
C	0	-0.0671275125	1.2213988475	-0.1264946594
C	0	1.0849488758	0.5221861413	-0.1050064304
H	0	-1.3101350652	-1.861256169	0.2573389133
H	0	1.1528007236	-1.5339357298	-0.7728682554
H	0	1.2325475315	-1.3491831235	0.9696420067
H	0	-2.2342470586	0.6005267202	0.0383861164
H	0	-0.1622410703	2.29605514	-0.2361652305
H	0	2.0887912915	0.9201072233	-0.1931195252

Imaginary Frequency :	None
<S <sup>2</sup> >	0.0000
Electronic Energy	-194.009854501
Zero-point correction	0.093074
Thermal correction to Energy	0.097236
Thermal correction to Enthalpy	0.098181

Thermal correction to Gibbs Free Energy 0.066472

B3LYP/3-21G

C	0	-0.7372143223	-0.9638142624	0.1359446999
C	0	0.7823349858	-0.9455811982	0.064588309
C	0	-1.2028510311	0.2980741857	0.0233532749
C	0	-0.0624524725	1.2312677859	-0.1277583619
C	0	1.0929629033	0.5338246871	-0.1066048768
H	0	-1.3178502381	-1.866640072	0.2582663894
H	0	1.1550066744	-1.538254187	-0.7828725021
H	0	1.2356980666	-1.3513502432	0.9800778959
H	0	-2.239259577	0.6051745609	0.0381231653
H	0	-0.1658669616	2.3018402722	-0.2366222582
H	0	2.095591657	0.9266024807	-0.1941109608

Imaginary Frequency : None  
<S<sup>2</sup>> 0.0000  
Electronic Energy -193.038274580  
Zero-point correction 0.093385  
Thermal correction to Energy 0.097488  
Thermal correction to Enthalpy 0.098432  
Thermal correction to Gibbs Free Energy 0.066794

B3LYP/6-31+G(d)

C	0	-0.7297990396	-0.9622267006	0.1354220591
C	0	0.776028798	-0.9379608472	0.064072199
C	0	-1.1981581302	0.3011295216	0.0228232823
C	0	-0.0663699614	1.2272782281	-0.1271421063
C	0	1.0899653187	0.526893482	-0.1057517508
H	0	-1.3170124896	-1.8657884174	0.2581100255
H	0	1.1585858192	-1.5412149487	-0.7741666105
H	0	1.2384691842	-1.3560453452	0.9719534295
H	0	-2.2407390724	0.6034666445	0.0383907823
H	0	-0.1638921816	2.3029592391	-0.2368012065
H	0	2.0945868276	0.9259407242	-0.1940285211

Imaginary Frequency : None  
<S<sup>2</sup>> 0.0000  
Electronic Energy -194.110327847  
Zero-point correction 0.092642  
Thermal correction to Energy 0.096796  
Thermal correction to Enthalpy 0.097740  
Thermal correction to Gibbs Free Energy 0.066037

B972/3-21G

C	0	-0.7337695025	-0.9626246767	0.1356679561
C	0	0.7798024267	-0.9425210199	0.0643773124
C	0	-1.2005144934	0.2986286226	0.0231837613

C	0	-0.0634503993	1.2290938639	-0.1274876464
C	0	1.0911269221	0.5306932619	-0.1061815813
H	0	-1.3137984066	-1.8644035034	0.2578546338
H	0	1.1512751729	-1.5336984152	-0.7828969591
H	0	1.2319536835	-1.346873085	0.9794655218
H	0	-2.2361915804	0.6037107584	0.038129911
H	0	-0.1650151258	2.2985632677	-0.2363231227
H	0	2.092606535	0.9230806666	-0.1935887977

Imaginary Frequency :	None
<S <sup>2</sup> >	0.0000
Electronic Energy	-192.968662349
Zero-point correction	0.094099
Thermal correction to Energy	0.098187
Thermal correction to Enthalpy	0.099131
Thermal correction to Gibbs Free Energy	0.067516

B972/6-31+G(d)

C	0	-0.7260989862	-0.9600215273	0.1350292911
C	0	0.772610207	-0.9338299014	0.0637857274
C	0	-1.1947381788	0.3009912145	0.0226757505
C	0	-0.0668936518	1.2239135243	-0.1267676377
C	0	1.0870785766	0.5237092483	-0.1052719095
H	0	-1.3117833676	-1.862594275	0.2575475718
H	0	1.1543507784	-1.5357922334	-0.7726361858
H	0	1.2340767841	-1.3510449398	0.9696833079
H	0	-2.2360700998	0.6013984229	0.0383844469
H	0	-0.162753092	2.2980031241	-0.2363393981
H	0	2.0904311964	0.9214545506	-0.1933470739

Imaginary Frequency :	None
<S <sup>2</sup> >	0.0000
Electronic Energy	-194.039603357
Zero-point correction	0.093396
Thermal correction to Energy	0.097540
Thermal correction to Enthalpy	0.098485
Thermal correction to Gibbs Free Energy	0.066798

mpwpw91/3-21G

C	0	-0.7378223116	-0.9699187548	0.1366065953
C	0	0.7837963929	-0.9473450326	0.064721447
C	0	-1.207190207	0.3023617194	0.0231030264
C	0	-0.0658474537	1.2363293261	-0.1281319618
C	0	1.099100881	0.5332415092	-0.1068387038
H	0	-1.3215386391	-1.8794343394	0.2597671589
H	0	1.1596329186	-1.5447578867	-0.7881150795
H	0	1.2408314	-1.3566377891	0.9861637712
H	0	-2.2510270023	0.6106935945	0.038084289
H	0	-0.1690442495	2.314389068	-0.2377946555

H	0	2.1089217634	0.9277347484	-0.1948679026
---	---	--------------	--------------	---------------

Imaginary Frequency :	None
<S <sup>2</sup> >	0.0000
Electronic Energy	-193.003636588
Zero-point correction	0.090917
Thermal correction to Energy	0.095132
Thermal correction to Enthalpy	0.096077
Thermal correction to Gibbs Free Energy	0.064265

#### VSXC/3-21G

C	0	-0.7371557406	-0.9671829861	0.1363100063
C	0	0.7831169131	-0.946527222	0.064653132
C	0	-1.2042073146	0.3014829038	0.0230470077
C	0	-0.0655592295	1.2332516913	-0.1278359381
C	0	1.0962767177	0.53312115	-0.1066702848
H	0	-1.3174739267	-1.8694304461	0.2585584073
H	0	1.1558657429	-1.539262801	-0.7826086025
H	0	1.2365648012	-1.3524371413	0.9799243045
H	0	-2.2405387308	0.607097423	0.0379619318
H	0	-0.1675229572	2.3034610099	-0.2367364961
H	0	2.0982769939	0.9256987339	-0.1941230837

Imaginary Frequency :	None
<S <sup>2</sup> >	0.0000
Electronic Energy	-193.109042779
Zero-point correction	0.092908
Thermal correction to Energy	0.097077
Thermal correction to Enthalpy	0.098021
Thermal correction to Gibbs Free Energy	0.066278

#### 1,3-Cyclopentadiene H shift TS UO3LYP/3-21G

C	0	0.413777	1.153229	-0.017513
C	0	-0.942564	0.754721	-0.037039
C	0	1.221627	0.000005	-0.010977
C	0	0.413785	-1.153226	-0.017513
C	0	-0.942558	-0.754728	-0.037039
H	0	0.759383	2.175123	0.029317
H	0	-1.819385	1.358112	-0.219136
H	0	-1.165540	-0.000004	1.045659
H	0	2.301111	0.000008	0.054467
H	0	0.759399	-2.175118	0.029317
H	0	-1.819374	-1.358125	-0.219136

Imaginary Frequency :	1308.2049i
<S <sup>2</sup> >	0.0000
Electronic Energy	-192.916086533
Zero-point correction	0.089504

Thermal correction to Energy	0.093292
Thermal correction to Enthalpy	0.094236
Thermal correction to Gibbs Free Energy	0.063130

UO3LYP/6-31+G(d)

C	0	0.412933	1.149706	-0.018222
C	0	-0.938339	0.742721	-0.039972
C	0	1.217104	0.000001	-0.008601
C	0	0.412935	-1.149705	-0.018222
C	0	-0.938337	-0.742723	-0.039972
H	0	0.754839	2.177040	0.029659
H	0	-1.822494	1.351841	-0.192195
H	0	-1.163324	-0.000001	1.014877
H	0	2.300851	0.000003	0.060118
H	0	0.754844	-2.177039	0.029659
H	0	-1.822491	-1.351845	-0.192195
Imaginary Frequency :				-1165.8757
<S <sup>2</sup> >				0.0000
Electronic Energy				-193.999148394
Zero-point correction				0.089224
Thermal correction to Energy				0.093071
Thermal correction to Enthalpy				0.094015
Thermal correction to Gibbs Free Energy				0.062841

UB1B95/3-21G

C	0	-0.51846	-1.82082	0.93529
C	0	0.90076	-1.80265	0.86845
C	0	-0.99426	-0.49746	0.81641
C	0	0.09842	0.38099	0.65401
C	0	1.30044	-0.37611	0.6861
H	0	-1.12667	-2.71	1.08205
H	0	1.54391	-2.66137	0.67627
H	0	1.42968	-1.03733	1.90569
H	0	-2.04143	-0.20001	0.84916
H	0	0.04206	1.46171	0.5491
H	0	2.2783	-0.04035	0.34102

Imaginary Frequency :				1400.0833i
<S <sup>2</sup> >				0.0000
Electronic Energy				-192.884344031
Zero-point correction				0.088801
Thermal correction to Energy				0.092509
Thermal correction to Enthalpy				0.093453
Thermal correction to Gibbs Free Energy				0.062447

UB1B95/6-31+G(d)

C	0	-0.703298383	-0.9849811521	0.1288671687
C	0	0.6994060658	-0.9656464925	0.0335526367

C	0	-1.1668187933	0.328583097	0.0131188939
C	0	-0.0899051906	1.2043929612	-0.1509229874
C	0	1.095533018	0.4482452795	-0.1471345157
H	0	-1.3038818408	-1.8674098998	0.3055854787
H	0	1.3789456489	-1.8039501278	-0.051696329
H	0	1.1598068901	-0.1988546424	0.9866313805
H	0	-2.2043050077	0.6304191506	0.1004590699
H	0	-0.1411717725	2.2825994869	-0.2247657997
H	0	2.1011057805	0.7736338747	-0.3811009773

Imaginary Frequency :	1153.8655 <i>i</i>
<S <sup>2</sup> >	0.0000
Electronic Energy	-193.968504779
Zero-point correction	0.089867
Thermal correction to Energy	0.093687
Thermal correction to Enthalpy	0.094631
Thermal correction to Gibbs Free Energy	0.063503

#### UB3LYP/3-21G

C	0	-0.7075202847	-0.990923354	0.1289293305
C	0	0.7021561729	-0.9819030249	0.0429731997
C	0	-1.1751186482	0.3299758521	0.0058173028
C	0	-0.0904733454	1.2114810679	-0.1525294648
C	0	1.1068264072	0.4624754381	-0.1416109999
H	0	-1.3123022383	-1.8672699597	0.3029209075
H	0	1.3743524473	-1.8170428193	-0.0770831583
H	0	1.1794000665	-0.199376316	1.0255107026
H	0	-2.2102524506	0.6299979297	0.0841320237
H	0	-0.1486329713	2.2861708631	-0.2278752022
H	0	2.1022133361	0.7808844265	-0.4090814834

Imaginary Frequency :	1366.0335 <i>i</i>
<S <sup>2</sup> >	0.0000
Electronic Energy	-192.985748798
Zero-point correction	0.089708
Thermal correction to Energy	0.093469
Thermal correction to Enthalpy	0.094413
Thermal correction to Gibbs Free Energy	0.063343

#### UB3LYP/6-31+G(d)

C	0	-0.7067709326	-0.9892299638	0.129040715
C	0	0.7024897119	-0.9709547842	0.0368378073
C	0	-1.1725479144	0.3298982169	0.0108434496
C	0	-0.0906905439	1.2097236629	-0.1519753211
C	0	1.1011083158	0.451820148	-0.1449865679
H	0	-1.3094443094	-1.871973778	0.3047974181
H	0	1.3805626083	-1.8110707172	-0.0569154641
H	0	1.1769668146	-0.2026280502	0.9947335993
H	0	-2.2117570687	0.6316169583	0.0935044999

H	0	-0.143655089	2.2890356167	-0.2269602719
H	0	2.1057952239	0.7774762914	-0.3877202786

Imaginary Frequency :	1236.5329 <i>i</i>
<S <sup>2</sup> >	0.0000
Electronic Energy	-194.064776640
Zero-point correction	0.089345
Thermal correction to Energy	0.093165
Thermal correction to Enthalpy	0.094109
Thermal correction to Gibbs Free Energy	0.062969

UB972/3-21G

C	0	1.0269843888	1.7060566248	0.6912217939
C	0	-0.3345916965	2.0684198033	0.6255544824
C	0	1.1177846867	0.3046998047	0.7243174993
C	0	-0.167842943	-0.2601871861	0.689620824
C	0	-1.1166203484	0.7814882177	0.6245071051
H	0	1.849922543	2.3994452698	0.7474551065
H	0	-0.7633773271	3.0345748858	0.4159097482
H	0	-0.9473763404	1.5588447125	1.6962967141
H	0	2.0361414658	-0.2534405454	0.8240745869
H	0	-0.4042504512	-1.3100842959	0.7444345876
H	0	-2.171531104	0.717274687	0.4140226841

Imaginary Frequency :	1316.8250 <i>i</i>
<S <sup>2</sup> >	0.0000
Electronic Energy	-192.918277983
Zero-point correction	0.090520
Thermal correction to Energy	0.094262
Thermal correction to Enthalpy	0.095206
Thermal correction to Gibbs Free Energy	0.064167

UB972/6-31+G(d)

C	0	-0.7046511804	-0.9867611096	0.1289947902
C	0	0.7008507572	-0.9673614938	0.0347688983
C	0	-1.169231592	0.3291340861	0.01213487
C	0	-0.0901414877	1.2065868482	-0.151304645
C	0	1.0977297993	0.4492053509	-0.1462618975
H	0	-1.3051013426	-1.8686793861	0.305879839
H	0	1.3799148515	-1.8052630188	-0.052741761
H	0	1.1632553229	-0.1999402948	0.9857063366
H	0	-2.2063975483	0.6307381999	0.0983774249
H	0	-0.141549888	2.2843418365	-0.2248566318
H	0	2.1025408261	0.7739805729	-0.3823573035

Imaginary Frequency :	1170.5820 <i>i</i>
<S <sup>2</sup> >	0.0000
Electronic Energy	-193.996446357
Zero-point correction	0.090169

Thermal correction to Energy	0.093975
Thermal correction to Enthalpy	0.094919
Thermal correction to Gibbs Free Energy	0.063805

umpwpw91/3-21G

C	0	-0.7111422454	-0.9964007017	0.1292242667
C	0	0.7060397866	-0.9867217526	0.0433072127
C	0	-1.181467399	0.3316043534	0.0046409812
C	0	-0.0907535249	1.2179320376	-0.1537587562
C	0	1.1126409973	0.4645499659	-0.1421576604
H	0	-1.3195050295	-1.8781749133	0.3091059092
H	0	1.3841515577	-1.8265231752	-0.0782182068
H	0	1.1803191888	-0.1987212462	1.0326509197
H	0	-2.2234392261	0.633876795	0.0855718063
H	0	-0.1488169141	2.300316987	-0.2248908393
H	0	2.1153847354	0.7834421373	-0.4117558527

Imaginary Frequency :	1274.1894i
<S <sup>2</sup> >	0.0000
Electronic Energy	-192.957017842
Zero-point correction	0.087386
Thermal correction to Energy	0.091254
Thermal correction to Enthalpy	0.092198
Thermal correction to Gibbs Free Energy	0.060971

UVSXC/3-21G

C	0	-0.7094632772	-0.9937462967	0.1293673801
C	0	0.7047332137	-0.9856195401	0.0402759768
C	0	-1.1779105671	0.3311229301	0.0088200897
C	0	-0.0907375347	1.2149020988	-0.1528508517
C	0	1.1106819815	0.4636646538	-0.1448979356
H	0	-1.313296484	-1.8690185515	0.3068662107
H	0	1.3788561877	-1.8192830241	-0.072418603
H	0	1.1632714431	-0.1955005212	1.0200943247
H	0	-2.2118817285	0.6313061722	0.0904773283
H	0	-0.1482390045	2.2890388168	-0.2245331687
H	0	2.1074666892	0.7815140327	-0.4047740474

Imaginary Frequency :	1324.9178i
<S <sup>2</sup> >	0.0000
Electronic Energy	-193.060039836
Zero-point correction	0.089172
Thermal correction to Energy	0.092984
Thermal correction to Enthalpy	0.093928
Thermal correction to Gibbs Free Energy	0.062784

UVSXC/6-31+G(d)

C	0	-0.70909132	-0.9926851937	0.1290720284
---	---	-------------	---------------	--------------

C	0	0.7055455985	-0.9745624551	0.0340005599
C	0	-1.1760715146	0.3313336761	0.0143855551
C	0	-0.0909254284	1.2137731579	-0.1528980619
C	0	1.1053696321	0.4525919753	-0.1483747432
H	0	-1.311102301	-1.8760273083	0.309293303
H	0	1.3873662547	-1.813853061	-0.0502808962
H	0	1.159577581	-0.1987518573	0.9868358516
H	0	-2.2155862595	0.6338055884	0.1021779601
H	0	-0.142687442	2.2942849952	-0.2236465681
H	0	2.113470361	0.7778346795	-0.3814916799

Imaginary Frequency :	1169.0322i
<S <sup>2</sup> >	0.0000
Electronic Energy	-194.149582353
Zero-point correction	0.088557
Thermal correction to Energy	0.092437
Thermal correction to Enthalpy	0.093381
Thermal correction to Gibbs Free Energy	0.062151

Bicyclo[2.1.0]pent-2-ene (125)

O3LYP/3-21G

C	0	0.356124	0.773378	-0.423479
C	0	1.254949	-0.000008	0.559406
C	0	-1.088501	0.676941	0.099891
C	0	-1.088485	-0.676954	0.099890
C	0	0.356128	-0.773356	-0.423506
H	0	0.740560	1.429422	-1.189099
H	0	0.992095	-0.000027	1.611880
H	0	2.319845	-0.000002	0.330246
H	0	-1.767191	1.427132	0.481455
H	0	-1.767158	-1.427161	0.481452
H	0	0.740558	-1.429375	-1.189151

Imaginary Frequency :	None
<S <sup>2</sup> >	0.0000
Electronic Energy	-192.884851703
Zero-point correction	0.092224
Thermal correction to Energy	0.096327
Thermal correction to Enthalpy	0.097272
Thermal correction to Gibbs Free Energy	0.065755

O3LYP/6-31+G(d)

C	0	0.344309	0.759998	-0.404074
C	0	1.261758	0.000000	0.536305
C	0	-1.084129	0.674301	0.096930
C	0	-1.084129	-0.674302	0.096930
C	0	0.344309	-0.759997	-0.404075
H	0	0.727875	1.397999	-1.194940

H	0	1.055445	-0.000001	1.606073
H	0	2.321522	0.000000	0.274526
H	0	-1.762712	1.429400	0.488592
H	0	-1.762711	-1.429401	0.488592
H	0	0.727875	-1.397996	-1.194943

Imaginary Frequency :	None
<S <sup>2</sup> >	0.0000
Electronic Energy	-193.971125517
Zero-point correction	0.091791
Thermal correction to Energy	0.095921
Thermal correction to Enthalpy	0.096865
Thermal correction to Gibbs Free Energy	0.065329

#### B1B95/3-21G

C	0	-0.4831313216	-0.7699157255	0.2705855556
C	0	1.0048111223	-0.9222208133	-0.0655937356
C	0	-1.0484648476	0.3068312593	-0.6650235196
C	0	-0.1642563207	1.2405340294	-0.2632444453
C	0	0.5263828966	0.2973567817	0.7305151236
H	0	-1.0284665363	-1.4661070371	0.8846017749
H	0	1.3143708872	-0.7723748416	-1.0924937381
H	0	1.5484917489	-1.6778869705	0.494950622
H	0	-1.7781510778	0.2583916069	-1.4581225613
H	0	0.0891857645	2.2303682378	-0.6093865669
H	0	0.8425200397	0.5120958149	1.7370165972

Imaginary Frequency :	None
<S <sup>2</sup> >	0.0000
Electronic Energy	-192.856495842
Zero-point correction	0.093015
Thermal correction to Energy	0.097083
Thermal correction to Enthalpy	0.098027
Thermal correction to Gibbs Free Energy	0.066572

#### B1B95/6-31+G(d)

C	0	0.3452626522	0.7560735227	-0.405556798
C	0	1.2484417618	0.0000148475	0.5391461439
C	0	-1.0767228403	0.6706327702	0.0960545086
C	0	-1.0767804157	-0.6706995921	0.0956741789
C	0	0.3453370727	-0.7560392467	-0.405653574
H	0	0.7324081788	1.394460006	-1.1898846617
H	0	1.0234069595	-0.0000317328	1.6021790155
H	0	2.3084104192	0.0001278116	0.2918048034
H	0	-1.7549531122	1.422932603	0.4843600595
H	0	-1.7550743804	-1.4231200954	0.4836214994
H	0	0.7325725504	-1.3942624017	-1.1900674728

Imaginary Frequency :	None
-----------------------	------

<S <sup>2</sup> >	0.0000
Electronic Energy	-193.940389375
Zero-point correction	0.092929
Thermal correction to Energy	0.097011
Thermal correction to Enthalpy	0.097955
Thermal correction to Gibbs Free Energy	0.066497

#### B3LYP/3-21G

C	0	-0.482830146	-0.7749751429	0.265721435
C	0	1.0140452775	-0.9314711675	-0.064490628
C	0	-1.0575129133	0.3133388688	-0.6643457414
C	0	-0.1718001531	1.2487790057	-0.2617514172
C	0	0.5329959241	0.2989165084	0.7284771462
H	0	-1.0284654806	-1.4696665889	0.8840719595
H	0	1.3371599121	-0.7950944134	-1.0900535728
H	0	1.5505765131	-1.685410077	0.5076363661
H	0	-1.7915399098	0.2685658901	-1.4553872147
H	0	0.0768069849	2.241897836	-0.6059549993
H	0	0.8460740455	0.5121789183	1.7380226939

Imaginary Frequency :	None
<S <sup>2</sup> >	0.0000
Electronic Energy	-192.950568752
Zero-point correction	0.092402
Thermal correction to Energy	0.096497
Thermal correction to Enthalpy	0.097441
Thermal correction to Gibbs Free Energy	0.065935

#### B3LYP/6-31+G(d)

C	0	-0.4692578765	-0.763137115	0.2498176375
C	0	1.0109748911	-0.9301664547	-0.0610370294
C	0	-1.0614722634	0.312357224	-0.6493351924
C	0	-0.1776273642	1.2462396457	-0.2471855271
C	0	0.5305401405	0.293662301	0.7051234018
H	0	-1.0073085404	-1.4548844154	0.8903390189
H	0	1.3610688546	-0.8195683804	-1.086393169
H	0	1.5394804262	-1.6830015134	0.5259342581
H	0	-1.7984743103	0.2677722892	-1.447160534
H	0	0.0727924115	2.2450137878	-0.5956584975
H	0	0.8334959929	0.490934626	1.7286391811

Imaginary Frequency :	None
<S <sup>2</sup> >	0.0000
Electronic Energy	-194.032814146
Zero-point correction	0.091858
Thermal correction to Energy	0.095976
Thermal correction to Enthalpy	0.096920
Thermal correction to Gibbs Free Energy	0.065395

## B972/3-21G

C	0	-0.4820824179	-0.7716614085	0.268036985
C	0	1.0083502845	-0.9256357685	-0.0654855837
C	0	-1.0529791616	0.3090125189	-0.6644044362
C	0	-0.1671634897	1.2444908547	-0.2618261743
C	0	0.5291490438	0.2973984028	0.7287233942
H	0	-1.0267686671	-1.4669183467	0.8838203336
H	0	1.3255828246	-0.7837702544	-1.0907870991
H	0	1.5467784998	-1.6796206221	0.5026346571
H	0	-1.7846747643	0.2623709179	-1.4556186668
H	0	0.0835794364	2.2354660842	-0.6063437466
H	0	0.8438571158	0.5108446248	1.7360294123

Imaginary Frequency :	None
<S <sup>2</sup> >	0.0000
Electronic Energy	-192.885868421
Zero-point correction	0.093308
Thermal correction to Energy	0.097360
Thermal correction to Enthalpy	0.098304
Thermal correction to Gibbs Free Energy	0.066866

## B972/6-31+G(d)

C	0	-0.12263	-1.15649	0.21509
C	0	1.355	-1.31731	-0.05116
C	0	-0.69809	-0.07801	-0.69644
C	0	0.19422	0.86506	-0.29031
C	0	0.8983	-0.07748	0.67983
H	0	-0.73518	-1.8545	0.77891
H	0	1.74095	-1.2379	-1.083
H	0	1.89586	-2.08228	0.53647
H	0	-1.51736	-0.1353	-1.39625
H	0	0.40603	1.89775	-0.52055
H	0	1.22671	0.21877	1.67219

Imaginary Frequency :	None
<S <sup>2</sup> >	0.0000
Electronic Energy	-193.963879854
Zero-point correction	0.091719
Thermal correction to Energy	0.095842
Thermal correction to Enthalpy	0.096786
Thermal correction to Gibbs Free Energy	0.065247

## mpwpw91/3-21G

C	0	-0.4869342288	-0.7778142041	0.2677227067
C	0	1.0167815049	-0.9324957812	-0.0680953649
C	0	-1.0625714354	0.310855506	-0.6661018979
C	0	-0.169528196	1.2539960085	-0.2602125439
C	0	0.5342010637	0.301704661	0.7329119023

H	0	-1.0317429162	-1.478135022	0.8930897827
H	0	1.3358211014	-0.7886391332	-1.1019853877
H	0	1.5588722923	-1.6924167594	0.5057349518
H	0	-1.7935488736	0.2611064714	-1.4701541816
H	0	0.0891564763	2.2495128148	-0.6142690319
H	0	0.8497496695	0.5110944876	1.7502350535

Imaginary Frequency :	None
<S <sup>2</sup> >	0.0000
Electronic Energy	-192.922001888
Zero-point correction	0.089983
Thermal correction to Energy	0.094188
Thermal correction to Enthalpy	0.095132
Thermal correction to Gibbs Free Energy	0.063460

#### VSXC/3-21G

C	0	-0.4927079678	-0.7733881298	0.2813684502
C	0	1.0088862368	-0.9250459118	-0.0679590468
C	0	-1.0489720162	0.3042766591	-0.674271324
C	0	-0.1583594039	1.2447130607	-0.269597822
C	0	0.5239607216	0.3014656516	0.7445674965
H	0	-1.0355252262	-1.4777358867	0.8895334174
H	0	1.2932523505	-0.7487716819	-1.1009060699
H	0	1.5629655659	-1.6845978954	0.4788225123
H	0	-1.7703234349	0.2525574849	-1.4759999596
H	0	0.1026352278	2.2303932362	-0.6247575489
H	0	0.850150094	0.5160267637	1.7486611258

Imaginary Frequency :	None
<S <sup>2</sup> >	0.0000
Electronic Energy	-193.025206546
Zero-point correction	0.091876
Thermal correction to Energy	0.096010
Thermal correction to Enthalpy	0.096954
Thermal correction to Gibbs Free Energy	0.065395

#### Bicyclo[2.1.0]pent-2-ene to 1,3-Cyclopentadiene ring-opening TS

#### UO3LYP/3-21G

C	0	-0.360617	1.060032	0.235719
C	0	-1.270032	-0.000001	-0.376049
C	0	1.077765	0.672940	-0.084074
C	0	1.077766	-0.672939	-0.084075
C	0	-0.360616	-1.060033	0.235720
H	0	-0.603814	1.454702	1.222762
H	0	-1.261804	-0.000002	-1.469590
H	0	-2.282947	-0.000001	0.028800
H	0	1.883390	1.366955	-0.284091
H	0	1.883390	-1.366954	-0.284094

H 0 -0.603811 -1.454694 1.222768

Imaginary Frequency : 629.0615i  
<S<sup>2</sup>> 0.6789  
Electronic Energy -192.843400217  
Zero-point correction 0.087750  
Thermal correction to Energy 0.092421  
Thermal correction to Enthalpy 0.093365  
Thermal correction to Gibbs Free Energy 0.060586

UO3LYP/6-31+G(d)

C 6 0 -0.349471 -1.043968 -0.224416  
C 6 0 -1.264693 0.000000 0.352969  
C 6 0 1.067360 -0.674270 0.083193  
C 6 0 1.067360 0.674270 0.083193  
C 6 0 -0.349471 1.043968 -0.224416  
H 1 0 -0.606767 -1.534215 -1.164681  
H 1 0 -1.308705 0.000000 1.450732  
H 1 0 -2.271339 0.000000 -0.071958  
H 1 0 1.883532 -1.369356 0.263723  
H 1 0 1.883532 1.369356 0.263723  
H 1 0 -0.606767 1.534215 -1.164681

Imaginary Frequency : 747.8628i  
<S<sup>2</sup>> 0.7405  
Electronic Energy -193.924840209  
Zero-point correction 0.087549  
Thermal correction to Energy 0.092193  
Thermal correction to Enthalpy 0.093137  
Thermal correction to Gibbs Free Energy 0.060454

UB1B95/3-21G

C 0 -0.358839 1.057103 0.236950  
C 0 -1.262595 -0.000002 -0.375292  
C 0 1.071771 0.670331 -0.083791  
C 0 1.071772 -0.670330 -0.083792  
C 0 -0.358838 -1.057105 0.236954  
H 0 -0.607020 1.471449 1.211191  
H 0 -1.245215 -0.000004 -1.466626  
H 0 -2.276697 -0.000002 0.019986  
H 0 1.878155 1.360799 -0.280961  
H 0 1.878157 -1.360797 -0.280966  
H 0 -0.607013 -1.471429 1.211206

Imaginary Frequency : 633.8457i  
<S<sup>2</sup>> 0.7122  
Electronic Energy -192.810958908  
Zero-point correction 0.088302  
Thermal correction to Energy 0.093024

Thermal correction to Enthalpy	0.093968
Thermal correction to Gibbs Free Energy	0.060986

UB1B95/6-31+G(d)

C	0	-0.173116	-1.223103	0.290864
C	0	1.295323	-1.247194	-0.009108
C	0	-0.847228	-0.329092	-0.690839
C	0	0.068022	0.615304	-0.969849
C	0	1.249761	0.245087	-0.142894
H	0	-0.524752	-1.295257	1.319039
H	0	1.546565	-1.766277	-0.941946
H	0	1.916858	-1.607103	0.811519
H	0	-1.858136	-0.442866	-1.067974
H	0	-0.003583	1.470746	-1.633328
H	0	1.583616	0.880255	0.676313

Imaginary Frequency :	762.9823i
<S <sup>2</sup> >	0.7791
Electronic Energy	-193.890401940
Zero-point correction	0.087970
Thermal correction to Energy	0.092679
Thermal correction to Enthalpy	0.093623
Thermal correction to Gibbs Free Energy	0.060700

UB3LYP/3-21G

C	0	0.362750	-1.043004	0.248549
C	0	1.272645	0.000000	-0.391246
C	0	-1.082358	-0.670072	-0.085314
C	0	-1.082358	0.670072	-0.085314
C	0	0.362750	1.043004	0.248549
H	0	0.609364	-1.418109	1.239881
H	0	1.245555	0.000000	-1.482505
H	0	2.290485	0.000000	-0.002352
H	0	-1.877674	-1.368953	-0.303126
H	0	-1.877674	1.368953	-0.303126
H	0	0.609364	1.418110	1.239881

Imaginary Frequency :	607.3250i
<S <sup>2</sup> >	0.6002
Electronic Energy	-192.914493435
Zero-point correction	0.088267
Thermal correction to Energy	0.092811
Thermal correction to Enthalpy	0.093755
Thermal correction to Gibbs Free Energy	0.061330

UB3LYP/6-31+G(d)

C	0	0.352887	-1.037361	0.233792
C	0	1.266492	0.000000	-0.366219

C	0	-1.071281	-0.672233	-0.084260
C	0	-1.071281	0.672233	-0.084260
C	0	0.352887	1.037361	0.233792
H	0	0.608839	-1.494516	1.190132
H	0	1.288036	0.000000	-1.463353
H	0	2.279495	0.000000	0.042810
H	0	-1.881719	-1.369135	-0.278395
H	0	-1.881719	1.369135	-0.278395
H	0	0.608840	1.494516	1.190132

Imaginary Frequency :	672.7052i
<S <sup>2</sup> >	0.6821
Electronic Energy	-193.993013351
Zero-point correction	0.087960
Thermal correction to Energy	0.092490
Thermal correction to Enthalpy	0.093434
Thermal correction to Gibbs Free Energy	0.061030

UB972/3-21G

C	0	-0.170639	-1.224383	0.316912
C	0	1.309893	-1.267403	-0.029719
C	0	-0.855689	-0.321313	-0.699119
C	0	0.057623	0.621085	-0.977538
C	0	1.258526	0.250295	-0.118763
H	0	-0.468826	-1.188378	1.362010
H	0	1.520287	-1.753079	-0.983475
H	0	1.941484	-1.642159	0.773645
H	0	-1.847850	-0.466399	-1.099037
H	0	0.010899	1.451544	-1.665668
H	0	1.497621	0.840692	0.762548

Imaginary Frequency :	626.9277i
<S <sup>2</sup> >	0.6566
Electronic Energy	-192.843759841
Zero-point correction	0.088736
Thermal correction to Energy	0.093342
Thermal correction to Enthalpy	0.094286
Thermal correction to Gibbs Free Energy	0.061678

UB972/6-31+G(d)

C	0	-0.350032	-1.040798	-0.227068
C	0	-1.261398	0.000000	0.355859
C	0	1.065858	-0.672224	0.083070
C	0	1.065858	0.672225	0.083070
C	0	-0.350033	1.040798	-0.227068
H	0	-0.606087	-1.521136	-1.169981
H	0	-1.295491	-0.000001	1.451168
H	0	-2.268508	0.000000	-0.062019
H	0	1.879443	-1.365583	0.266232

H	0	1.879443	1.365584	0.266232
H	0	-0.606087	1.521137	-1.169980

Imaginary Frequency :	720.0631 <i>i</i>
<S <sup>2</sup> >	0.7342
Electronic Energy	-193.920924772
Zero-point correction	0.088531
Thermal correction to Energy	0.093110
Thermal correction to Enthalpy	0.094054
Thermal correction to Gibbs Free Energy	0.061515

umpwpw91/3-21G

C	0	-0.360740	1.072257	0.230409
C	0	-1.274356	0.000000	-0.369656
C	0	1.080362	0.676790	-0.083265
C	0	1.080362	-0.676790	-0.083265
C	0	-0.360740	-1.072257	0.230409
H	0	-0.606069	1.485942	1.216472
H	0	-1.276742	0.000000	-1.470586
H	0	-2.290720	0.000000	0.044376
H	0	1.895137	1.372202	-0.277268
H	0	1.895137	-1.372202	-0.277269
H	0	-0.606069	-1.485941	1.216472

Imaginary Frequency :	653.6793 <i>i</i>
<S <sup>2</sup> >	0.6898
Electronic Energy	-192.883258367
Zero-point correction	0.085695
Thermal correction to Energy	0.090496
Thermal correction to Enthalpy	0.091440
Thermal correction to Gibbs Free Energy	0.058304

UVSXC/3-21G

C	0	-0.366798	1.064741	0.246728
C	0	-1.260402	-0.000003	-0.392278
C	0	1.074885	0.673597	-0.085073
C	0	1.074887	-0.673597	-0.085075
C	0	-0.366797	-1.064743	0.246734
H	0	-0.607635	1.399559	1.256434
H	0	-1.187840	-0.000006	-1.483187
H	0	-2.288775	-0.000002	-0.033343
H	0	1.878609	1.365376	-0.291283
H	0	1.878611	-1.365373	-0.291289
H	0	-0.607625	-1.399530	1.256453

Imaginary Frequency :	559.1379 <i>i</i>
<S <sup>2</sup> >	0.6461
Electronic Energy	-192.987893792
Zero-point correction	0.087302

Thermal correction to Energy	0.092098
Thermal correction to Enthalpy	0.093042
Thermal correction to Gibbs Free Energy	0.059810

